Biochemical Analysis of the Immunity-Related GTPase Irga6

In Vivo and *In Vitro*;

The Role of the Myristoyl Group

Inaugural-Dissertation

zur

Erlangung des Doktorgrades

der Mathematisch-Naturwissenschaftlichen Fakultät

der Universität zu Köln

vorgelegt von

Nataša Papić

aus Belgrad, Serbien

Köln 2007

To my family

Table of contents

1. Introduction

1.1 GTPases - general mechanism of GTP hydrolysis

An estimated 10–18% of all known gene products contain the mononucleotide-binding fold, which forms part of the P-loop domain (G1 motif) of both guanosine triphosphatases (GTPases) and adenosine triphosphatases (ATPases) (Leipe et al., 2002). However, the biological roles of GTPases and ATPases are very different. ATP hydrolysis liberates the energy needed to move motor proteins and accelerate metabolic reactions. Instead, GTP hydrolysis appears to have evolved exclusively to regulate guanine nucleotide-binding proteins, either through promoting their action as molecular switches or their self-assembly as mechanoenzymes (MacMicking, 2004).

The conversion of guanosine triphosphate (GTP) to guanosine diphosphate (GDP) and inorganic phosphate (Pi) by GTP binding proteins (GTPases) is a fundamental process in living cells. GTP hydrolysis controls numerous vital functions, including cellular growth and differentiation (Ras family; (Vojtek and Der, 1998), cytoskeletal dynamics and transcription (Rho/Rac/Cdc42 family; (Mackay and Hall, 1998), vesicular transport (Rab family; (Schimmoller et al., 1998), membrane trafficking (Arf family; (Moss and Vaughan, 1998), nucleocytoplasmic transport and mitotic spindle assembly (Ran family; (Hetzer et al., 2002), translation and protein translocation (EF-Tu, EF-G, SRP; (Chu et al., 2004), endocytosis (dynamin; (Hinshaw, 2000; Hunn, 2007); (Song and Schmid, 2003); (Praefcke and McMahon, 2004), as well as cell-autonomous resistance against a variety of intracellular pathogens (Mx, GBP and IRG families; (Martens and Howard, 2006).

GTPases function as molecular switches, generally cycling between GTP-bound, active and GDP-bound, inactive form (figure 1.1). Only in the activated state these proteins interact with and activate downstream effectors, which in turn trigger cellular responses. GTP hydrolysis returns GTPases to their inactive state, thereby terminating downstream signalling (Scheffzek and Ahmadian, 2005).
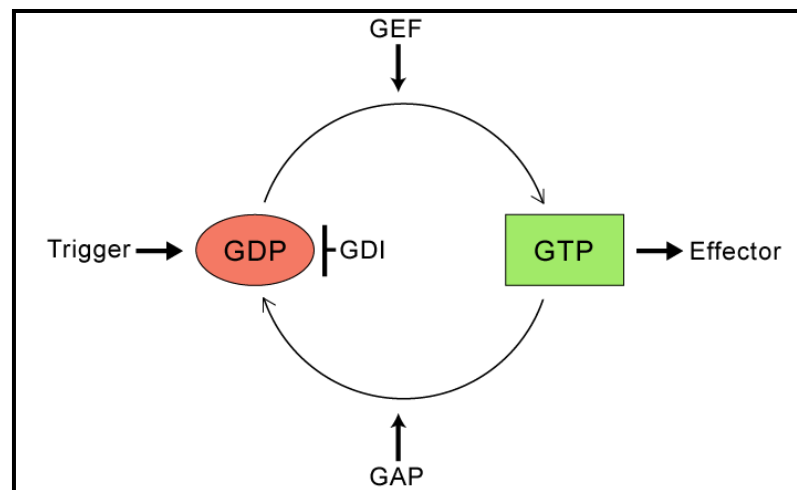
Figure 1.1. GTPase cycle

The GDP-bound form of the GTP-binding protein is considered inactive, whereas the GTP-bound form represents the active form interacting with effector proteins. For many GTPases, but not all, transition between GDP- and GTP-bound states is regulated by different proteins. GDIs prevent dissociation of GDP, keeping the GTPase in the inactive form. GEF activity catalyses the release of GDP and the subsequent uptake of GTP. GAP activity triggers GTP hydrolysis, terminating the active state and restoring the inactive GDP form.

1.1.1. Nucleotide binding domain of GTPases

Common for all GTPases analysed to date is a nucleotide-binding domain (Leipe et al., 2002). The core of the GTP binding motif consists of central six-stranded beta sheets, five parallel and one antiparallel, surrounded by five alpha helices (figure 1.2). Binding of guanine nucleotide is mediated by five motifs termed G1–G5, of which the G1 [G(X)$_4$GK(S/T)], G3 [DXXG], and G4 [(N/T)KXD] motifs are more or less universally conserved.

G1 motif G(X)$_4$GK(S/T) (also referred to as P-loop) stabilises the phosphates of GDP and GTP of the bound nucleotide by hydrogen bonds formed by both lysine and serine/threonine residues (Kjeldgaard et al., 1996). In addition, the side chain of the Ser/Thr residue coordinates the position of magnesium ion, necessary for the catalytic activity of GTPases. In most of the known structures, the Asp residue in G3 motif DXXG is involved in binding a magnesium ion via a water molecule. Furthermore, the Asp residue appears to form a hydrogen bond with the conserved Ser/Thr residue in the G1 motif. In the GTP-bound form, this aspartic acid interacts

with the γ-phosphate. The G4 motif (N/T)KXD determines the specificity for the guanine base (Kjeldgaard et al., 1996).
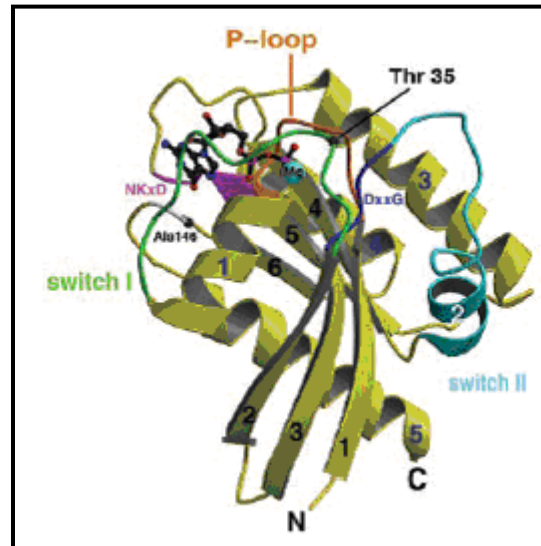
Figure 1.2. The strucure of the GTP-binding domain
Ribbon plot of the minimal GTP-binding domain is shown, with the conserved sequence elements and the switch regions in different colors as indicated (Vetter and Wittinghofer, 2001).

1.2. Regulation of GTPase activity

The fraction of protein molecules in the GTP-bound state depends on the relative rates of two reactions: dissociation of GDP from the GDP-bound protein and hydrolysis of bound GTP, characterized by $k_{dissGDP}$ and k_{catGTP} rate constants respectively. Thus, the proportion of protein in the active GTP-bound state can be increased either by accelerating $k_{dissGDP}$ or by reducing k_{catGTP} (Bourne et al., 1990), performed for many GTPases by specific ligands.

Three groups of structurally distinctive proteins regulate GTPase cycle of some of the GTPases. Guanine-nucleotide dissociation inhibitors (GDIs) trap GTPases in an inactive, GDP-bound state whereas guanine-nucleotide exchange factors (GEFs) catalyze the release of GDP and the subsequent uptake of GTP. GTPase activating proteins (GAPs) accelerate the rate of GTP hydrolysis and thereby terminate downstream signaling.

1.2.1. Guanine-nucleotide dissociation inhibitors (GDI)

Guanine-nucleotide dissociation inhibitors for Rho and Rab family proteins have been identified. GDIs bind to the prenylated COOH-terminus of small GTPases and thereby shield the hydrophobic tail from the aqueous environment. GTPase-GDI complexes constitute a cytoplasmic pool of prenylated proteins, allowing Rab and Rho proteins to be recycled between different membrane compartments in the cell (Vetter and Wittinghofer, 2001). However, no GDI candidates have been reported for the large GTPases like dynamin, Mx, GBP or IRG proteins.

1.2.2. Guanine-nucleotide exchange factors (GEF)

GEFs constitute a highly diverse group of proteins in the cell (Sprang, 2001). They contain a variety of regulatory and protein-protein interaction domains (Cerione and Zheng, 1996) and they can be differentially expressed in a tissue-specific manner (Sprang, 2001). GEFs often possess multiple signal transduction modules allowing their activation by the interaction with various upstream regulators (Hoffman and Cerione, 2002). In addition, GEFs can be also activated by the phosphorylation (Kato et al., 2000). Thus, they can respond to various intra- and extracellular signals often resulting in their translocation to a specific membrane compartment where they than activate GTPases. Although diverse in structure, GEFs use a common mechanism to release nucleotide either by disrupting the magnesium ion binding site in the GTP binding proteins (Worthylake et al., 2000) or, in addition, by influencing γ-phosphate binding site and the P-loop (Sprang, 2001). GEF-GTPase nucleotide-free complex is dissociated by rebinding of the nucleotide (Hutchinson and Eccleston, 2000), normally GTP because of its higher concentration in cells (Kleinecke and Soeling, 1979) and because for most of the GTPases the affinity for GTP is higher than that for GDP. In the case of the large GTPases it has been argued that no GEF activity is required, on the ground of the low nucleotide binding affinity of these GTPases (Uthaiah et al., 2003).

1.2.3. GTPase-activating proteins (GAP)

GTP-hydrolysis by GTP-binding proteins is usually very slow but can be accelerated upon interaction with GTPase-activating proteins (GAPs). GAPs stimulate GTP hydrolysis in two ways: by supplying a catalytic arginine to the GTPase active site to facilitate the transition state and by reducing the flexibility of the switch segments, stabilising them in a catalytically functional state (Scheffzek et al., 1997). An exposed loop of the GAP inserts into the catalytic site of an appropriate GTPase, allowing the interaction of an arginine side chain (the arginine finger) with the β-phosphate of GTP. In addition, the arginine finger forms a hydrogen bond with the side chain of catalytically important glutamine (Gln61 in Ras) (Scheffzek et al., 1998). The exception is Rap1GAP, which uses a catalytic asparagine instead of an arginine (Daumke et al., 2004). Other variations, not involving a separate GAP protein, have been reported. In heterotrimeric G proteins, as well as in the human guanylate-binding protein hGBP1, the critical arginine residue is part of the GTP-binding protein itself and is supplied *in cis* (Sprang, 1997; Prakash et al., 2000b) whereas dynamins and Irga6 provide it *in trans* by self-association (Tuma and Collins, 1994; Uthaiah et al., 2003).

1.3. Dynamins

Dynamins are large GTPases (98 kDa) found in yeast, plants and animals. They have been implicated in various cellular processes, such as vesicular trafficking and scission, organelle fusion and division and in cytokinesis (Praefcke and McMahon, 2004).

Classical dynamins consist of five domains: GTP-binding domain; middle domain, with no sequence homology to any known structural motif; pleckstrin homology domain (PH), which binds preferentially to phosphoinositides, in particular to phosphoinositide(4,5)biphosphate [$PI(4,5)P_2$]; GTPase effector domain (GED), acting as a GAP for dynamin; proline rich domain (PRD), playing an important role in protein-protein interaction (Hinshaw, 2000).

1.3.1. Dynamin as GTPase

Dynamin was found in a monomer-tetramer equilibrium in solution (Hinshaw and Schmid, 1995; Tuma and Collins, 1995; Eccleston et al., 2002). It has low binding affinity for nucleotides, with dissociation constant in the micromolar range (Stowell et al., 1999; Binns et al., 2000; Marks et al., 2001). Considering the cellular nucleotide concentration (Kleinecke and Soeling, 1979) and that dynamin binds GTP 40-fold more tightly that GDP, it is expected that dynamin would predominantly exist in GTP-bound form in the cell.

Dynamin tetramers have a relatively high intrinsic rate of hydrolysis (k_{cat} of ~200 min^{-1}), which increases upon self-assembly of dynamin into oligomeric structures (Tuma and Collins, 1994; Hinshaw and Schmid, 1995). Up to 50-fold stimulation of GTP hydrolysis was shown to be mediated by dynamin itself, namely by GTPase effector domain (GED) (Sever et al., 1999), in this way providing its own GAP.

Self-assembly of dynamin tetramers into ring-like structure is spatially limited to the membranes, where the pleckstrin homology and another, yet unidentified, domain mediate lipid binding and proper positioning of dynamins (Burger et al., 2000). Although GTP binding is not necessary for membrane recruitment itself (Tuma and Collins, 1995; Burger et al., 2000), membrane tubulation and vesicle scission require GTP incorporation and its subsequent hydrolysis, respectively (Sweitzer and Hinshaw, 1998; Stowell et al., 1999; Marks et al., 2001).

The exact mechanism of dynamin function is still under dispute. The fact that GTP-bound dynamin oligomers tubulate membranes *in vitro* (Hinshaw and Schmid, 1995) and *in vivo* (Marks et al., 2001) and that the vesicle scission requires GTP hydrolysis led to the model describing dynamin as mechanochemical enzyme. Alternatively, dynamin is considered as regulatory protein, recruiting effectors proteins in GTP-bound form via the proline rich domain (Praefcke and McMahon, 2004).

1.4. IFN-inducible GTPases

1.4.1. Mx proteins

Murine Mx1 was the first IFN-inducible GTPase implicated in cell-autonomous resistance against intracellular pathogens. Mx1 locus was discovered more than 40 years ago through a polymorphism in influenza virus resistance among different mouse strains. The A2G mouse was found to be resistant while all other strains were susceptible (Lindenmann et al., 1963). Resistance behaved genetically as a single dominant trait (Lindenmann, 1964). The resistance phenotype was confirmed at the cellular level *in vitro* as well (Lindenmann et al., 1978), indicating its cell-autonomous character. Mx genes were found in all vertebrates (Staeheli and Haller, 1985). In mouse and humans two Mx genes were characterized, Mx1 and Mx2, and MxA and MxB, respectively, and they were found to be induced by type I IFN (Goetschy et al., 1989; Simon et al., 1991).

Mx proteins are large GTPases (70-80 kDa) consisting of N-terminal GTP-binding domain and C-terminal domain involved in protein-protein interactions. Recombinant MxA hydrolyses GTP to GDP with a turnover rate of 27 min^{-1} (Richter et al., 1995). High GTPase activity and several fold stronger binding of GTP than GDP suggest that most MxA proteins *in vivo* could be in the GTP-bound form. Although no lipid-binding motif has been identified, purified MxA binds to lipid vesicles in a nucleotide-independent manner (Accola et al., 2002). *In vivo*, MxA partly co-localised with the smooth endoplasmic reticulum but the relevance of MxA lipid binding to its antiviral function is not clear. In the presence of GDP, however, MxA protein in solution formed evenly shaped rings that condensed to spirals or stacks of rings after incubation with GTPγS (Kochs et al., 2002). The oligomerisation property of Mx proteins was also confirmed by gel filtration analysis of both recombinant human His-tagged MxA (Richter et al., 1995) and mouse Mx1 (Melen et al., 1992). MxA was shown to form homo-oligomers *in vivo* as well (Ponten et al., 1997) and the C-terminus of the protein, containing a putative leucine zipper, was required for the interaction. In mouse Mx1, the only Mx protein localising to the nucleus, the same domain carries a nuclear localisation signal. Both cytoplasmic and nuclear Mx proteins are found in granular and dotty structures, generally considered as Mx oligomers.

Mx proteins are antiviral resistance factor. Transfected murine Mx1 confers resistance against influenza virus even in the absence of IFN induction (Staeheli et al., 1986; Arnheiter et al., 1990), implying that other IFNα/β induced factors are not essential for protection against the virus, thought they may play a significant role in establishing the antiviral state (Staeheli et al., 1986). Human MxA blocks nuclear import of Thogoto virus nucleocapsids by GTP-dependent interaction of its C-terminal domain with a nucleoprotein (Kochs and Haller, 1999a; Kochs and Haller, 1999b). Cytoplasmic MxA inhibits the multiplication of both influenza virus and vesicular stomatitis virus (Zurcher et al., 1992b). Interestingly, when moved to the nucleus with the help of a foreign nuclear transport signal, MxA not only retained its activity against influenza virus but was actually more effective, exerting its function by blocking primary transcription of influenza virus like mouse Mx1, whose natural location is the cell nucleus (Krug et al., 1985; Pavlovic et al., 1992). Nuclear localisation of mouse Mx1 protein is, however, necessary for inhibition of influenza virus (Zurcher et al., 1992a).
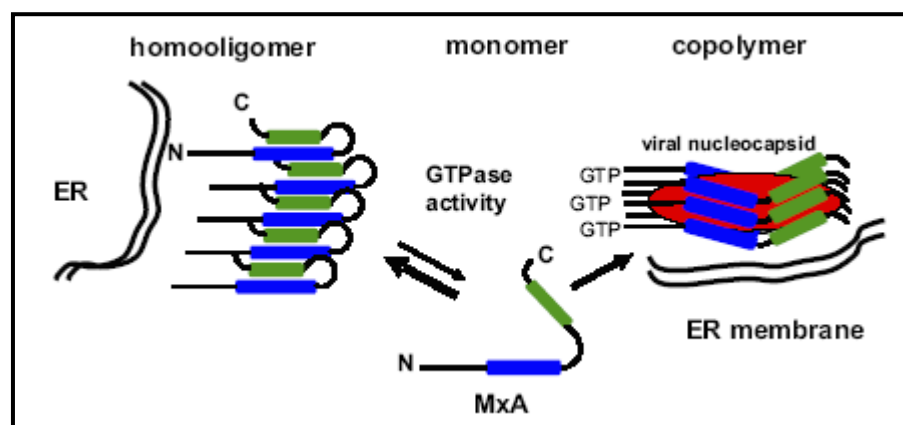
Figure 1.3. Model of MxA-MxA interaction mediated by the carboxyl-terminal region (Haller et al., 2007)

MxA can form two types of assemblies. In the absence of infection, MxA forms oligomers by intermolecular association of the LZ domain of one molecule (green box) with the CID of another molecule (blue box). These assemblies represent a storage form of antivirally inactive molecules, from which antivirally competent monomers are transiently released. In infected cells, MxA monomers bind to viral targets, such as nucleocapsids or nucleocapsid-like structures (red shape).

Mx proteins fold into three functional domains (Haller et al., 2007): N-terminal GTP-binding domain, containing self-assembly motif (Nakayama et al., 1993), central interactive domain (CID) and C-terminal leucine zipper domain (LZ). It has been reported that the C-terminal LZ domain interacts with both GTP-binding domain (Schwemmle et al., 1995) and with the CID of another Mx molecule (Schumacher and Staeheli, 1998). Based on these findings, a model for Mx antiviral function has been proposed (Di Paolo et al., 1999; Janzen et al., 2000; Haller and Kochs, 2002). It proposes that MxA proteins exist in two forms in the cell: an active monomeric and an inactive oligomeric form. The oligomers may represent a storage form of Mx molecules preventing their activation without the presence of the specific target. Prerequisite for MxA oligomer formation is the folding of the C-terminal LZ domain (in green in figure 1.3.) (Di Paolo et al., 1999; Haller and Kochs, 2002). Folded LZ domain interacts with both CID (in blue, figure 1.3.) and self-assembly sequence in the GTP-binding motif of another MxA molecule, giving rise to the formation of large aggregates. After viral infection, cellular or viral protein(s) induce the dissociation of the MxA oligomers, releasing antivirally competent monomers. MxA monomers bind to viral targets, such as nucleocapsids or nucleocapsid-like structures (red shape, figure 1.3.) and sort them to locations where they are trapped and degraded. The exact mechanism of how monomeric Mx inhibits viral activity is not resolved. MxA needs to be in the GTP-bound form in order to interact with Thogoto virus nucleocapsid (Kochs and Haller, 1999a) though GTP hydrolysis itself seems not to be required (Janzen et al., 2000).

1.4.2. The guanylate-binding proteins (GBPs)

The response of cells to IFNγ is dominated by the induction of two families of GTPases, the IRG family and the guanylate-binding proteins (GBPs). There are seven GBP genes described in human, hGBP1-7 (Cheng et al., 1991; Olszewski et al., 2006) and eleven in mouse, mGBP1-11 (Degrandi, in press) and the family is well conserved in vertebrates (Robertsen et al., 2006). Despite their massive induction upon IFNγ treatment, only a weak antipathogenic effect of hGBP1 against vesicular stomatitis virus (VSV) and encephalomyocarditis virus (ECMV) *in vitro* has been reported (Anderson et al., 1999). Additionally, hGBP1 and mGBP2 were proposed to

have a role in regulation of vasculogenesis by proinflammatory cytokines (Guenzi et al., 2001; Guenzi et al., 2003) and IFN-mediated cell growth (Gorbacheva et al., 2002), respectively.

GBPs are large GTPases (65-67 kDa), consisting of an N-terminal GTP-binding motif and very elongated C-terminal helical domain (Prakash et al., 2000a). The G4 motif, TLRD, responsible for the recognition of the guanine moiety of the nucleotide, is characterized by unique substitution of conserved lysine at the position 2 to the hydrophobic leucine (Praefcke et al., 1999). Three of the human (hGBP1, hGBP2 and hGBP5) and mouse (mGBP1, mGBP2 and mGBP5) GBPs posses a C-terminal CaaX box, resulting in farnesylation of hGBP1 and isoprenylation of all others (Nantais et al., 1996; Stickney and Buss, 2000).

The mechanism of GTP hydrolysis by hGBP1 is well studied. The binding affinity of hGBP1 for GTP, GDP and GMP is very low (0.5-2.4 μM) (Praefcke et al., 2004), due to high nucleotide dissociation rates. In the presence of GMP and GDP, hGBP1 was found as a monomer, but it is dimeric in the GTP-bound state and tetrameric in GDP-AlFx stabilised transition state (Prakash et al., 2000a; Praefcke et al., 2004). GTP-dependent dimerisation of hGBP1 results in at least an eight-fold increase in GTP hydrolysis by providing the catalytic arginine *in cis* (Prakash et al., 2000b; Ghosh et al., 2006). The unique position of hGBP1 amongst known GTPases is demonstrated by the hydrolysis of GTP to GDP and GMP (Schwemmle and Staeheli, 1994; Praefcke et al., 1999), leaving predominantly GMP as a product of hydrolysis (85-95% at 37°C; (Kunzelmann et al., 2006). Although GTP is hydrolysed in two successive cleavages of γ- and β-phosphates, GDP in solution cannot serve as a substrate. The crystal structure of hGBP1 in complex with the non-hydrolysable GTP analog GppNHp (Prakash et al., 2000b) illustrated that the largest structural changes involve guanine and phosphate caps around GTP-binding site, suggesting a shift of the nucleotide toward the catalytic centre after GTP hydrolysis by positioning the β-phosphate of GDP at the same place as the γ-phosphate of GTP was located before.

Recent data document subcellular localisation of hGBP1 to the Golgi apparatus (Modiano et al., 2005). Redistribution from the cytosol to the Golgi occurs when hGBP1 is in the GDP-AlFx transition state and requires isoprenylation and the presence of another, so far unidentified IFNγ-induced factor. Although the lipid modification of hGBP1 was shown to be important for the relocalisation of this protein

to the Golgi, its role in hGBP1 function *in vivo*, nor its effect on the biochemical properties of hGBP1 *in vitro* are not known.

1.4.3. Very large inducible GTPase (VLIG)

VLIG-1 protein, with a molecular weight of approximately 280 kDa, is the largest known GTPase (Klamp et al., 2003). Its expression is massively induced by IFNγ, and to a somewhat lesser extent by IFNβ. The GTP-binding domain of VLIG-1 is related to that of other IFN-inducible resistance GTPases, in particular with Mx and GBP proteins. In the assay using nucleotide-agaroses it was shown that VLIG-1 binds strongly to GDP-agarose and very weakly to GTP- and GMP-agaroses, indicating that this protein is, indeed, a GTP-binding protein (Klamp et al., 2003). The largest part of the long protein sequence does not share any structural similarities with any other protein. Recently, it has been reported that the central part of VLIG-1 exhibit 43% similarity to the CARD6 protein (Dufner and Mak, 2006), microtubule-interacting protein that positively modulates NF-kappaB activation (Dufner et al., 2006). However, the role of this central VLIG-1 region in its potential immunity-related function is unknown.

1.4.4. Immunity-related GTPases (IRGs)

IFNγ induction of mouse macrophages results in an immense transcription activation. Of estimated 1300 genes induced (Ehrt et al., 2001), messages of GBP and IRG protein families are the most abundant (Boehm et al., 1998), indicating their importance in immune response to pathogen infections.

IRG proteins are typically 47 kDa in molecular weight, with a canonical GTP-binding domain positioned approximately 80 amino acid from the N-terminus. Analysis of the N-terminal sequence revealed that more than half of the mouse GTPases could be myristoylated. In mouse, three of the IRG proteins are characterized by the unique substitution of the universally conserved lysine in G1 motif (GX_4GKS) to the methionine (GX_4GMS), implying a distinct catalytic mechanism

for GTP hydrolysis. Thus, based on the sequence of the G1 motif, IRG proteins can be grouped into GKS and GMS subfamily (Boehm et al., 1998).

1.4.4.1. Genomic structure of IRG genes

The genome structure of IRG genes in the C57BL/6 mouse strain was analysed in detail (Bekpen et al., 2005). There are all together 25 coding units present, of which 24 contain IFN-responsive GAS and ISRE motifs in their promotor, resulting in their strong induction upon IFNγ stimulation. Exception is the Irgc gene, which is not induced by IFNγ nor does it possess IFN-response elements in its promotor. Interestingly, the only human full-length gene, *IRGC*, is an ortholog with 90% identity to the Irgc mouse gene. As in the mouse, human IRGC protein is constitutively expressed in male gonad (Rohde, 2007). In human genome, another Irg-like gene fragment was identified, containing only part of the GTP-binding domain of an IRGM protein. Although some IRG genes were found in zebrafish, there are no clear homologs in invertebrates below the Cephalohordates (Bekpen et al., 2005). The Cephalochordate *Branchiostoma floridae* has a large family of IRG genes (Hunn, 2007). Absence of IFN-induced IRG proteins in humans show that they either possess alternative mechanisms effective against intracellular pathogens or they deploy other already known mechanisms more efficiently (Bekpen et al., 2005).

1.4.4.2. Localisation of IRG proteins

Analysis of cellular localisation of five of the IRG members, Irga6, Irgb6, Irgd, Irgm1 and Irgm3 (IIGP1, TGTP, IRG-47, LRG-47 and IGTP, in old nomenclature) in IFNγ-induced mouse fibroblasts and macrophages, revealed different levels of membrane association of these proteins (Martens et al., 2004). Irgm1 and Irgm3 were found almost exclusively bound to the membranes whereas, in contrast, Irgd protein was mainly soluble. Irga6 and Irgb6 partitioned roughly equally between the membrane bound and soluble fractions. Co-staining with different organelle markers localised Irgm1 and Irgm2 to the Golgi apparatus and Irgm3 to the endoplasmic reticulum (Martens, 2004; Martens et al., 2004). Irga6 and Irgb6 were found

predominantly co-localising in a reticular pattern with ER markers, contrasting findings reporting Irga6 association with Golgi markers (Zerrahn et al., 2002).

1.4.4.3. The involvement of IRG proteins in resistance to intracellular pathogens

Consistent with their strong inducibility by IFNγ, many members of the IRG family have been implicated in resistance against intracellular pathogens in mice, both of bacterial and protozoan origin: *Mycobacterium tuberculosis* (MacMicking et al., 2003), *Mycobacterium avium* (Feng et al., 2004), *Salmonella typhimurium* (Taylor et al., 2004), *Listeria monocytogenes* (Collazo et al., 2001), *Chlamydia trachomatis* (Nelson et al., 2005; Bernstein-Hanley et al., 2006), *Chlamydia psittaci* (Miyairi et al., 2007), *Tripanosoma cruzi* (Santiago et al., 2005), *Leishmania major* (Feng et al., 2004) and *Toxoplasma gondii* (Taylor et al., 2000; Collazo et al., 2001; Halonen et al., 2001; Butcher et al., 2005; Martens et al., 2005; Ling et al., 2006). Involvement of different IRG proteins in resistance against these pathogens is shown in table 1.1. Influence of IRG proteins in viral infections is limited to reports correlating overexpression of Irgb6 and relative reduced plaque formation by vesicular stomatitis virus but not herpes simplex virus in L cells (Carlow et al., 1998) and even weaker effect for Coxackie virus in Hela cells expressing Irgm2 (Zhang et al., 2003). Ebola virus and mouse cytomegalovirus have failed to reveal a susceptibility phenotype (Taylor et al., 2000).

Although several studies document susceptibility of IRG-deficient mice to various pathogens, little is known about the mechanism of their function. Irgm1-defficient mice infected with *M. avium* display severe lymphopenia at the site of bacterial replication (Feng et al., 2004) whereas pathology of *T. gondii* infected Irgm3-deficient mice was contributed to the overproduction of inflammatory cytokines (Taylor et al., 2000). Recently, infection with *C. psittaci* revealed that C57BL/6J mice were 10^5-fold more resistant than DBA/2J mice due to differential expression of both Irgb10 and Irgm2 proteins (Miyairi et al., 2007). Microarrays of infected peritoneal lavage showed over 10-fold upregulation of neutrophil-recruiting chemokines in susceptible mice and over 100-fold increase in macrophage differentiation genes in resistant mice. Massive neutrophil recruitment was seen in susceptible in comparison

to resistant mice indicating that the susceptibility pattern involves the stimulation of different inflammatory pathways.

	Wild type	IIFNγ-/-	Irgm1-/-	Irgm3-/-	Irgd-/-	Irga6-/-	Irgb10	Irgm2
Mycobacterium tuberculosis	R	S	S	R	R	ND	ND	ND
Mycobacterium avium	R	S	S	R	ND	ND	ND	ND
Listeria monocytogenes	R	S	S	R	R	R	ND	ND
Salmonella typhimurium	R	S	S	R	R	ND	ND	ND
Chlamydia trachomatis	R	S	ND	Sc	ND	Si	Si	ND
Chlamydiy psittaci	R	S	ND	ND	ND	ND	Ss Si	Ss Si
Toxoplasma gondii	R	S	S	S Sc	S Rc	R Sc	ND	ND
Trypanosoma cruzi	R	S	S	R	ND	ND	ND	ND
Leishmania major	R	S	S	S	ND	R	ND	ND

Table 1.1. Susceptibilities of IRG-deficient mice and cells to intracellular pathogens (modified from (Martens and Howard, 2006)

R, wild type or knockout mouse resistant; S, knockout mouse sensitive; ND, not done; Rc, knockout cells resistant; Sc knockout cells sensitive; Ss, wild type mouse strain DBA/2J sensitive; Si, RNAi wild-type cells sensitive.

1.4.4.4. The involvement of IRG proteins in cell-autonomous resistance to intracellular pathogens

Loss of resistance of Irgm1- and Irgm3-deficient mice to infection with *T. gondii* correlates with the loss of IFNγ-dependent resistance in infected cells *in vitro* (Halonen et al., 2001; Butcher et al., 2005), demonstrating the role of IRG proteins in cell-autonomous resistance. Effect of IRG proteins in challenging pathogen infections is not redundant (Collazo et al., 2001; Butcher et al., 2005; Bernstein-Hanley et al., 2006; Miyairi et al., 2007), indicating that they may regulate each other's functions in infected cells. Five of the known IRG proteins, Irgb6, Irga6, Irgd, Irgm2 and Irgm3 were found concentrated at the parasitophorous vacuole membrane in IFNγ-induced astrocytes infected with *T. gondii* (Martens et al., 2005), already 15 min after infection. Both Irga6 and Irgm3 were found to be involved in *T. gondii* vacuole vesiculation and disruption in astrocytes and macrophages (Martens et al., 2005; Ling et al., 2006), effectively striping parasite of its membranes. A series of disruption

events was proposed involving parasitophorous vacuole membrane (PVM) ruffling, PVM vesiculation, disruption, and parasite plasma membrane stripping, leading to lysosomal degradation of the parasite (Ling et al., 2006). Disruption of *T. gondii* containing vacuoles, measured by uracil incorporation, was slightly decreased in Irga6-deficient cells, although Irga6-deficient mice showed no significant susceptibility to *T. gondii* infection (Martens et al., 2005).

Irgm1 protein was not found on parasitophorous vacuole (Martens et al., 2005) but associated with phagosomes containing *M. tuberculosis* in IFNγ-induced macrophages (MacMicking et al., 2003). Recruitment of Irgm1 to the mycobacterial phagosome seems not to require a pathogen-derived signal since this relocalisation occurs as well during phagocytosis of latex beads in fibroblasts and macrophages (Martens et al., 2004). Absence of Irgm1 results in delayed and limited phagosome acidification in Irgm1-deficient cells (MacMicking et al., 2003).

A role of Irgm1 in induction of autophagy has been also proposed (Gutierrez et al., 2004). As autophagosome-like vacuoles were closely associated with disrupted *T. gondii*-containing vacuoles (Martens et al., 2005; Ling et al., 2006), susceptibility of Irgm1-deficient mouse to *T. gondii* infection could be explained by inability of cells to engulf disrupted vacuole into the autophagosome. Because autophagy also targets cytosolic pathogens (Rich et al., 2003; Deretic, 2005), its promotion by Irgm1 may also explain how Irgm1 helps mice to resist infections by *L. monocytogenes* (Collazo et al., 2001) and *T. cruzi* (Santiago et al., 2005).

1.4.4.5. Biochemical properties of IRG proteins

GTPase activities of three of the IRG proteins, Irga6, Irgb6 and Irgm3, have been reported. Partly purified GST-Irgb6 and GST-Irgm3 proteins were shown to hydrolyse GTP to GDP *in vitro* (Taylor et al., 1996; Carlow et al., 1998). Weak GTP hydrolysis was also demonstrated for FLAG-Irgm3 immunoprecipitated from NIH/3T3 fibroblasts (Taylor et al., 1997). It is suggested that cellular Irgm3 is predominantly GTP-bound (Taylor et al., 1997), although nucleotide-binding affinity were not measured. Both endogenous, IFNγ-induced Irgm3 and transfected FLAG-Irgm3 proteins were shown to be mostly in the GTP-bound form in cells (up to 96%), indicating that the IFNγ state of the cell does not influence the activity of this protein

(Taylor et al., 1997). However, recombinant Irga6 protein is the only IRG member whose biochemical and enzymatic properties were studied in detail.

Recombinant Irga6, purified from *Escherichia coli*, crystallized as a dimer in the nucleotide-free and GDP-bound state (Ghosh et al., 2004). Structure shows Irga6 folding into helical and G domain, consisting of 6-stranded β sheets surrounded by 6 α helices. Helical domain is unique, being built from both N- and C-terminal helices (figure 1.4.). Since recombinant Irga6wt contained a short non-canonical N-terminal extension derived from the GST fusion (Uthaiah et al., 2003) and, in addition, because prokaryotes do not expressed enzymes necessary for protein myristoylation (Heuckeroth et al., 1988), the structural position of the N-terminal myristoyl group could not be determined.
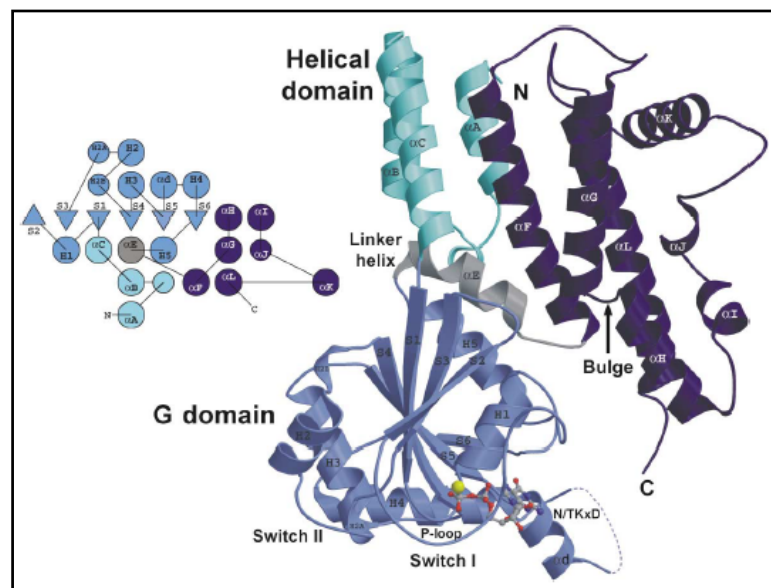
Figure 1.4. Structure of Irga6 (Ghosh et al., 2004)

Irga6 binds to GTP and GDP with dissociation constants in the micromolar range with at least 10 times higher affinity for GDP than for GTP (Uthaiah et al., 2003). Considering cellular nucleotide concentration, 330µM GTP and 120 µM GDP (Kleinecke and Soeling, 1979), Irga6 in cells should be predominantly GDP-bound. It hydrolyses GTP to GDP but not to GMP, and the GTPase activity is concentration-dependent with a maximum GTP turnover rate of 2 min^{-1}. Magnesium ions were found to be essential for the GTPase reaction. Irga6 oligomerises in the presence of

GTP, and the oligomers resolve as GTP hydrolysis proceeds. Micromolar nucleotide affinities and oligomerisation-dependent hydrolytic activity are properties that Irga6 shares with other large GTPases, GBPs, Mx proteins and with the paradigm of the self-activating GTPases, the dynamins. As in all other large GTPases (Boehm et al., 1998; Prakash et al., 2000a; Danino and Hinshaw, 2001; Haller and Kochs, 2002; Klamp et al., 2003), the catalytically important Gln61[Ras] in Irga6 is replaced by a hydrophobic amino acid, suggesting the requirement for a different catalytic residue (Mishra et al., 2005). Irga6 oligomer formation and GTP hydrolysis is necessary for AlFx to bind and trap the complex in AlFx-GDP transition state, indicating that the oligomer is the catalytically active form in which an additional catalytic residue can be provided *in cis* or *in trans* (Uthaiah et al., 2003).

Since recombinant Irga6wt, purified from *E. coli* was not myristoylated, it is not clear whether IFNγ-induced Irga6wt in cells share the same biochemical properties with the recombinant Irga6wt *in vitro*. It has been reported that the lipid modification affects enzymatic activity of Rac GTPase (Molnar et al., 2001) or the nucleotide binding affinities of small GTPase Arf1 (Randazzo et al., 1995). However, there is no information about the role of the myristoyl group in the enzymatic properties of Irga6.

1.5 Lipid modifications and membrane-binding properties of GTPases

Lipid modifications, both extra- and intracellularly oriented, are increasingly recognised as important mechanisms for targeting proteins within cells and for controlling their activity. Intracellularly oriented lipid modifications include reversible S-acylation (palmitoylation) as well as covalent myristoylation and prenylation (farnesylation and geranylgeranylation) (Magee and Seabra, 2005). These hydrophobic moieties are found on a wide variety of proteins and are thought to regulate signal transduction, movement of a signaling protein within the cell and its final destination and reversible protein-protein and protein-membrane associations (Resh, 2006).

1.5.1 S-acylation

S-acylation is a unique modification that is reversible *in vivo* and can therefore regulate protein localisation and function (Milligan et al., 1995). Nearly all S-acylated proteins contain palmitate, a saturated sixteen-carbon fatty acid, linked through thioester bond to one or more cysteine residues. Addition of palmitate is not limited to the N- or C-terminus of the protein and there is no consensus-binding motif. Palmitoylated cysteine residues are often found near sites of N-myristoylation or prenylation where they increase membrane-binding energy, although mono- and di-palmitoylation alone can localise protein to the plasma membrane (McCabe and Berthiaume, 1999; Baker et al., 2003; Magee and Seabra, 2005) and the Golgi region (Perez de Castro et al., 2004; Magee and Seabra, 2005), respectively.

1.5.2. Prenylation

Protein prenylation is a posttranslational reaction that occurs in the cytosol. A 15-carbon (farnesyl) or 20-carbon (geranylgeranyl) isoprenoid are linked irreversibly through thioether bond to one or more cysteine residues at or near the C terminus of the protein. Many prenylated proteins contain a C-terminal 'CaaX box' (Cys-aliphatic-aliphatic-X) and the 'X' amino acid determines whether the cysteine within the CaaX box is farnesylated by farnesyltransferase (X is not leucine) or geranylgeranylated by geranylgeranyltransferase I (X is leucine) (Konstantinopoulos et al., 2007). Upon prenylation, proteins are translocated to the ER where the three C-terminal amino acids (aaX) are cleaved (Boyartchuk et al., 1997) and, subsequently, the C-terminal prenylated cysteine residue carboxymethylated (Gelb, 1997).

For small G proteins, the number of prenyl groups as well as their identity influence protein targeting. RhoB exists in farnesylated and geranylgeranylated forms; farnesylated RhoB is targeted to the plasma membrane, whereas geranylgeranylated RhoB localises to late endosomes (Gomes et al., 2003). Most Rab proteins are doubly geranylgeranylated at the two cysteine residues at the C-terminus (Zerial and McBride, 2001; Goody et al., 2005) and localise to endosomes, whereas monogeranylgeranylated Rabs mistarget to the ER and are nonfunctional (Calero et al., 2003; Gomes et al., 2003). Geranylgeranylated Rab proteins are in the

cytosol in complex with a GDI molecule, which sequester the prenyl groups to form a soluble complex. Rab-GDI interaction is strongly dependent on Rab prenylation and the presence of GDP (Sasaki et al., 1990; Sasaki et al., 1991). Upon association with appropriate membrane (Soldati et al., 1994), GDI is released from the Rab protein which, anchored to the membrane via its geranygeranyl groups, can interact with a membrane-localised GEF. Process of membrane association and GDI release often involves proteins known as GDI-displacement factors (GDFs), which are proposed to catalyse Rab-GDI dissociation at particular membrane surfaces (Pfeffer and Aivazian, 2004). GTP-bound Rab senses its target proteins and the interaction is terminated upon GAP-dependent GTP hydrolysis, allowing soluble Rab-GDI complex formation (Behnia and Munro, 2005). Similar mechanism was reported for Rho (Dransart et al., 2005) and Ras (Pechlivanis and Kuhlmann, 2006) GTPases.

GBP proteins are also characterized by presence of the C-terminal CaaX box, predicting protein modification either by farnesylation (hGBP1 and mGBP5) or geranygeranylisation (hGBP2, hGBP5, mGBP1 and mGBP2) (Vestal et al., 2000; Vestal, 2005). However, *in vivo* prenylation was only shown for mGBP2 (Vestal et al., 2000) and hGBP1 (Modiano et al., 2005). Redistribution of soluble hGBP1 to the Golgi is GTP-dependent and requires both farnesylation and IFNγ-induced factor (Modiano et al., 2005).

1.5.3. Myristoylation

Approximately 0.5% of all eukaryotic proteins are modified by co-translational binding (Olson and Spizz, 1986; Wilcox et al., 1987) of myristate (rare 14-carbon fatty acid) to the N-terminal glycine residue (Kamps et al., 1985) on a variety of eukaryotic and viral proteins (Resh, 2006). After the initiating methionine is removed by methionine aminopeptidase, myristate is linked through an amide bond to the N-terminal glycine in the reaction catalysed by N-myristoyltransferase (Farazi et al., 2001). Myristoylation absolutely requires N-terminal glycine residue at position 1 and preferentially small, polar serine and, to a lesser extent, threonine residue at position 5 (Maurer-Stroh et al., 2002).

N-myristoylation alone does not provide sufficient hydrophobicity to stably anchor proteins to a lipid bilayer but rather promotes weak and reversible protein-

membrane and protein-protein interactions (Peitzsch and McLaughlin, 1993; Silvius and l'Heureux, 1994; Murray et al., 1997; Murray et al., 1998). Stable membrane association of N-myristoylated proteins requires a second lipid-binding motif. This secondary signal can be either palmitoyl group, attached by palmitoyl acyltransferases residing in the target membrane domain (Schroeder et al., 1996) or N-terminal stretch of basic amino acids associating electrostatically with negatively charged phospholipids (Murray et al., 1997; Murray et al., 1998).

Alternatively, regulated membrane association of myristoylated proteins is achieved by ligand-promoted conformational changes, so-called switches. In myristoyl-electrostatic switch, phosphorylation within the N-terminal polybasic motif introduces negative charge and reduces the electrostatic component of bilayer interaction, thus releasing the protein from the membrane (McLaughlin and Aderem, 1995). In the case of myristoyl-ligand switches, the myristoylated N-terminus is, in the absence of ligand, sequestered in a hydrophobic binding site located on the protein (Bhatnagar and Gordon, 1997). Binding of ligand induces a protein conformational change that exposes the myristoyl moiety, allowing the protein to associate with membranes (Zozulya and Stryer, 1992; Ames et al., 1995).

The small GTPase ADP-Ribosylation Factor-1 (ARF1) provides one example of a myristoyl-ligand switch, interacting with the membrane through two components: the myristate, which gives a basal affinity for lipid regardless of the protein conformation (Franco et al., 1995), and a protein region that becomes available for membrane binding only when ARF switches to the active, ARF-GTP conformation. In the GDP-bound form, ARF1 is soluble, with hydrophobic residues of the N-terminal amphipathic peptide buried in the protein core. When ARF switches to the GTP state, these residues insert into membrane lipid layer (Antonny et al., 1997).

Eleven members of IRG protein family are shown to carry the amino-terminal myristoylation signal MGxxxS. However, lipid modification of only one of them, namely Irga6, was reported (Martens et al., 2004). Even though the N-terminus of Irga6 targets EGFP to membranes in a myristoyl-dependent manner, myristoylation is not absolutely necessary for membrane association of Irga6 itself since only a minor increase of cytosolic pool of nonmyristoylated Irga6, relative to the wild type protein, was found (Martens et al., 2004). Apart from the influence on the resting localisation of Irga6, nothing is known about the effect of the myristoyl group on Irga6 activity and its relocalisation to the PVM.

1.6. The aim of this study

Immunity-Related GTPases (IRG), represented by 25 coding units in the mouse genome, are implicated in resistance against a variety of bacterial and protozoal pathogens (table 1.1.). Several studies have documented the susceptible phenotype of IRG-deficient mice upon challenge with various pathogens, but the exact mechanism of their function in cell-autonomous immunity is still not known.

This study attempts to understand the role of IRG proteins in cell-autonomous immunity by analysis of one member of IRG family, Irga6. Identification of Irga6 interaction partners in IFNγ-induced cells could give more insight into the function of Irga6. Because IRG proteins show non-redundancy in resisting pathogen infection (Collazo et al., 2001; Butcher et al., 2005; Bernstein-Hanley et al., 2006; Miyairi et al., 2007) and, thus, probably regulate each other's functions, association of Irga6 with other IRG proteins was also analysed.

Recombinant nonmyristoylated Irga6wt was shown to form GTP-dependent, catalytically active homooligomers *in vitro* (Uthaiah et al., 2003), characterized by increased GTPase activity. However, there was no information about Irga6 self-association *in vivo*. Therefore, the ability of Irga6 to form GTP-dependent homooligomers *in vivo* was studied in an attempt to analyse the nucleotide state of Irga6 in IFNγ-induced cells and possible changes of Irga6 activity during infection.

IRG proteins possess few obvious structural features, apart from the GTP-binding domain itself, which would indicate their function *in vivo*. One exception is Irga6, which has a myristoylation sequence (MGQLST) at the N-terminus. Additionally, Triton X-114 partitioning demonstrated the hydrophobic character of native Irga6 (Martens et al., 2004) that was dependent on the integrity of the myristoylation motif, indicating, all together, that Irga6wt is probably myristoylated *in vivo*. In this study, it was attempted to analyse the role of the myristoyl group in Irga6 activity *in vivo* and in the ability of Irga6 to relocalise to the parasitophorous vacuole membrane of *Toxoplasma gondii*.

The structure and biochemical properties of purified, recombinant, nonmyristoylated Irga6 protein have been intensively studied *in vitro* and are well characterised (Uthaiah et al., 2003; Ghosh et al., 2004). However, there have been reports demonstrating that the lipid modification significantly affects the enzymatic properties of the GTPases in the presence of lipid vesicles and membranes. Addition

of membranes increased GTP hydrolysis of only prenylated Rac GTPase and had hardly any effect on the nonprenylated protein (Molnar et al., 2001). Myristoylation of the small GTPase Arf1 strongly influences its nucleotide binding affinities. In the absence of lipids, Arf1 has a higher affinity for GDP than for GTP, whereas, in the presence of phospholipids, Arf1 affinity for GTPγS is much higher than for GDP (Randazzo et al., 1995).

In addition to identifying the role of myristoyl group on Irga6 function *in vivo*, this study also aimed to purify the myristoylated Irga6 and analyse its GTPase activity as well as nucleotide binding affinities in the presence and absence of lipid vesicles. The analysis of biochemical properties of myristoylated Irga6 would, hopefully, contribute to better understanding of the function of Irga6 in *T. gondii* infected cells and give more insight in its role in the vesiculation and disruption of the parasitophorous vacuole membrane and degradation of the parasite.

2. Material and Methods

2.1 Reagents and Cells

2.1.1 Chemicals, Reagents and Accessories

All chemicals were purchased from Aldrich (Steinheim), Amersham-Pharmacia (Freiburg), Applichem (Darmstadt), Baker (Deventer, Netherlands), Boehringer Mannheim (Mannheim), Fluka (Neu-Ulm), GERBU (Gaiberg), Merck (Darmstadt), Pharma-Waldhof (Düsseldorf), Qiagen (Hilden), Riedel de Haen (Seelze), Roth (Karlsruhe), Serva (Heidelberg), Sigma-Aldrich (Deisenhofen) or ICN biochemicals, Oxoid, (Hampshire UK). Developing and fixing solutions for Western Blot detection were from Amersham Pharmacia (Freiburg), Luminol from Sigma Aldrich (Deisenhofen), Coumaric acid from Fluka (Neu-Ulm). Deionised and sterile water (Seral TM) was used for all the buffers and solutions, Ultra pure water derived from Beta 75/delta UV/UF from USF Seral Reinstwassersysteme GmbH, (Baumbach) equipped with UV (185/254nm) and ultrafiltration (5000 kd cut off), or from Milli-Q-Synthesis (Millipore).

2.1.2 Equipment

Centrifuges used were: Biofuge 13, Heraeus; Sigma 204; Sigma 3K10; Labofuge 400R, Heraeus; Sorvall RC-5B, Du Pont instruments; Optima TLX Ultracentrifuge, Beckmann and Avanti J-20 XP, Beckman. BioRAD Gel dryer, Model-583; BioRad Power pack 300 or 3000; electrophoresis chambers from FMC Bioproducts (Rockland Maine US); Gel Electrophoresis Chamber, Cambridge electrophoresis; Biorad Mini Protean II; PTC-100, MJ Research Inc.; ÄKTA P-920, OPC-900, Frac-950, Amersham; Centrifuge tubes 15ml, TPP Switzerland; 50ml Falcon, BectonDickenson; Zeiss Axioplan II fluorescence microscope equipped with a Quantix cooledCCD camera.

2.1.3 Materials

Sterile filters FP 030/3 0,2 μm and ME 24 0,2 μm (Schleicher und Schüll, Dassel); Nitrocellulose transfer membrane PROTRAN (Schleicher und Schüll, Dassel); 3MM Whatmann Paper (purchased via LaboMedic); 100 Sterican 0,50 x 16mm hypodermic needles (Braun AG, Melsungen); 0.2µm and 0.45µm sterile filters (Schleicher und Schuell, Dassel); X-OMAT LS and AR X-ray films, Kodak. All plastic ware for cell culture was from Sarstedt (Nümbrecht) or Greiner (Solingen).

2.1.4 Enzymes/ Proteins

Restriction enzymes (New England Biolabs); "Complete Mini" protease inhibitor cocktail (Roche, Mannheim); Pyrococcus furiosus (Pfu) DNA Polymerase (Promega, Mannheim); T4 DNA ligase (New England Biolabs); RNase A (Sigma); shrimp alkaline phosphatase (SAP) (USB, Amersham); PageRuler™ Prestained Protein Ladder (Fermentas); PageRuler™ Protein Ladder (Fermentas); SigmaMarker™ Wide Range (Sigma); GeneRuler™ DNA Ladder Mix (Fermentas).

2.1.5 Kits

Plasmid Maxi and Midi kit (Qiagen, Hilden),
Terminator-cycle Sequencing kit version 3 (ABI),
QuikChange TM Site directed mutagenesis kit (Stratagen),
Rapid PCR product purification Kit (Roche, Mannheim),

2.1.6 Vectors

pGW1H (British Biotech),
pGEX-4T2 (Amersham),
pVL1393 (BD Biosciences),
pEGFP-N3 (BD Bioscience Clontech).

2.1.7 Cell lines

L929 (CCL-1) and gs3T3 (Invitrogen) mouse fibroblasts were cultured in IMDM or DMEM supplemented with 10% FCS (Biochrom AG, Berlin), 2 mM L-Glutamine, 1 mM sodium pyruvate, 100 U/ml penicillin and 100 µg/ml streptomycin, all from Gibco BRL. Hybridoma 10D7 and 10E7 cells were grown in IMDM, supplemented with 5% FCS (Biochrom AG, Berlin), 2 mM L-Glutamine, 1 mM sodium pyruvate, 100 U/ml penicillin and 100 µg/ml streptomycin, all from Gibco BRL. *Sf9* insect cells, cloned from IPLB-*Sf21* derived from pupal ovarian tissue of the Fall armyworm, *Spodoptera frugiperda,* were grown in Insect-Xpress^TM Medium (Lonza) or in TNM-FH Insect Medium (Sigma).

2.1.8 Media

Luria Bertani (LB) medium
    10 g bacto tryptone, 5 g yeast extract, 10 g NaCl, distilled water 1l
LB plate medium
    10 g bacto tryptone, 5 g yeast extract, 10 g NaCl, 15 g agar, distilled water 1l
IMDM (Iscove's Modified Dulbecco's Medium) supplemented with 10% FCS (Biochrom AG, Berlin), 2 mM L-glutamine, 1 mM sodium pyruvate, 1x non-essencial amino acids, 100 U/ml penicillin, 100 µg/ml streptomycin (all from Gibco BRL)
DMEM (Dulbecco's Modified Eagle Medium) supplemented with 10% FCS (Biochrom AG, Berlin), 2 mM L-glutamine, 1 mM sodium pyruvate, 1x non-essencial amino acids, 100 U/ml penicillin, 100 µg/ml streptomycin (all from Gibco BRL)
Insect-Xpress^TM Medium with L-glutamine (Lonza)
TNM-FH Insect Medium (Modified Grace's Medium) with L-glutamine and sodium bicarbonate (Sigma)

2.1.9 Bacterial and protozoan strains

Escherichia coli DH5α: *80dlacZ* ΔM15, recA1, endA1, gyrA96, thi-1, hsdR17 (r_B^-,
m_B^+), supE44, relA1, deoR, Δ*(lacZYA-argF)*U169

Escherichia coli BL-21: *E. coli* B, F⁻, omp T, hsd S (r_B^-, m_B^-), gal, dcm

Toxoplasma gondii Me49

2.1.10. Serological reagent

2.1.10.1. Primary antibodies and sera

Name	Immunogen	Species	Concentration	Dilution	Origin
10D7	recombinant mouse Irga6wt	mouse monoclonal	1-3 µg/µl	WB: 1:2000 IF: 1:500 IP: 10µl/ 50µl PAS	Jens Zerrahn, Berlin
10E7	recombinant mouse Irga6wt	mouse monoclonal	1-3 µg/µl	WB: 1:2000 IF: 1:500 IP: 10µl/ 50µl PAS	Jens Zerrahn, Berlin
5D9	recombinant mouse Irga6wt	mouse monoclonal	1-3 µg/µl	IP: 10µl/ 50µl PAS	Jens Zerrahn, Berlin
165	recombinant mouse Irga6wt	rabbit polyclonal	1-3 µg/µl	WB: 1:25000 IF: 1:8000 IP: 7µl/ 50µl PAS	
2600	peptide KLGRLERPHRD	rabbit polyclonal		IF: 1:4000 IP: 7µl/ 50µl PAS	EUROGENTEC
αIGTP clone 7	Mouse Irgm3 aa 283-423	mouse monoclonal	0.25 µg/µl	WB: 1:2000	BD Transduction laboratories
A20 (sc11079)	N-teminal peptide of Irgb6	goat polyclonal	0.2 µg/µl	WB: 1:500	Santa Cruz

2.1.10.2. Secondary antibodies and antisera

donkey-α-mouse Alexa 488, donkey-α-rabbit Alexa 546, donkey-α-mouse Alexa 546,
donkey-α-rabbit Alexa 488 (all Molecular Probes), goat-α-mouse kappa light chain-

FITC (Southern Biotech), donkey-α-rabbit (Amersham), goat-α-mouse HRP (Amersham), donkey-α-goat HRP (Santa Cruz), DAPI (Roche).

2.2 Molecular Biology

All plasmids and constructs were amplified, cloned or propagated using protocols adapted from Sambrook, J., Fritsch, E.F., and Maniatis, T., Vol. 1, 2, 3 (1989), or from the cited references.

2.2.1 Agarose gel electrophoresis

DNA was analysed by agarose gel electrophoresis (1x TAE; 0.04 M Tris, 0.5 mM EDTA, pH adjusted to 7.5 with acetic acid) The DNA was stained with ethidium bromide (0.3 µg/ml), a fluorescent dye which intercalates between nucleotide bases, and the migration of the DNA molecules was visualized by using bromophenol blue.

2.2.2 Generation of Irga6 expression constructs

pGW1H-Irga6cTag1 construct was made by amplification of Irga6cTag1 sequence from pGEX-4T-2-Irga6cTag1 by using IIGP-SAL5 as forward and IIGPm3 as reverse primers. IIGPm3 primer introduces new *Sal*I site after the stop codon (marked in red) and, additionally, mutates the internal *Sal*I restriction site (residue in green). PCR product was digested with *Sal*I and ligated into the *Sal*I-digested pGW1H vector.

IIGP-SAL5 forward 5'-CCCCCCCCCGTCGACCACCATGGGTCAGCTGTTCTCTTCACCTAAG-3'
IIGPm3 reverse 5'-CCCCCCCCCGTCGACTCAGTCACGATGCGGCCGCTCGAGTCGGCCTAG-3

Following mutations were introduced in both pGW1H-Irga6wt and pGW1H-Irga6cTag1 constructs using listed primers:
pGW1H-Irga6-G2A forward 5'-GAGTCGACCACCATGGCTCAGCTGTTCTCTTCA-3'
pGW1H-Irga6-G2A reverse 5'- TGTAGAGAACAGCTGAGCCAGGGTGGTCGACTC-3'

Δ7-12 forward 5'-GGGTCAGCTGTTCTCTAATAATGATTTGCCC-3'

Δ7-12 reverse 5'- GGGCAAATCATTATTAGAGAACAGCTGACCC-3'

K82A forward 5'-GGGAGACGGGATCAGGGGCGTCCAGCTTCATCAATACCC-3'

K82A reverse 5'- GGGTATTGATGAAGCTGGACGCCCCTGATCCCGTCTCCC-3'

S83N forward 5'-GGAGACGGGATCAGGGAAGAACAGCTTCATCAATACCCTG-3'

S83N reverse 5'- CAGGGTATTGATGAAGCTGTTCTTCCCTGATCCCGTCTCC-3'

E106A forward 5'-GCTAAAACTGGGGTGGTGGCGGTAACCATGGAAAG-3'

E106A reverse 5'-CTTTCCATGGTTACCGCCACCACCCCAGTTTTAGC-3'

Primers listed below were used to introduce mutations only in pGW1H-Irga6wt construct.

T21I forward 5'-CCCTCCAGCTTTATTGGTTATTTTAAGAAATTTAATACGG-3'

T21I reverse 5'-CCGTATTAAATTTCTTAAAATAACCAATAAAGCTGGAGGG-3'

G22E forward 5'-CCCTCCAGCTTTACTGAGTATTTTAAGAAATTTAATACGG-3'

G22E reverse 5'-CCGTATTAAATTTCTTAAAATACTCAGTAAAGCTGGAGGG-3'

F24L forward 5'-GCCCTCCAGCTTTACTGGTTATTTGAAGAAATTTAATACGGG-3'

F24L reverse 5'-CCCGTATTAAATTTCTTCAAATAACCAGTAAAGCTGGAGGGC-3'

Δ7-25 forward 5'-CCACCATGGGTCAGCTGTTCTCTAAATTTAATACGGG-3'

Δ7-25 reverse 5'- CCCGTATTAAATTTAGAGAACAGCTGACCCATGGTGG-3'

Δ2-12 forward 5'-CGAGATCTAGAGTCGACCACCATGAATAATGATTTGCCC-3'

Δ2-12 reverse 5'- GGGCAAATCATTATTCATGGTGGTCGACTCTAGATCTCG-3'

Following primers were used to make deletions in pEGFP-N3-Irga6-1-33 construct, containing first 33 Irga6 amino acids. This way, three constructs were created containing first 20, 23 and 25 Irga6 amino acids, respectively.

Δ21-33 forward 5'-CCTCCAGCTTTGTCGACGGTACCGCG-3'

Δ21-33 reverse 5'-CGCGGTACCGTCGACAAAGCTGGAGG-3'

Δ24-33 forward 5'-GCTTTACTGGTTATGTCGACGGTACCGCG-3'

Δ24-33 reverse 5'- CGCGGTACCGTCGACATAACCAGTAAAGC-3'

Δ26-33 forward 5'-GGTTATTTTAAGGTCGACGGTACCGCGGGC-3'

Δ26-33 reverse 5'-GCCCGCGGTACCGTCGACCTTAAAATAACC-3'

To create pVL-Irga6wt construct, pGEX-Irga6wt was digested with *Sma*I and *Not*I restriction enzymes. Appropriate fragment containing Irga6wt was excised from the

agarose gel and ligated into the pVL1393 vector, which was already digested with *Sma*I and *Not*I. Thrombin cleavage site (underlined), between Irga6wt sequence and the stop codon was introduced by site directed mutagenesis using pVL-Irga6wt-thrombin forward and pVL-Irga6wt-thrombin reverse primers. Sequence encoding six histidine residues (in red) behind the thrombine cleavage site was introduced by pVL-Irga6wt-thrombin-His forward and pVL-Irga6wt-thrombin-His reverse primers. Site directed mutagenesis was used to create G2A and S83N mutation in pVL-Irga6wt-thrombin-his construct using pVL-Irga6wt-G2A, pVL-Irga6wt-G2A and S83N forward, S83N reverse primers, respectively.

pVL-Irga6wt-thrombin forward 5'-GAGATATGTTTAAGAAAC<u>CTGGTCCCCCGCGGCTCG</u>TAGGTCGACTCGAGCGG-3'

pVL-Irga6wt-thrombin reverse 5'-CCGCTCGAGTCGACCTA<u>CGAGCCGCGGGGGACCAG</u>GTTTCTTAAACATATCTC-3'

pVL-Irga6wt-thrombin-His forward 5'-GGTCCCCCGCGGCTCGCATCATCACCATCACCATTAGGTCGACTCGAGCGG-3'

pVL-Irga6wt-thrombin-His reverse 5'-CCGCTCGAGTCGACCTAATGGTGATGGTGATGATGCGAGCCGCGGGGGACC-3'

pVL-Irga6wt-G2A forward 5'-GGGTCGACCACCATGGCTCAGCTGTTCTCTTCACC-3'

pVL-Irga6wt-G2A reverse 5'-GGTGAAGAGAACAGCTGAGCCATGGTGGTCGACCC-3'

2.2.3 Cloning of PCR amplification products

Amplified PCR products were purified using the rapid PCR purification Kit (Roche) and eluted with 100 µl 10mM Tris, pH 8.5. DNA yield was monitored by agarose gel electrophoresis and DNA fragments were digested with the appropriate restriction endonuclease (New England Biolabs) according to the suppliers' protocol. Restriction enzymes were used at a 5-10 fold over-digestion. Following restriction, DNA fragments were again column purified using the rapid PCR purification Kit (Roche) and DNA yield was monitored by agarose gel electrophoresis.

2.2.4 Purification of DNA fragments from agarose gels

DNA fragments were loaded on agarose gels of the suitable percentage after incubation with appropriate restriction endonucleases. After proper separation of the fragments, DNA was visualized under a low energy UV source and cut out of the gel using a clean blade. DNA fragments were eluted from the gel with the rapid PCR purification Kit (Roche) according to the manufactures protocol. Purity and yield of the DNA was determined by agarose gel electrophoresis and UV spectroscopy.

2.2.5 Ligation

The appropriate cloning vector was cut with the respective restriction enzyme(s) (10 U/ 1 µg DNA) for 1 h under according to the restriction enzyme suppliers' protocol. After the first hour the same amount of restriction enzyme and 0.1 U of shrimp alkaline phosphatase were added to the reaction followed by 1.5 h incubation. Following restriction, DNA fragments were column purified using the rapid PCR purification Kit (Roche) and DNA yield was monitored by agarose gel electrophoresis. Vector and the appropriate cut insert were mixed at a ratio of 1:3 and ligated with T4-DNA ligase in a total volume of 10 µl at 16°C over-night according to the manufactures protocol. As control, the same reaction without insert was carried out which should not yield any colonies after transformation into competent DH5α.

2.2.6 Preparation of competent cells

A single colony from a particular *E .coli* strain was grown over-night in 2 ml LB medium with 0.02 M MgSO4/ 0.01 M KCl with vigorous shaking (~300 rpm). It was diluted 1:10 into fresh medium with the same constituents and grown for 90 min, at 37°C to an OD_{600} of 0.45. Cultures were incubated on ice for 10 min after which the cells were pelleted by centrifugation at 6000 rpm at 4°C for 5 min. Cells were resuspended in TFB I (30 ml/ 100 ml culture), incubated 5 min on ice, pelleted again by centrifugation at 6000 rpm at 4°C for 5 min and finally resuspended in TFB II (4 ml per 100 ml culture). 100 µl aliquots of the competent bacteria were frozen at –80°C.

Composition of the buffers:

TFB I (30 mM KOAc/ 50 mM $MnCl_2$/ 100 mM $RbCl_2$/ 10 mM $CaCl_2$/ 15% w/v glycerin, pH 5.8)

TFBII (10 mM MOPS, pH 7.5/ 75 mM $CaCl_2$/ 100 mM $RbCl_2$/ 15% w/v glycerin)

Both the solutions were sterilized and stored at 4°C.

2.2.7 Transformation of competent bacteria

100 µl of competent bacteria were thawed on ice and gently mixed 3-4 times. 5 µl of the ligation reaction was added to the cells followed by incubation for 20 min on ice Cells were then heat-shocked for 45 sec at 42°C followed by a further incubation on ice for 2 min. Antibiotic free LB medium was added to a total volume of 1 ml and cells were rolled at 37°C for 1 h. The culture was spun at 9000 rpm for 2 min and 800 µl of the supernatant was removed. The cell pellet was resuspended in the remaining 200 µl medium in the 1.5 ml reaction tube and plated on a LB agar plate supplemented with the appropriate antibiotics.

2.2.8 Plasmid isolation

For screening a large number of cultures for clones containing the desired insert, 4 ml LB cultures with the appropriate antibiotics were inoculated with single colonies picked from a ligation plate and grown over-night at 37°C, 250 rpm. All following steps were performed at room temperature. 1.5 ml of the cultures was transferred into a 1.5 ml reaction tube and pelleted by centrifugation at 23000 g for 5 min. The supernatant was discarded and pellet resuspended in 100 µl P1 (50 mM Tris, pH 8.0/ 10 mM EDTA/ 100µg/ml RNase A). After addition of 100 µl P2 (200mM NaOH/ 1% SDS) the reaction was gently mixed and incubated for 5 min. 140 µl of P3 (3M potassium acetate, pH 5.5) was added and the reaction was spun for 15 min at 23000 g. The supernatant (~340 µl) was transferred into a new tube and 700 µl of 100% ethanol was added. After mixing, the reaction was spun for 15 min at 23000 g and the supernatant was removed. The pellet was washed by addition of 700 µl of 70% ethanol and spun at 23000 g. After removal of the supernatant the pellet was

air-dried and resuspended in 50 µl 10mM Tris pH 8.0. 5 µl of the plasmid preparation was cut with the appropriate restriction enzyme(s) in a total volume of 50 µl for 1 h and 10 µl of the reactions were subjected to agarose gel electrophoresis to identify insert-containing clones.

For preparation of large amounts of plasmid, the Qiagen Midi and Maxi Plasmid Preparation Kits were used according to the manufactures instructions.

2.2.9 Determination of the concentration of DNA

The concentration of DNA was measured using a spectrophotometer at 260 nm. The purity of the DNA solution was determined using the ratio of OD readings at 260 nm and 280 nm. Pure preparations of DNA have an OD_{260}/OD_{280} ratio of 1.8. The concentration was calculated according to the following equation. c = A260 x 50 µg/ml x dilution factor.

2.2.10 Site directed mutagenesis

Site directed mutagenesis was carried out using a modified protocol supplied with "QuikChangeTM XL Site-Directed Mutagenesis" Kit from Stratagene. The amplification was carried out using 20 ng plasmid as template, 125 ng of the sense and antisense oligonucleotide as primers and 2.5 U of Pfu-polymerase (Promega) in a total volume of 50 µl. The following program was used: 1. 95°C, 30 sec; 2. 95°C, 30 sec; 3. 55°C, 60 sec; 4. 68°C, 15 to 20 min (back to step 2., 15 to 18 times); 5. 68°C, 15 min. After amplification 1 µl *Dpn*I (20 U, New England Biolabs) was added to the reaction and incubated for 1.5 h at 37°C. 5 µl of the reaction was used to transform 200 µl competent DH5α. As control the whole procedure was carried out without addition of Pfu-polymerase. Ideally no colonies are found on the final LB agar plate for the control reaction.

2.2.11 DNA Sequencing

All constructs generated were verified by sequencing. DNA was sequenced using the *ABI Prism*R *BigDye*TM Terminator Cycle Sequencing Ready Reaction Kit (PE Applied Biosystems), using fluorescently labeled dideoxynucleotides based on the dideoxy-chain termination. Template DNA (0.5 µg), the respective primer (10 pmole) and 2 µl *Big Dye*TM terminator ready reaction mix (ABI) were combined in a total volume of 10 µl and the sequencing reaction was carried out as follows: 25x (96°C, 30 sec; 50°C, 15 sec; 60°C, 4 min). Sequencing was done on an automated sequencer (ABI 373A).

2.2.12. Transduction of insect *Sf9* cells

2×10^6 *Sf9* cells (BD Biosciences) were plated on 60 mm tissue culture plate so that the cells density was around 70% confluent. Cells were allowed to attach firmly, about 5 min. Old medium was aspirated from the cells and 1 ml of Transfection buffer A added. In parallel, 0.5 µg BaculoGold^{TM} DNA was mixed with 3.5 µg recombinant pVL1393 Baculovirus Transfer Vector, containing Irga6, Irga6 G2A or Irga6 S83N DNA as insert. Content was mixed well by flicking the tube and incubated at RT for 5 min. Subsequently, 1 ml of Transfection buffer B was added and mixure was pipetted drop-by-drop on to the plates with Transfection buffer A. After 4 h incubation at 27°C, medium was aspirated and 3 ml of TNM-FH Insect medium (Sigma) was added and incubated for 5 days at 27°C (transfection). 5×10^6 *Sf9* cells in 10 cm plate were then infected with 150 µl of transfection in 10 ml TNM-FH medium (infection) and incubated for 3 days at 27°C. Virus was further amplified by incubation of 500 µl of infection with 2×10^7 *Sf9* cells in 15 cm dish in 15 ml TNM-FH medium for 3 days at 27°C (amplification). 18 ml of amplified virus was used to infect 300 ml of *Sf9* cell liquid culture (2×10^6 *Sf9*/ml) (in Insect-Xpress, Lonza) for protein purification and cells were grown for 2 days at 27°C at 80 rpm.

2.3. Expression and purification of recombinant proteins

2.3.1. Expression and purification of Irga6 proteins from *E. coli*

pGEX-4T-2-Irga6wt was transformed into BL-21 *E. coli* strain. Cells were grown at 37°C to OD_{600} of 0.8 when the protein expression was induced by 0.1 mM isopropyl-β-D thiogalactoside (IPTG) at 18°C over-night. Cells were harvested (5000 g, 15 min, 4°C), frozen at –20°C, resuspended in 10 ml PBS/ 2 mM DTT/ "CompleteMini protease inhibitor cocktail without EDTA" (Roche) per liter of culture and lysed using microfluidiser (EmulsiFlex-C5, Avestin) at a pressure of 150 MPa. The lysates were cleared by sequential centrifugation at 50000 g 15 min and 75000 g 30 min at 4°C. The soluble fraction was purified on the glutathion-sepharose affinity column (GSTrap FF 5ml, Amersham) equilibrated with PBS/ 2 mM DTT. The GST domain was cleaved by over-night incubation with thrombin (20 U/ml, (Serva)) on the resin at 4°C. Free Irga6 was eluted with PBS/ 2 mM DTT and protein content in fraction analysed by SDS-PAGE and visualised by Coomassie staining. The positive fractions were pooled and subjected to the size exclusion chromatography on Superdex 75 column (HiLoad 26/60 Superdex 75 prep grade, Amersham) equilibrated with 50 mM Tris/HCl pH 7.4/ 5 mM $MgCl_2$/ 2 mM DTT. The fractions were analysed by SDS-PAGE and those containing Irga6 concentrated in a centrifugal concentrator (Vivascience) with a 10-kDa cut-off filter. Aliquots were shock-frozen in liquid nitrogen and stored at –80°C. The concentration of protein was determined by UV spectrophotometry at 280 nm.

2.3.2. Purification of Irga6 proteins from *Sf9* cells

700 ml of *Sf*9 culture infected with appropriate virus for 2 days was pelleted at 2500 g for 10 min at 4°C. Pellet was resuspended in 150 ml 0.1% Thesit/ 150 mM NaCl/ 3 mM $MgCl_2$/ 20 mM Imidazol/ 2 mM DTT/ PBS/ protease inhibitors and incubated for 1 h at 4°C while rotating. Lysate was passaged 10 times trough 20G needle and centrifuged 1 h at 50000 g at 4 °C and subsequently 1 h at 75000 g. Lysate was loaded on hisTrap HP 5ml column (Amersham) with fow rate of 0.5 ml/min in lysis buffer. Column was subsequently washed with 5 column volume (CV) of lysis buffer

and 15 CV of washing buffer (0.1% Thesit/ 150 mM NaCl/ 3 mM MgCl$_2$/ 60 mM Imidazol/ 2 mM DTT/ PBS). Elution was done at flow rate of 0.25 ml/min with 0.1% Thesit/ 150 mM NaCl/ 3 mM MgCl$_2$/ 250 mM Imidazol/ 2 mM DTT/ PBS and fractions analysed by Coomassie staining. Fractions containing Irga6 protein were pooled together and incubated with 150 U/ml of thrombin (Serva) for 12 h at 4°C. After ultracentrifugation at 45000 g/ 30 min/ 4°C, samples were loaded on HiLoad 26/60 Superdex 200 prep grade column (Amersham) with 0.05% Thesit/ 5 mM MgCl$_2$/ 2 mM DTT/ 50 mM Tris pH 7.4 at flow rate of 1 ml/min. Fractions with Irga6 protein were incubated with 1 ml Ni-NTA Superflow beads (Qiagen) for 1 h at 4°C to separate thrombin-cleaved (in the SN) from uncleaved Irga6 (bound to the beads). Cleaved and purified Irga6 was concentrated in a centrifugal concentrator (Vivascience) with a 10-kDa cut-off filter. Aliquots were shock-frozen in liquid nitrogen and stored at –80°C. The concentration of protein was determined by UV spectrophotometry at 280 nm. Uncleaved protein was eluted from beads by boiling for 5 min in the SDS-PAGE sample buffer.

2.4. Biochemical methods

2.4.1. Dynamic light scattering

Recombinant proteins, at the concentrations of 25 and 80 µM, were incubated with 10 mM GDP or GTP in B1 buffer (5 mM MgCl$_2$/ 2 mM DTT/ 50 mM Tris pH 7.4) in the presence or absence of 0.05% Thesit. Dynamic light scattering (DLS) was performed by using DynaPro molecular sizing instrument equipped with a MicroSampler temperature control unit (MSTC800, Protein Solutions). The scattering of light from a 750 nm wavelength solid-state laser (25 MW) by the sample was measured at 37°C for 20 min in a Quartz cuvette (acquisitio time 10 sec). Data was obtained and analysed using the DYNAMICS software (v.5 and v.6). The hydrodynamic radius (R_H) was calculated from the translational diffusion coefficient (D_T), obtained by autocorrelation of the data, using the Stokes-Einstein Equation ($R_H = k_b T / 6\pi\mu D_T$; k_b: Boltzmann constant, T: absolute temperature in Kelvin, µ: solvent viscosity). The molecular weight (MW) was estimated from the hydrodynamic radius R_H using the

standard curve of MW versus R_H for globular proteins (MW=(R_H factor*R_H)^{Power}, for globular proteins R_H factor=1.68, Power=2.3398).

2.4.2. GTP hydrolysis assay

Hydrolysis activities of recombinant proteins were determined by resuspending 25 µM protein in 50 mM Tris pH 7.4/ 5 mM $MgCl_2$/ 2 mM DTT in the final volume of 18 µl. 50 µl of 100 mM or 10 mM GTP was mixed with 1 µl of αP^{32}GTP. 2 µl of the nucleotide mix was added to the protein, so that the final concentration of GTP was 10 mM or 1 mM, and samples were placed immediately at the 37°C. At indicated time points, 0.6 µl of reaction mixed was taken and applied onto the PEI Cellulose F thin layer chromatography (TLC) plates (Merck). After air-drying, plates were run in 1 M acetic acid/ 0.8 M LiCl. Signals were detected using BAS 1000 phosphor imager analysis system (Fuji) and quantified with the AIDA Image Analyser v3 software (Raytest).

2.5. Cell biology

2.5.1. Transfection

Cells were transiently transfected for 24 h at 37°C using FuGENE 6 Transfection Reagent (Roche) according to the manufacturer's protocol. DNA (µg): FuGENE6 (µl) ratio was always 1:3. For transfection of cells in 6 well plate or in 60 mm dish 1 µg or 2 µg of DNA was used respectively.

2.5.2.Induction with IFNγ

Cells were induced with 200 U/ml of murine IFNγ (Cell Concepts) for 24 h at 37°C.

2.5.3. Hypotonic lysis

$1\text{x}10^7$ L929 cells, induced with 200 U/ml IFNγ or transfected with appropriate construct for 24 h, were washed once with PBS, collected by scraping and disrupted in 1 ml of hypotonic buffer/ 3 mM $MgCl_2$/ "CompleteMini protease inhibitor cocktail without EDTA" (Roche) for 1 h at 4°C while rotating (hypotonic buffer (10 mM Tris pH 7.5/ 10 mM NaCl/ 1.5 mM $MgCl_2$) was sterilised and kept at 4°C). Lysate were cleared by high-speed centrifugation (23000 g/ 30 min/ 4°C) and supernatant kept as a soluble fraction. Pellet was washed twice with hypotonic buffer, resuspended in 1 ml of appropriate lysis buffer, incubated 1 h at 4°C and cleared by centrifugation as above. Supernatant of this step was kept as membrane fraction.

2.5.4. Triton X-114 partitioning assay

480 ng of recombinant proteins were resuspended in 500 µl 1% Tx-114/ 3 mM $MgCl_2$/ PBS, incubated on ice for 5 min. and subsequently at room temperature for 5 min to induce phase separation. After the solution turned cloudy the tube was spun for 1 min with 23000 g at RT. The aqueous phase (~450 µl) was transferred into new tube and the detergent phase was adjusted with PBS to the same volume as the aqueous phase and stored on ice (D1). 50 µl of the aqueous phase was taken and stored on ice (A1). The remaining 400 µl of the aqueous phase were adjusted to 1% Triton X-114 by addition of an appropriate volume of ice cold 10% Triton X-114 (~44 µl). The tube was incubated on ice until the solution turned clear and was again shifted to room temperature to induce phase separation. The following steps are described above. The procedure was repeated three times. For Tx-114 partitioning analysis of cellular proteins, $6\text{x}10^6$ L929 cells, either IFNγ induced or transfected with Irga6wt or Irga6-G2A, were lysed in 500 µl 1% Tx-114/ 3 mM $MgCl_2$/ PBS for 1 h at 4°C. Upon scraping, lysates were centrifuged for 15 min at 3000 g at 4°C to remove nuclei. Supernatants were incubated for 5 min at room temperature to induce phase separation and subsequently centrifuged for 1 min at 23000 g at RT. The following steps were conducted as described above. Samples were subjected to SDS-PAGE and protein detected with 10D7 antibody.

2.5.5. Cross-linking

1×10^6 L929 cells per sample were induced with 200 U/ml IFNγ for 24 h or left untreated. Cells were washed with PBS, collected by scraping and mixed in 100 µl PBS/ 3 mM $MgCl_2$/ protease inhibitors with the cross-linkers (all from Pierce biotechnology): DSP (Dithiobis (succinimidylpropionate),) and EGS (Ethylene glycolbis (succinimidylsuccinate)), or their analogs DTSSP (Dithiobis (sulfosuccinimidylpropionate)) and Sulfo-EGS (Ethylene glycolbis (sulfosuccinimidylsuccinate)) in the presence of 0.1 U Streptolysin O (Murex Diagnostics Limited). Concentration of cross-linkers used was 0.25-2 mM. Mixtures were incubated for 2 h at 4°C or 30 min at RT respectively and cross-linking reaction was subsequently quenched with 50 mM Tris pH 7.5 for 15 min at 4°C. Afterwards, cells were lysed in 100 µl 1%Tx-100 (Sigma)/ 3 mM $MgCl_2$/ protease inhibitors for 1 h/ 4°C, span at 23000 g/ 30 min/ 4°C, boiled for 5 min in the presence or absence of 5% β-mercaptoethanol (Sigma) in SDS-PAGE sample buffer and subjected to the SDS-PAGE and Western blott.

2.5.6. Treatment with aluminium fluoride

300 µl 10 mM $AlCl_3$ (final concentration 300 µM) was added to 10 ml of IMDM containing no FCS and mixed by vigorous shaking. Subsequently, 166 µl of 600 mM NaF was added, mixed and applied on confluent L929 cells in 10 cm dish, previously induced with IFNγ or transfected for 24 h. Cells were incubated for 30 min at 37°C, then washed with cold PBS and collected by scraping. Cell pellets were lysed in 0.1% Thesit or 80 mM OGP/ 3 mM $MgCl_2$/ PBS with 300 µM $AlCl_3$ and 10 mM NaF, with or without 0.5 mM GTP for 1 h at 4°C.

2.5.7. Antibody purification

Hybridoma cells producing monoclonal 10D7 or 10E7 antibody were grown in 50 ml IMDM (supplemented with 5% FCS, 2 mM L-glutamine, 1 mM sodium pyruvate, 1x non-essencial amino acids, 100 U/ml penicillin, 100 µg/ml streptomycin (Gibco BRL))

in T-175 for 7 days at 37°C. Culture was centrifuged at 300 g/ 10 min/ 4°C, supernatant was frozen at –20°C and cell pellet diluted 1:10 in 50 ml medium and cells grown again for a week. Supernatants containing secreted antibody (400 ml) were centrifuged at 2800 g for 30 min at 4°C. Supernatant was applied on Protein A sepharose column (6 ml) by gravity flow and column subsequently washed with 400 ml cold PBS. Antibody was eluted by applying elution buffer (50 mM Sodium Acetat pH 3.5/ 150 mM NaCl) and 1 ml fractions were collected in eppendorf tubes already containing 56 µl of neutralization buffer (1M Tris pH 11). Concentration of protein was determined by measuring absorption at 280 nm and fractions containing antibodies were pooled together. Buffer was exchanged by dilution of antibody-containing sample in 20 ml of papain buffer (0.075 M phosphate buffer pH 7.0/ 0.075 NaCl/ 0.002 M EDTA) and concentrated in centrifugal concentrator (Vivascience) with a 10-kDa cut-off filter at 2000 g at 4°C. Buffer exchange was done five times subsequently. Concentration of antibody was determined by using formula conc Ab (mg/ml)= 0.8 x $A_{280.}$.

2.5.8. Papain digestion

0.5 mg of 10E7 or 10D7 antibodies were digested with 5 µg of papain (papain: globulin ratio was 1:100), in the presence of 0.01 M cysteine in 100 µl papain buffer (0.075 M phosphate buffer pH 7.0/ 0.075 NaCl/ 0.002 M EDTA). Mixtures were incubated at 37°C, and at indicated time points, reaction was stopped by adding 0.5 M iodoacetamide in papain buffer to the final concentration of 50 mM, and incubated at RT for 30 min. Samples were boiled in the SDS-PAGE sample buffer in the presence (reducing conditions) or absence (non-reducing conditions) of 5% β-mercaptoethanol and subjected to SDS-PAGE. Proteins were detected by staining of gels in Coomassie solutions.

2.5.9. Size Exclusion Chromatography

2.5.9.1. Size Exclusion Chromatography of cell lysates

$7x10^6$ L929 cells were lysed in 400 µl hypotonic buffer (10 mM Tris pH 7.5/ 10 mM NaCl/ 1.5 mM $MgCl_2$) or in PBS/ 0.1% Thesit (Fluka) or 80 mM OGP (Calbiochem)/ 3 mM $MgCl_2$ with protease inhibitors 1 h at 4°C while rotating, cleared by ultracentrifugation (45000 g/ 30 min/ 4°C) and supernanatant was loaded on the pre-equilibrated Superose 6 10/300 GL column with 0.2 ml/min, fraction size 0.2 ml, fractionation start at 0.3 CV and set pressure of 1 MPa. Column was run on ÄKTA P-920, OPC-900, Frac-950 and results evaluated using UNICORN 5.01.

2.5.9.2. Size exclusion chromatography of 10E7 and 10D7 fragments

600 µl of papain-digested antibodies was loaded on the HiLoad 26/60 Superdex 75 prep grade column (Amersham) and ran in papain buffer (0.075 M phosphate buffer pH 7.0/ 0.075 NaCl/ 0.002 M EDTA) at flow rate of 0.5 ml/min. Fractionation was started after 100 ml and 2ml fractions were collected.

2.5.10. Immunoprecipitation

$1x10^6$ L929 or $6x10^5$ gs3T3 cells per sample were precultured for 12 h, induced with 200 U/ml IFNγ (Cell Concepts, Umkirch, Germany) and/ or transfected for 24 h or left untreated, washed with cold PBS and harvested by scraping. Cells were lysed in 200 µl 0.1% Thesit or 80 mM OGP/ 3 mM $MgCl_2$/ PBS/ "CompleteMini protease inhibitor cocktail without EDTA" (Roche) per sample for 1 h at 4°C in the absence of nucleotide or in the presence of 0.5 mM GDP (Sigma), GTP (Sigma), GTPγS (Sigma), mant GDP (Jena Bioscience), mant GTPγS (Jena Bioscience), 300 µM $AlCl_3$ (Sigma) and 10 mM NaF (Sigma) at 4°C while rotating. Lysates were passaged 10 times trough 25G needle (B.Braun Melsungen AG) and cleared by high-speed centrifugation (23000 g for 30 min at 4°C). In the case of recombinant proteins, 170 or 240 ng of proteins, upon high speed centrifugation, were resuspended in 200 µl of

0.1% Thesit or 80 mM OGP/ 3 mM MgCl$_2$/ PBS/ "CompleteMini protease inhibitor cocktail without EDTA" in the presence or absence of nucleotides.

50 µl of wet Protein A Sepharose ^{TM} CL-4B (Amersham) beads per sample were incubated with 10 µl 10D7or 10E7 monoclonal mouse αIrga6 antibody or 7 µl 165 (αIrga6) or 2600 (αcTag1) polyclonal rabbit sera for 1 h at 4°C while rotating. Beads were pelleted by short centrifugation (2000 g/ 1min), washed 5x with PBS and once with 0.2 M boric acid pH 9.0 (Merck). Bound antibodies were cross-linked with 20 mM DMP (Sigma) in 0.2 M boric acid pH 9.0 for 30 min at RT. Beads were washed once, incubated with 0.2 M ethanolamine pH 8.0 (Sigma) for 2 h at 4°C while rotating and then washed once with PBS and once with lysis buffer. Lysates were incubated with prepared beads for 2 h at 4°C while rotating and then washed twice with lysis buffer and twice with PBS/ 3 mM MgCl$_2$. Proteins bound to the monoclonal mouse antibodies were eluted by boiling for 10 min in 30 µl 100 mM Tris/HCl pH 8.5/ 0.5% SDS with SDS-PAGE sample buffer (50 mM Tris/HCl pH 6.1/ 1% SDS/ 5% glycerol/ 0.0025% brommephenol blue (Sigma)/ 0.7% β-mercaptoethanol). Proteins bound to the polyclonal rabbit serum were eluted by incubation in 50 µl 100 mM Tris/HCl pH 8.5/ 0.5% SDS for 30 min at RT, residual beads removed by filtration (filter tubes, pore size 0.45 µm, Millipore) and eluates then boiled for 5 min with SDS-PAGE sample buffer.

2.5.11. Pull-down

BL-21 cells transformed with pGEX-4T-2, pGEX-4T-2-Irga6wt and pGEX-4T-2-Irga6-S83N respectively, were grown to an optical density (OD$_{600nm}$) of 0.8 at 37°C in 500 ml LB/ 100 µg/ml ampicillin prior to induction of protein expression with 0.1 mM IPTG at 18°C over-night. Cells were harvested by centrifugation (5000 g/ 15 min/ 4°C), resuspended in 10 ml PBS/ 2 mM DTT/ "CompleteMini protease inhibitor cocktail without EDTA" (Roche) and lysed using microfluidiser (EmulsiFlex-C5, Avestin) at a pressure of 150 MPa. The lysates were cleared by sequential centrifugation at 50000 g 15 min and 75000 g 30 min at 4°C. Lysates were incubated with 700 µl of glutathion sepharose suspension (High Performance, Amersham) for 2 h at 4°C and washed 10x with PBS/ 2 mM DTT prior to storage as 1:1 suspention in PBS/ 2 mM DTT at 4°C. 30 µl of 1:1 protein bound glutathion sepharose were washed once with

PBS/ 5 mM MgCl$_2$/ 1 mM DTT and preincubated with or without 1 mM nucleotide (GDP, GTPγS (both from Sigma), or mant GTPγS (Jena Bioscience)) in 500 µl PBS/ 5 mM MgCl$_2$/ 1 mM DTT for 1-2 h at RT. Beads were washed with lysis buffer (PBS/ 0.1% Thesit/ 3 mM MgCl$_2$/ "CompleteMini protease inhibitor cocktail without EDTA" (Roche)) in the presence of 10 µM of the respective nucleotide.

1.25x10^6 gs3T3 cells were precultured for 24 h, induced with 200 U/ml IFNγ (Cell Concepts, Umkirch, Germany) for 24 h, washed once with PBS and harvested by scraping. Cells were lysed in 500 µl lysis buffer with or without 0.5 mM GDP,GTPγS or mant GTPγS for 1 h at 4°C. Lysates were cleared by centrifugation (23000 g/ 30 min/ 4°C), mixed with nucleotide pretreated protein-glutathion sepharose and incubated at 4°C over-night. Beads were washed twice with lysis buffer, twice with PBS/ 5 mM MgCl$_2$ prior to elution of bound cellular proteins in 30 µl 100 mMTris pH 8.5/ 0.5% SDS for 30 min at RT. Eluates were boiled for 5 min in the presence of SDS-PAGE sample buffer, separated by 10% SDS-PAGE and subjected to Western blot.

2.5.12. Immunofluorescence

Cells were grown on coverslips, fixed with PBS/ 3% paraformaldehyde (PFA) for 20 min and subsequently washed 3x with PBS. Cells were permeabilized with PBS/ 0.1% saponin (washing buffer) followed by a blocking step with PBS/ 0.1% saponin/ 3% BSA (fractionV) (blocking buffer) for 1 h. Coverslips were incubated with primary antibodies (diluted in blocking buffer) in a humid chamber for 1 h at RT and subsequently washed 3x 5 min with washing buffer. Incubation with secondary antibodies was done as described for primary antibodies for 30 min at RT and washed 3x as described above. Coverslips were mounted on slides with ProLong® Gold antifade reagent (Invitrogen), sealed with nail polish and cleaned with deionised water. DAPI, used to stain DNA (300 nM), was added to the secondary antibody solution. Images were taken with a Zeiss Axioplan II fluorescence microscope equipped with an AxioCam MRm camera (Zeiss). Images were processed with Axiovision rel. 4.6 software (Zeiss).

2.5.12.1. Immunofluorescence with antibody fragments

gs3T3 cells were induced with 200 U/ml of IFNγ for 24 h and then infected with *T. gondii* Me49 strain with MOI 8 for 2 h. Upon fixation, cells were labelled with 10D7, 10D7 C3 fraction (both 10 µg/ml) or with no antibody for 1 h at RT. As secondary antibody either donkey-α-mouse IgG Alexa 488 (Invitrogen) or goat-α-mouse kappa light chain-FITC (Southern Biotech) antibodies were used.

2.5.13. Western blotting

After SDS-PAGE, proteins were transferred to nitrocellulose transfer membranes (Schleicher&Schuell) by electroblotting. The gel was placed in contact to a nitrocellulose transfer membrane, and was sandwiched between four sheets of 3 MM Whatmann paper, two porous pads, and two plastic supports on either side, soaked in a transfer buffer containing 25 mM Tris/ 190 mM glycine. The sandwich was then placed between platinum plate electrodes, with the nitrocellulose membrane facing the anode, and the transfer was carried out at RT for 1 h with a current of 0.5 V. Ponceau S staining was used to locate proteins (0.1%(w/v) Ponceau S (Sigma) in 5% (v/v) acetic acid) after Western blotting. Membranes were blocked with PBS/ 5% milk powder/ 0.1% Tween 20 or Western Blotting Blocking Reagent (Roche) at room temperature for 1 h or over-night at 4°C. Antisera/ antibodies were diluted in PBS/ 5% FCS/ 0.1% Tween 20 or PBS/ 5% Western Blotting Blocking Reagent. Bands were visualized with enhanced chemiluminescence (ECL) substrate.

2.5.13.1. Western blotting with antibody fragments

60 ng of recombinant Irg6wt per sample was loaded in every second slot of a 10% polyacrylamide gel and blotted on the nitrocellulose transfer membrane. Membrane was cut in stripes so that each stripe contains a lane with Irga6wt and they were blocked in Western Blocking Reagent (Roche) (1:10 dilution in PBS) at RT for 1 h. Whole antibodies or their fragments were diluted to a concentration of 10 µg/ml (1:20 dilution in blocking buffer) and that concentration was considered as 1:1. Serial of

dilutions was made further, 1:3, 1:9, 1:27 and 1:81. Each stripe was incubated with appropriate antibody dilutions at 4°C over night and goat-α-mouse HRP coupled antibody was used as secondary antibody. Signals were quantified using ImageQuant TL v2005 (Amersham).

2.5.14. Colloidal Coomassie staining

Gel was washed 30 min in H_2O and subsequently placed in incubation solution (17% ammonium sulfate/ 20% MeOH/ 2% phosphoric acid). After 60 min incubation, 330 mg/ 500ml of solid Coomassie Brilliant Blue G-250 (Serva) was added to the solution and incubated 1-2 days. Gel was destained by incubation for 1 min in 20% MeOH and stored in 5% acetic acid. All was done at RT and while shaking.

2.5.15. Silver staining (method modified according to Blum)

Gel was washed twice for 20 min with 30% EtOH, once for 20 min with H_2O and sensitised with 0.2 g/l sodium thiosulfate for 1 min. After 3x 20 sec washing with H_2O, gel was incubated in 2 g/l $AgNO_3$/ 750 µl/l formaldehyde (FA) for 20 min. After 2x 20 sec H_2O washes, gel was developed in 30 g/l sodium carbonate/ 500 µl/l FA/ 4 mg/l sodium thiosulfate until the background came up. The reaction was stopped by incubation in 5% acetic acid for 10 min. Gel was washed 2x 10 min in H_2O and kept in 20% EtOH/ 3% glycerol. All was done at RT.

3. Results

3.1. Chemical cross-linking of IFNγ-induced Irga6

3.1.1. Irga6 is found in higher molecular weight complex upon chemical cross-linking

Irga6, a member of the IRG family, hydrolyses GTP to GDP with a specific rate that is dependent on the concentration of the enzyme, demonstrating a cooperative mechanism of GTP hydrolysis (Uthaiah et al., 2003). In agreement with the cooperative activity, Irga6 is characterised by formation of enzymatically active GTP-dependent oligomers *in vitro* (Uthaiah et al., 2003). However, almost nothing was known about whether and under what circumstances Irga6 forms higher molecular weight complexes *in vivo.* In contrast to *in vitro* conditions, in cells Irga6 might not only self-associate but also form interactions with other cellular components.

In order to analyse molecular associations of Irga6 *in vivo,* chemical cross-linking was performed. Reactive groups that can be targeted using a cross-linker include primary amines, sufhydryls, carbonyls, carbohydrates and carboxylic acid. Because primary amines are commonly found in proteins, homobifunctional *N*-hydroxysuccinimide (NHS) esters were used as cross-linking reagents. Since it is difficult to predict the proximity between reactive groups different cross-linkers were tested: membrane-permeable DSP (Dithiobis (succinimidylpropionate)) and EGS (Ethylene glycolbis(succinimidylsuccinate)) as well as their water-soluble analogs DTSSP (Dithiobi(sulfosuccinimidylpropionate)) and Sulfo-EGS (Ethylene glycolbis (sulfosuccinimidylsuccinate)). Cross-linking with membrane-insoluble DTSSP and Sulfo-EGS was performed in the presence of Streptolysin-O (SLO). SLO is a protein produced by *Staphylococcus aureus*, which interacts primarily with cholesterol molecules and upon oligomerisation forms pores in the membranes (30-35 nm in diameter) thus allowing transport of ions and macromolecules into the cell (Bhakdi et al., 1996).

L929 fibroblasts, either IFNγ-induced or untreated, were collected form the tissue culture plates and resuspended in PBS containing $MgCl_2$. DSP and EGS, being lipophilic and membrane-permeant, were added to the cells at a final concentration of 1mM. DTSSP and Sulfo-EGS were incubated with the cells at a

concentration of 1 mM but in the presence of 0.1 U of SLO. Cross-linking was performed for 2 h at 4°C and subsequently quenched in the presence of 50 mM Tris pH 7.5 for 15 min at 4°C, since Tris contains primary amines that compete with the cross-linking of the proteins. Cells were lysed in 100 µl of 1% Tx-100 for 1 h at 4°C, the lysates were cleared by high-speed centrifugation and boiled in SDS-PAGE sample buffer in the absence of β-mercaptoethanol. Lysates were subjected to SDS-PAGE and Western blotting and Irga6 was detected by mouse monoclonal 10D7 antibody (figure 3.1.).
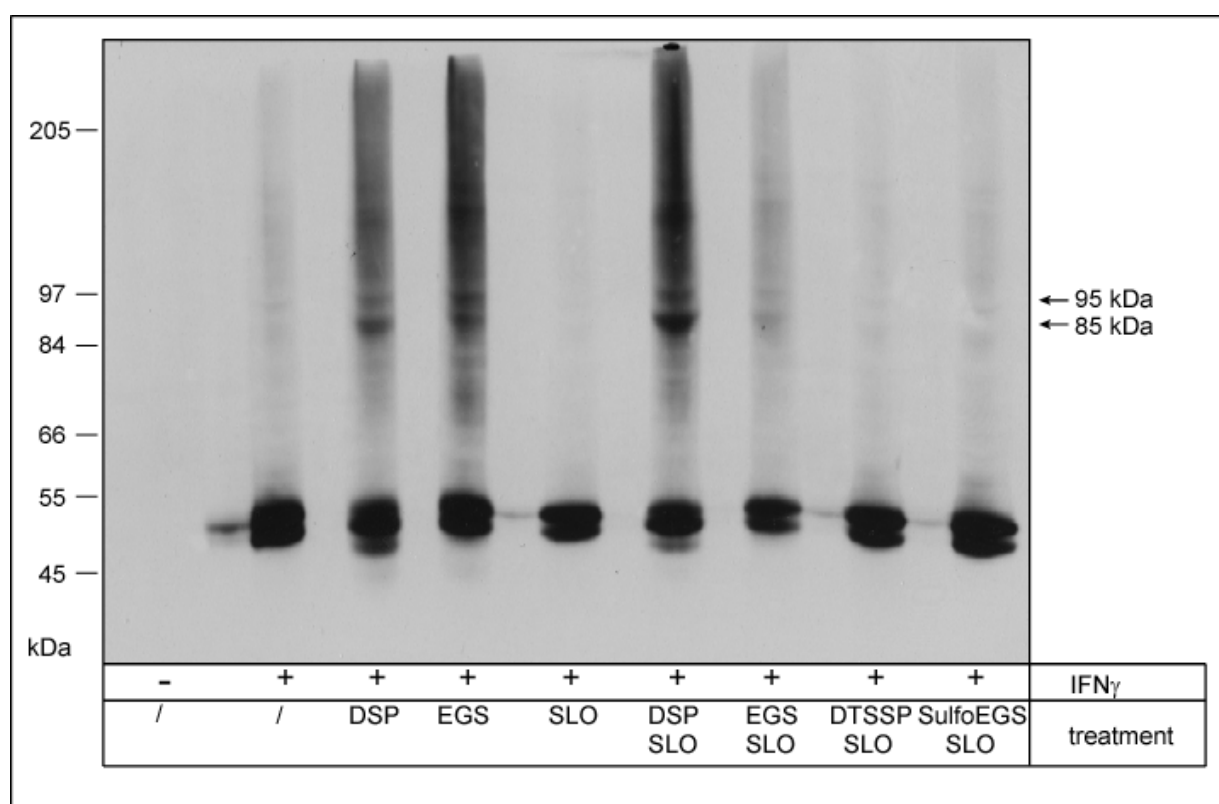
Figure 3.1. Cross-linking of Irga6 in IFNγ-induced L929 fibroblasts
L929 fibroblasts, induced or not induced with 200 U/ml of IFNγ, were treated with different cross-linkers (DSP, DTSSP, EGS and Sulfo-EGS) at concentration of 1 mM, in the presence or absence of 0.1 U SLO for 2 h at 4°C. Reaction was quenched with 50 mM Tris pH 7.5 for 15 min at 4°C, lysates boiled in the absence of β-mercaptoethanol in SDS-PAGE sample buffer, subjected to SDS-PAGE and Irga6 protein detected with 10D7 antibody in Western blot.

Incubation of cells in the presence of membrane-permeable cross-linkers DSP and EGS, both in the presence and in the absence of SLO, resulted in formation of

Irga6-containing complexes that were approximately 85 and 95 kDa in size, marked by the arrows in figure 3.1., indicating interaction of Irga6 with another protein of molecular weight of around 50 kDa. In this experiment, IFNγ-induced Irga6 atypically ran as a double band, even in the absence of cross-linkers. The nature of this additional band is unclear. Unsuccessful Irga6 cross-linking with DTSSP and SulfoEGS suggested that sulfonated cross-linkers could not be used for efficient trapping of Irga6 molecules in high-molecular weight complexes.

3.1.2. Analysis of cross-linking conditions

In order to increase the amount of cross-linked Irga6, IFNγ-induced L929 cells were incubated with rising concentrations of DSP either for 2 h at 4°C or for 30 min at room temperature (RT), as explained above. Lysates were boiled in the absence of reducing agent and Irga6 detected by 10D7 antibody on Western blot.
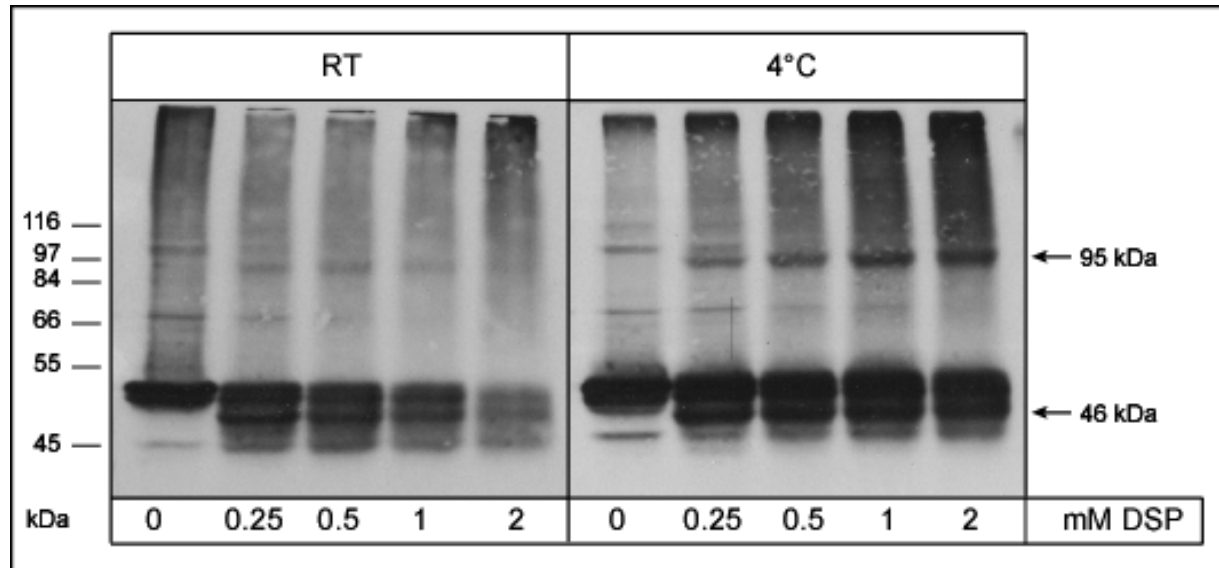
Figure 3.2. Cross-linking of Irga6 with different DSP concentration at 4°C and RT
IFNγ-induced L929 cells were incubated with rising concentration of DSP either for 2 h at 4°C or for 30 min at RT. Upon quenching of cross-linking reaction, lysates were boiled in the absence of β-mercaptoethanol and Irga6 proteins were identified by staining with 10D7 antibody in Western blot.

Amount of Irga6 detected in a 95 kDa complex increased with the rising concentration of the cross-linker at 4°C, as depicted in figure 3.2., with the maximum reached in the presence of 2 mM of DSP. In contrast, cross-linking of Irga6 at RT was very inefficient. Intriguingly, a 85 kDa complex containing Irga6 could not be identified. Possible explanations are that the gel resolution was inefficient to separate 85 and 95 kDa complexes or, alternatively, it indicates high instability of this Irga6-containing complex *in vivo*. In addition, DSP cross-linking at both 4°C and RT resulted in strong Irga6 signal at the size of approximately 46 kDa, representing either degradation product of Irga6 or intra-cross-linked Irga6 molecule adopting more globular form and thus running faster in SDS-PAGE.

In order to isolate Irga6-containing cross-linked complexes and analyse their composition, a concentration of 2 mM DSP and incubation for 2 h at 4°C were used as cross-linking condition in further experiments.

3.1.3. Immunoprecipitation of cross-linked Irga6

To be able to identify an Irga6-binding partner by mass spectrometry, immunoprecipitation experiments were conducted to isolate DSP cross-linked complexes. Lysed IFNγ-induced L929 cells treated with 2 mM DSP were incubated for 2 h at 4°C with Protein A sepharose beads coupled either with polyclonal 165 serum (figure 3.3.) or monoclonal antibodies 10E7 or 5D9 (data not shown). Bound proteins were eluted by incubation in 100 mM Tris/HCl pH 8.5/ 0.5% SDS for 30 min at RT. Lysates (10% of the total sample) and immuoprecipitated proteins (IP) were subjected to SDS-PAGE and analysed by Western blot with αIrga6 antibodies or by silver staining of polyacrylamide gels.

Upon immunoprecipitation with αIrga6 polyclonal serum 165, strong signal for the monomeric Irga6 protein and much weaker signal for cross-linked 95 kDa Irga6-containing complex could be detected in Western blot, as indicated in figure 3.3. Even though silver-stained polyacrylamide gels revealed monomeric Irga6 in immunoprecipitates, the cross-linked Irga6-containing band at 95 kDa could not be identified. In general, the efficiency of Irga6 cross-linking varied in different experiments. In addition, during immunoprecipitation cross-linked Irga6-containing complex was always binding weakly than the monomeric Irga6. Varying the ratio

between the fibroblasts and the antibody-coupled Protein A sepharose beads did not improve the yield of the immunoprecipitated cross-linked Irga6 complex. Therefore, DSP cross-linking could not by exploited further to identify the Irga6 interaction partners.
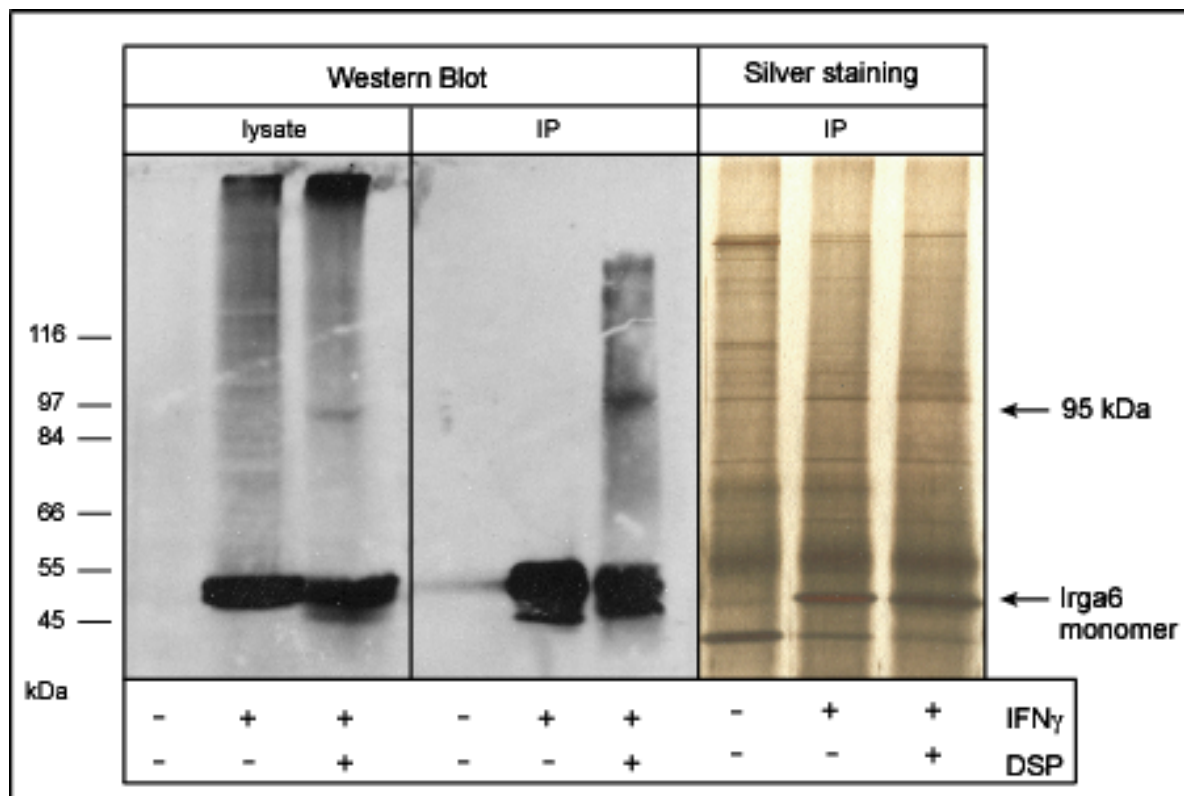
Figure 3.3. Immunoprecipitation of cross-linked Irga6 complexes
IFNγ-induced L929 lysates with Irga6-containing complexes formed in the presence of 2 mM DSP were immunoprecipitated with rabbit polyclonal serum 165. Irga6 was detected either by 10D7 antibody in Western blot or by silver staining of polyacrylamide gel.

3.2 Size Exclusion Chromatography

3.2.1. Size Exclusion Chromatography of Irga6 proteins in Thesit

To analyse in another way whether Irga6 exists in a monomeric form or in any kind of a complex *in vivo*, size exclusion chromatography was carried out. IFNγ-induced L929 cells were disrupted in hypotonic buffer, the soluble fraction separated

and subsequently the membrane fraction lysed in 0.1%Thesit/ 3 mM MgCl$_2$/ PBS. Both soluble and membrane fractions were fractionated on a Superose 6 10/300 GL column using 0.1%Thesit/ 3 mM MgCl$_2$/ PBS as running buffer, the fractions separated by SDS-PAGE and detected in Western blot using monoclonal 10D7 antibody.

Irga6 induced with IFNγ, isolated from both membrane fraction (figure 3.4.(a)) as well as from soluble fraction (figure 3.4.(b)) separated into two forms, one running at the size of a monomer (~50 kDa), the other running much bigger, at the size of approximately 150 kDa. Often the proportion of Irga6 molecules in the oligomeric form was much larger than in the monomeric form. This behavior is not only due to the presence of IFNγ-induced factors since exogenous, transfected Irga6wt, in the absence of IFNγ induction, also ran in a similar manner, though most of the protein was found in higher molecular weight fractions, as shown in figure 3.4.(c). It was observed that, in general, transfected Irga6wt (as well as Irga6 mutants) runs on Western blot as a double band, independently of the antibodies used for detection. Interestingly, this upper band in the size exclusion analysis was fractionated exclusively at the size of a monomer (figure 3.4.(c)). As depicted in figure 3.4.(d), transfected Irga6-G2A, which cannot be myristoylated since it lacks N-terminal glycine necessary for covalent linkage of myristoyl group, was found only in the low molecular weight fractions. Recombinant nonmyristoylated Irga6wt, expressed and purified from a bacterial expression plasmid, also ran as monomer (figure 3.4.(e)).

Size exclusion analysis of Irga6 proteins in 0.1% Thesit, illustrated in figure 3.4. revealed Irga6wt at the position expected for the monomer (~50 kDa) but also in fractions with a molecular weight of 150 kDa, both in the presence and in the absence of other IFNγ-induced factors. There are four possible explanations for Irga6 presence in higher molecular weight complexes. Irga6wt could interact with ubiquitously expressed protein, in an IFNγ-independent manner. Since recombinant Irga6wt *in vitro* forms GTP-dependent homooligomers (Uthaiah et al., 2003), alternative possibility is that the Irga6-containing complex in non-induced cells could represent Irga6 homooligomers, whereas in IFNγ-induced cells they could be either Irga6-homooligomers or heterooligomers, containing Irga6wt in complex with another IFNγ-induced protein. However, nonmyristoylated proteins, recombinant Irga6wt and transfected Irga6-G2A, were found exclusively in the monomeric form, rather suggesting that the myristoyl group itself influences running behavior of Irga6

proteins in size exclusion chromatography. Interestingly, the upper band of transfected Irga6wt (figure 3.4.(c)) was found only in the later fractions, allowing the assumption that part of the transfected Irga6 protein is left unmyristoylated in cells *in vivo*. Finally, since concentration of 0.1% Thesit is above critical micellar concentration (~0.005%; (Black, 2002), interaction of Irga6 monomer (~50 kDa) with Thesit micelle (~90 kDa) could result in Irga6wt protein running as a complex of 150 kDa in size.
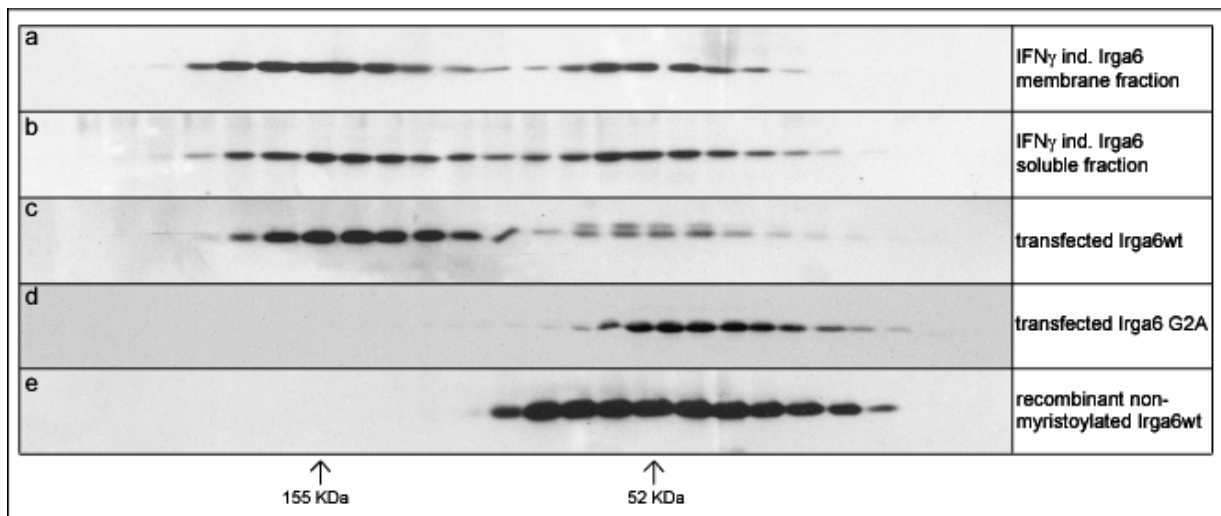
Figure 3.4. Size Exclusion Chromatography of Irga6 proteins in 0.1% Thesit

Proteins were fractionated on the Superose 6 10/300 GL in the presence of 0.1% Thesit/ 3 mM $MgCl_2$/ PBS. (a) IFNγ-induced Irga6, membrane fraction; (b) IFNγ-induced Irga6, soluble fraction; (c) transfected Irga6wt; (d) transfected Irga6-G2A; (e) recombinant nonmyristoylated Irga6wt. Irga6 proteins were detected with 10D7 antibody in Western blot.

3.2.2. Size Exclusion Chromatography of IFNγ-induced Irga6 in Octyl-β-D glucopyranoside

Since the concentration of Thesit used in experiments above was over the critical micellar concentration (CMC of Thesit is ~0.005%; (Black, 2002), it was necessary to exclude the possibility that the presence of Irga6 in the higher molecular weight complexes was a result of association of the protein with a Thesit micelle (about 90 kDa). Therefore, another nonionic detergent was considered, namely Octyl-β-D-glucopyranoside (OGP), with a much smaller micellar molecular weight of

7.89 kDa (Black, 2002). IFNγ-induced L929 cells were lysed in 80 mM OGP (2.3%)/ 3 mM MgCl$_2$/ PBS, lysate separated again on the Superose 6 column in the same buffer and Irga6 detected as described above.

Irga6 protein, induced with IFNγ, in the presence of OGP displayed wide distribution in size, shown in figure 3.5., indicating that use of different detergents might affect Irga6 running behavior and/or conformation in a detergent-specific manner. Nevertheless, the majority of Irga6 protein in the presence of OGP was found running between 67 and 200 kDa, confirming that the presence of Irga6 in fractions associated with higher molecular weight components is not due to the protein-micelle association.
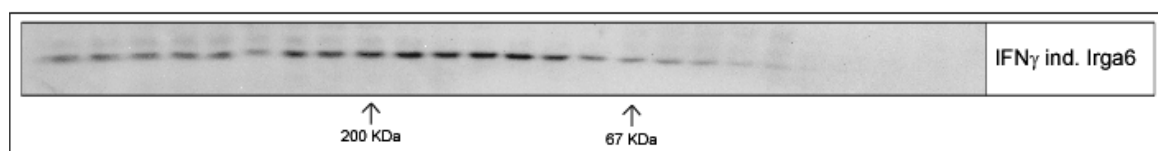
Figure 3.5. Size Exclusion Chromatography of IFNγ-induced Irga6 in the presence of OGP
L929 fibroblasts, induced with IFNγ for 24 h, were lysed in 80 mM OGP/ 3 mM MgCl$_2$/ PBS. Lysate was fractionated on the Superose 6 10/300 GL in the same buffer and fractions analysed by SDS-PAGE and Western blot with 10D7 antibody.

3.2.3. Size Exclusion Chromatography of IRG proteins in Thesit

Both IFNγ-induced and transfected Irga6 proteins were found in the higher molecular weight complexes upon size exclusion, independent of detergents used (figures 3.4. and 3.5.) However, these complexes may not be of the same nature. Although presence of transfected Irga6 in 150 kDa complex, in the absence of IFNγ induction, suggests that Irga6 proteins could form homooligomers, involvement of other IFNγ-induced proteins as Irga6 binding partner in IFNγ-stimulated cells could be possible as well.

As other IRG proteins are IFNγ-induced, and, therefore, could potentially interact with Irga6 in the IFNγ-induced cells, their running behaviour was analysed in size exclusion chromatography. L929 fibroblasts were induced with IFNγ, lysed in lysis buffer containing 0.1% Thesit and, upon fractionation on the Superose 6

column, IRG proteins were detected on Western blot with the following antibodies: 10D7 (for Irga6), αIGTP (for Irgm3) and A20 (for Irgb6). In contrast to Irga6, Irgb6 ran only at the size of a monomer whereas Irgm3 was present exclusively in the higher molecular weight fractions, as depicted in figure 3.6..

The presence of both Irga6 and Irgm3 in the higher molecular weight fractions indicated the possible interaction of these proteins in the IFNγ-induced cells, which was further characterized.
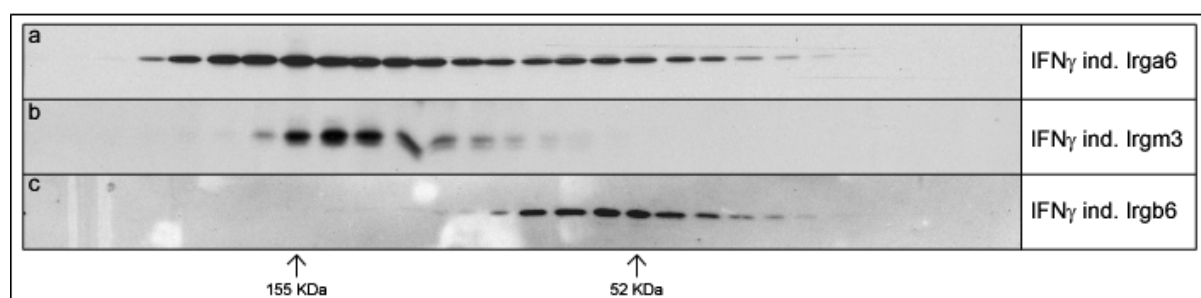
Figure 3.6. Size Exclusion Chromatography of IFNγ-induced IRG proteins in 0.1% Thesit
IFNγ-induced L929 cell lysate was fractionated on the Superose 6 10/300 GL in the presence of 0.1% Thesit/ 3 mM $MgCl_2$/ PBS and analysed by SDS-PAGE and Western blot with respective antibodies: (a) 10D7 (for Irga6); (b) αIGTP (for Irgm3); (c) A20 (for Irgb6).

3.3. Irga6-Irgm3 interactions

3.3.1. Co-immunoprecipitation of Irgm3 with Irga6 (in collaboration with Julia Hunn)

In order to further analyse a possible interaction between Irga6 and Irgm3 proteins, a series of co-immunoprecipitation experiments was conducted. gs3T3 fibroblasts, induced with IFNγ or left untreated, were lysed at 4°C in buffer containing 0.1% Thesit in the absence of nucleotide or in the presence of 0.5 mM GDP or GTPγS. Lysates were incubated with Protein A sepharose beads coupled with rabbit polyclonal serum 165. Bound proteins were eluted by incubation in 100 mM Tris/HCl pH 8.5/ 0.5% SDS for 30 min at RT. Eluates were boiled for 5 min in SDS-PAGE

sample buffer, subjected to SDS-PAGE on 7.5% polyacrylamide gels and Irga6 and Irgm3 detected with 10D7 and αIGTP antibodies, respectively, on Western blot.

Figure 3.7. presents results of two independent experiments and shows that Irga6 can co-immunoprecipitate Irgm3 from IFNγ-induced cell lysate in the absence of any exogenous nucleotide and, to a lesser extent, with additional 0.5 mM GDP. Importantly, Irga6-Irgm3 interaction was almost completely inhibited in the presence of 0.5 mM GTPγS, the non-hydrolysable form of GTP. There was no unspecific binding of proteins from the non-induced lysates detected by either αIrga6 or αIrgm3 antibodies. In contrast to Irga6, which was strongly precipitated with αIrga6 serum-coupled beads independently of the nucleotide present, co-immunoprecipitated Irgm3 was detected only after long exposure times (5-10 min) suggesting a greatly sub-stoichiometric interaction.
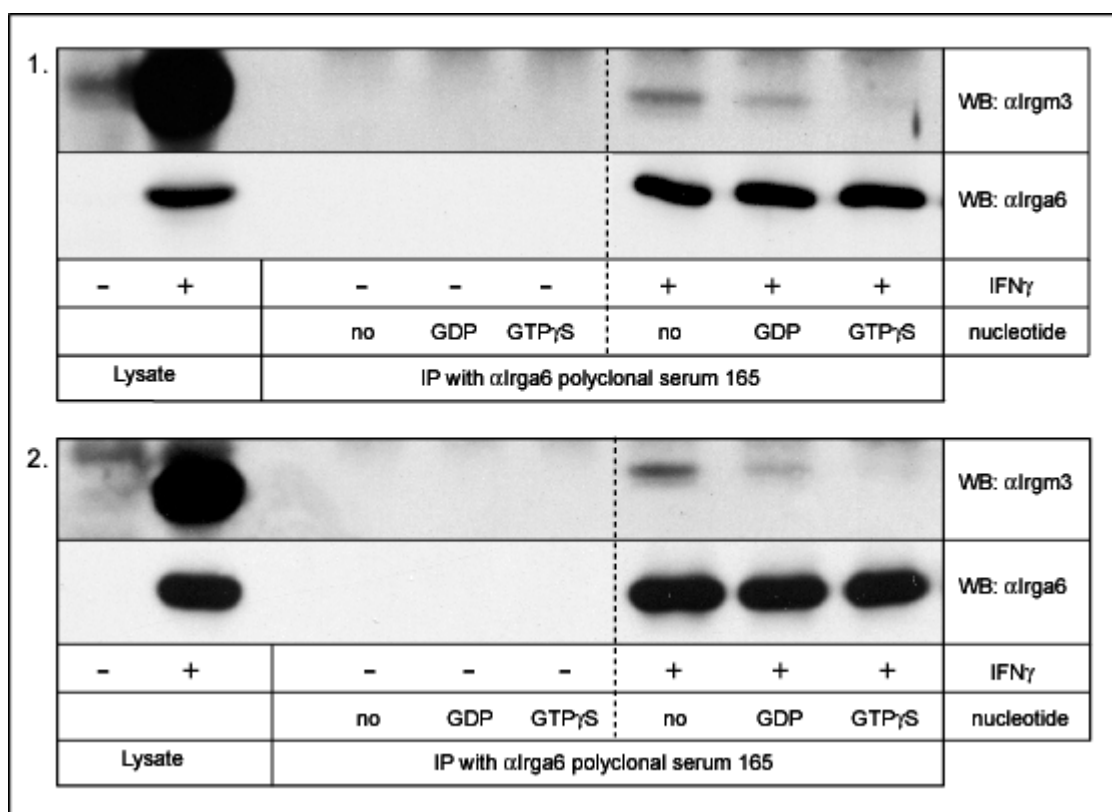
Figure 3.7. Co-immunoprecipitation of Irgm3 with Irga6

gs3T3 cells, induced with IFNγ or left untreated, were lysed in 0.1% Thesit/ 3 mM MgCl$_2$/ PBS in the absence or presence of 0.5 mM GDP or GTPγS. Lysates were incubated with Protein A sepharose beads coupled with αIrga6 polyclonal serum 165. Irga6 and Irgm3 were analysed by SDS-PAGE and Western blot by staining with 10D7 and αIGTP respectively. (1) and (2) represent results from two independent experiments.

The weak signal for co-immunoprecipitated Irgm3 could be explained by the transient nature of the Irga6-Irgm3 complex *in vivo* and /or its strong instability during precipitation procedure. Alternatively, since presence of exogenous GDP decreases the amount of co-immunoprecipitated Irgm3, it could be that Irga6 and/or Irgm3 interact with other IFNγ-induced factors that compete with Irga6-Irgm3 complex formation in the presence of GDP. Finally, since Irga6-Irgm3 interaction is decreased in the presence of GDP and practically absent in the presence of GTPγS, it could be argued that the hydrolysis of GTP is necessary for the Irga6-Irgm3 complex formation.

3.3.2. Pull-down of Irgm3 with GST-Irga6 fusion proteins (in collaboration with Julia Hunn)

In order to confirm co-immunoprecipitation results and, in addition, to analyse the nucleotide state of Irga6 while interacting with Irgm3, pull-down experiments were performed. Fusion proteins GST-Irga6wt, GST-Irga6-S83N or GST alone, expressed in *E. coli* from pGEX-4T2-Irga6wt, pGEX-4T2-Irga6-S83N and pGEX-4T2 vectors respectively, were bound to Gluthathione Sepharose beads. Conjugated beads were preincubated with or without 1 mM nucleotide (GDP, GTPγS or mant GDP) in 5 mM $MgCl_2$/ 1 mM DTT/ PBS for 2 h at RT. IFNγ-induced gs3T3 cells were lysed in 0.1% Thesit/ 3 mM $MgCl_2$/ PBS with or without 0.5 mM GDP, GTPγS or mant GDP for 1 h at 4°C and subsequently mixed with nucleotide-pretreated protein-glutathione sepharose beads. Upon over-night incubation at 4°C, bound cellular proteins were eluted in 100 mM Tris pH 8.5/ 0.5% SDS for 30 min at RT. Eluates were analysed on 10% SDS-PAGE and Irgm3 detected with αIGTP antibody in Western blot. The amount of conjugated beads was visualised by Ponceau S staining of the membrane upon protein transfer. Figures 3.8.(a) and (b) display results of two independent experiments.

Strong signal of Irgm3 was detected upon incubation of IFNγ-induced fibroblasts with GST-Irga6wt in the presence of GDP, as shown in figure 3.8.(a) and (b). Absence of significant Irgm3 signal in the presence of GDP upon pull-down with GST-Irga6-S83N, nucleotide-binding deficient mutant (Hunn, 2007), indicates that the Irga6 has to be in the GDP-bound state in order to interact with Irgm3 (figure 3.8.(b)).

The presence of GTPγS, the non-hydrolysable form of GTP, inhibited the Irga6-Irgm3 association almost completely, confirming that this interaction is GDP-dependent.
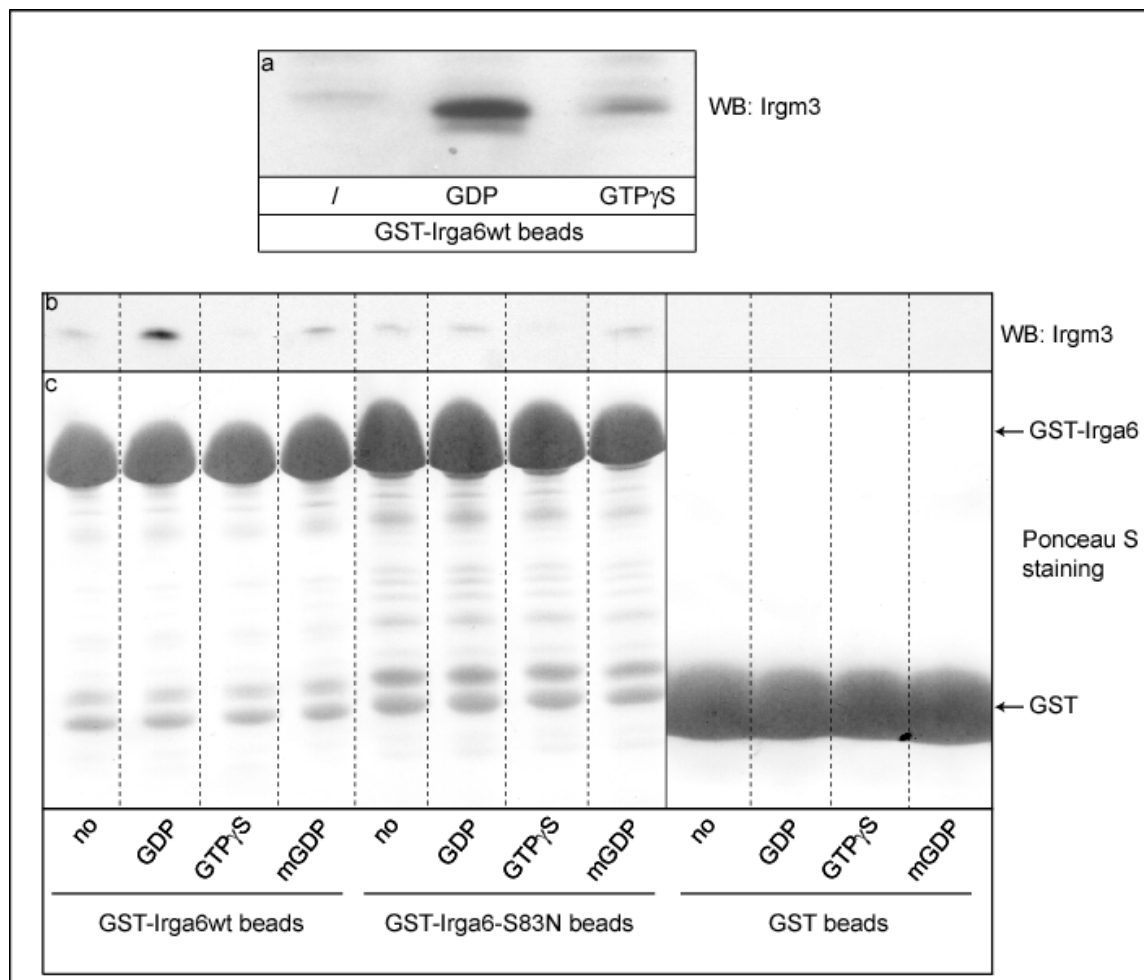
Figure 3.8. Pull-down of IFNγ-induced Irgm3 with GST-Irga6 proteins
GST-Irga6wt, GST-Irga6-S83N and GST proteins were coupled to Gluthathione Sepharose beads and preincubated with or without 1 mM GDP, GTPγS or mant GDP. IFNγ-induced gs3T3 fibroblasts were lysed in 0.1% Thesit/ 3 mM MgCl$_2$/ PBS in the presence or absence of 0.5 mM GDP, GTPγS or mant GDP; (a) and (b): Irgm3 was detected with αIGTP antibody in Western blot; (c): Ponceau S staining of the nitrocellulose transfer membrane.

Nucleotides labelled with mant, a large fluorescent group, interfere with oligomerisation of recombinant Irga6 since the mant group inserts between two binding interfaces preventing protein interaction via GTP-binding domains (Pawlowski, unpublished data). Since the incubation of fibroblast lysate and GST-Irga6wt beads with mant GDP reduced Irgm3 signal to the basal level (figure 3.8.(b)),

it is likely that the GDP-dependent Irga6-Irgm3 interaction happens via GTP-binding domains of these proteins. In pull-downs with both GST-Irga6wt and GST-Irga6-S83N a weak nucleotide-independent signal for Irgm3 was detected in the absence of nucleotide or in the presence of GDP and mant GDP, but not in the presence of GTPγS (figure 3.8.(b)). This difference in Irgm3 signal strength was not due to unspecific binding of Irgm3 protein to the gluthathion sepharose beads, since incubation of Irgm3-containing cell lysates with GST-coupled beads resulted in no Irgm3-specific staining. It rather represents the basal affinity of these molecules that is independent of their nucleotide state. In addition, results described above are not affected by varying amount of GST fusion protein determined by Ponceau S staining in figure 3.8.(c).

Pull-down experiments, using GST-Irga6 fusion proteins coupled to the gluthathione sepharose beads and IFNγ-induced cell lysates, suggest that Irgm3 and Irga6 interact in the GDP-dependent manner. Only in the presence of GDP Irga6 and Irgm3 interacted strongly, over the background level seen in figure 3.8.(b). Since nucleotide-binding deficient Irga6-S83N mutant could not form strong interaction with Irgm3, it is probable that Irga6 has to be in GDP-bound form in order to interact with Irgm3. Practically no interaction between Irgm3 and Irga6 proteins was detected in the presence of GTPγS, which traps molecules in the GTP-like state. This result allows the possibility that Irga6 and/or Irgm3 molecules, when activated, could have other binding partners.

3.4. Irga6 nucleotide-dependent self-interactions

3.4.1. αcTag1 immunoprecipitation

Presence of transfected Irga6 in a 150 kDa size complex in size exclusion analysis (figure 3.4.(c)), in the absence of any other IFNγ-induced protein, suggested the possibility of Irga6 homointeraction in cells. It has been reported that purified, recombinant Irga6wt *in vitro* can interact with itself and form GTP-dependent oligomers (Uthaiah et al., 2003). However, nothing was known about potential self-interaction of Irga6 molecules *in vivo*.

In order to address this question, a series of co-immunoprecipitions was conducted, in the presence of different nucleotides from detergent lysates of IFNγ-induced or non-induced L929 or gs3T3 fibroblasts. To be able to distinguish Irga6 molecules in the potential homooligomer, a tagged version of Irga6 was generated. This tag was cloned at the C-terminus of Irga6wt and therefore named cTag1. The cTag1 modification of Irga6wt replaces the last two amino acids (RN) with residues KLGRLERPHRD. It is know from *in vitro* and *in vivo* data that Irga6cTag1 has the same biochemical properties as Irga6wt (Uthaiah et al., 2003; Martens et al., 2005), thus, the cTag1 could be considered as a neutral tag. Two specific rabbit polyclonal sera against cTag1 were raised, named 2600 and 2601 and analysed for specificity (data not shown). The 2600 serum was used in further co-immunoprecipitation and immunofluorescence experiments.
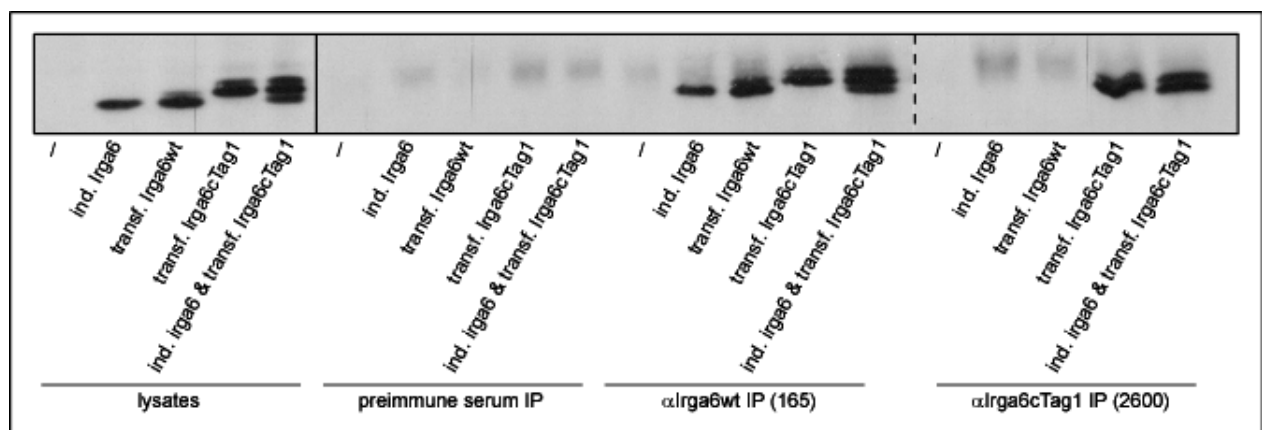
Figure 3.9. Immunoprecipitation of tagged or not tagged Irga6 with 165 and 2600 sera in L929 cells

IFNγ-induced or transfected Irga6wt or Irga6cTag1 were immuoprecipitated either with preimmune, 165 (αIrga6) or 2600 (αcTag1) sera. Irga6 proteins were detected with 10D7 antibody in Western blot.

To test the specificity of αcTag1 serum, IFNγ-induced Irga6, as well as Irga6wt and Irga6cTag1, expressed from transiently transfected pGW1H-Irga6wt and pGW1H-Irga6cTag1 plasmids (further on referred as transfected Irga6wt or Irga6cTag1) in L929 fibroblasts, were immunoprecipitated with preimmune serum, αIrga6-specific 165 or αcTag1-specific 2600 sera. Upon SDS-PAGE, Irga6 proteins were detected with 10D7 antibody in Western blot. Figure 3.9. indicates that the

serum 2600 specifically recognises only cTag1-tagged Irga6 in contrast to the serum 165, which equally well binds to IFNγ-induced or transfected Irga6 proteins, regardless of the tag presence. The specificity of the serum 2600 was retained even when Irga6cTag1 was transfected into IFNγ-induced cells. Upon transfection, Irga6 proteins always appear as a double band in Western blots, independently of the antibody used for detection, where the ratio of the upper band to the lower band varies in intensities. As seen in figure 3.4.(c), in size exclusion chromatography the upper band ran as a monomer in contrast to the lower band, which was also present in fractions associated with higher molecular weight components. Interestingly, both sera were able to precipitate upper and lower form of transfected Irga6 proteins.

3.4.2. Co-immunoprecipitation of IFNγ-induced Irga6 with transfected Irga6cTag1

To analyse the potential interaction between Irga6 molecules in cellular contexts, co-immunoprecipitation experiments were conducted. L929 fibroblasts were either simultaneously induced with IFNγ and transfected with Irga6cTag1 (i+t) or induced and transfected separately and mixed just prior to lysis ((i)+(t)), in order to distinguish if the potential interaction occurs *in vivo*, inside cells or *ex vivo*, during lysis. Cells were lysed in 80 mM OGP/ 3 mM $MgCl_2$/ PBS in the absence of nucleotides or in the presence of 0.5 mM GDP, GTP or GTPγS.

Additionally, cells were preincubated with 300 μM $AlCl_3$ and 10 mM NaF for 30 min at 37°C, prior to lysis, which was done in the presence of $AlCl_3$ and NaF, with or without 0.5 mM GTP. In aqueous solution fluoride and aluminium can form tetrahedral aluminium fluoride complex (AlFx), analog of a phosphate group (Strunecka et al., 2002). *In vitro* data with recombinant Irga6 showed that AlFx could replace the leaving γ-phosphate in the oligomer after GTP hydrolysis and thus lock the protein in the GTP-like bound oligomeric state (Uthaiah et al., 2003). As aluminium fluoride complexes are able to penetrate plasma membranes, incubation of AlFx with intact cells results in binding of AlFx to the GTPases during GTP hydrolysis, keeping them trapped in the GTP-like bound form *in vivo* (Hart et al., 1998). Lysates were incubated with Protein A sepharose beads coupled to the 2600

serum, eluates subjected to the 7.5% SDS-PAGE and Irga6 proteins detected with 10D7 antibody.
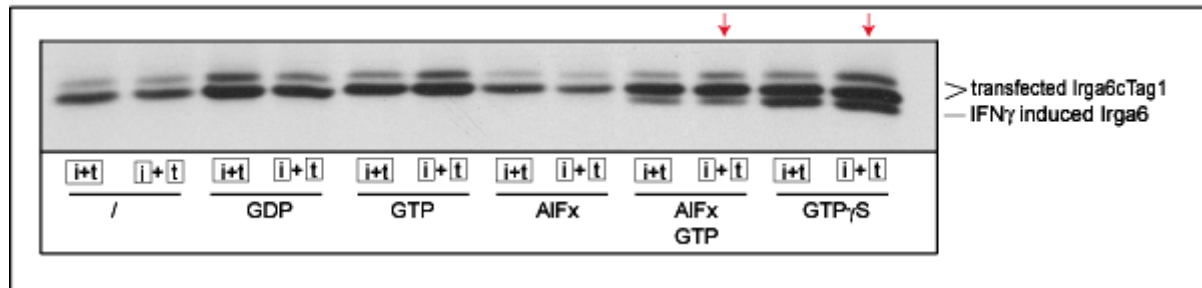
Figure 3.10. Co-immunoprecipitation of IFNγ-induced Irga6 with transfected Irga6cTag1 in lysates of L929 fibroblasts

L929 fibroblasts were either simultaneously (I+t) or separately ((i)+(t)) induced with IFNγ and transfected with Irga6cTag1, lysed in the presence of nucleotides and AlFx, and immunoprecipitated with αcTag1 serum. Irga6 proteins were detected with 10D7 antibody in Western blot.

IFNγ-induced Irga6 could be co-immunoprecipitated with Irga6cTag1 in the presence of GTPγS and in the presence of GTP and AlFx, shown in figure 3.10., indicating that Irga6 can form at least homodimers when the protein is locked in the GTP-bound state. Absence of co-immunoprecipitated endogenous Irga6 in the presence of GTP suggests that, under these conditions, self-associated GTP-dependent Irga6 complexes are disrupted upon GTP hydrolysis that can occur during co-immunoprecipitation procedure. This result confirms that Irga6 GTP-dependent homooligomers can be isolated only if they are trapped in the GTP-bound state. Incubation of cells in the presence of AlFx did not result in detection of Irga6 homooligomers, indicating that, at least in IFNγ-induced cells, Irga6 does not self-associate *in vivo*. This conclusion could be further strengthened by the fact that GTP-dependent homooligomers were built during the cells lysis. Namely, co-immunoprecipitated IFNγ-induced Irga6 could be found in samples that were induced with IFNγ and transfected with Irga6cTag1 separately and mixed prior to lysis ((i)+(t)), both in the presence of GTPγS and GTP with AlFx, implying that Irga6 can form homooligomers during lysis, *ex vivo* (figure3.10., marked with red arrows).

Thus, Irga6, in the presence of IFNγ-induced factors, cannot form GTP-dependent homooligomers in intact cells *in vivo*.

3.4.3. Effect of IFNγ induction on co-immunoprecipitation of Irga6 proteins

As described previously, in IFNγ-induced L929 cells Irga6 interacts with Irgm3 in the presence of GDP but not in the presence of GTPγS, the non-hydrolysable form of GTP. It was tempting to postulate that Irgm3 and/or other IFNγ-induced factors keep Irga6 in an inactive, GDP-bound form. In the absence of these factors Irga6 might get activated thought GTP-binding *in vivo* and be detectible in GTP-dependent oligomers without adding exogenous GTPγS. In order to analyse the effect of IFNγ on Irga6 homointeraction, L929 fibroblasts were either simultaneously induced with IFNγ and transfected with Irga6cTag1 or not induced by IFNγ but double transfected with Irga6wt and Irga6cTag1. Cells were lysed in 0.1% Thesit/ 3 mM $MgCl_2$/ PBS and co-immunoprecipitation was done as described above.

In the IFNγ-induced background, Irga6 could interact with Irga6cTag1 only in the presence of GTPγS and AlFx+GTP (figure 3.11.(a) and (b)). However, in cells that were only transfected, Irga6wt could be co-immunoprecipitated with Irga6cTag1 also in the presence of AlFx alone, depicted by arrows in figure 3.11.(a) and (b), indicating that IFNγ-induced factors prevent self-association, and, thereby, probably the activation of Irga6 in intact cells. Same results were obtained when gs3T3 fibroblasts were used (data not shown). The use of different detergents for cell lysis (Thesit and OGP) did not affect self-interaction of Irga6 proteins. Incubation of lysates in the presence of mant GTPγS almost completely prevents co-immunoprecipitation of Irga6 proteins (figure 3.11.(b)), thus indicating that binding of Irga6 molecules occurs through interaction of GTP-binding domains.

In summary, Irga6 can form GTP-dependent homooligomers in cell lysates, independently of other IFNγ-induced factors, in the presence of GTPγS or GTP and AlFx. Exogenously added GTP and AlFx as well as nonhydrolysable GTPγS trap Irga6 molecules in a GTP-like state and, thus, allow building of GTP-dependent Irga6 homooligomers *ex vivo*. Although this interaction does not reflect the Irga6 state *in vivo*, it does show that cellular Irga6 molecules possess the intrinsic property to self-interact in the GTP-dependent manner.
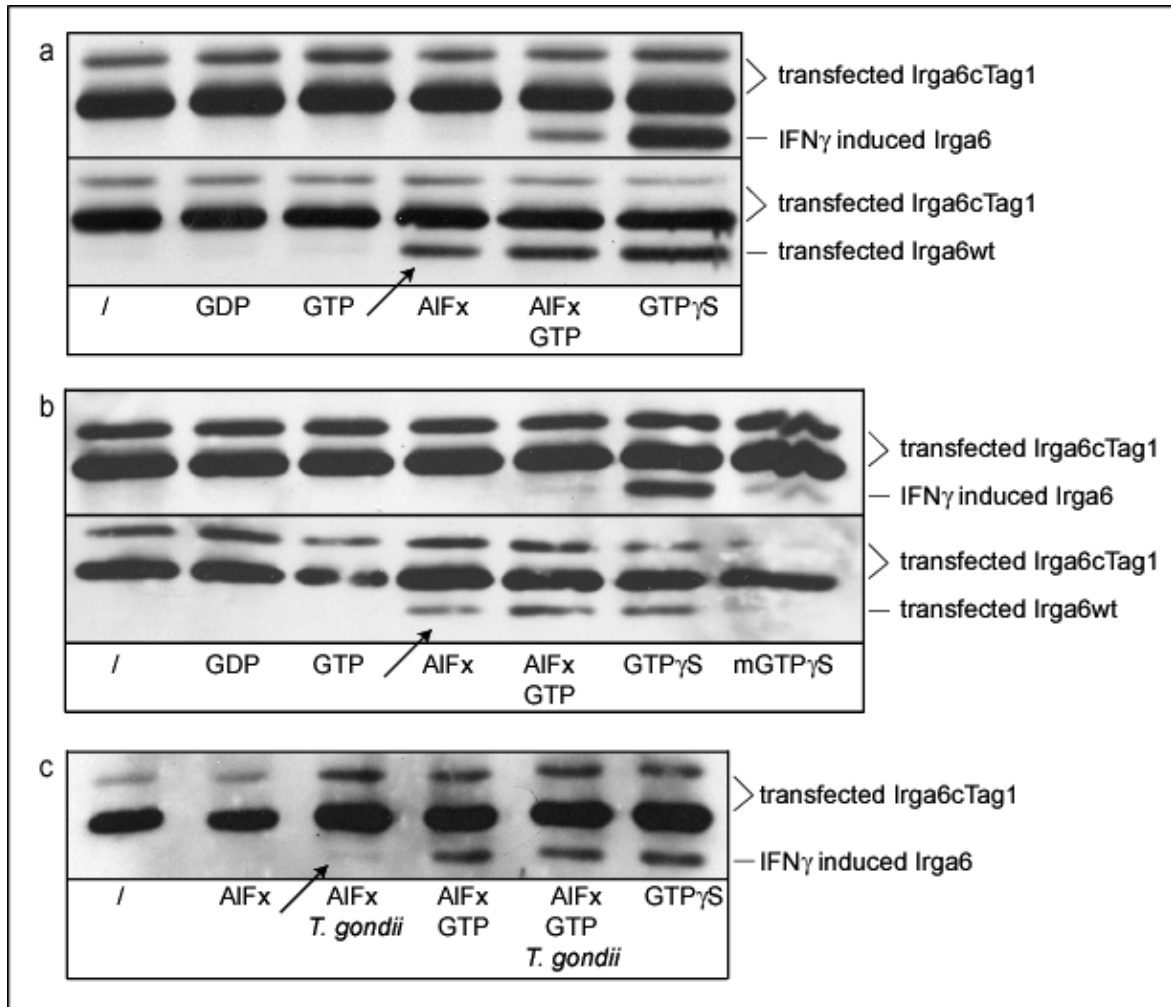
Figure 3.11. Co-immunoprecipitation of Irga6 with Irga6cTag1 in the presence or absence of IFNγ

In (a) and (b), L929 fibroblasts, simultaneously induced with IFNγ and transfected with Irga6cTag1 or double transfected with Irga6wt and Irga6cTag1, were lysed in the presence of nucleotides and AlFx and immunoprecipitated with αcTag1 serum; in (c), gs3T3 fibroblasts, induced with IFNγ and transfected with Irga6cTag1, were infected with *T. gondii* Me49 strain, lysed in the presence of nucleotides and AlFx and immunoprecipitated with αcTag1 serum. Irga6 proteins were detected with 10D7 antibody.

However, incubation of cells in the presence of AlFx alone resulted in trapping of Irga6 homooligomers only in the absence of other IFNγ-induced factors, indicated by the arrows in figures 3.11.(a) and (b). This result demonstrates that Irga6 proteins can indeed form homooligomers in intact cells, *in vivo*, but only if other IFNγ-induced factors are missing. These IFNγ-induced proteins could, therefore, play a role of activation inhibitors for Irga6 molecules, keeping them in an inactive, GDP-bound

form. Irgm3 could be one of these proteins since it appears to interact with Irga6 in the GDP- but not in GTP-bound form, as reported in chapters 3.3.1 and 3.3.2.

When mouse astrocytes (Martens et al., 2005) or gs3T3 fibroblasts (Hunn, 2007) are infected with *Toxoplasma gondii* Me49 strain, Irga6 is rapidly, within few minutes (Khaminetz, unpublished data) translocated to the parasitophorous vacuole (PV). Together with other IRG proteins, Irga6 participates in the destruction of *T. gondii* PV (Martens et al., 2005).To analyse whether under these condition, IFNγ-induced Irga6 can be found in an active, GTP-bound state, gs3T3 cells were simultaneously induced with IFNγ and transfected with Irga6cTag1 for 24 h and subsequently infected for 2 h with Me49 *T. gondii* strain with multiplicity of infection (MOI) of 10. Cells were then lysed in 0.1% Thesit/ 3 mM $MgCl_2$/ PBS and co-immunoprecipitation was done as described above. As shown in figure 3.11.(c), it was indeed possible to visualize a very faint signal of co-immunoprecipitated IFNγ-induced Irga6 in the presence of AlFx alone, indicated by the arrow, leading to the conclusion that, upon infection, IFNγ-induced Irga6 could be activated *in vivo*. However, the amount of co-immunoprecipitated Irga6 was very weak and the result was not always reproducible. Therefore, to analyse the presence of activated Irga6 proteins around *T. gondii* PVM another method has to be employed.

3.4.4. Effect of mutations on co-immunoprecipitation of Irga6 proteins

Recombinant Irga6wt, expressed and purified from *E. coli*, forms GTP-dependent homooligomers *in vitro* (Uthaiah et al., 2003). However, this protein is not myristoylated and, thus, may not reflect the properties of Irga6 proteins expressed in cells. Cellular, myristoylated Irga6 can form homooligomers in the presence of GTPγS, as shown in figure 3.11.. Even though this interaction occurs *ex vivo*, in the cell lysates, it could be used to test the ability of various Irga6 mutants to form GTP-dependent self-associations. Irga6 proteins, with mutations in the N-terminal as well as in the GTP-binding domain, were analysed in their ability to form homooligomers in the presence or absence of GTPγS, in order to confirm that Irga6 homointeraction is indeed GTP-dependent.

Irga6-G2A mutant protein cannot be myristoylated whereas Irga6-Δ7-12 construct, which has the indicated six amino acids deleted, is still able to covalently

bind myristoyl group. From *in vitro* data with recombinant protein, it is known that both K82A and E106A mutants have nucleotide binding properties of a wild type Irga6 but cannot hydrolyse GTP (Pawlowski, unpublished data). On the other hand, the S83N mutant binds both GDP and GTP very inefficiently (Hunn, 2007). Mutations were introduced both in Irga6wt and Irga6cTag1 proteins. L929 fibroblasts were double transfected, lysed in 0.1% Thesit/ 3 mM MgCl$_2$/ PBS and immunoprecipitated in the presence or absence of GTPγS with αcTag1 serum.

As depicted in the figure 3.12., Irga6wt and Irga6-Δ7-12 show strong self-interaction only in the presence of GTPγS. The Irga6-G2A mutant interacts with itself in a GTP-dependent manner but very weakly. However, both K82A and E106A mutants form homooligomers independently of any additional nucleotide. Interestingly, Irga6-E106A mutant ran much smaller in SDS-PAGE than other Irga6 proteins. Finally, the S83N mutant did not show any self-interaction, even in the presence of GTPγS.
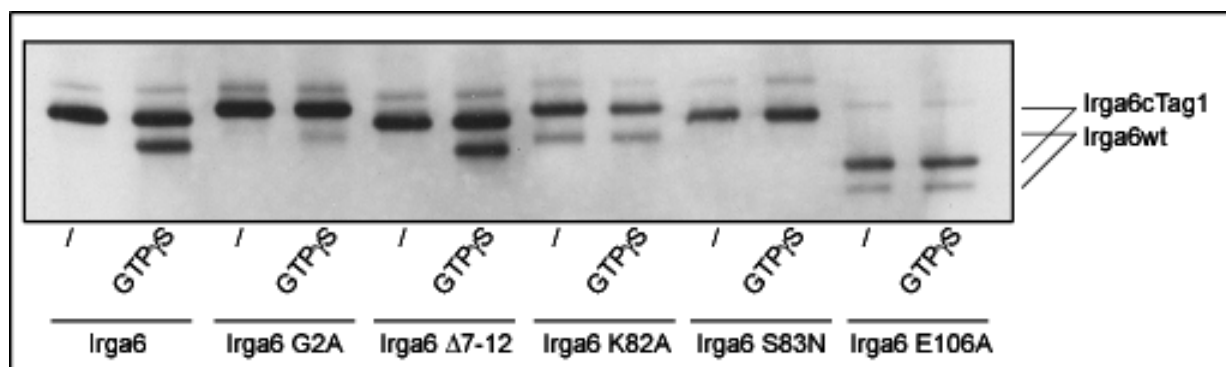
Figure 3.12. Co-immunoprecipitation of Irga6wt and mutant proteins
L929 fibroblasts were double transfected with Irga6wt and Irga6cTag1, with or without mutations. Cells were lysed in the presence or absence of GTPγS and immunoprecipitated with αcTag1 serum. Irga6 proteins were detected with 10D7 antibody in Western blot.

Indeed, Irga6 interacts with itself in a GTP-dependent manner, since mutants that cannot hydrolyse GTP form homooligomers even in the absence of exogenously added GTPγS, probably exploiting cellular GTP. In agreement with that, nucleotide-binding deficient mutant did not exhibit homooligomerisation, confirming the nucleotide-dependent nature of the Irga6 self-interaction. The deletion of six amino

acids (Δ7-12) at the N-terminus of Irga6 did not affect self-association of this protein. In contrast, absence of myristoyl group severely impaired the ability of Irga6 to form homooligomers. Although this effect occurs *ex vivo*, it still might indicate that lipid modification could have a significant role in Irga6 function *in vivo*.

3.5. IFNγ-induced factors are necessary for proper localisation of Irga6

When Irga6 is induced with IFNγ, it is localised in immunofluorescence in a reticular pattern, with the signal overlapping with those of ER proteins like TAP, Calnexin or ERP60 (Martens et al., 2004). In contrast to IFNγ-induced Irga6 (figure 3.13.(a)), transfected Irga6wt, as well as tagged Irga6cTag1, forms small dots or larger aggregates, whose presence is independent of the amount of protein expressed in cells (figure 3.13.(b),(c),(d)).

However, when L929 fibroblast were simultaneously induced with IFNγ and transfected with Irga6cTag1, cells with low amount of transfected Irga6cTag1 showed normal ER-like reticular localisation of exogenous protein, as in figure 3.13.(g). The amount of transfected Irga6cTag1 in these "low transfected cells" roughly equals the amount of Irga6 upon IFNγ-induction.

After quantification, of all cells that were simultaneously induced with IFNγ and transfected with Irga6cTag1, 16.5% showed relocalisation of exogenous Irga6cTag1, and always those with low amount of transfected protein (figure 3.14.(g), whereas high (40.5%) and medium (43%) transfected cells displayed no relocalisation of transacted Irga6cTag1, as in figures 3.14 (e) and (f) respectively. Transfected Irga6cTag1 was detected with rabbit polyclonal αcTag1 serum 2600.

Thus, IFNγ-induced factors are required not only for keeping Irga6 proteins in an inactive form prior to infection (figure 3.11.) but are also necessary for proper, ER localisation of Irga6. This effect of IFNγ is dose-dependent since only cells expressing relatively low amount of Irga6cTag1 show relocalisation of transfected Irga6 proteins.
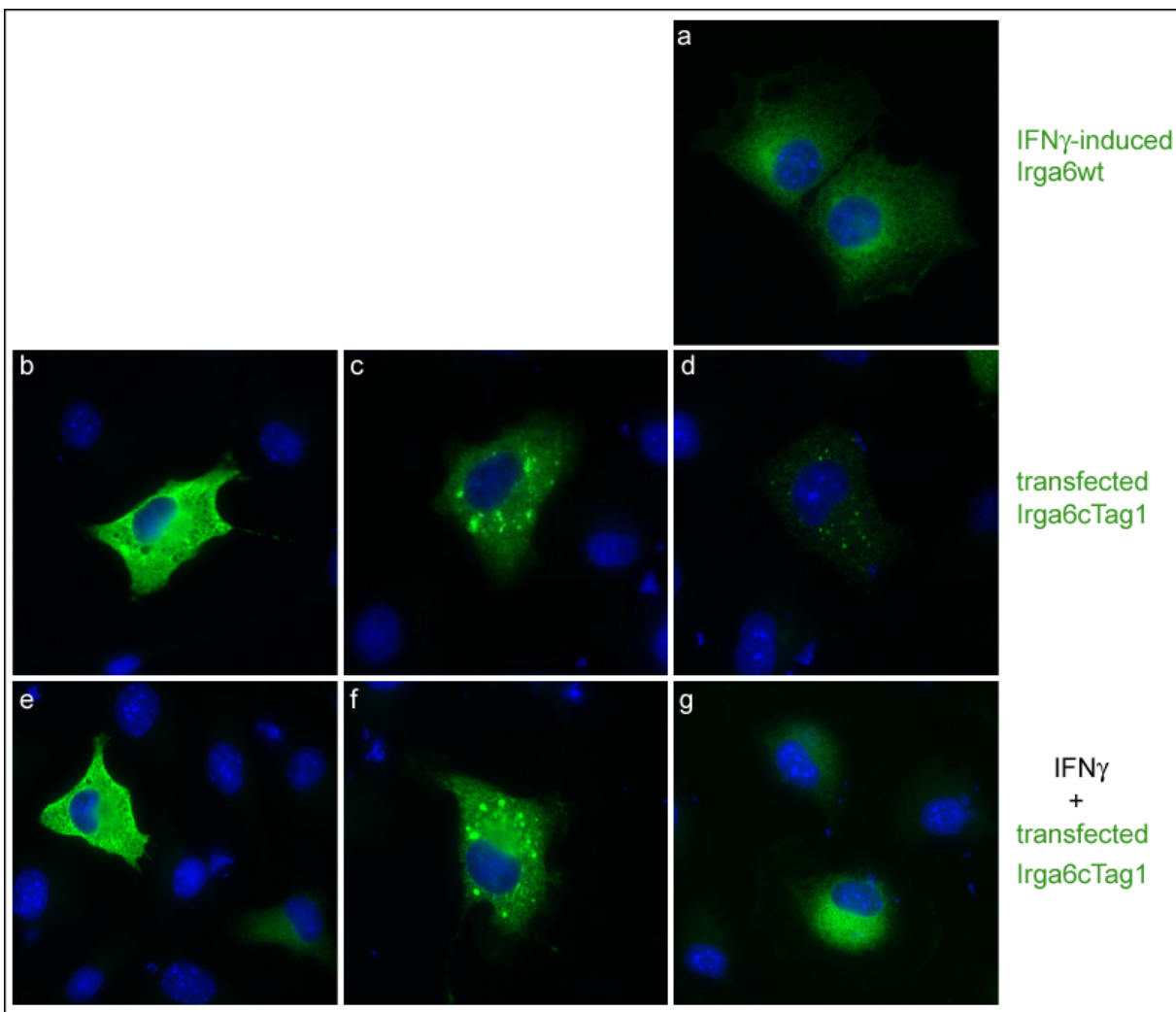
Figure 3.13. Localisation of IFNγ-induced and transfected Irga6cTag1 in L929 cells

Localisation of IFNγ-induced Irga6 (a), transfected Irga6cTag1 without IFNγ (b, c, d) or with IFNγ induction (e, f, g). (b) and (e) represent high transfected cells, (c) and (f) medium and (d) and (g) low transfected cells. IFNγ-induced Irga6 in (a) was detected with αIrga6 10E7 antibody (green); transfected Irga6cTag1 (b, c, d, e, f, g) was detected with αcTag1 serum 2600 (green).

3.6. 10D7 antibody in immunofluorescence recognises transfected Irga6 and Irga6 on *T. gondii* PV but not Irga6 that is relocalised to the ER

IFNγ-induced Irga6 localises to the ER in contrast to transfected Irga6cTag1, which adopt punctual localisation, forming aggregates of different size (figure 3.13.). In the IFNγ-induced cells, transfected Irga6cTag1 can be partly relocalised to the ER. It appears that Irga6 on the ER, either IFNγ-induced or relocalised, is kept in an

inactive, GDP-bound form by GMS proteins. Transfected Irga6cTag1, in the absence of inhibitory effect of GMS proteins, can form GTP-dependent homooligomers *in vivo* (figure 3.11.), and the Irga6-positive aggregates seen throughout the cell might represent this active form of Irga6.
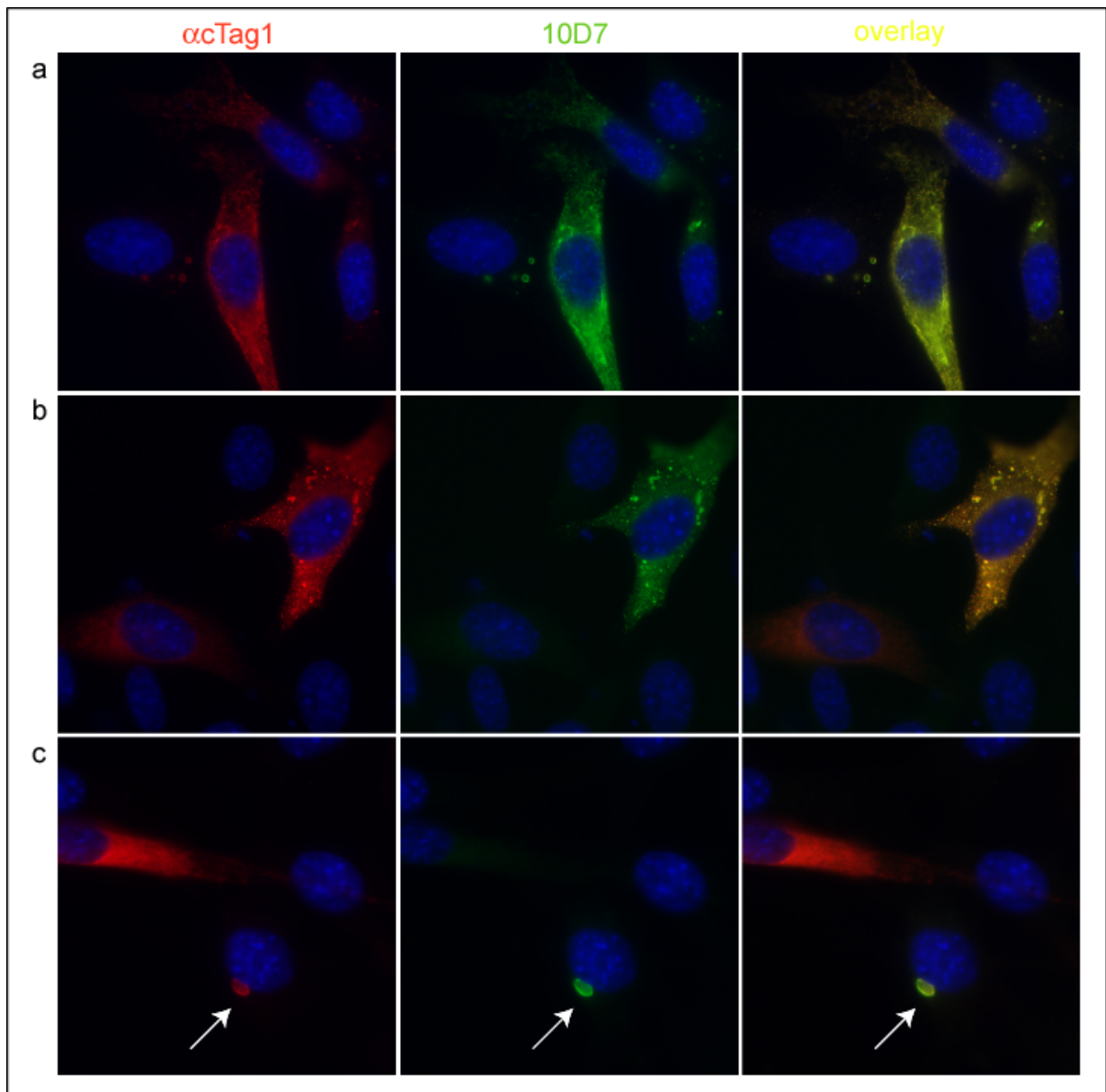
Figure 3.14. Detection of transfected Irga6cTag1 with 10D7 antibody in gs3T3 fibroblasts
(a) cells transfected with Irga6cTag1; (b) cells simultaneously induced with IFNγ and transfected with Irga6cTag1; (c) cells induced with IFNγ and transfected with Irga6cTag1 24 h prior to 2 h infection with *T. gondii* Me49 strain with MOI 8. αcTag1 staining is shown in red and 10D7 staining in green. Parasitophorous vacuole is indicated by the arrow.

Upon infection with *Toxoplasma gondii*, IFNγ-induced Irga6 protein is found at the parasitophorous vacuole membrane (Martens et al., 2005). It is proposed that Irga6 at the PVM is in GTP-bound form and actively participate in the disruption of the parasitophorous vacuole containing *T. gondii* (Martens et al., 2005). However, no formal proof has been reported. Co-immunoprecipitation assay, performed in order to detect GTP-dependent Irga6 homooligomers in *T. gondii*-infected cells *in vivo*, was not efficient (figure 3.11.(c)), implying that another method had to be used to identify potentially activated Irga6 molecules on the PVM.

It has been observed that, in immunofluorescence analysis, 10D7 antibody, one of the αIrga6 monoclonal antibodies, does not recognise IFNγ-induced Irga6 on the ER, but does detect transfected Irga6 (Schroeder, 2005). To analyse whether this antibody binds to Irga6 on the PVM, gs3T3 cells were either transfected with Irga6cTag1 (figure 3.14.(a)), simultaneously transfected with Irga6cTag1 and induced with IFNγ (figure 3.14.(b)) or transfected with Irga6cTag1 and induced with IFNγ 24 h prior to 2 h infection with *T. gondii* Me49 strain with MOI 8 (figure 3.14.(c)). Transfected Irga6cTag1 was analysed by staining with both αcTag1 serum 2600 (red) and with monoclonal antibody 10D7 (green).

As described previously, 10D7 recognised Irga6cTag1 in cells that were only transfected, regardless of the amount of protein present (figure 3.14.(a)). However, 10D7 did not stain relocalised Irga6cTag1 in cells that were simultaneously transfected and induced with IFNγ, whereas aggregated Irga6cTag1 was still detected (figure 3.14.(b)). Transfected Irga6cTag1 accumulating around PV containing *T. gondii* Me49 strain in IFNγ-induced cells was also detected with 10D7 antibody, as shown in figure 3.14.(c).

Since 10D7 antibody binds to mis-localised transfected Irga6 as well as to Irga6 around *T. gondii*-containing vacuoles but not to Irga6 at the ER, it was tempting to postulate that the 10D7 antibody recognises a specific, namely, active conformation of Irga6 *in vivo.* Another option would be that the 10D7 is a low affinity antibody and, thus, efficiently binds only to the densely packed Irga6 molecules in aggregates or around *T. gondii*-containing PV. In order to distinguish between these two possibilities, the binding affinity of 10D7 antibody was analysed further, in comparison with the monoclonal antibody 10E7, which fails to discriminate between IFNγ-induced and aggregated or vacuole-bound Irga6 (Schroeder, 2005).

3.7. 10D7 antibody affinity determination

3.7.1. Purification of 10D7 and 10E7 Fab and Fc fragments

Antibody binding to antigen is noncovalent and reversible and the strength of this interaction is termed affinity (Harlow, 1988). However, overall stability of the antibody-antigen complex depends not only on the intrinsic affinity of an antibody for the epitope but also on the valency of the antibody and antigen. The measure of this overall stability of the complex between antibody and antigen is named avidity.

Most immunochemical procedures involve multivalent interactions, which greatly stabilise immune complexes, resulting in practically irreversible reactions. Antibodies are multivalent and antigens can be also multivalent either because they contain multiple copies of the same epitope (as in homopolymer) or because they contain multiple epitopes recognised by different antibodies. Multimeric interactions allow low-affinity antibody to bind tightly to the antigens, transforming a low affinity antibody to an antibody of high avidity.

10D7, belonging to the IgG1 class of antibodies (Zerrahn, personal communication), is bivalent. Densely packed Irga6 molecules either in aggregates following transfection into uninduced cells, or around *T. gondii* PV, could act as a multivalent antigen in contrast to more distributed, probably monomeric Irga6 molecules bound to the ER in resting cells. If 10D7 is a low affinity antibody, bivalent interaction with Irga6 in aggregates and around PV will increase its avidity and result in strong binding. If that is the case, then papain-cleaved, monomeric 10D7 Fab fragments will not be able to bind efficiently to concentrated Irga6, illustrated in figure 3.15.. In contrast, if 10D7 is a high affinity antibody, its monomeric Fab fragments will retain their strong binding property.

An IgG molecule is a symmetrical dimer consisting of four polypeptide chains: two identical heavy chains and two identical light chains held together by interchain disulfide bonds (Harlow, 1988). Conventionally, antibodies are thought of as having three protein domains, two identical antigen-binding sites called Fab fragments (fragments of antigen binding) connected by a hinge region to an effector domain known as the Fc fragment (crystallisable fragment). Treatment with papain protease results in digestion of the antibody in the hinge region, releasing the two Fabs (consisting of a light chain and N-terminal domain of a heavy chain, bridged by

disulfide bond) and one Fc fragment (consists of two C-terminal parts of heavy chains connected by two disulfide bridges). The principal sites of papain cleavage are found an the amino-terminal side of the disulfide bonds that hold the light and the heavy chains together thus resulting in release of two Fab fragments with molecular weight of around 45-55 kDa and one Fc fragment of 50 kDa, under non-reducing conditions (figure 3.18.). However, mouse monoclonal antibodies from the different classes show a wide degree of variation of secondary papain cleavage sites in the flexible hinge region, which usually results in a presence of additional fragments of different sizes.
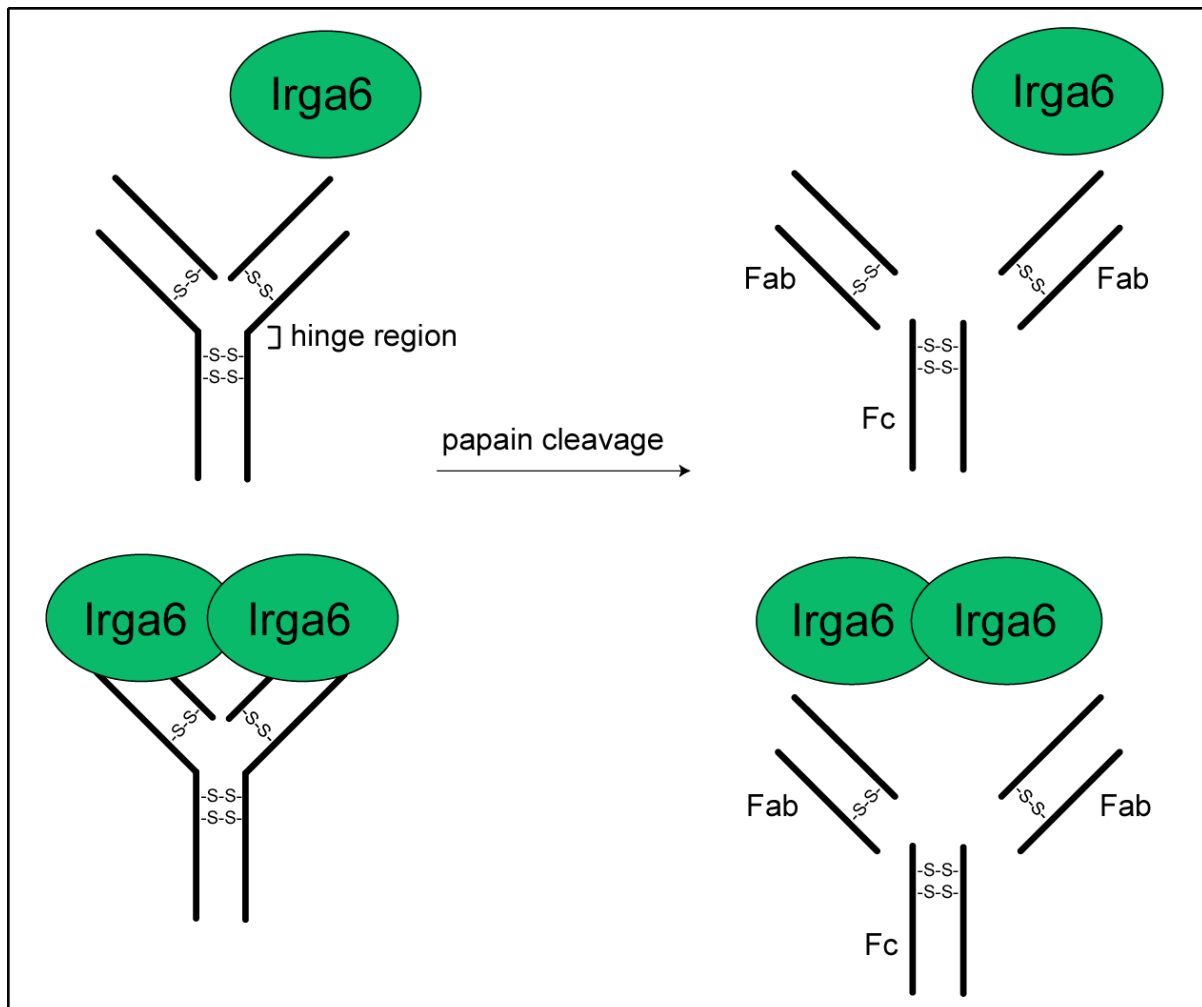
Figure 3.15. Properties of a low affinity antibody
If 10D7 is a low affinity antibody, bivalent interaction of 10D7 with Irga6 in aggregates and around PV will increase the avidity of the complex and will result in strong binding. However, its papain-cleaved Fab fragments will not be able to bind efficiently to the densely packed Irga6 molecules.

To test papain digestion condition, 10E7 antibody was digested with papain (papain: globulin ratio was 1:100) in the presence of 0.01 M cysteine (Gorini et al., 1969). Mixtures were incubated at 37°C for 1 h and at indicated time points (figure 3.16.) 20 µl of sample were taken for cleavage efficiency analysis. The digestion reaction was stopped by adding iodoacetamide to the final concentration of 50 mM and incubation at RT for 30 min. Samples were then boiled in the SDS-PAGE sample buffer in the presence (reducing conditions) or absence (non-reducing conditions) of 5% β-mercaptoethanol. Upon SDS-PAGE, proteins were visualised by staining of gel in Coomassie Brilliant Blue solutions.
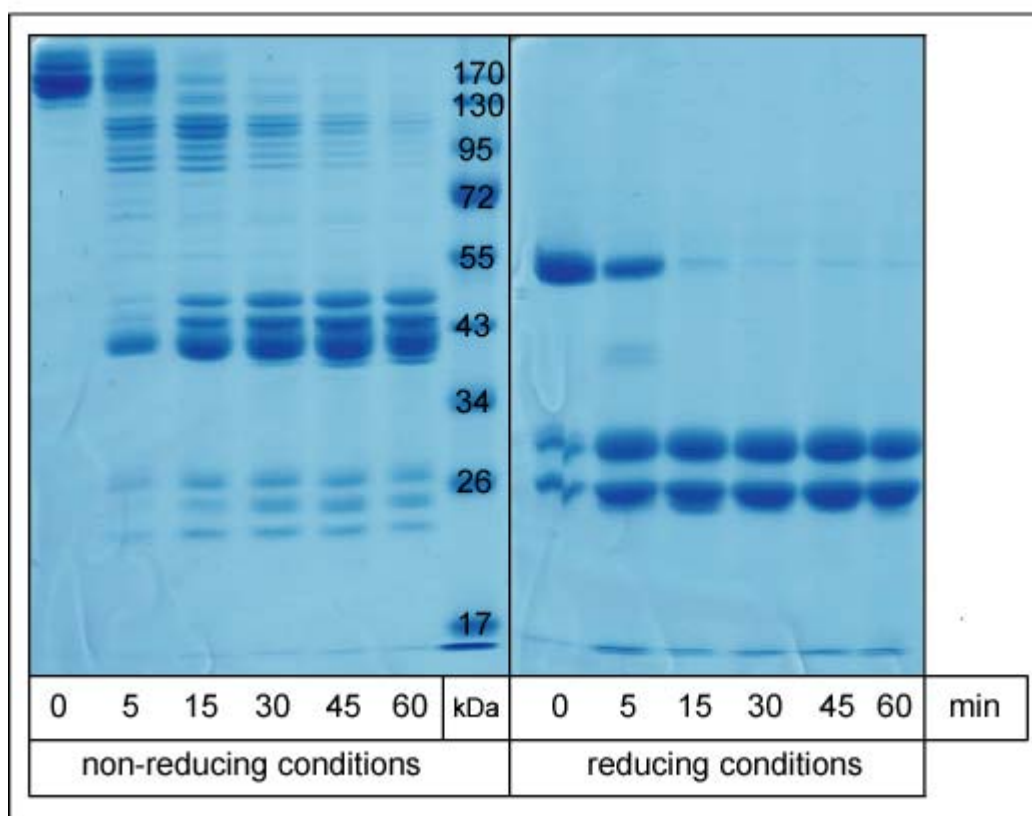
Figure 3.16. Papain digestion of mouse monoclonal 10E7 antibody

10E7 antibody was incubated with papain and 0.01 M cysteine at 37°C and at indicated time points (0, 5, 10, 15, 30, 45 and 60 min) 20 µl of mixture was taken. Reaction was stopped by adding iodoacetamide to a final concentration of 50 mM and incubation at RT for 30 min. Upon boiling in the SDS-PAGE sample buffer in the presence or absence of 5% β-mercaptoethanol and SDS-PAGE, proteins were detected by staining in Coomassie Brilliant Blue solutions.

Figure 3.16. shows that most of the antibody was cleaved in the first 15 minutes of papain digestion, but even after 1 h there was a small amount of antibodies that was only partially digested. Under non-reducing conditions, three major bands between 40 and 50 kDa were observed whereas after boiling in the presence of reducing agent only two bands of 25 and 30 kDa were present.

In order to get more complete digestion of antibodies, both 10D7 and 10E7 antibodies were incubated as described above, but for longer time periods, up to 4 h, and analysed under non-reducing conditions. As figure 3.17. depicts, 2 h incubation with papain was enough to cleave most of the antibodies and those conditions were used in further experiments.
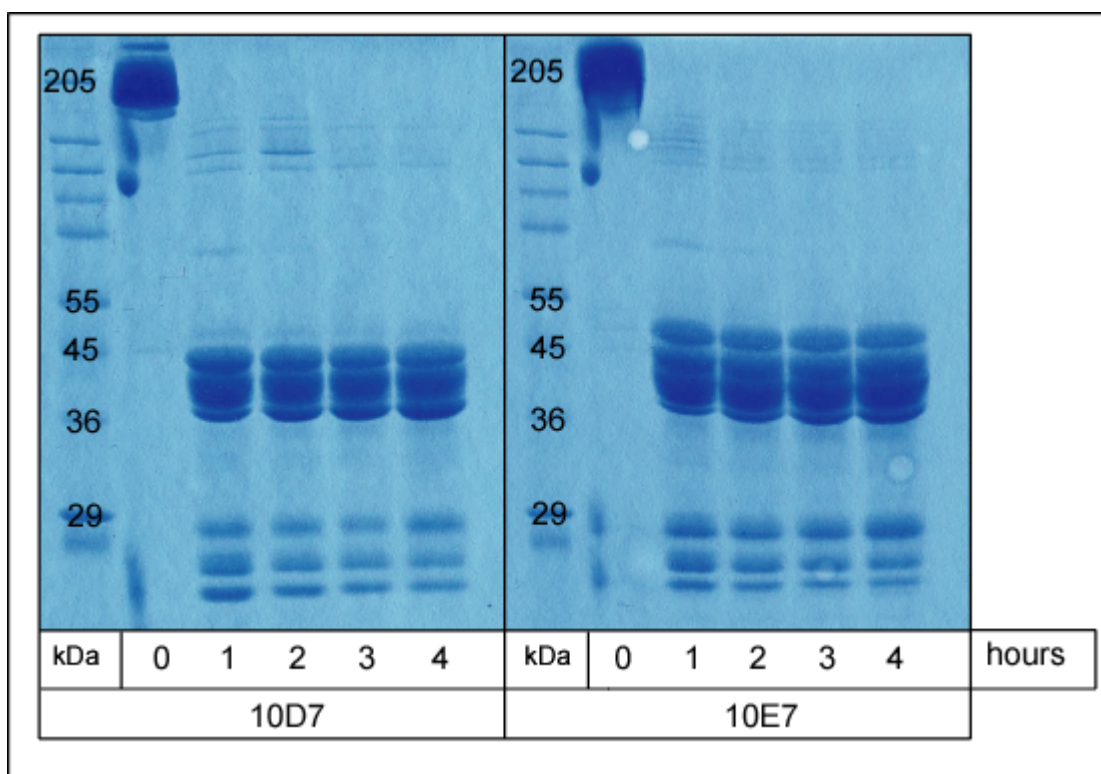
Figure 3.17. Papain cleavage of 10D7 and 10E7 antibodies
10D7 and 10E7 antibodies were incubated with papain at 37°C for up to 4 h. Upon termination of reaction, samples were subjected to SDS-PAGE and stained with Coomassie Brilliant Blue. No reducing agent was used.

To further separate papain-cleaved fragments from non-cleaved whole antibody molecules, digestions were subjected to size exclusion chromatography on

a Superdex 75 column (HiLoad 26/60 Superdex 75 prep grade, Amersham) under non-reducing conditions. This column was chosen for its separation range of 3-70 kDa, thus only monovalent fragments should be separated whereas uncleaved antibody of 150 kDa in size should be excluded.
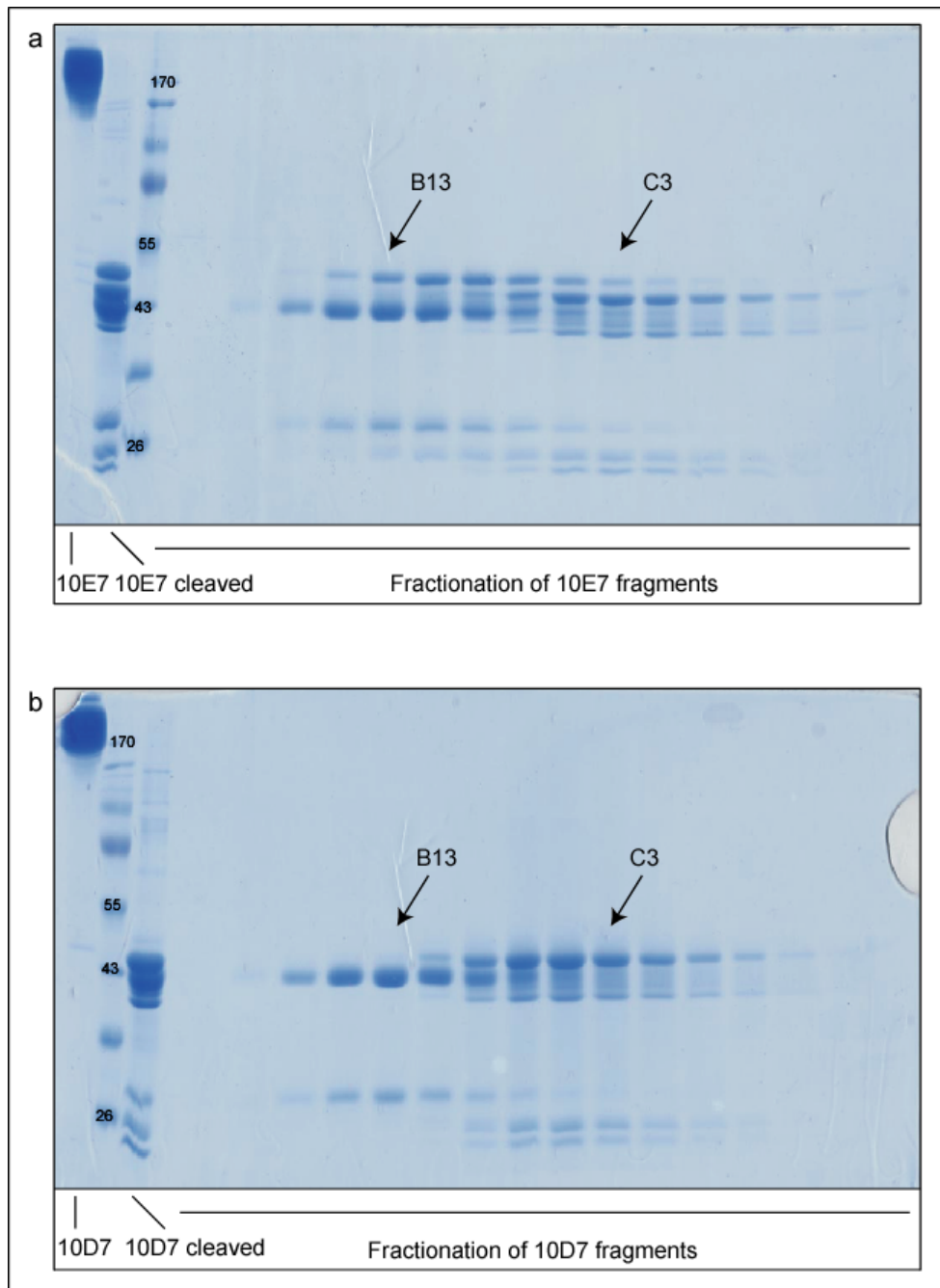
Figure 3.18. Size exclusion chromatography of 10E7 and 10D7 fragments
Papain cleaved 10E7 (a) and 10D7 (b) antibodies were separated on a Superdex 75 column. Fractions were subjected to SDS-PAGE and protein detected by Coomassie Brilliant Blue staining. No reducing agent was used.

Indeed, after size exclusion, there was no trace of uncleaved antibody in fragment fractions detectable by Coomassie Brilliant Blue staining (figure 3.18.). Antibody fragments from both 10E7 and 10D7 were detected in fractions B11-C7, corresponding to sizes 55-42 kDa. In following experiments fractions B13 and C3 were assayed.

3.7.2. Determination of affinity of 10D7 and 10E7 fragments in Western blot

The Irga6 binding affinity of purified 10D7 and 10E7 papain-cleaved fractions, as well as the affinities of whole 10D7 and 10E7 antibodies were analysed in Western blot. Recombinant Irg6wt was loaded on a polyacrylamide gel and blotted on the nitrocellulose transfer membrane. The membrane was cut in strips so that each strip contained a lane with Irga6wt and they were blocked in Western Blocking Reagent (1:10 dilution in PBS) at RT for 1 h. 10D7 and 10E7 as well as 10D7 B13, 10D7 C3, 10E7 B13 and 10E7 C3 fractions (figure 3.18.) were diluted to a concentration of 10 µg/ml (in 1:20 diluted blocking buffer) and that concentration was considered as 1:1. Serial of dilutions of antibodies and their fragments was made further, 1:3, 1:9, 1:27 and 1:81. Each strip was incubated with appropriate antibody dilution and goat-α-mouse HRP-coupled antibody was used as secondary detection reagent (figure 3.19.(a)). Signals were quantified using ImageQuant TL v2005 (Amersham) and plotted against logarithmic values of antibodies in µg/ml as in figure 3.19.(b).

As depicted in figure 3.19.(b), 10D7 antibody showed much higher titre to Irga6 than 10E7 at equal concentration. Interestingly, the titre of the C3 fraction of 10D7, containing only monovalent Fab fragments, was only third of the titre of bivalent 10E7. In the case of both 10D7 and 10E7 antibodies, C3 fractions displayed higher titres for Irga6 than earlier eluting B13 fractions, excluding the possibility that the strong αIrga6 signal originated from trailing of uncleaved antibody during separation on the Superdex 75 column.

Both uncleaved 10D7 and 10E7 antibodies appeared to have higher titres than the C3 fragments. However, the secondary HRP-coupled detection reagent was raised against whole mouse monoclonal IgG antibody. Stronger signals for the native

antibodies could be, at least partially, due to binding of the detection reagent to the constant region of the uncleaved antibodies
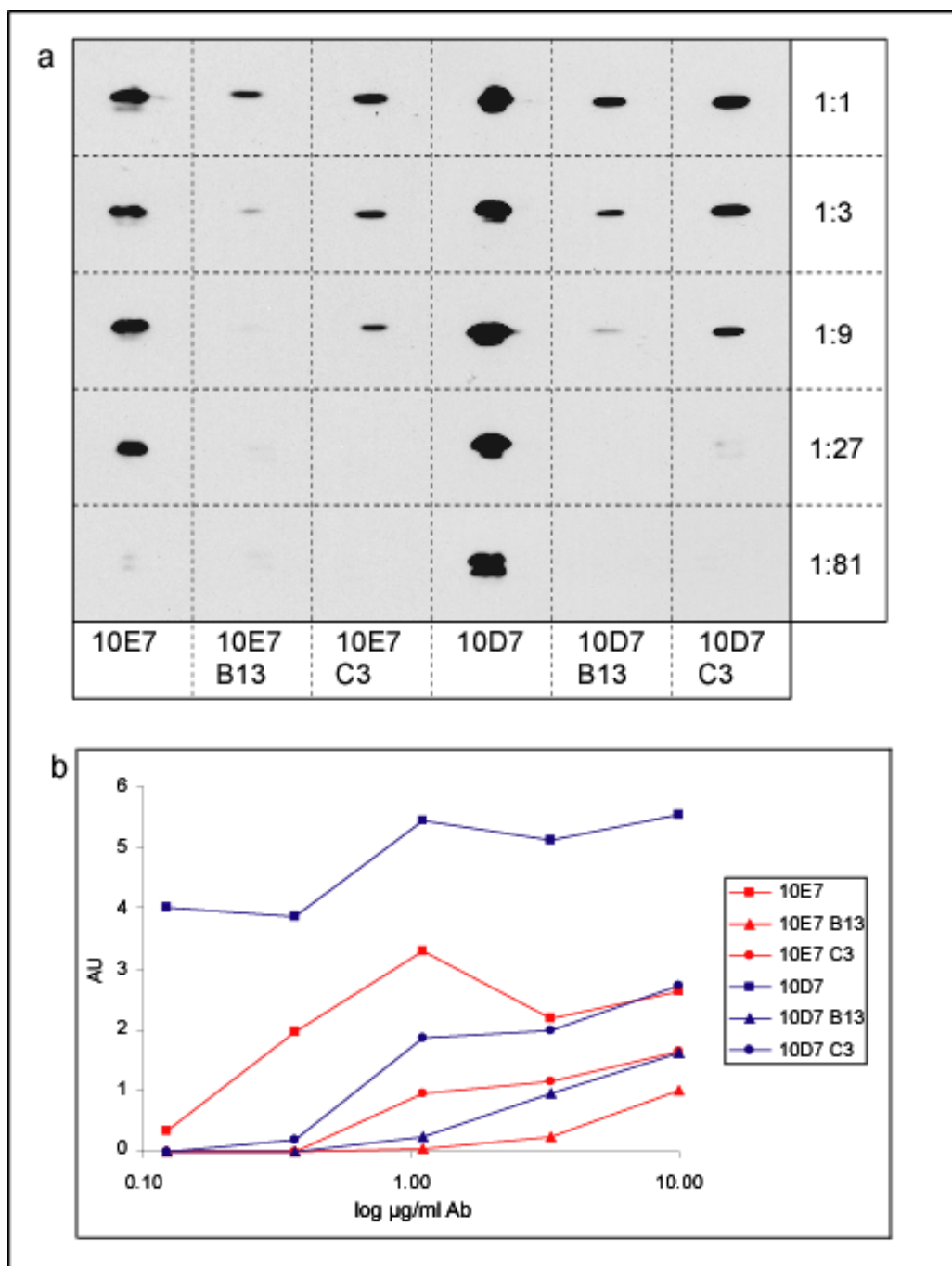
Figure 3.19. Titration of 10D7 and 10E7 fragments on Irga6 Western blot

Affinity of antibodies was analysed by binding to the recombinant Irga6 fixed to the nitrocellulose membrane. 10 µg/ml of antibodies was considered as 1:1 and further dilutions were made, 1:3, 1:9, 1:27 and 1:81. Goat-α-mouse-HRP antibody was used as a secondary detection reagent, (a). Signals were quantified using ImageQuant TL v2005 (Amersham) and plotted against logarithmic values of concentration of antibodies used, (b).

3.7.3. Estimation of the relative affinities of 10D7 antibody and 10D7 C3 fragments in immunofluorescence

In order to compare the behaviour of 10D7 and 10D7 C3 fragments in a biological context, immunofluorescence analysis was conducted. gs3T3 fibroblasts were induced with 200 U/ml of IFNγ for 24 h and then infected with *T. gondii* Me49 strain with MOI 8 for 2 h. Upon fixation, cells were labelled with native 10D7 or 10D7 C3 Fab fragments (both 10 µg/ml) for 1 h at RT. To avoid the fluorescent signal due to the constant region of the uncleaved antibody, a secondary antibody goat-α-mouse kappa light chain-FITC (αkappa) antibody was used. Images were taken with a Zeiss Axioplan II fluorescence microscope equipped with an AxioCam MRm camera (Zeiss) and acquisition times are depicted in figure 3.20. Binding affinity was evaluated by the acquisition time necessary to detect Irga6 signal of equal intensity around *T. gondii* PV.

As seen earlier (figure 3.14.(c)), the 10D7 antibody binds to the Irga6 molecules around *T. gondii* PV. If 10D7 is a low affinity antibody, its Fab fragments (in fraction C3), which are unable to form bivalent interactions with antigens and therefore have low avidity, will bind to Irga6 molecules very inefficiently. This would result in longer exposure time necessary to detect signal of Irga6 around PV with 10D7 C3 fragments compared to noncleaved 10D7 antibody.

However, when secondary α-mouse kappa light chain-FITC antibody was used, Irga6 rings, labelled with the whole 10D7 antibody (figure 3.20.(a)) as well as with 10D7 C3 fragment (figure 3.20.(b)), were detected after 400 ms in both cases. Thus, 10D7 C3 fragment detect Irga6 around PV vacuoles as efficiently as the whole 10D7 antibody, indicating that 10D7 is a high affinity antibody when detecting Irga6 in the vacuole-bound or aggregated state. Thus, the failure of 10D7 to detect non-aggregated Irga6 presumably implies that there is a conformational change between Irga6 molecules in resting, IFNγ-induced state and Irga6 molecules in aggregates or bound to the *T. gondii* vacuole.
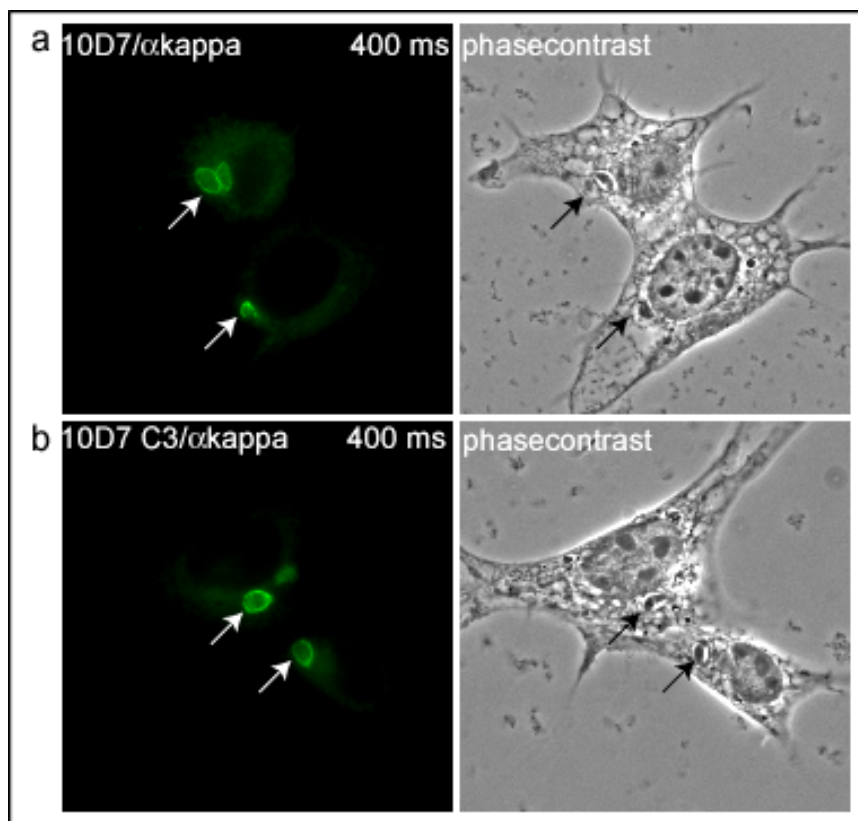
Figure 3.20. Detection of Irga6 rings around PV using 10D7 antibody and 10D7 C3 fragments
gs3T3 fibroblasts were induced with IFNγ and infected for 2 h with *T. gondii* Me49 strain. Irga6 was detected with 10 µg/ml of 10D7 antibody or 10D7 C3 fraction (10D7 C3); as secondary detection reagent goat-α-mouse kappa light chain-FITC (αkappa) was used.

3.8. The 10D7 epitope is located between amino acids 20-25 of Irga6

Previous experiments reported that the 10D7 epitope resides in the first 68 amino acids of the Irga6 molecule (Martens, 2004). In order to locate the epitope of the 10D7 antibody more precisely, various deletion constructs of Irga6wt were cloned into the pEGFP-N3 vector. Constructs pEGFP-N3-Irga6-1-20, pEGFP-N3-1-23 and pEGFP-N3-1-25, containing first 20, 23 or 25 amino acids of Irga6 respectively fused N-terminally of EGFP, were transfected into L929 fibroblasts. The EGFP signal was used to identify transfected cells and the presence of the epitope in these fusion proteins was detected by staining with 10D7 (red).

As depicted in figure 3.21., 10D7 antibody could not bind to the first 20 aa of Irga6 (figure 3.21.(a)), whereas in 30% of transfected cells it did bind to Irga6-1-23

(figure 3.21.(b)). Finally, 100% of cells containing Irga6-1-25 peptide were 10D7 positive (figure 3.21.(c)). This result indicates that 10D7 epitope is largely situated between amino acid 20-25.
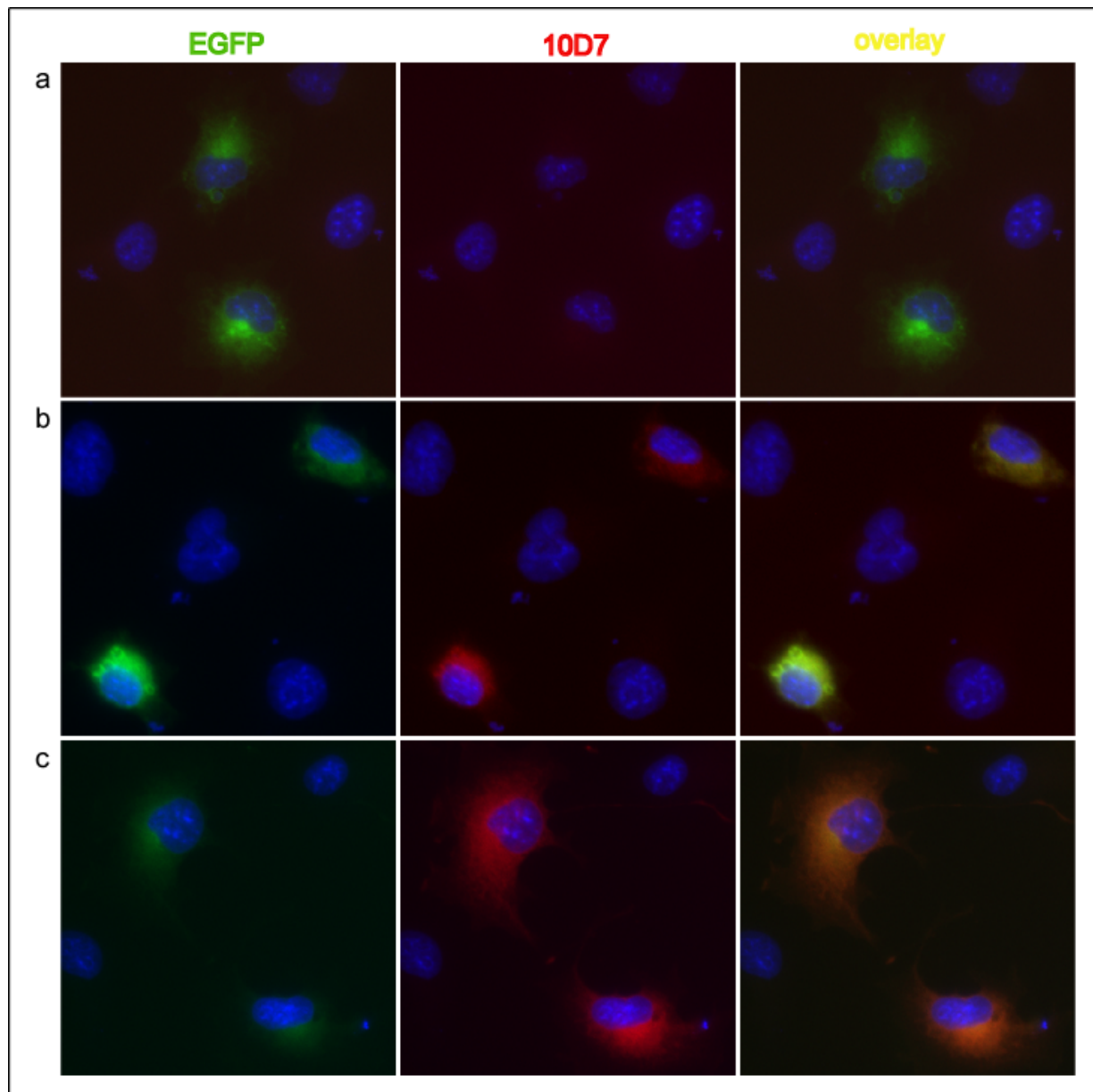
Figure 3.21. 10D7 epitope is between Irga6 amino acids 20-25

L929 fibroblasts were transfected with pEGFP-Irga6-1-20 (a), pEGFP-Irga6-1-23 (b) or pEGFP-Irga6-1-25 (c). EGFP signal was used to detect transfected cells and 10D7 epitope was analysed by staining with 10D7 antibody (red).
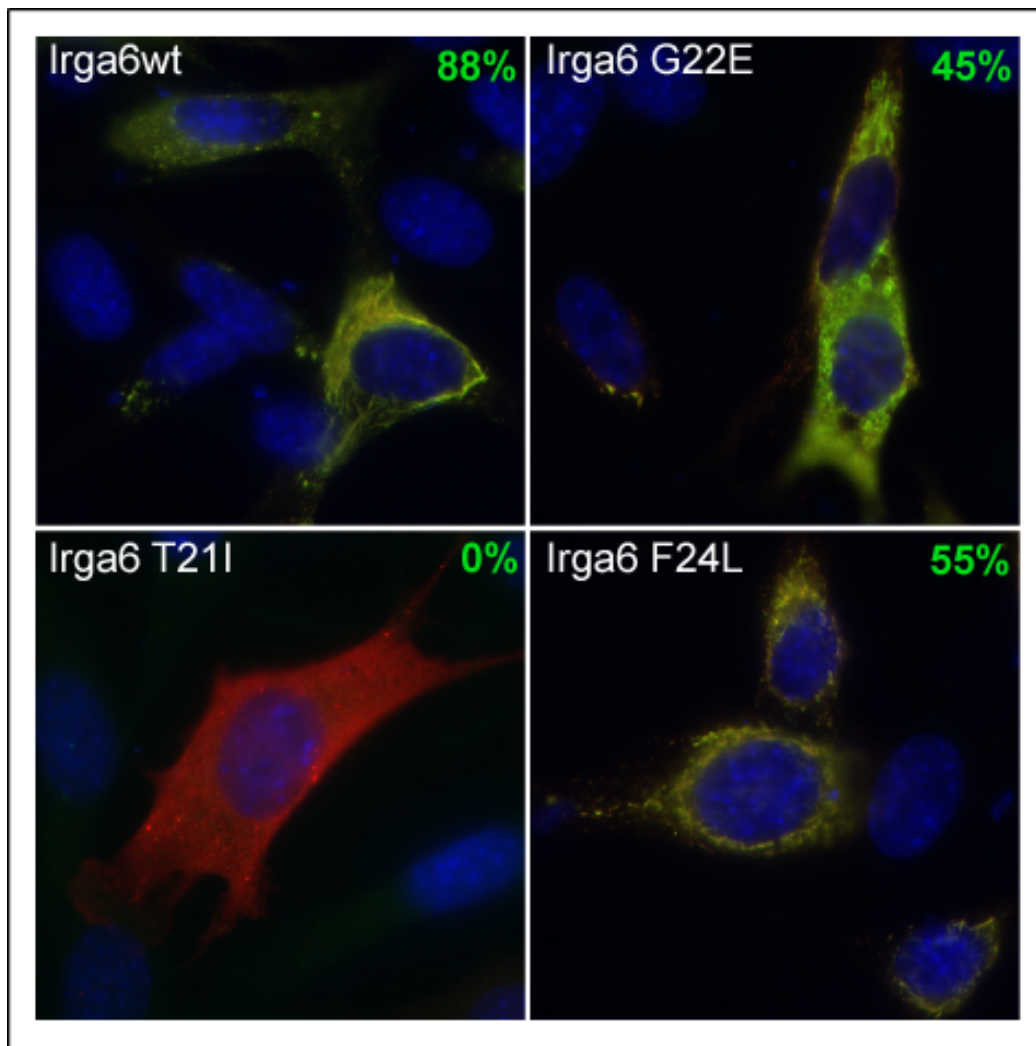
Figure 3.22. Irga6-T21I protein is 10D7-negative

L929 fibroblasts were transfected with Irga6wt, Irga6-T21I, Irga6-G22E and Irga6-F24L. Proteins were detected with αIrga6 serum 165 (red) and 10D7 (green). Only overlays are shown. Numbers represent percentage of transfected cells showing 10D7 positive signal.

In contrast to Irga6, homologues protein Irga2 cannot be detected by 10D7 (Zeng, personal communication). In the region where the 10D7 epitope is located, Irga6 and Irga2 differ in three residues. In order to identify which of them is necessary for 10D7 to bind to the Irga6 molecules, site directed mutagenesis was used to introduce T21I, G22E and F24L mutations into pGW1H-Irga6wt vector, respectively. L929 fibroblasts were transfected with respective constructs, the Irga6 protein detected with αIrga6 serum 165 (red) and 10D7 (green) and overlays depicted in

figure 3.22. The 165 serum was used to detect transfected cells and the number of 10D7 positive cells for each construct was determined.

Figure 3.22. indicates that 88% of cells transfected with Irga6wt were 10D7 positive. Cells expressing Irga6-G22E and Irga6-F24L mutant proteins were 45% and 55% 10D7 positive, respectively. In contrast, none of the cell containing Irga6-T21I mutant displayed 10D7 signal, suggesting that the threonine residue in position 21 in Irga6 is the most important for 10D7 recognition.

The 10D7 epitope was also analysed in Western blot. L929 fibroblasts were transfected with Irga6wt, Irga6-G2A, Irga6-Δ2-12, Irga6-Δ7-25 and Irga6-F24L and lysed in 0.1% Thesit/ 3 mM $MgCl_2$/ PBS. Lysates were subjected to SDS-PAGE and Irga6 proteins were detected with monoclonal mouse antibodies 10D7 and 10E7.

Figure 3.23. shows that deletion of amino acids 7-25 and F24L mutation resulted in complete or almost complete loss of 10D7 epitope, respectively. Deletion of amino acids 2-12 or the absence of the myristoyl group in Irga6-G2A mutant had no effect on the 10D7 recognition, thus excluding the involvement of the very N-terminal region of Irga6 protein in the 10D7 epitope.
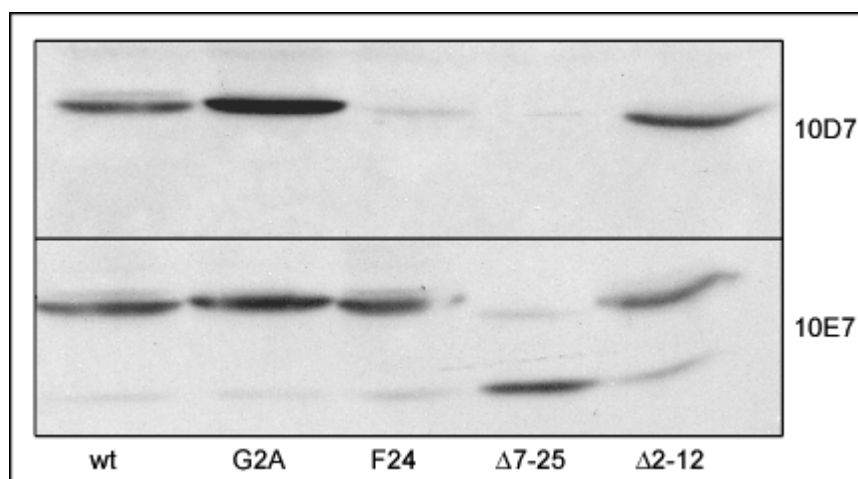
Figure 3.23. Western blot analysis of the 10D7 epitope
L929 fibroblasts were transfected with Irga6wt, -G2A, -F24L, -Δ7-25 and -Δ2-12 constructs and lysates run on SDS-PAGE. Proteins were detected with 10D7 and 10E7 antibodies.

In conclusion, the 10D7 epitope is located between amino acid 20-25 in Irga6 molecule, where the mutation of threonine at position 21 to isoleucine shows the

strongest effect on 10D7 binding. The myristoyl group and first 12 N-terminal amino acids of Irga6 protein are not part of the 10D7 epitope, as illustrated in figure 3.23..

The exact position of the epitope in the structural model of Irga6, as well as orientations of side chains of T21, Y23, F24 and K25 amino acids, are depicted in red in figure 3.24.(a) and (b) respectively. T21 and K25 residues point to the solvent, whereas Y23 and F24 residues are located in the interhelical space, between helices αB, αC and αF. The fact that the epitope is a part of the first α helix in Irga6 molecule suggests that the GTP-binding domain itself is excluded from the 10D7 recognition sequence.
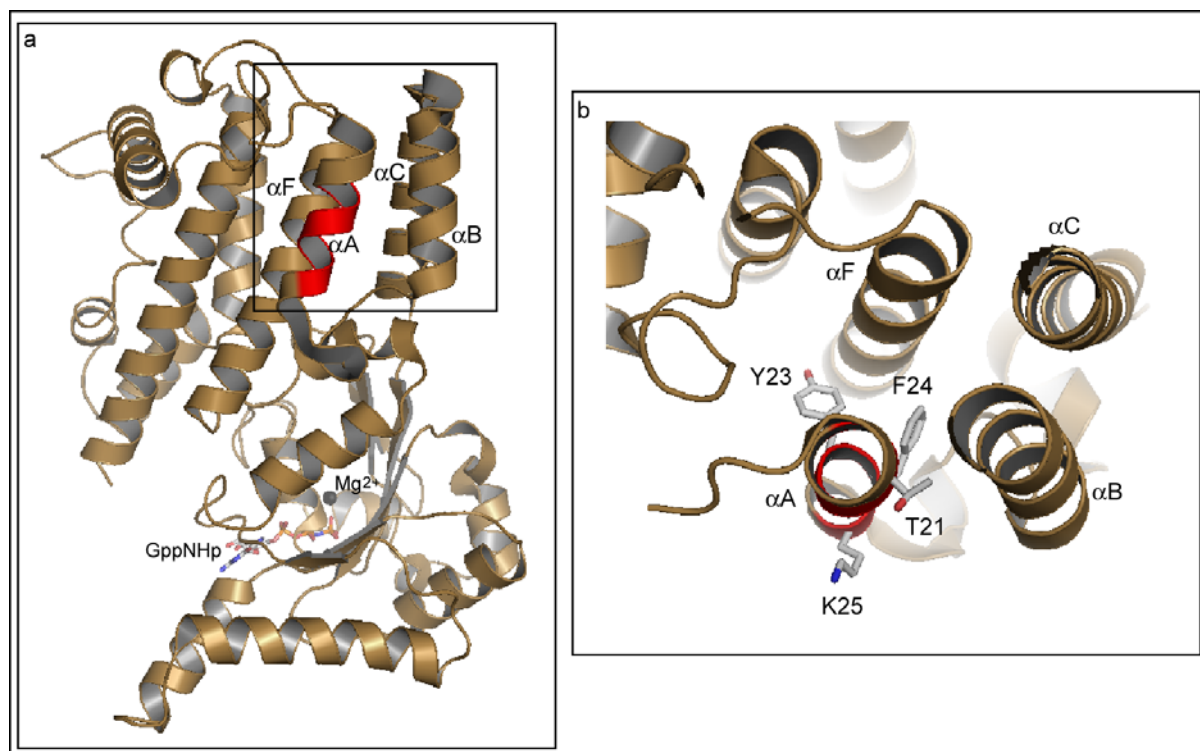
Figure 3.24. Location of the 10D7 epitope in the Irga6 molecule

(a) 10D7 epitope, marked in red, includes amino acids 20-25 but not the myristoyl group, first 12 N-terminal amino acids nor the GTP-binding domain. GppNHp and Mg^{2+} are shown as atomic stick figure and black sphere respectivly; (b) orientation of side chains of T21, Y23, F24 and K25 amino acids in the Irga6 structure.

3.9. 10D7 immunoprecipitations

3.9.1. 10D7 precipitates Irga6 proteins in the presence of OGP but not in the presence of Thesit

10D7, in immunofluorescence analysis, binds to Irga6 proteins in aggregates and around *T. gondii* PV, but not to the Irga6 in its resting localisation, on ER (figure 3.14.). This is not an effect of aggregation per se since it is not lost in 10D7 Fab fragments (chapter 3.7.). The most possible explanation for the differential binding specificities of 10D7 to monomeric and aggregated or assembled Irga6 would be that it recognises a specific conformation of Irga6 molecule.

To examine this possibility, a series of immunoprecipitation experiments was carried out. Purified recombinant Irga6wt was diluted in buffers containing either no detergent, 80 mM OGP or 0.1% Thesit, using 10% FCS or noninduced L929 cell lysate to block the unspecific binding of protein to Protein A sepharose beads. Samples were incubated with Protein A sepharose coupled to 10D7 (D), 10E7 (E) or no antibodies (/) for 2 h at 4°C. Bound proteins were eluted by incubation in 100 mM Tris/HCl pH 8.5/ 0.5% SDS for 30 min at RT, eluates boiled for 5 min with SDS-PAGE sample buffer and analysed by SDS-PAGE and Western blot. Irga6 was detected by rabbit polyclonal serum 165.
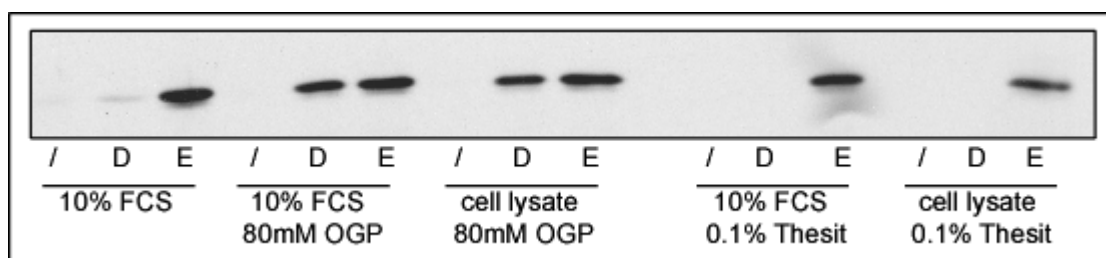
Figure 3.25. Immunoprecipitation of recombinant Irga6wt with 10D7 (D) and 10E7 (E) monoclonal antibodies

Purified recombinant Irga6wt was incubated with Protein A sepharose coupled with 10D7 (D), 10E7 (E) or no antibodies (/) in the presence of OGP, Thesit or without any detergent. FCS or non-induced cell lysate were used to prevent unspecific binding of Irga6 to the beads. Irga6 was detected by rabbit αIrga6 polyclonal serum 165.

10E7 antibody could immunoprecipitate recombinant Irga6wt regardless of detergents present, as shown in figure 3.25.. In contrast, 10D7 could precipitate Irga6 only in the presence of OGP but not in Thesit or in the absence of detergent, indicating that the Irga6 conformation recognised by 10D7 in immunoprecipitation experiments is detergent-dependent.

Effect of detergents on 10D7 immunoprecipitation of IFNγ-induced and transfected Irga6 proteins was analysed next. L929 fibroblasts were induced with IFNγ (ind.) or transfected with Irga6wt (transf.) for 24 h. Cells were lysed in buffers containing either 0.1% Thesit or 80 mM OGP for 1 h at 4°C. In parallel, recombinant Irga6wt (rec.) was diluted in Thesit- or OGP-containing noninduced L929 cell lysate, as mentioned above. Samples were incubated with Protein A sepharose beads coupled with either 10D7, 10E7 or with no antibodies (/) for 2 h at 4°C. Upon incubation of beads in 100 mM Tris/HCl pH 8.5/ 0.5% SDS for 30 min at RT, eluated proteins were boiled for 5 min with SDS-PAGE sample buffer, separated by SDS-PAGE and Irga6 proteins detected by rabbit polyclonal serum 165 in Western blot.
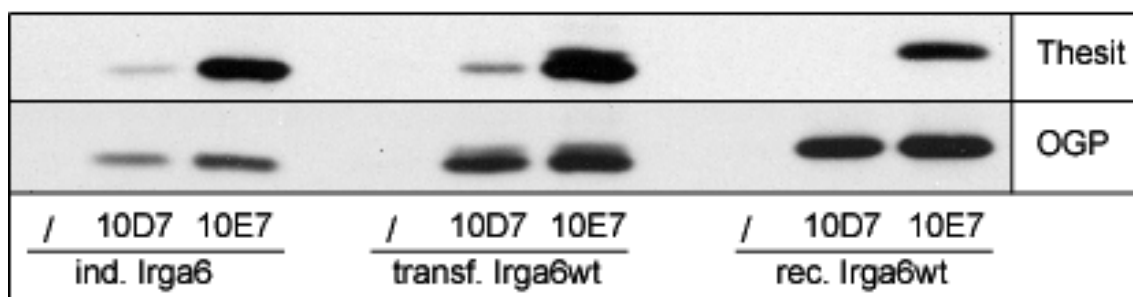
Figure 3.26. Immunoprecipitation of Irga6 with 10D7 and 10E7 in the presence of Thesit or OGP
L929 fibroblasts, induced with IFNγ (ind.) or transfected with Irga6wt (transf.), were lysed in the presence of 0.1% Thesit or 80 mM OGP. Purified recombinant Irga6wt (rec.) was diluted in non-treated L929 cell lysates also in the presence of either Thesit or OGP. Samples were incubated with Protein A sepharose coupled to the 10D7 and 10E7 or no antibodies (/) for 2 h at 4°C. Eluates were subjected to the SDS-PAGE and Irga6 proteins detected by serum 165 in Western blot.

As figure 3.26. indicates, in the presence of OGP, 10D7 and 10E7 immunoprecipitate all Irga6 proteins (IFNγ induced, transfected and recombinant) with the similar efficiency. However, in the presence of Thesit, only 10E7 could efficiently immunoprecipitate Irga6 proteins. 10D7 bound both IFNγ-induced and

transfected Irga6 very weakly and failed completely to immunoprecipitate recombinant Irga6wt, confirming that 10D7 precipitates Irga6 proteins in detergent–dependent manner. As it was mentioned earlier, 10D7 in immunofluorescence does not recognise Irga6 on ER but does bind to transfected Irga6 molecules as well as Irga6 on the parasitophorous vacuoles. Thus, it appears that, in immunoprecipitation experiments, the aggregated or vacuole-bound conformation of Irga6 can be induced by binding of OGP but not by Thesit.

3.9.2. Effect of nucleotide in Irga6 immunoprecipitation by 10D7

IFNγ-induced factors are necessary for proper, ER localisation of Irga6 (figure 3.13.). In addition, the Irga6 protein in the GDP-bound state interacts with a member of the GMS family, Irgm3 (chapter 3.3.). It was tempting to assume that Irga6 in the resting state, bound to the ER, is in an inactive, GDP-bound form. In the absence of IFNγ-induced factors, Irga6 is found localised in dotty structures throughout the cell (figure 3.13.) and can form GTP-dependent homooligomers (figure 3.11.(a)). Finally, GTP-dependent Irga6 homooligomers could be visualized in IFNγ-induced cells upon infection with *T. gondii* (figure 3.11.(c)). As 10D7 stains Irga6 proteins around *T. gondii* PV and in aggregates but not when they are localised to the ER (figure 3.14.), it might be possible that 10D7 recognises the GTP-bound form of Irga6.

The effect of nucleotides on 10D7 immnuprecipitation of Irga6 was tested. Samples, as described above, were incubated with Protein A sepharose coupled with 10D7 or 10E7 in the absence of nucleotides or in the presence of 0.5 mM GDP or GTPγS. Bound proteins were eluted by boiling of beads for 5 min in SDS-PAGE sample buffer and eluates than analysed by SDS-PAGE and Western blot. Irga6 was detected by rabbit polyclonal serum 165.

In the presence of OGP there was no effect of nucleotide, both antibodies immunoprecipitated equally well all Irga6 proteins, shown in figure 3.27. In the presence of Thesit, however, again, there was no precipitation of recombinant Irga6wt by 10D7 antibody. In contrast, 10D7 showed stronger binding to IFNγ-induced and transfected Irga6 in the presence of GTPγS than in the presence of GDP or in the absence of exogenously added nucleotides. In this experiment, low signal for IFNγ-induced and recombinant Irga6 immunoprecipitated by 10E7 in the

presence of GTPγS is probably result of an unequal gel loading. In all other experiments, 10E7 bound Irga6 proteins equally well, regardless of nucleotide or detergent present.

Taken together, it appears that 10D7 antibody, in the presence of Thesit, binds preferentially to the GTP-bound state of IFNγ-induced and transfected Irga6 but, interestingly, not to recombinant protein.
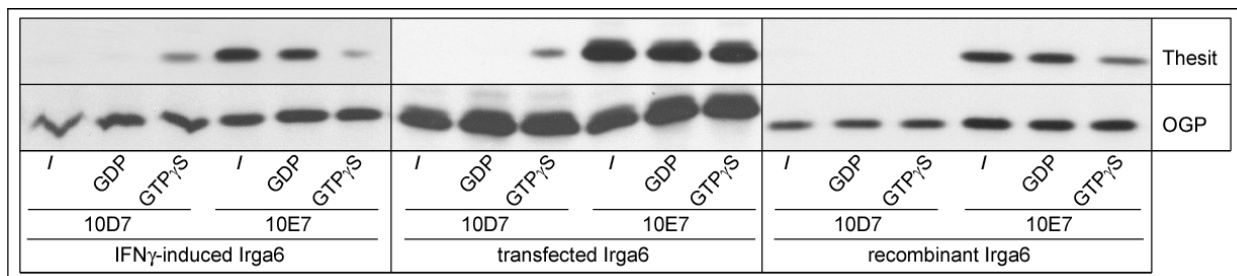
Figure 3.27. Immunoprecipitation of IFNγ-induced, transfected and recombinant Irga6 proteins by 10D7 and 10E7 antibodies in the presence of different nucleotides

L929 fibroblasts, induced with IFNγ or transfected with Irga6wt, were lysed in the presence of 0.1% Thesit or 80 mM OGP. Recombinant Irga6wt was diluted in non-treated L929 cell lysates also in the presence of either Thesit or OGP. Samples were incubated in the absence of nucleotide or in the presence of 0.5 mM GDP or GTPγS with Protein A sepharose coupled to the 10D7 or 10E7 for 2 h at 4°C. Eluates were subjected to SDS-PAGE and Irga6 proteins detected by serum 165 in Western blot.

3.9.3. Effects of detergents on binding of Irga6 to 10D7

The influence of other detergents on 10D7 immunoprecipitation of Irga6 was tested further. L929 fibroblasts were transfected with Irga6wt and lysed in the absence or presence of 0.5 mM GTPγS with different detergents: 80 mM OGP, 0.1% Thesit, 20 mM CHAPS, 1% Triton X-100, 1% Triton X-114, 0,7% SDS or 1% Digitonin (figure 3.28.).

Nonionic detergents Thesit and Digitonin as well as the zwitterionic detergent CHAPS showed nucleotide-dependent immunoprecipitation of Irga6 by 10D7. When lysed with these detergents, Irga6 was immunoprecipitated up to10 times stronger in the presence of GTPγS than in its absence. Thus, results with Thesit, CHAPS and Digitonin suggest that the 10D7 determinant is modified by nucleotide binding.

On the other hand, Irga6 was efficiently precipitated even in the absence of GTPγS in nonionic OGP, Triton X-110, Triton X-114 and ionic SDS, suggesting that these detergents induce the 10D7-exposed Irga6 conformation probably independently of nucleotide.
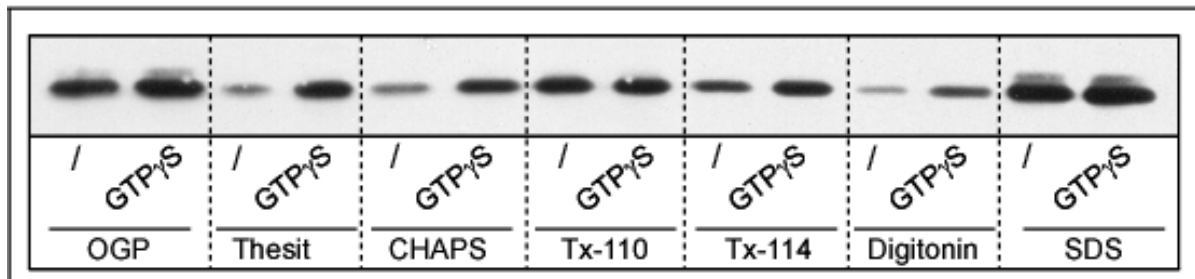
Figure 3.28. Effects of detergents on binding of Irga6 to 10D7
L929 fibroblasts were transfected with Irga6wt and lysed in the absence or presence of 0.5 mM GTPγS with different detergents: 80 mM OGP, 0.1% Thesit, 20 mM CHAPS, 1% Triton X-100, 1% Triton X-114, 0,7% SDS or 1% Digitonin. Bound proteins were eluted by boiling in SDS-PAGE sample buffer and detected with 165 serum in Western blot.

3.9.4. Effects of mutations in Irga6 on binding of Irga6 to 10D7

To confirm that 10D7 antibody preferentially recognises a GTP-bound form of the Irga6 molecule, different Irga6 mutants were tested for their ability to bind to 10D7 in the presence of nucleotides. Two mutations in the G1 binding motif were introduced. Irga6-K82A has wild type nucleotide binding affinity but no GTPase activity, whereas Irga6-S83N essentially binds no nucleotide (Hunn, 2007). In addition, Irga6-E106A mutant was tested, that caries mutation in the primary interaction interface (Pawlowski, unpublished data). This mutant binds nucleotides with the wild type affinities but cannot hydrolyse GTP, similarly to the K82A mutant. In addition, nonmyristoylated Irga6-G2A protein as well as Irga6-Δ7-12 mutant were analysed, in order to study the influence of the myristoyl group and the N-terminus of Irga6 protein on the 10D7 binding.

L929 fibroblasts were transfected with Irga6wt, Irga6-G2A, -Δ7-12, -K82A, -S83N and -E106A respectively. Cells were lysed in 0.1% Thesit, lysates bound to 10D7-coupled beads in the presence of 0.5 mM GTPγS and bound proteins eluted by

boiling. Eluates and 10% of corresponding lysates were subjected to the SDS-PAGE and Irga6 proteins detected with 165 serum in Western blots. Signals from immunoprecipitated Irga6 proteins were normalised to the signal of corresponding lysates (data not shown) and value for imunoprecipitated Irga6wt in the presence of GTPγS set as 100%. Figure 3.29. shows representative immunoprecipitation results and mean values of quantified signals from at least three independent experiments.

10D7 immunoprecipitated Irga6wt in the presence of GTPγS with up to 10 fold higher efficiency than in the absence of exogenous nucleotide. Two mutants, K82A and E106A, which are not able to hydrolyse bound GTP and are expected to be constitutively in GTP-bound state *in vivo*, displayed strong binding to 10D7 independently of nucleotide added. The S83N mutant that, on the other hand, exhibits essentially no GDP or GTP binding, was precipitated by 10D7 very inefficiently, even when GTPγS was added to the lysates.

Therefore, 10D7 indeed recognises GTP-bound Irga6. This leads to conclusion that IFNγ-induced Irga6wt in the resting state is in inactive, GDP-bound form, and therefore unable to interact with 10D7 antibody. Upon infection with *Toxoplasma gondii*, Irga6wt is found accumulating around parasitophorous vacuoles in the active, GTP-bound conformational state, with the 10D7 epitope exposed.

Additionally, Irga6-G2A mutant, that cannot be myristoylated, was precipitated very weakly and only in the presence of GTPγS, indicating that myristoyl group has an important role in GTP-dependent conformational change of Irga6. Finally, Irga6-Δ7-12, lacking six amino acids at the N-terminus, bound to 10D7 in a nucleotide-independent manner, suggesting that this region might be responsible for blocking of 10D7 epitope when Irga6 is in the GDP-bound state.

Thus, 10D7 determinant is positively affected by the presence of the myristoyl group and by GTP binding. It is, however, negatively affected by the residues 7-12 at the N-terminus of the protein. In other words, GTP binding to Irga6 results in a conformational change involving GTP-binding domain, myristoyl group and N-terminal region between amino acids 7-12.
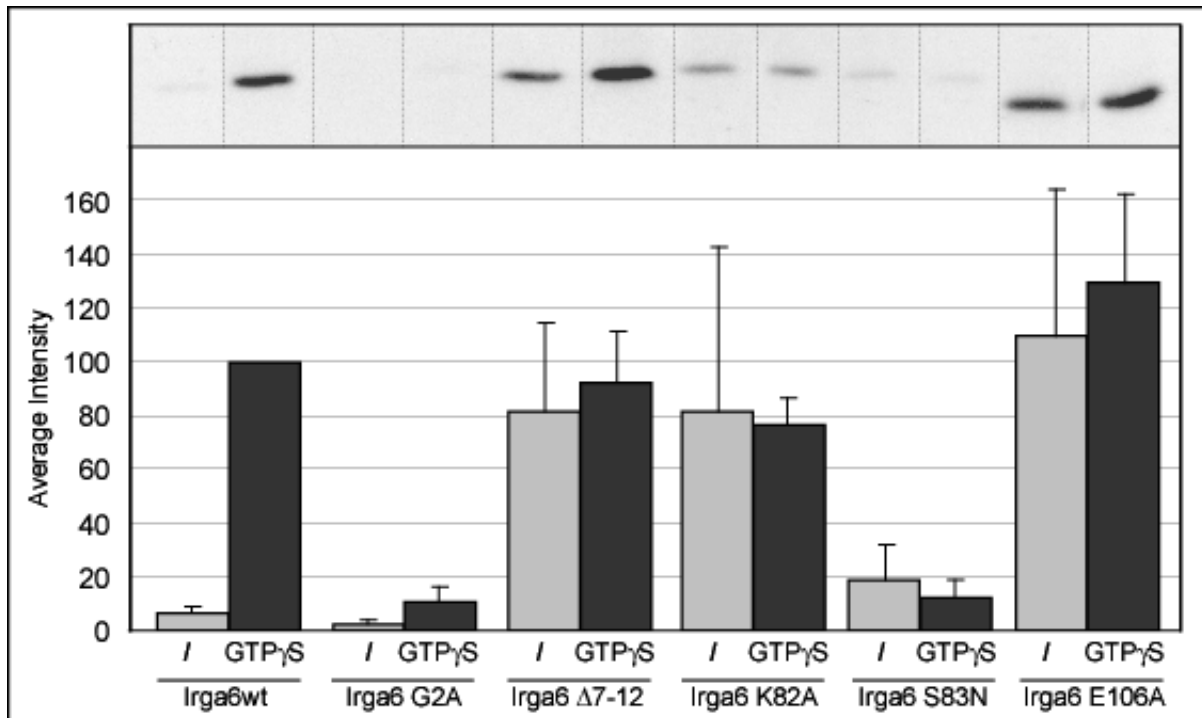
Figure 3.29. Effect of mutations on binding of Irga6 to 10D7

L929 fibroblasts were lysed in 0.1% Thesit in the absence or presence of 0.5 mM GTPγS. Lysates were incubated with Protein A sepharose coupled to 10D7 and bound protein eluted by boiling in SDS-PAGE sample buffer. Eluates were subjected to SDS-PAGE and detected in Western blot by 165 serum. Signals were quantified using ImageQuant TL v2005 and normalised mean values of at least three independent experiments are show in the histogram.

3.9.5. Immunofluorescence analysis of Irga6 mutants

Transfected Irga6cTag1 forms dotty, 10D7-positive structures throughout the cell. However, it can be partly relocalised to the ER in the presence of IFN-induced factors and those relocalised proteins are not stained by 10D7, as illustrated in figure 3.14. (b). In order to confirm that Irga6 bound to the ER is in an inactive form, the following constructs were analysed in immunofluorescence: Irga6cTag1-wt, Irga6cTag1-G2A, Irga6cTag1-Δ7-12, Irga6cTag1-S83N, Irga6cTag1-K82A and Irga6cTag1-E106A. gs3T3 cells were either only transfected (figure 3.30. (/)) or simultaneously transfected and induced with IFNγ (figure 3.30. (IFNγ)). Cells were stained with 10D7 antibody (green) and αcTag1 serum (red), which was used to identify transfected cells. The number of cells that displayed a 10D7 signal was given as a percentage of total number of transfected cells.

As depicted in table 3.1., 100% of cells transfected with Irga6cTag1-wt, were 10D7 positive and they all showed aggregated, dotty localisation of protein. When cells were simultaneously induced with IFNγ and transfected with Irga6cTag1-wt, more than half of transfected cells were 10D7 negative and in those cells transfected Irga6cTag1-wt showed endogenous, ER-like localisation, indicating that relocalised Irga6 is in GDP-bound form.

Irga6cTag1-G2A protein formed very fine and small aggregates that were distributed through the whole cell. Surprisingly, all cells expressing the G2A mutant were 10D7 positive in the absence of IFNγ induction even though it showed inefficient binding to the 10D7 antibody in immunoprecipation experiments (figure 3.29.). Upon IFNγ induction, only about 40% of transfected cells displayed a 10D7 positive signal. Interestingly, the Irga6cTag1-G2A mutant was often found aggregated in the nucleus in the presence of IFNγ induction. The discrepancy between results in immunoprecipitation and immunofluorescence in the case of Irga6cTag1-G2A mutant could be due to the different conditions under which these experiments were conducted. In immunofluorescence analysis, cells were fixed in paraformaldehyde and then permeabilized with 0.1% Saponin, in contrast to immunoprecipitation where cells were lysed in 0.1% Thesit.

	Cells with 10D7 positive signal (%)	
	transfection	transfection + IFNγ induction
Irga6cTag1 **wt**	**100**	**45.51**
Irga6cTag1 **G2A**	**100**	**41.89**
Irga6cTag1 **Δ7-12**	**100**	**79.61**
Irga6cTag1 **S83N**	77.68	47.15
Irga6cTag1 **K82A**	87.64	91.73
Irga6cTag1 **E106A**	86.76	84.78

Table 3.1. Percentage of cells with 10D7 positive signal
Following Irga6 proteins were tested: Irga6cTag1-wt, Irga6cTag1-G2A, Irga6cTag1-Δ7-12, Irga6cTag1-K82A, Irga6cTag1-S83N and Irga6cTag1-E106A. Cells were either transfected or transfected and induced with IFNγ simultaneously. Cells were stained with 10D7 antibody and αcTag1 serum that was used to detect transfected cells. Number of cells with 10D7 signal is given as percentage of total number of transfected cells.

Transfected Irga6cTag1-Δ7-12, even in IFNγ-induced cells, was 10D7 positive in 80-95% of cells, consistent with the fact that deletion of N-terminal amino acids exposes the 10D7 epitope.

Irga6cTag1-S83N proteins showed no aggregation even in the absence of IFNγ induction. Nevertheless, in almost 78% of transfected cells 10D7 signal could be detected. In the presence of IFNγ-induced factors, more then half of Irga6cTag1-S83N transfected cells were 10D7 negative. However, 10D7 staining of Irga6cTag1-S83N was, in general, much weaker in intensity than staining of any other Irga6 protein tested, indicating the weak binding of 10D7 to this mutant.

Around 90% of cells transfected with either Irga6cTag1-K82A or Irga6cTag1-E106A were 10D7 positive, independently of IFNγ induction, and no relocalisation was observed, confirming that Irga6 bound to the ER is in inactive, GDP-bound form in contrast to aggregated, GTP-bound Irga6.
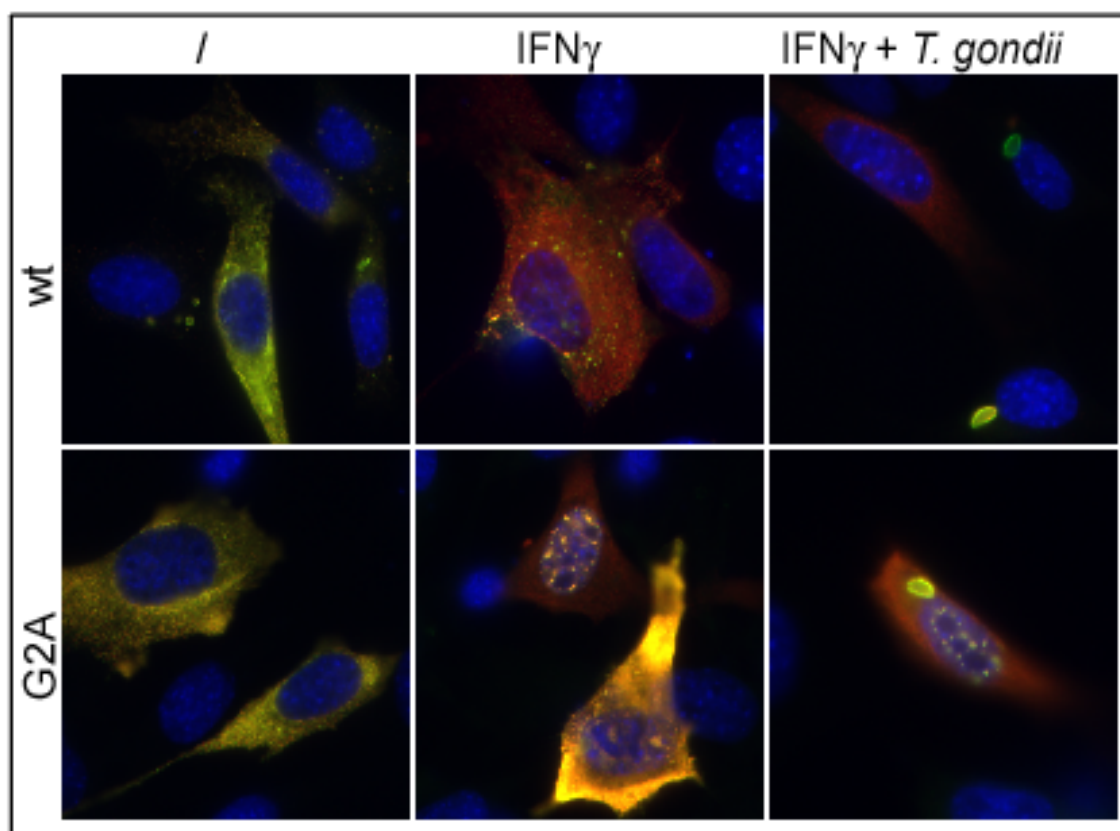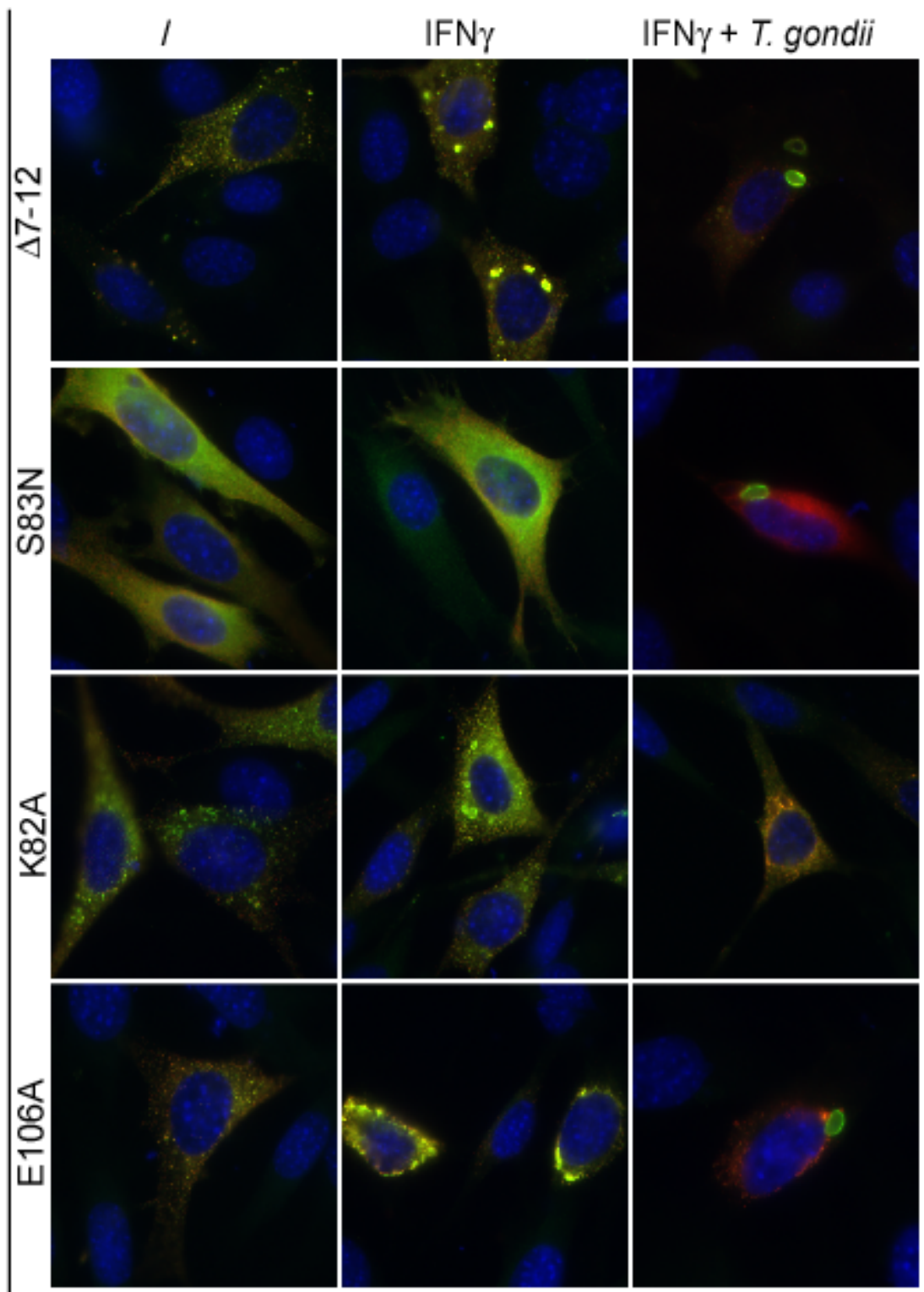
Figure 3.30. 10D7 staining of Irga6 proteins in immunofluorescence analysis

Irga6cTag1-wt, Irga6cTag1-G2A, Irga6cTag1-Δ7-12, Irga6cTag1-S83N, Irga6cTag1-K82A and Irga6cTag1-E106A proteins were tested. gs3T3 fibroblasts were either only transfected (/), transfected and induced with IFNγ (IFNγ) or transfected, induced with IFNγ and infected with *T. gondii* Me49 strain (IFNγ+*T. gondii*). Cells were stained with 10D7 antibody (green) and αcTag1 serum (red) that was used to identify transfected cells. Only overlays are presented.

91

As mentioned earlier, 10D7 antibody recognises Irga6 proteins accumulating around *T. gondii* PV (figure, 3.14.(c)). On the other hand, it has been already reported that Irga6cTag1-K82A protein, which does not hydrolyse bound GTP, act as a dominant negative mutant, preventing wt protein to target to the PV (Martens et al., 2005). Therefore, the ability of other Irga6 mutants to accumulate around *T. gondii* PV and their influence on the endogenous Irga6 was analysed.

gs3T3 fibroblasts were simultaneously induced with IFNγ and transfected with Irga6cTag1-wt, Irga6cTag1-G2A, Irga6cTag1-Δ7-12, Irga6cTag1-S83N, Irga6cTag1-K82A and Irga6cTag1-E106A, respectively, 24 h prior to infection with *Toxoplasma gondii* strain Me49 with MOI 8 (figure 3.30. (IFNγ+*T. gondii*)). Cells were stained with 10D7 antibody (green) and αcTag1 serum (red) and only parasitophorous vacuoles in transfected cells were analysed. Presence of only 10D7 positive ring around PV indicates presence of only endogenous, IFNγ-induced Irga6 protein. In contrast, both 10D7 and αcTag1 staining around PV evidence vacuolar targeting of transfected protein.

	Counted vacuoles	No rings (%)	Only 10D7 positive rings (%)	10D7 and αcTag1 positive rings (%)
Irga6cTag1 **wt**	90	30	0	70
Irga6cTag1 **G2A**	150	46.67	34	19.33
Irga6cTag1 **Δ7-12**	93	28	0	72
Irga6cTag1 **S83N**	91	53.85	46.15	0
Irga6cTag1 **K82A**	117	92.31	0.85	6.84
Irga6cTag1 **E106A**	66	93.34	1.52	4.54

Table 3.2. Determination of number of PV coated with transfected Irga6cTag1 proteins
gs3T3 fibroblasts were simultaneously induced with IFNγ and transfected with Irga6cTag1-wt, Irga6cTag1-G2A, Irga6cTag1-Δ7-12, Irga6cTag1-K82A, Irga6cTag1-S83N and Irga6cTag1-E106A proteins respectivly, 24 h prior to infection with *T. gondii* Me 49 strain. Cells were stained with 10D7 antibody and αcTag1 serum. Only vacuoles in transfected cells were counted.

Table 3.2. illustrates that, when Irga6cTag1-wt and -Δ7-12 proteins were transfected, 70% of PV were both 10D7 and αcTag1 positive. There was no vacuole

with only 10D7 staining found, indicating that Δ7-12 mutation does not prevent PV targeting nor it inhibits accumulation of endogenous Irga6 around PV.

In contrast, 34% of PV in cells transfected with Irga6cTag1-G2A were only 10D7 positive, whereas 19% had both 10D7 and αcTag1 staining. This indicates that the targeting of the Irga6 proteins to the PV strongly depends on myristoyl group.

In cells transfected with Irga6cTag1-S83N, only 10D7 positive rings around PV were found, suggesting that this mutant is unable to relocalise to the PV and that the presence of endogenous Irga6 on the vacuoles is not inhibited.

Both Irga6cTag1-K82A and -E106A mutants exhibit strong dominant negative effect on endogenous Irga6 protein since, in the case of both mutants, only one PV with 10D7 staining was found. In addition, there were few vacuoles with both 10D7 and αcTag1 staining.

Intensities of 10D7 and αcTag1 signal around PV were measured. Images were taken with the same exposure time and the pixel intensities of rings were detected using ImageJ software.

In cells transfected with Irga6cTag1-wt, -Δ7-12, -K82A and -E106A, average intensities of 10D7 and αcTag1 rings for each protein were very similar (figure 3.31.), suggesting the both endogenous and transfected Irga6 proteins are relocalised to the PVM. However, in cells transfected with Irga6cTag1-S83N, no αcTag1 positive ring around PV could be measured confirming the inability of this nucleotide-binding deficient mutant to target PV. In the case of Irga6cTag1-G2A, average intensity of 10D7 rings was twice as strong as intensity of αcTag1 rings, indicating inefficient relocalisation of non-myristoylated transfected protein to the parasitophorous vacuole.

Dominant-negative effect of Irga6-K82A and -E106A mutants could be explained by the ability of the endogenous Irga6wt to associate with constitutively active mutant proteins in cells before reaching the PVM. As Irga6-S83N mutant practically does not bind nucleotides, it cannot target PVM nor it can interact with the endogenous Irga6 protein. Nonmyristoylated Irga6-G2A inefficiently binds to the PVM through probably two effects. As this mutant builds homooligomers very inefficiently in lysates of transfected cells (figure 3.12.), it might act as a chain terminator, preventing also the endogenous protein from further association. Alternatively, or in addition, absence of myristoyl group in the homooligomer can destabilise its membrane attachment and result in oligomer disassembly from the PVM.
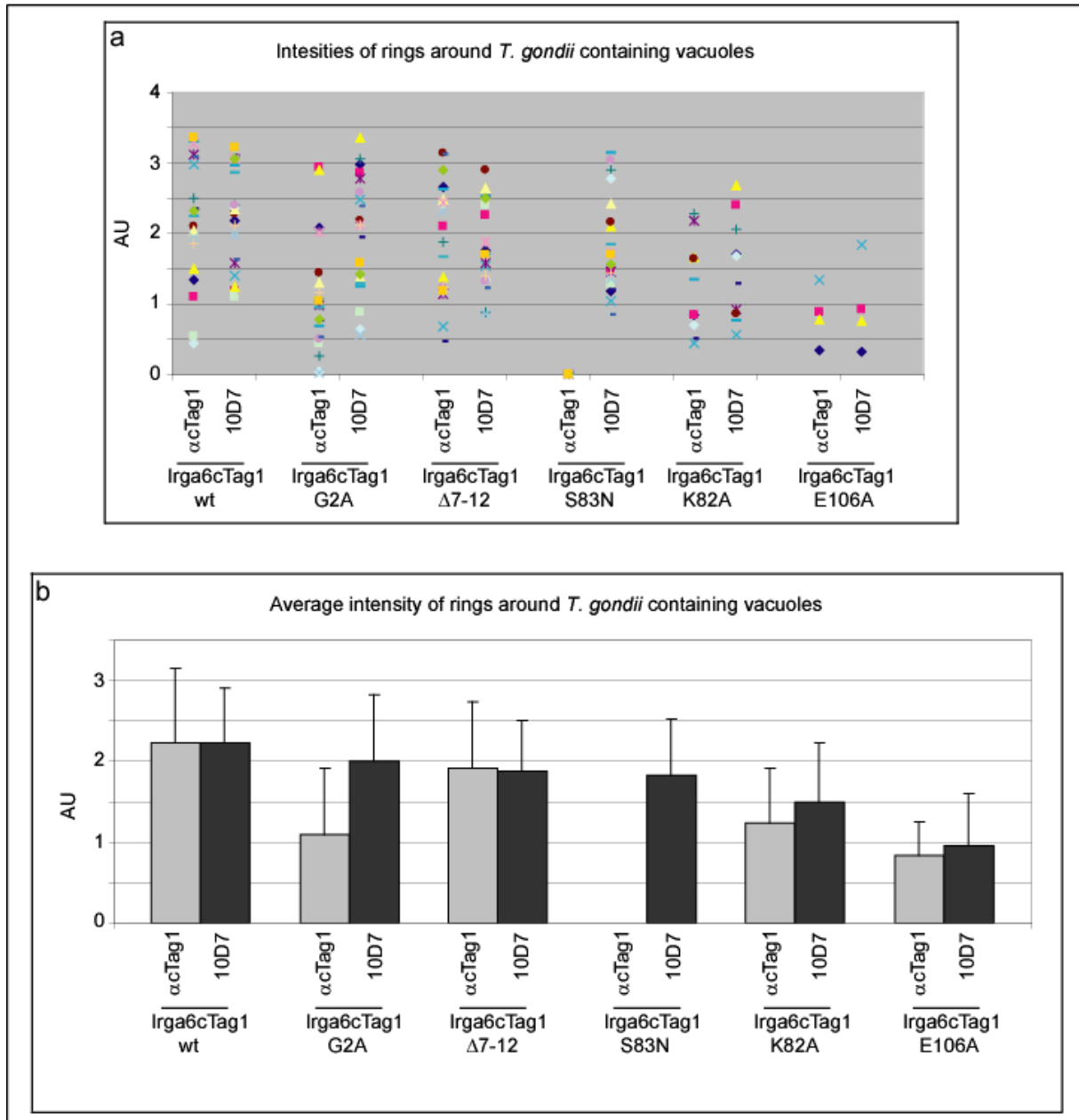
Figure 3.31. Pixel intensities of 10D7 and αcTag1 positive rings

gs3T3 fibroblasts were simultaneously induced with IFNγ and transfected with Irga6cTag1-wt, Irga6cTag1-G2A, Irga6cTag1-Δ7-12, Irga6cTag1-K82A, Irga6cTag1-S83N and Irga6cTag1-E106A proteins, 24 h prior to infection with *T. gondii* Me 49 strain. Cells were stained with 10D7 antibody and αcTag1 serum. Images were taken with the same exposure time and the pixel intensities of rings were detected using ImageJ software. (a) pixel intensities of individual 10D7 and cTag1 positive ring around PV; (b) average intensities of 10D7 and cTag1 positive rings around PV.

3.10. Biochemical analysis of recombinant myristoylated Irga6

The myristoyl group is apparently involved in conformational change of Irga6 protein induced upon GTP binding (figure 3.29.). In addition, unmyristoylated Irga6cTag1-G2A mutant is less efficient in targeting *T. gondii* PV (table 3.2.), indicating that the myristoyl group might be necessary for proper binding of Irga6 to the parasitophorous vacuole membrane.

Structure and biochemical properties of Irga6 protein, expressed and purified from *E. coli*, have been intensively studied *in vitro* (Uthaiah et al., 2003; Ghosh et al., 2004). However, this recombinant protein could not be myristoylated due to the N-terminal thrombin cleavage site associated with the GST-fusion protein (Uthaiah et al., 2003) and also because prokaryotes do not express enzymes necessary for protein myristoylation (Heuckeroth et al., 1988). Thus, in order to study biochemical properties of myristoylated Irga6 *in vitro*, Irga6 with a normal N-terminus was expressed and purified from insect *Sf9* cells.

3.10.1. Purification of myristoylated Irga6

Myristoylated Irga6wt as well as Irga6 G2A and S83N mutants were expressed using Baculovirus Expression Vector System (BEVS). This system allows expression of genes from different sources in insect cells. The likelihood that expressed Irga6wt would be myristoylated in these cells was supported by the fact that several post-translational modifications have been reported to occur, such as glycosylation, phosphorylation, acylation, isoprenylation, and others. In order to purify Irga6 proteins from *Sf9* cells, they were expressed with the C-terminal thrombin cleavage site (LVPRGS), followed by six histidines (Irga6-thrombin-his). Upon purification over NiNTA column and thrombin cleavage, Irga6 proteins would contain four additional amino acids at the C-terminus, LVPR. To assure that this small C-terminal tag does not influence the biochemical properties of the enzyme, Irga6 protein with this tag was expressed and purified from *E. coli* (Irga6-LVPR). GTP hydrolysis and oligomerisation properties of Irga6-LVPR and Irga6wt protein were indistinguishable (data not shown), indicating that these four amino acids do not affect the enzymatic properties of Irga6 protein.
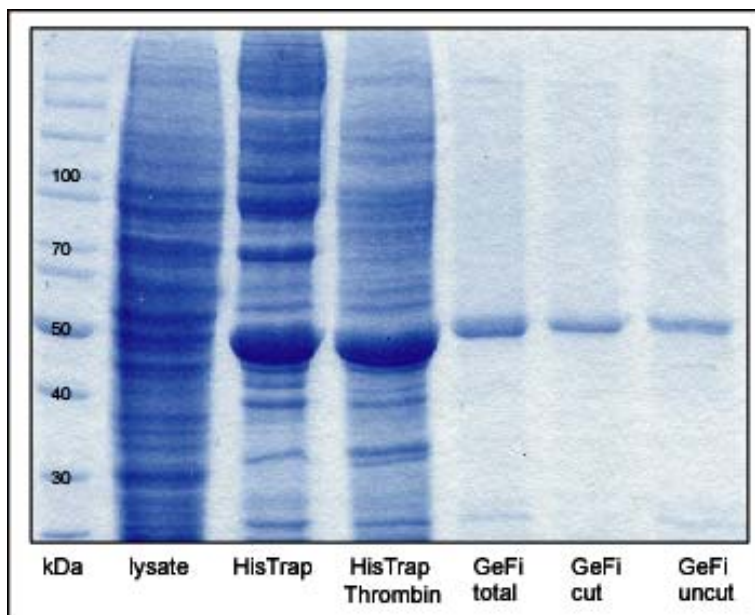
Figure 3.32. Purification of myristoylated Irga6wt

Sf9 cell containing Irga6wt-thrombin-his were lysed in 0.1% Thesit/ 150 mM NaCl/ 3 mM $MgCl_2$/ 20 mM Imidazol/ 2 mM DTT/ PBS. Lysate was purified over HisTrap HP 5ml column, bound protein eluted with 0.1% Thesit/ 150 mM NaCl/ 3 mM $MgCl_2$/ 250 mM Imidazol/ 2 mM DTT/ PBS (HisTrap) and cleaved with 150 U/ml of thrombin o/n at 4°C (HisTrap Thrombin). Irga6 was further purified over a Superdex 200 prep grade column (GeFi total) with 0.05% Thesit/ 5 mM $MgCl_2$/ 2 mM DTT/ 50 mM Tris pH 7.4 and incubated with NiNTA beads to separate cleaved (GeFi cut) from uncleaved protein (GeFi uncut). Proteins were analysed on SDS-PAGE and were stained with Coomassie Brilliant Blue.

Sf9 culture, infected with appropriate recombinant virus for 2 days at 27°C, was lysed in 0.1% Thesit/ 150 mM NaCl/ 3 mM $MgCl_2$/ 20 mM Imidazol/ 2 mM DTT/ PBS and loaded on HisTrap HP 5ml column in lysis buffer. After washing steps, elution of protein was done with 0.1% Thesit/ 150 mM NaCl/ 3 mM $MgCl_2$/ 250 mM Imidazol/ 2 mM DTT/ PBS and fractions analysed by Coomassie Brilliant Blue staining (figure 3.32., HisTrap). Fractions containing Irga6-thrombin-his protein were pooled together and incubated with 150 U/ml of thrombin for 12 h at 4°C (figure 3.32., HisTrap Thrombin). Afterwards, samples were loaded on HiLoad 26/60 Superdex 200 prep grade column with 0.05% Thesit/ 5 mM $MgCl_2$/ 2 mM DTT/ 50 mM Tris pH 7.4 as the running buffer. Fractions with Irga6 protein (figure 3.32, GeFi total) were incubated with 1 ml Ni-NTA beads for 1 h at 4°C to separate thrombin-cleaved (figure 3.32., GeFi cut) from uncleaved Irga6 (figure 3.32., GeFi uncut). Uncleaved protein was eluted from beads by boiling for 5 min in the SDS-PAGE sample buffer.

3.10.2. Triton X-114 partitioning assay

In order to analyse whether Irga6 proteins, purified from *Sf9* cells, are lipid modified, the Triton X-114 partitioning assay was performed. The Triton X-114 assay applies the general property of non-ionic detergents, namely that they undergo phase separation at a particular temperature (cloud point) to yield a detergent-rich (D) and an aqueous (A) layer. The cloud point of Triton X-114 is around 22°C, thus it can be used to separate lipid-soluble from hydrophilic molecules at RT (Bordier, 1981; Bhairi, 2001). This assay has been previously used to analyse lipid modification of mammalian Irga6wt and Irga6-G2A mutant. Upon lysis in 1% Triton X-114, Irga6wt partitioned into detergent phase whereas G2A mutant protein, which cannot be myristoylated, stayed in the aqueous phase (Martens et al., 2004).
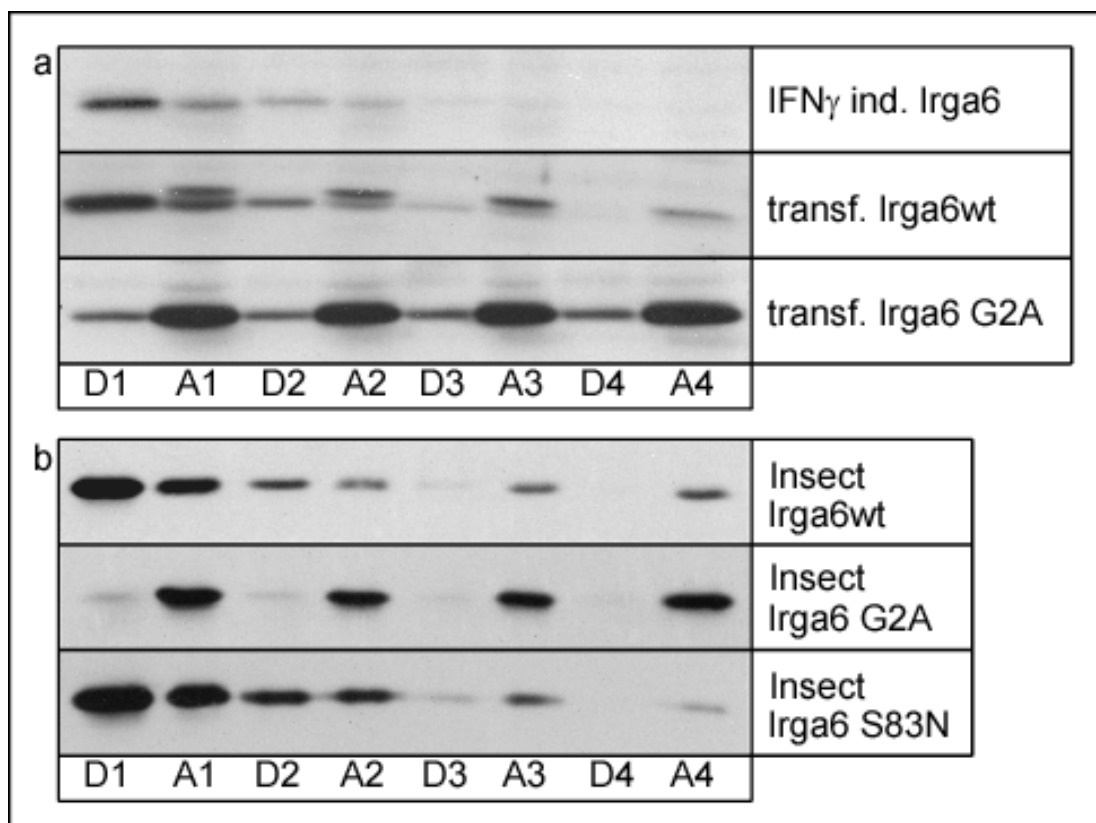
Figure 3.33. Tx-114 partitioning of Irga6 proteins

Lysates from L929 fibroblasts induced with IFNγ or transfected with Irga6wt or Irga6-G2A (a) or recombinant Irga6wt, -G2A or -S83N proteins purified from *Sf9* cells (b), were separated into detergent-soluble and aqueous fractions by the Triton X-114 partitioning assay. Samples were subjected to the SDS-PAGE and Irga6 proteins detected with 10D7 antibody.

Upon purification from *Sf9* cells, Irga6wt, Irga6-G2A and Irga6-S83N were analysed for the presence of lipid modification using Triton X-114 partitioning assay by dilution in 1% Tx-114/ 3 mM $MgCl_2$/ PBS (figure 3.33.(b)). In parallel, L929 fibroblasts, either IFNγ-induced or transfected with Irga6wt or Irga6-G2A (figure 3.33.(a)), were lysed in the same buffer for 1 h at 4°C and subjected to the Tx-114 assay as well. Partitioning of Irga6 proteins was done in four successive steps. Samples were subjected to SDS-PAGE and protein detected with 10D7 antibody.

As depicted in figure 3.33.(a), nonmyristoylated, transfected Irga6-G2A partitioned into aqueous phase. In contrast, approximately 70% of IFNγ-induced Irga6 and the lower band of transfected Irga6wt partition into detergent phase in each partitioning step, indicating that they are lipid modified. Interestingly, the upper band of transfected Irga6wt stayed in aqueous phase throughout the whole partitioning assay indicating that a proportion of transfected Irga6 in mammalian cells is not efficiently myristoylated. The same band, in the size exclusion chromatography (figure 3.4.) was running at the size of a monomer, paralleling the running behaviour of transfected Irga6-G2A, confirming that the transfected Irga6wt protein in the upper band is not myristoylated.

Irga6-G2A, expressed and purified from insect *Sf9* cells, partitioned into aqueous phase, illustrated in figure 3.33.(b). Irga6wt and Irga6-S83N purified from insect cells partition into detergent phase in each partitioning step, indicating that they are lipid modified. In insect cells, lipid modification was not 100% efficient since approximately 5% of Irga6wt and somewhat less than 5% of Irga6-S83N were found in the aqueous phase.

In order to confirm that the lipid modification of Irga6 proteins containing intact N-terminus is indeed a myristoyl group, Irga6wt and Irga6-G2A, purified from insect cells, were analysed by mass spectrometry. Only the Irga6wt protein was shown to be myristoylated at the N-terminus. In contrast, mass spectrometric data indicated that the Irga6-G2A protein is N-terminally acetylated.

3.10.3. Effect of the myristoyl group on running behaviour of recombinant Irga6 proteins in Size Exclusion Chromatography

IFNγ-induced, myristoylated Irga6 protein, when analysed by size exclusion chromatography, ran mostly at an apparent molecular weight of 150 kDa, both in the presence of 0.1% Thesit and 80 mM OGP (figures 3.4. and 3.5.). In contrast, nonmyristoylated proteins, transfected Irga6-G2A and recombinant Irga6wt purified from *E. coli* (from now on referred to as Bact Irga6wt), were running at the size of a monomer (figure 3.4.).

During the purification of Irga6 proteins from insect cells (Ins Irga6wt, -G2A, -S83N) similar observations were made. As explained in chapter 3.10.1., the last step of purification of Ins Irga6 proteins is size exclusion chromatography on a HiLoad 26/60 Superdex 200 prep grade column in the presence of 0.05% Thesit. Even though the calculated values for the sizes of eluted proteins may not reflect the exact molecular weight of the protein, it was clear that recombinant Ins Irga6-G2A (in red) and Bact Irga6wt (in blue) eluted approximately at the size of a monomer, depicted in figure 3.34.. In contrast, myristoylated, recombinant Ins Irga6wt (in green) and Ins Irga6-S83N (in black) ran at an apparent molecular weight of over 200 kDa. Although myristoylated proteins showed only a very small increase in size in SDS-PAGE analysis (not more than1-2 kDa), the myristoyl group had a strong effect on the elution of Irga6 protein in size exclusion chromatography. Since the effect of other detergents on recombinant Irga6 proteins was not tested, it is possible that the myristoyl group, exposed in the presence of Thesit micelle, results in this size shift. However, it is more likely that the myristoyl groups of more than one Irga6 protein insert into the detergent micelle, providing higher local concentration of the protein around the micelle.
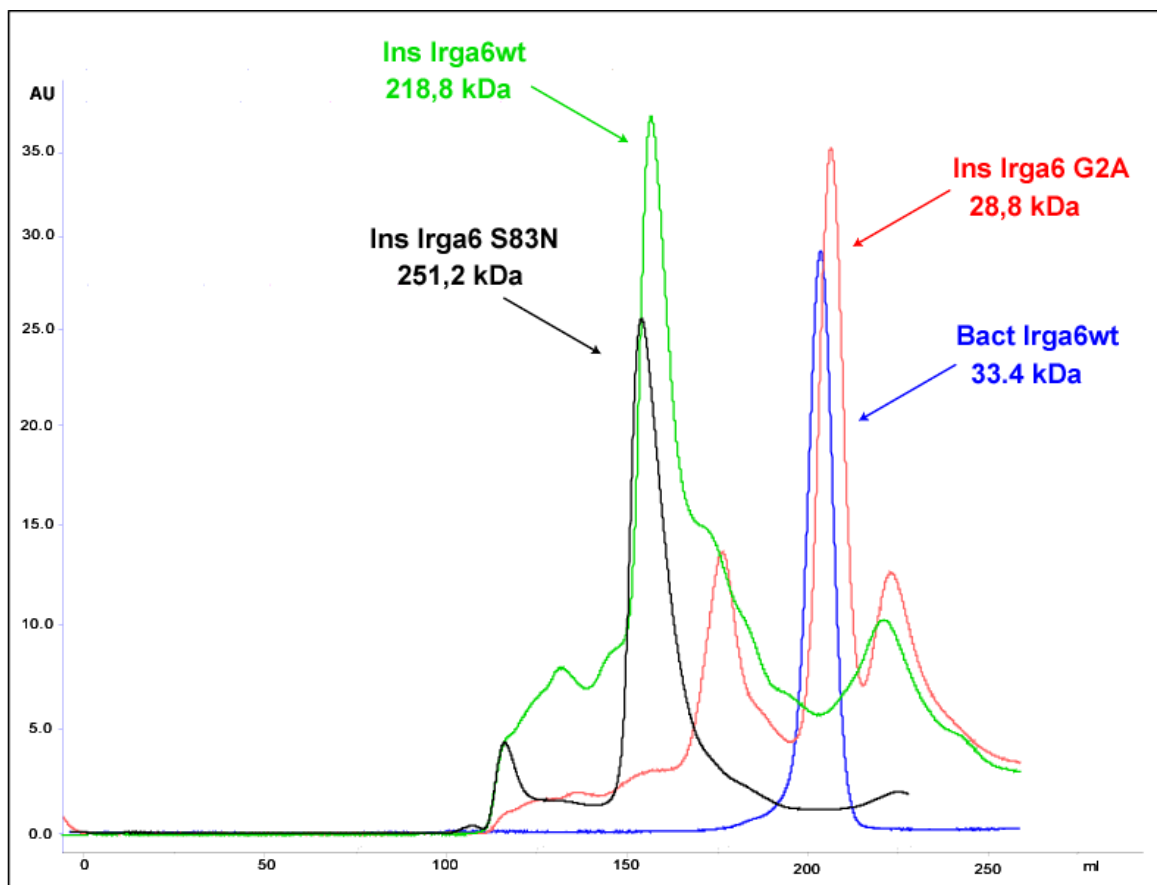
Figure 3.34. Running behaviour of recombinant Irga6 protein in size exclusion chromatography Recombinant protein expressed and purified from *E. coli* (Bact Irga6wt in blue) or from Sf9 cells (Ins Irga6wt in green, Ins Irga6-G2A in red and Ins Irga6-S83N in black) were analysed on a HiLoad 26/60 Superdex 200 prep grade column in the buffer containing 0.05% Thesit/ 5 mM MgCl$_2$/ 2 mM DTT/ 50 mM Tris pH 7.4. Molecular weights of the proteins in depicted peaks were calculated using calibration curve obtained by running marker proteins under the same conditions.

3.10.4. Dynamic light scattering of Ins-Irga6 proteins

During the purification on a size exclusion column in the presence of 0.05% Thesit, myristoylated proteins, Ins Irga6wt and Ins Irga6-S83N, were found running at the size of 200-250 kDa, whereas nonmyristoylated Ins Irga6-G2A was running as a monomer, at 50 kDa. This observation suggested that the oligomerisation properties of myristoylated Irga6 proteins might be different from those of Bact Irga6 or nonmyristoylated Ins Irga6-G2A.

Ins Irga6 proteins (at a concentration of 25 µM) as well as Bact Irga6wt (25 and 80 µM) were incubated with 10 mM GDP or GTP in the presence or absence of

100

0.05% Thesit. Oligomerisation was analysed using dynamic light scattering at 37°C for 20 min and change in hydrodynamic radius (R) was plotted against time (figure 3.35.).

Confirming previous results ((Uthaiah et al., 2003); Pawlowski, unpublished data), Bact Irga6wt showed a striking increase in hydrodynamic radius upon addition of GTP. At a protein concentration of 80 µM high molecular forms of Bact Irga6wt were detected within seconds and at concentration of 25 µM the process took longer, 2-3 minutes (figure 3.35.(a)). Interestingly, in the presence of 0.05% Thesit, GTP-dependent oligomer formation was much faster, taking only few seconds even at the protein concentration of 25 µM (figure 3.35.(b)). The addition of GDP to 80 µM Bact Irga6wt in the present of detergent resulted in the formation of high molecular weight structure only after 800 seconds of incubation (figure3.35.(b)).

The incubation of 25 µM of myristoylated Ins Irga6wt and Ins Irga6-S83N in the presence of 0.05% Thesit resulted in the formation of higher molecular weight structures after approximately 180 seconds, in presence of both GTP and GDP (figure 3.35.(c)). Nonmyristoylated Ins-Irga6-G2A showed an increase in size in the presence of GTP and detergent much later (500 sec).

The fact that both wild type Ins Irga6wt and nucleotide binding deficient Ins Irga6-S83N form higher molecular weight structure in the presence of both GTP and GDP argues against nucleotide-dependent oligomerisation. It is rather that the presence of the myristoyl group induces the formation of the Ins Irga6 complexes, probably via binding of myristoyl groups to the detergent micelle.
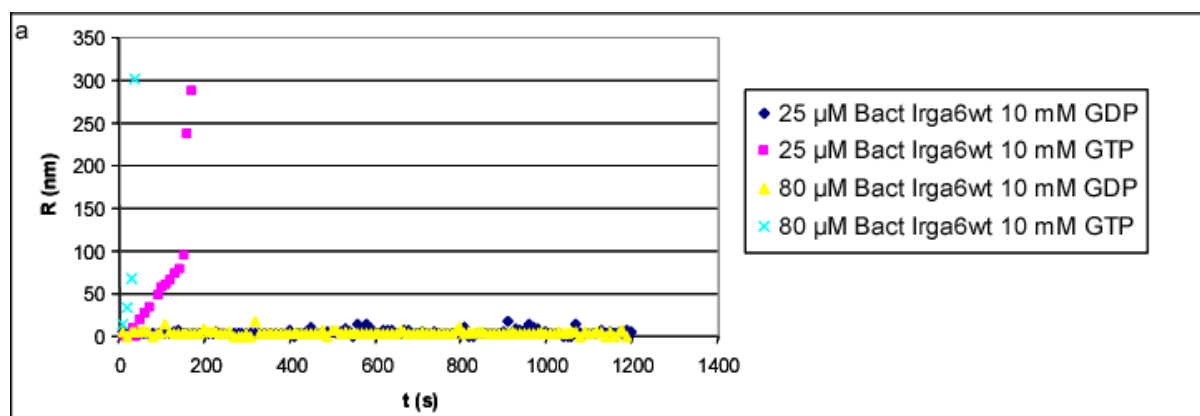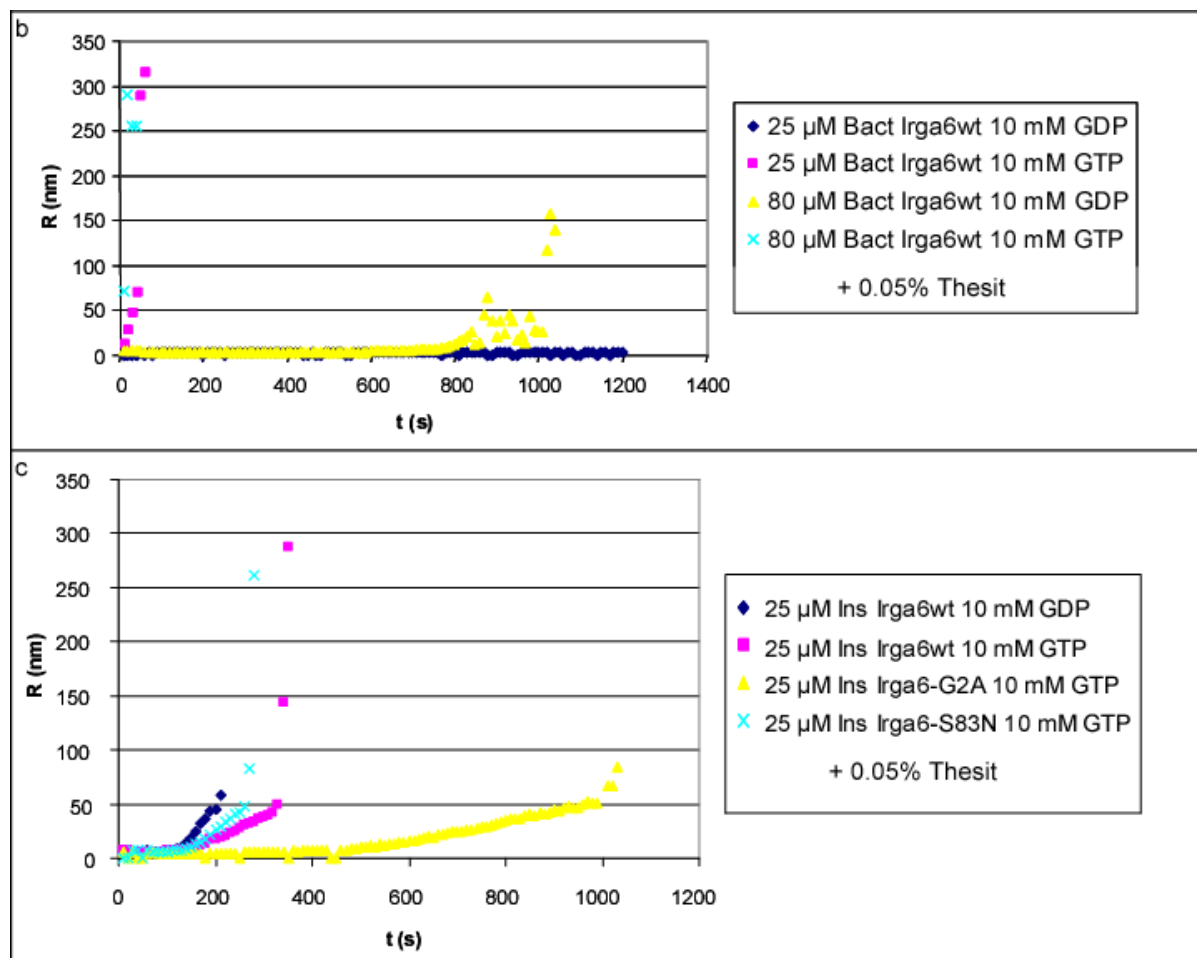
Figure 3.35. Dynamic light scattering of Ins Irga6wt, Ins Irga6-G2A, Ins Irga6-S83N and Bact Irga6wt

25 and 80 µM of Bact Irga6wt were incubated with 10 mM GDP or GTP in the absence (a) or presence (b) of 0.05% Thesit. In (c), 25 µM of Ins Irga6 proteins were incubated with 10 mM GDP or GTP in the presence of Thesit. Measurements were done at 37°C and changes of hydrodynamic radius were plotted against time.

3.10.5. 10D7 immunoprecipitation of Ins-Irga6 proteins

It has been proposed that the binding of GTP to the Irga6 molecule induces a conformational change, which affects the GTP-binding domain, the N-terminal region and the myristoyl group as well (chapter 3.9.4.). The 10D7 antibody, recognising only the active form of Irga6 protein, can, therefore, efficiently precipitate Irga6wt in the presence of GTPγS, but not nonmyristoylated Irga6-G2A or nucleotide-binding deficient mutant Irga6-S83N, as illustrated in figure 3.29. On the other hand, as discussed in the previous chapter, the myristoyl group induces the formation of Ins

Irga6wt- and Ins Irga6-S83N-containing complexes independent of nucleotide present. As it was not possible to purify the recombinant myristoylated Ins Irga6 proteins without detergent (data not shown), it was assumed that the myristoyl group has to be inserted into the Thesit micelle during purification. 10D7 immunoprecipitation of Ins Irga6 proteins could provide the opportunity to test whether this potential repositioning of myristoyl group could mimic the conformation of Irga6 molecule in its active state.
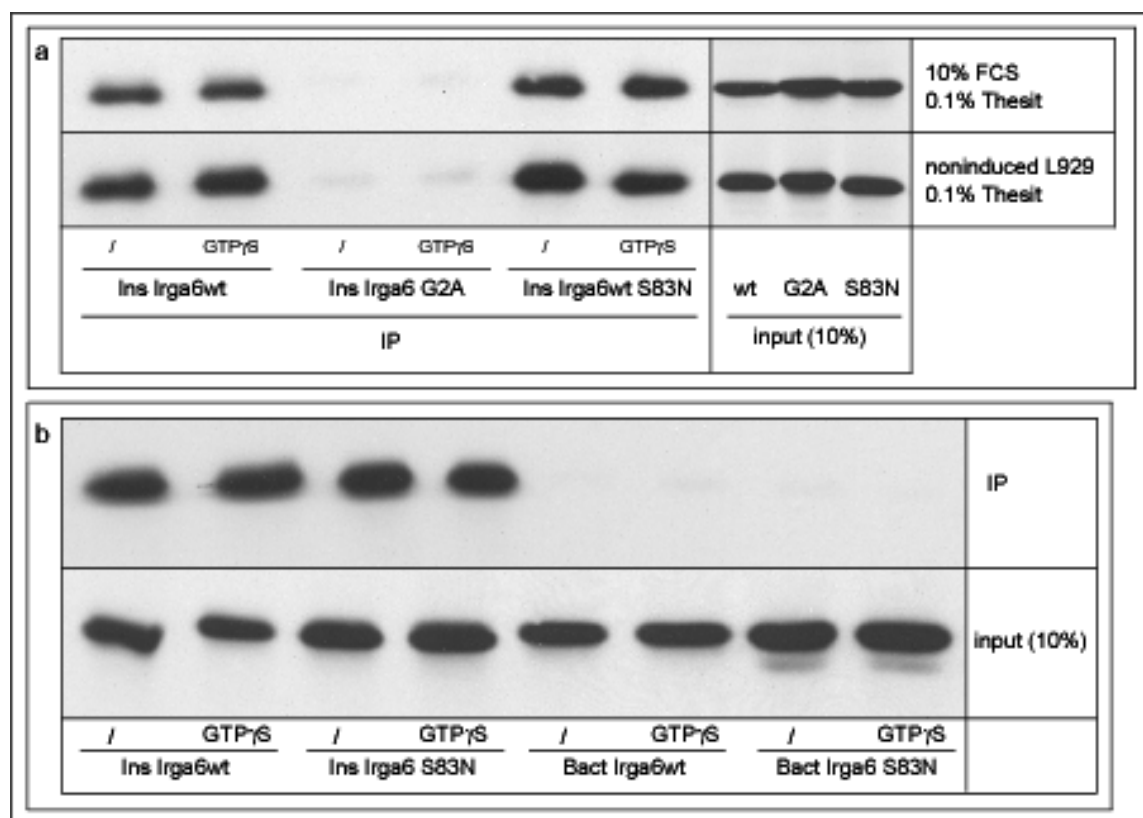
Figure 3.36. 10D7 immunoprecipitation of recombinant Ins Irga6 and Bact Irga6 proteins
(a) Ins Irga6wt, -G2A and -S83N were diluted in either 10% FCS/ 0.1% Thesit/ PBS or in noninduced L929 cell lysate/ 0.1 % Thesit/ PBS in the presence or absence of 0.5 mM GTPγS; (b) Ins Irga6wt, -S83N and Bact Irga6wt, -S83N were diluted in noninduced L929 cell lysate/ 0.1 % Thesit/ PBS in the presence or absence of 0.5 mM GTPγS. Samples were incubated with 10D7-coupled Protein A sepharose beads and bound protein eluted by boiling in SDS-PAGE sample buffer (IP). 10% of the sample prior to immunoprecipitation was loaded to control the amount of protein in each sample (input). Irga6 proteins were detected with 165 serum in Western blot.

Ins Irga6wt, -G2A and -S83N were diluted either in 10% FCS/0.1% Thesit/PBS or in noninduced L929 cell lysate/0.1 % Thesit/PBS in the presence or absence of 0.5 mM GTPγS. Samples were incubated with 10D7-coupled Protein A sepharose beads for 2 h at 4°C and bound protein eluted by boiling in SDS-PAGE sample buffer. As depicted in figure 3.36.(a), 10D7 was not able to immunoprecipitate recombinant nonmyristoylated Ins Irga6-G2A. In contrast to the result obtained with cellular proteins, 10D7 could equally well bind Ins Irga6wt and Ins Irga6-S83N, independently of nucleotide present.

To confirm these results, immunoprecipitation was done not only with Ins Irga6wt, -S83N but also with Bact Irga6wt and Bact Irga6-S83N. Again, only myristoylated Ins Irga6wt and -S83N were bound by 10D7 both in the presence and absence of GTPγS (figure 3.36.(b)). As expected, nonmyristoylated Bact Irga6wt and -S83N were not immunoprecipitated by 10D7 antibody, confirming the involvement of the myristoyl group in the Irga6 conformational state recognised by 10D7 antibody.

3.10.6. Hydrolysis properties of myristoylated Irga6

Nonmyristoylated, recombinant Irga6wt, expressed and purified from *E. coli* (Bact Irga6wt), hydrolyses GTP to GDP (Uthaiah et al., 2003). Therefore, hydrolysis properties of Ins Irga6wt, Ins Irga6-G2A and Ins Irga6-S83N proteins were analysed.

Ins-Irga6wt, Ins-Irga6-G2A, Ins-Irga6-S83N, as well as Bac-Irga6wt, all at a concentration of 25 µM, in the presence or absence of 0.05% of Thesit, were incubated at 37°C with 10 mM GTP containing 20 µCi/ml of $\alpha P^{32}GTP$. At indicated time points, samples of reaction mix were subjected to thin layer chromatography (TLC). Signals were detected using BAS 1000 phosphor imager analysis system and quantified with the AIDA Image Analyser v3 software.

As shown in figure 3.37., Ins Irga6-S83N did not hydrolyse GTP at all whereas all other proteins tested did. Ins Irga6wt and Ins Irga6-G2A hydrolysed GTP with roughly the same efficiency. Presence of 0.05% Thesit seems to increase the hydrolysis activity of Bac-Irga6wt.

Analysis of GDP and GMP levels upon hydrolysis revealed dramatic differences between myristoylated Irga6 (Ins-Irga6wt) and nonmyristoylated Ins

Irga6-G2A and Bact Irga6wt. While nonmyrystoylated Irga6 proteins hydrolysed GTP to GDP only, myristoylated Ins Irga6wt hydrolysed GTP to GDP and GMP as well.
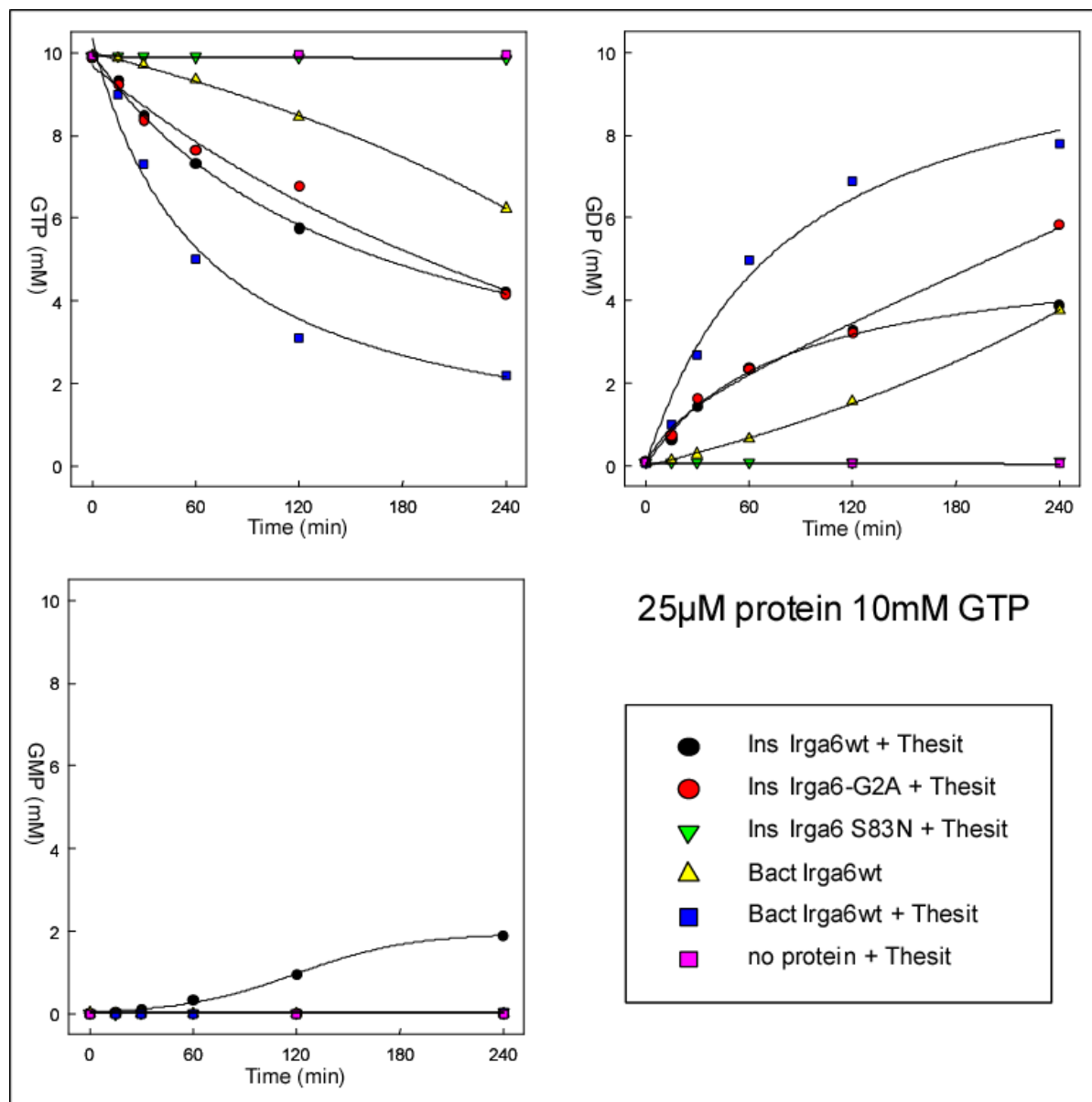
Figure 3.37. Hydrolysis properties of Irga6 proteins

25 µM of Ins Irga6wt, -G2A, -S83N and Bact Irga6wt were incubated with 10 mM of GTP containing 20 µCi/ml of αP^{32}GTP. After indicated time points, probes were subjected to TLC. Signals were detected using BAS 1000 phosphor imager analysis system and quantified with the AIDA Image Analyser v3 software.

To confirm this result, 25 µM of Ins Irga6wt, Ins Irga6-G2A and Ins Irga6-S83N were incubated with either 10 mM or 1 mM GTP containing 20 µCi/ml of αP³²GTP, as described above.
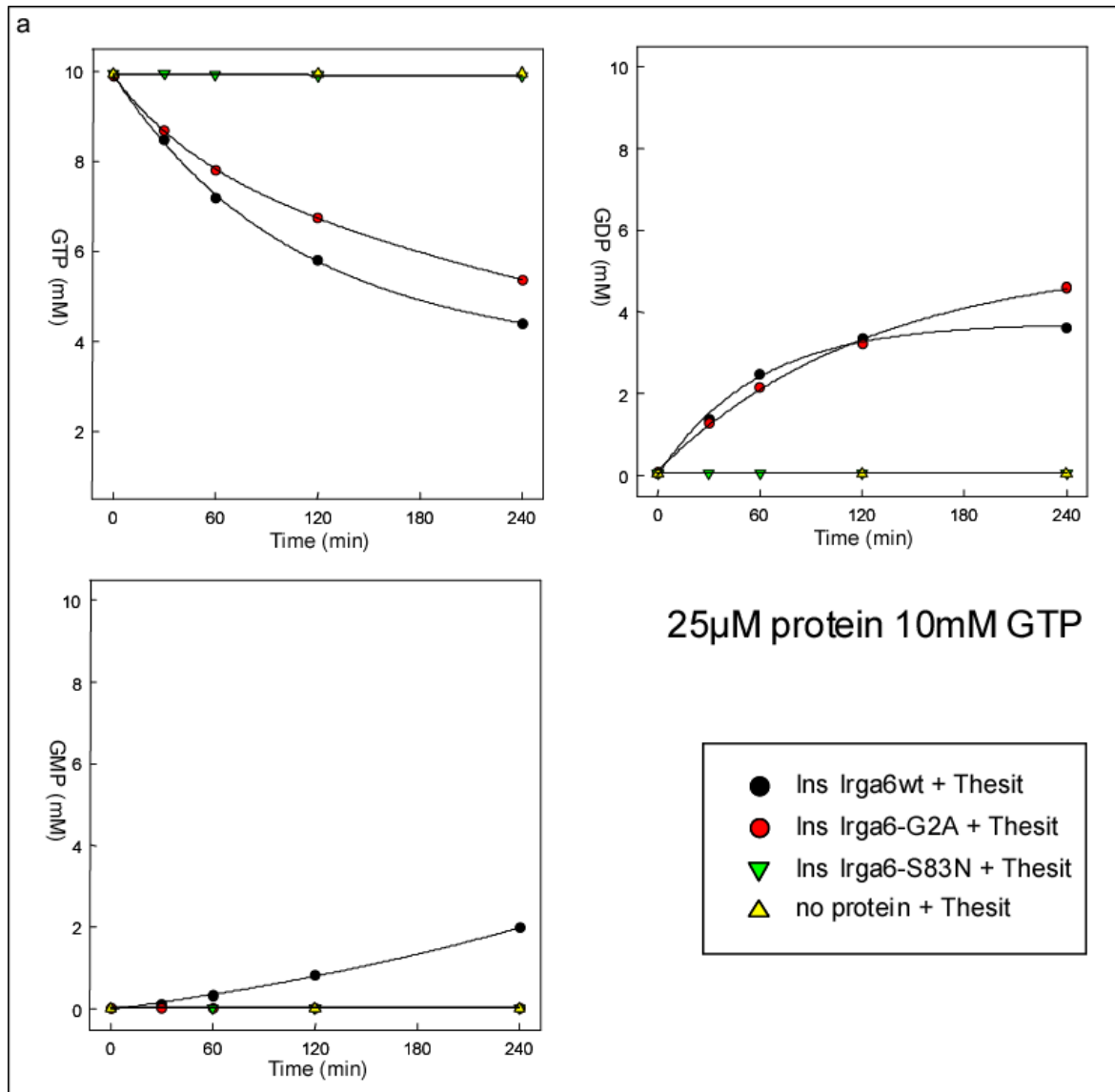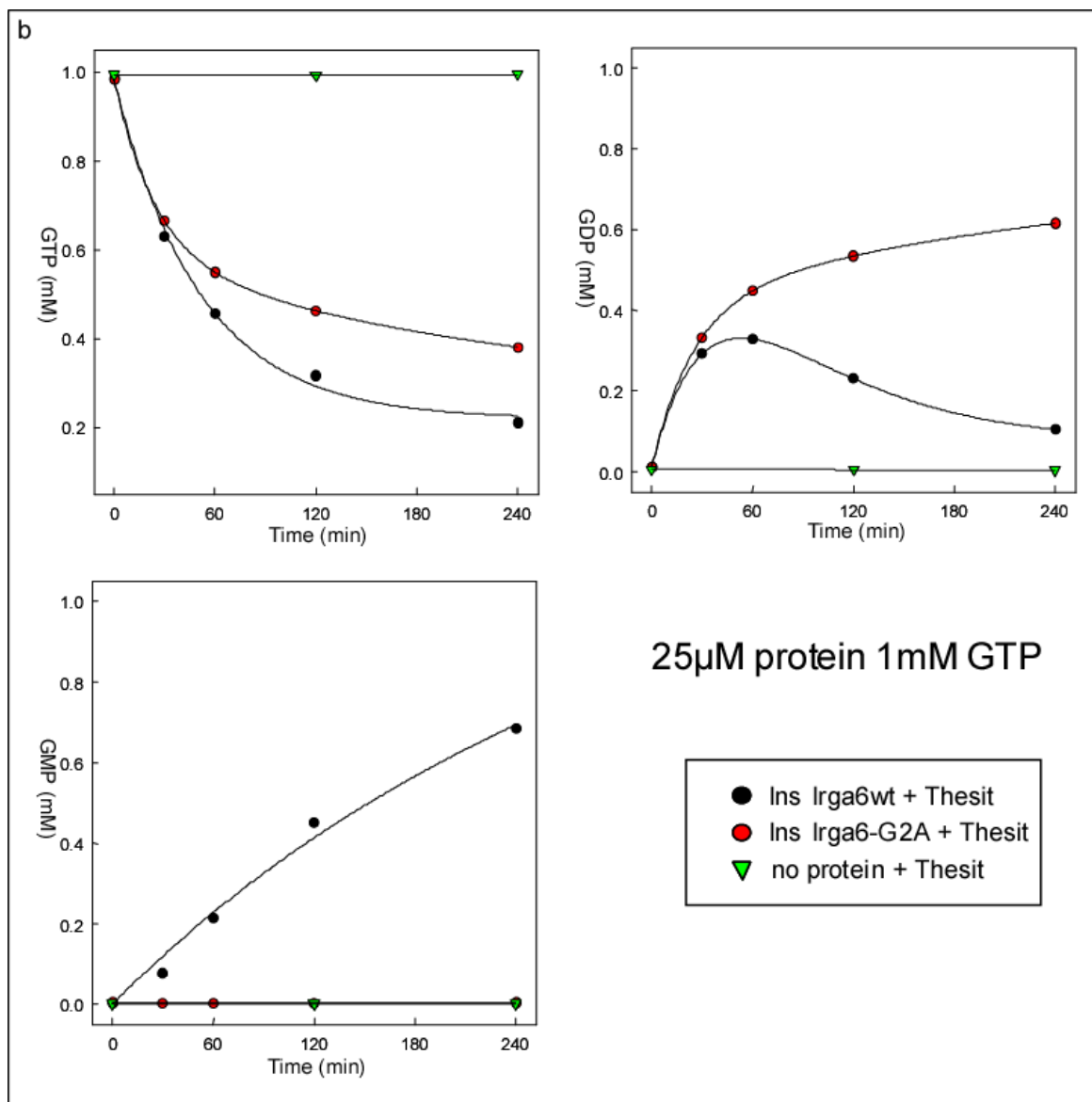
Figure 3.38. Hydrolysis activity of Ins Irga6 proteins

(a) 25 µM Ins Irga6wt, -G2A and -S83N were incubated with 10 mM GTP containing 20 µCi/ml of αP^{32}GTP, as described above; (b) 25 µM Ins-Irga6wt and Ins-Irga6-G2A were incubated with 1 mM GTP containing 20 µCi/ml of αP^{32}GTP.

Upon 4 h incubation of Ins-Irga6 proteins with 10 mM GTP (figure 3.38.(a)), 40% and 50% of GTP was hydrolysed by Ins Irga6-G2A and Ins Irga6wt respectively. While Ins Irga6-G2A hydrolysed GTP only to GDP, 60% of GTP hydrolysed by Ins-Irga6wt was in the form of GDP and 40% in the form of GMP. There was no hydrolysis activity of Ins Irga6-S83N detected.

After protein incubation with 1 mM GTP (figure 3.38.(b)), up to 60% of GTP was hydrolysed to GDP by Ins Irga6-G2A after 4 h. In contrast, 80% of GTP was

hydrolysed by Ins Irga6wt in the same time frame. In the case of Ins Irga6wt, the amount of GDP increased in the first 60 min of hydrolysis reaction but then decreased significantly in the next 3 h. Amount of GMP obtained by Ins Irga6wt hydrolysis of GTP was increasing steadily during time. As a result of Ins Irga6wt hydrolysis of GTP for 4 h, the amount of GMP obtained was approximately 6 times higher than the amount of GDP.

Thus, recombinant myristoylated Irga6wt protein exhibits strikingly different hydrolysis properties compared to the nonmyristoylated protein. Since the GDP concentration rises in the first hour of Ins Irga6wt hydrolysis and decreases in the next three hours, it is assumed that GTP hydrolysis to GMP by Ins Irga6wt does not occur in two successive steps while the nucleotide remains bound, as in hGBP1 (Prakash et al., 2000b). It is more likely that GTP is hydrolysed to GDP only but, as the GDP concentration rises, GDP itself becomes a substrate for Ins Irga6wt and is further hydrolysed to GMP.

4. Discussion

Results in this study demonstrate that the Irga6 activity in IFNγ-induced cells is regulated by other members of IRG family and by the infectious status of the cell. Irgm3, a member of the GMS family, interacts with Irga6 in the presence of GDP and, together with other two GMS proteins, keeps Irga6 in inactive form at the ER. Infection with *T. gondii* results in the relocalisation of activated, GTP-bound Irga6 to the parasitophorous vacuole membrane. GTP binding promotes the conformational change of Irga6, which involves GTP-binding domain, N-terminal 12 amino acids and the myristoyl group.

Recombinant myristoylated Irga6wt and nonmyristoylated Irga6-G2A proteins show striking differences in their biochemical properties *in vitro*. In addition to their different running behavior in size exclusion chromatography, myristoylated Irga6wt hydrolyses GTP to GDP and GMP, in contrast to Irga6-G2A, which hydrolyses GTP to GDP only.

Thus, both *in vivo* and *in vitro* data suggest that the myristoyl group plays an important role in Irga6 enzymatic activity and, therefore, in Irga6 function in cells.

4.1. Irga6 interacts with Irgm3 in a GDP-dependent manner

Endogenous, IFNγ-induced Irga6 protein localises in the reticular pattern, with the signal overlapping with those of endoplasmic reticulum (ER) proteins like TAP, Calnexin or ERP60 (Martens et al., 2004). In contrast to IFNγ-induced Irga6 (figure 3.13.(a)), Irga6wt (Martens, 2004) and Irga6cTag1 (figure 3.13.(b),(c),(d)), transacted into cells not induced with IFNγ, form small dots or larger aggregates distributed throughout the cell. This aggregation of transfected Irga6 proteins in the absence of IFNγ-induced factors is dose-independent since Irga6-containing dots are found even in cells expressing a very low level of transfected protein (figure 3.13.(d)). The Irga6-S83N mutant, characterized by very low binding affinity for both GDP and GTP *in vitro* (Hunn, 2007), was distributed in transfected fibroblast cytoplasmin a "smooth" pattern (figure 3.30.). Inability of Irga6-S83N proteins to adopt punctate morphology

indicates that the Irga6 aggregation in cells not induced with IFNγ is dependent on the nucleotide-binding integrity of the protein.

However, transfected Irga6cTag1 can be relocalised to the ER compartment if the cell is, in addition, simultaneously induced with IFNγ, as in figure 3.13.(g). This relocalisation effect of IFNγ induction is dose-dependent, since only cells expressing low amount of transfected Irga6 proteins showed distributed, ER-like localisation of exogenous protein. The amount of transfected Irga6cTag1 in cells that are able to relocalise exogenous protein approximately equals the amount of Irga6 induced by IFNγ. In other words, IFNγ-induced and transfected cells, which are able to relocalise exogenous Irga6, contain at most twice as much Irga6 as cells only induced with IFNγ. This indicates that Irga6 protein and the IFNγ-induced factors, necessary for its proper localisation to the ER, are expressed in certain equilibrium in IFNγ-induced cells, allowing the relocalisation of only limited additional amount of Irga6 molecules.

Several IFNγ-induced IRG proteins have been implicated in resistance against pathogen infections and their role is not redundant (Martens and Howard, 2006). This nonredundancy in function suggests that IRG proteins might regulate each other in cells, both prior to and during infection, possibly by direct interaction.

Effect of IRG proteins on the relocalisation of Irga6 was studied in gs3T3 fibroblasts, stably transfected with Irga6 DNA (gs3T3-Irga6), whose transcription is stimulated by synthetic hormone Mifepristone (GeneSwitch, Invitrogen). In these cells Mifepristone induces expression of Irga6 protein in an IFNγ-negative background (Hunn, 2007). Mifepristone-induced Irga6 formed aggregates, as seen in transiently transfected cells (Hunn, 2007). However, simultaneous transfection of the three GMS proteins, Irgm1, Irgm2 and Irgm3, carrying the unique substitution of the universally conserved lysine in G1 motif (GX_4GKS) to the methionine (GX_4GMS) (Boehm et al., 1998), into Mifeprestone-induced gs3T3-Irga6 cells resulted in Irga6 relocalisation to the ER in up to 80% of transfected cells (Schroeder, 2005). The effect of GMS proteins was nucleotide-dependent since their GMN mutants, carrying serine to asparagine substitution in their G1 binding motif and, thus, being unable to bind nucleotides (in analogy to Irga6; (Hunn, 2007), were not able to relocalise Irga6 molecules (Schroeder, 2005).

Thus, only Irgm1, Irgm2 and Irgm3 proteins are necessary and sufficient for localisation of Irga6 to the ER, indicating that GMS proteins are, either direct or indirectly, interaction partners of Irga6 in IFNγ-induced cells.

Irga6-Irgm3 interaction was confirmed by yeast-two hybrid screen (Hunn, 2007), co-immunoprecipitation and pull-down experiments (chapters 3.3.1. and 3.3.2. respectively). Irga6 could co-immunoprecipitate Irgm3 from the IFNγ-induced gs3T3 cell lysate, in the absence of any exogenously added nucleotide and, to a lesser extent, in the presence of additional GDP (figure 3.7.). Presence of GTPγS, nonhydrolysable form of GTP, almost completely inhibited Irga6-Irgm3 interaction.

However, the Irga6 and Irgm3 co-precipitation was greatly sub-stoichiometric. The weak signal for co-immunoprecipitated Irgm3 could be explained by the transient nature of the Irga6-Irgm3 complex *in vivo* and/or instability during the precipitation procedure. Alternatively, since the addition of exogenous GDP decreased the amount of co-immunoprecipitated Irgm3, it could be that Irga6 and/or Irgm3 interact with other IFNγ-induced factors that compete with Irga6-Irgm3 complex formation in the presence of GDP.

Pull-down experiments, using GST-Irga6 fusion proteins coupled to gluthathione sepharose beads and IFNγ-induced cell lysates, indicate the GDP-dependent Irgm3-Irga6 interaction (figure 3.8.). Only in the presence of GDP Irga6 and Irgm3 interacted strongly, over the background level. The background signal is not due to unspecific binding of Irgm3 to the gluthathion sepharose beads or GST alone. It rather seems to represent a basal affinity of these molecules for each other that is independent of their nucleotide state. Since the nucleotide-binding deficient Irga6-S83N mutant could not form a complex with Irgm3, it is probable that Irga6 has to be in GDP-bound form in order to interact strongly with Irgm3. As incubation of fibroblast lysate and GST-Irga6wt beads with mant GDP reduced Irgm3 signal to the basal level, the GDP-dependent Irga6-Irgm3 interaction might occur via GTP-binding domains of these proteins since mant group interferes with the dimeric Irga6 interactions occurring through the GTP-binding domain (Pawlowski, unpublished data).

In conclusion, active Irgm1, Irgm2 and Irgm3 proteins are necessary and sufficient for localisation of Irga6 to the ER. As Irgm3 interacts with Irga6 protein in the presence of GDP, it is possible that IFNγ-induced Irga6, at the ER, is kept in an inactive, GDP-bound state by the three GMS proteins.

A yeast- two hybrid screen revealed not only interactions between Irga6 and GMS protein, but also strong affinities of other GKS for GMS proteins (Hunn, 2007). It is, therefore, expected that the interactions between IRG proteins *in vivo* have to be

tightly regulated. An excess or deficiency of any of them, especially GMS proteins since they are represented by only one gene in the mouse genome, would result in instability of the whole system. That might explain the non-redundancy of IRG proteins in the experiments done with mice or cells deficient in one of the IRG members (Collazo et al., 2001; Butcher et al., 2005; Bernstein-Hanley et al., 2006; Miyairi et al., 2007). Interestingly, overexpression of Irgm3 rendered mouse embryonic fibroblasts more susceptible to *Chlamydia trachomatis* infection (Bernstein-Hanley et al., 2006). In the view that Irgm3 interacts with Irga6 in the GDP-bound form, overexpression of Irgm3 could strengthen the inhibitory effect on Irga6 activation upon infection and, therefore, prevent the efficient relocalisation of Irga6 to the PVM.

4.2. Irga6 forms GTP-dependent homooligomers *in vivo* in the absence of IFNγ-induced factors

Recombinant Irga6wt, expressed and purified from *E. coli*, was shown to form GTP-dependent homooligomers (Uthaiah et al., 2003) resulting in an increased GTPase activity of the protein. Upon GTP hydrolysis, Irga6 oligomers are dissolved. Addition of AlFx*,* which plays the role of the leaving γ-phosphate and mimics the transition state of GTP hydrolysis (Mittal et al., 1996), could trap Irga6wt in the oligomeric form when GTP is bound and being hydrolysed. Binding of AlFx to Irga6-GDP complex when the oligomer is preformed indicates that the oligomer is the catalytically active form in which an additional catalytic residue can be provided *in cis* or *in trans* (Uthaiah et al., 2003).

In this study, the ability of Irga6 proteins to form self-associations *in vivo* was analysed. Transfected Irga6cTag1 and Irga6wt, either transfected or IFNγ-induced, in the cell lysates formed homooligomers in the presence of GTPγS or in the presence of GTP and AlFx (figure 3.11.(a)). Exogenously added GTP and AlFx as well as nonhydrolysable GTPγS trap Irga6 molecules in GTP-like state and, thus, allow building of GTP-dependent Irga6 complexes. The number of Irga6 molecules in these GTP-dependent complexes was not resolved. For simplicity reasons, throughout this study, the homooligomer is considered only to be more than a monomer.

Mant-labeled nucleotides interfere with oligomerisation of recombinant Irga6 by insertion between two binding interfaces preventing protein interaction via GTP-binding domains (Pawlowski, unpublished data). Incubation of lysates in the presence of mant GTPγS almost completely prevented self-interaction of Irga6 molecules (figure 3.11.(b)), thus indicating that the self-association of cellular Irga6 proteins occurs through the interaction of GTP-binding domains. This GTP-dependent homooligomerisation of Irga6 molecules, both in the presence of GTPγS and GTP with AlFx, takes place in the cell lysate, thus, *ex vivo* (figure 3.10.). Namely, co-immunoprecipitated IFNγ-induced Irga6 could be found in samples that were induced with IFNγ and transfected with Irga6cTag1 separately and mixed prior to lysis ((i)+(t)), excluding the possibility that this interaction occurred in the cell. Nevertheless, this result suggests that cellular Irga6 proteins can form GTP-dependent self-interactions, similar to the recombinant Irga6wt *in vitro*.

It has been reported that AlFx can bind to oligomeric recombinant Irga6 *in vitro* (Uthaiah et al., 2003). AlFx can penetrate plasma membranes of intact cells and, thus, trap GTPases in GTP-like, GDP+AlFx transition state *in vivo* (Hart et al., 1998). Incubation of intact cells in the presence of AlFx alone resulted in trapping of Irga6 homooligomers only in the absence of other IFNγ-induced factors, indicated by the arrow in figure 3.11.(a). This result demonstrates that Irga6 proteins can indeed form homooligomers in intact cells, *in vivo*, but only if other IFNγ-induced factors are missing.

As discussed earlier, transfected Irga6 proteins form small dots or larger aggregates throughout the cell. In contrast, Irga6 in IFNγ-induced cells is localised to the ER. Three GMS proteins, Irgm1, Irgm2 and Irgm3, were reported to be necessary and sufficient to position Irga6 molecules to the ER. As Irga6 interacts with Irgm3 in the GDP-bound form, the role of GMS proteins, in general, might be to keep Irga6 in an inactive, GDP-bound form on the ER, prior to infection. In the absence of IFNγ induction, there is no inhibitory effect of GMS proteins on Irga6, therefore Irga6 can get activated and can form GTP-dependent homooligomers that disassemble upon hydrolysis unless stabilised by AlFx molecules. These Irga6 homooligomers might be represented by the Irga6-positive dots and aggregates in cells not induced by IFNγ (figure 3.13.).

4.3. Possible Irga6 homooligomers in cells infected with *Toxoplasma gondii*

Toxoplasma gondii, an apicomplexan protozoan pathogen, actively invades the host cell (Morisaki et al., 1995; Dobrowolski and Sibley, 1996; Sibley, 2004). Within host cells, *T. gondii* replicates in parasitophorous vacuoles (PVs) formed during invasion by invagination of the plasma membrane (Suss-Toby et al., 1996). Parasitophorous vacuole membrane (PVM) is devoided of most host plasma membrane proteins (Mordue et al., 1999a; Charron and Sibley, 2004) and does not fuse with the host cell endocytic compartment and mature to lysosomes (Joiner et al., 1990; Mordue et al., 1999b).

Irgm1, Irgm3 and Irgd are implicated in resistance against *T. gondii* infection (Taylor et al., 2000; Collazo et al., 2001). Susceptibility to infection, related to the absence of these proteins, was shown in knockout mice and in isolated cells, *in vitro* (Halonen et al., 2001; Butcher et al., 2005), thus implying involvement of IRG proteins in cell-autonomous resistance. In order to understand the mechanism of IRG protein function and how they potentially regulate each other, detailed analysis of these proteins during infection with *T. gondii* is being conducted.

It has been reported that IFNγ-induced IRG proteins (Irgb6, Irga6, Irgd, Irgm3, Irgm2 (Martens et al., 2005) and Irgb10 (Koenen-Waisman, unpublished data)) relocalise from their resting localisation to the PVM upon infection with the nonvirulent *T. gondii* strain Me49. IRG protein accumulation around the PVM is not random. In contrast, it seems to be highly organized and follows a certain hierarchy. Approximately 80% of PVM in infected gs3T3 fibroblasts are coated with Irgb6 (Koenen-Waisman, unpublished data) and this process is very rapid; the first Irgb6-positive PVs are detected within two minutes of infection (Khaminetz, unpublished data). In addition, Irgb6 does not require any other IRG protein for PVM targeting (Hunn, 2007). In contrast, Irga6 binds to the PVM very inefficiently in the absence of other IRG proteins (Hunn, 2007). Irga6 accumulates around PVM in the presence of Irgb6. Additionally, the presence of GMS proteins is also required for relocalisation of Irga6 to the PVM (Hunn, 2007), probably by positioning Irga6 to the ER and preventing its activation prior to infection. The prerequisite for Irgd accumulation around *T gondii*-containing vacuole is presence of Irgb6 and Irga6 molecules at the PVM. Finally, only vacuoles coated with three GKS proteins, Irgb6, Irga6 and Irgd, contain Irgm3- and Irgm2-positive signals (Koenen-Waisman, unpublished data).

IFNγ-induced astrocytes and primed macrophages effectively resist *T.gondii* infection by stripping the parasite of its membranes (Martens et al., 2005; Ling et al., 2006). A series of disruption events was proposed involving parasitophorous vacuole membrane (PVM) ruffling, PVM vesiculation, disruption, followed by parasite plasma membrane stripping, leading to lysosomal degradation of the parasite (Ling et al., 2006). Both Irgm3 and Irga6 proteins were found to be involved in *T. gondii* vacuole vesiculation and disruption in astrocytes and macrophages, respectively (Martens et al., 2005; Ling et al., 2006).

Involvement of an active Irga6 protein in *T. gondii* PVM disruption would imply the presence of GTP-dependent Irga6 homooligomers in the cells induced with IFNγ and infected with *T. gondii*, as GTP binding results in self-association of Irga6 molecules. As shown above, there was no evidence for Irga6 homooligomerisation in cells stimulated with IFNγ and not infected with *T. gondii*. AIFx was unable to trap any oligomers in these cells. This result was consistent with the evidence that the "resting" Irga6 is held in a GDP-dependent state, probably by transient interaction with GMS proteins. However, after infection with *T. gondii*, the relocalisation of Irga6 to the PV depends on the integrity of the nucleotide binding site (Martens et al., 2005) and probably requires GTP binding. It was, therefore, possible that AIFx could detect this by trapping oligomers in IFNγ-induced, *T. gondii*-infected cells. Indeed, it was possible to detect evidence for some oligomers (figure 3.11.(c), indicated by the arrow). However, this band was very weak and not always detectable. This co-immunoprecipitation assay appears not really to be sensitive enough for this purpose, though the result is promising. Low level of Irga6 homooligomerisation in IFNγ-induced cells infected with *T. gondii* could be explained by the inefficiency of this assay. Homooligomerisation is analysed by the coimmunoprecipitation of IFNγ-induced Irga6wt by the transfected Irga6cTag1 (chapter 3.4.2.). Treatment with IFNγ results in the protein induction in practically all cells. In contrast, DNA transfection of fibroblasts using FuGENE6 transfection reagent (Roche) is very inefficient, resulting in expression of transfected protein in only 5-10% of cells. Finally, even when high MOI of *T. gondii* were used (MOI>10), not all cells were infected and, in addition, only 70% of PVs were coated with Irga6. Thus, only 3.5-7% of cells were in the condition where Irga6 homooligomers could be detected by co-immunoprecipitation, which is not enough to obtain a clear result and make a valid conclusion. Another method has

to be employed in order to analyse the presence of activated Irga6 proteins around *T. gondii* PVM.

4.4. Analysis of the binding affinity of the αIrga6 monoclonal 10D7 antibody

IFNγ-induced Irga6 localises to the ER and accumulates around PVM upon infection with *T. gondii,* as discussed earlier. Transfected Irga6cTag1 adopts punctate localisation, forming aggregates of various size. In IFNγ-induced cells, transfected Irga6cTag1 can be partly relocalised to the ER. It is presently cosidered that Irga6 on the ER, either IFNγ-induced or relocalised, is kept in an inactive, GDP-bound form by GMS proteins prior to infection. Upon infection, IFNγ-induced Irga6 protein is found at the PVM, presumably in the active form. The argument continues, that transfected Irga6cTag1 protein, in the absence of inhibitory effect of GMSs, activates spontaneously in the absence of infection, and the Irga6-positive aggregates seen throughout the cell might, therefore, represent the active form of Irga6.

10D7, one of the αIrga6 monoclonal antibodies, in immunofluorescence analysis does not recognise Irga6 on the ER, either IFNγ-induced or relocalised (figure 3.14.(b)). In contrast, transfected Irga6cTag1 protein (figure 3.14.(a)) or Irga6cTag1 around PV containing the Me49 strain of *T. gondii* (figure 3.14.(c)) is stained by 10D7 antibody.

It was, therefore, tempting to postulate that 10D7 antibody recognises only active, GTP-bound Irga6. The plausible alternative, however, is that the 10D7 is a low affinity antibody, which efficiently binds only to the densely packed, probably oligomerised, Irga6 molecules in aggregates or around *T. gondii*-containing PV.

Multimeric interactions allow a low-affinity antibody to bind tightly to an antigen, transforming a low affinity antibody to an antibody of high avidity (Harlow, 1988). 10D7 belongs to the IgG1 class of antibodies (Zerrahn, personal communication), and is, therefore, bivalent. Densely packed Irga6 molecules, either in aggregates or around *T. gondii* PV upon transfection, could act as a multivalent substrate in contrast to distributed, possibly monomeric Irga6 molecules bound to the ER. If 10D7 were a low affinity antibody, bivalent interaction with Irga6 in aggregates

116

and around PV would increase its avidity, which would result in stronger binding. This could be tested by creating monovalent 10D7 antibody Fab fragments by papain cleavage. Single Fab fragment could not be able to bind more efficiently to oligomers than to monomeric molecules. In contrast, if 10D7 is a high affinity antibody, sensitive to a distinctive conformational state associated with PV-bound or aggregated Irga6, then Fab fragments would show the same sensitivity as the native antibody.

The IgG molecule is a symmetrical dimer consisting of four polypeptide chains: two identical heavy chains and two identical light chains held together by interchain disulfide bonds (Harlow, 1988). Treatment with papain protease results in digestion of the antibody into two Fabs (fragments of antigen binding), consisting of a light chain and the N-terminal domains of a heavy chain, bridged by disulfide bonds, and one Fc fragment (crystallisable fragment), which consists of two C-terminal parts of heavy chains connected by disulfide bridges. The principal sites of papain cleavage are found at the amino-terminal side of the disulfide bonds that hold the light and the heavy chains together thus resulting in release of two Fab fragments with molecular weight of around 45-55 kDa and one Fc fragment of 50 kDa, under non-reducing conditions (Harlow, 1988). However, mouse monoclonal antibodies from the different classes show a wide degree of variation of secondary papain cleavage sites, which usually results in the presence of additional fragments of different sizes.

Indeed, papain cleavage of monoclonal antibodies 10D7 and 10E7,which does not distinguish aggregated and dispearsed Irga6 molecules, resulted in formation of three to four major fragments, having molecular weights between 42 and 55 kDa under non-reducing conditions, both in SDS-PAGE and in size exclusion chromatography (figure 3.18.). As it will be discussed later, fragments in later fractions, named C3, of both antibodies showed stronger αIrga6 binding than those in earlier fractions (B13 in figure 3.18.). It can be, therefore, assumed that the majority of the Fab fragments of 10D7 and 10E7 represent the strongest bands in C3 fractions, whereas Fc fragments are found in the earlier, B13 fractions.

Relative binding affinities of purified 10D7 and 10E7 papain-cleaved fractions, compared with whole 10D7 and 10E7 antibodies for Irga6 proteins were analysed in Western blot and in immunofluorescence. Western blot analysis revealed that, in general, 10D7 antibody and its fragments in B13 and C3 fractions bound at higher dilutions to the recombinant Irga6 than 10E7 antibody and its fragments. Fragments in C3 fractions, presumably Fabs, of both antibodies displayed binding at higher

dilutions than earlier B13 fractions, excluding the possibility that the strong αIrga6 signal originated from the uncleaved antibody trailing in the size exclusion column.

Even though 10D7 C3 fraction bound to the recombinant Irga6 almost as efficiently as non-cleaved 10E7 antibody, uncleaved 10D7 antibody bound at higher dilutions than its C3 fragments. Since secondary HRP-coupled antibody raised against the whole mouse monoclonal IgG antibody was used for detection, it could not be determined if the stronger 10D7 signal was due to the higher binding affinity compared to its Fabs or it resulted from an additional signal from the secondary HRP antibody binding to the constant region of uncleaved 10D7 antibody.

Immunofluorescence analysis provided clearer view on the relative binding affinity of 10D7 and its fragments. To avoid the signal coming from the constant region of an uncleaved antibody, goat-α-mouse kappa light chain-FITC was used as a secondary detection reagent, which binds only to the light chain of the antibody. IFNγ-induced gs3T3 cells were infected with Me49 strain of *T. gondii* and stained by 10D7 and its fragments in C3 fraction. Relative binding affinity was estimated by the acquisition time necessary to detect Irga6 signal of equal intensity around *T. gondii* PV. If 10D7 were low affinity antibody, its Fab fragments, which are unable to form bivalent interactions with antigens and therefore have low avidity as well, would bind to Irga6 molecules on *T. gondii* PV very inefficiently. This would result in longer exposure time necessary to detect signal of Irga6 around PV with 10D7 C3 fragments compared to noncleaved 10D7 antibody.

When secondary α-mouse kappa light chain-FITC antibody was used, Irga6 rings around PV, labelled with the whole 10D7 antibody as well as with 10D7 C3 fraction were detected after the same exposure time (figure 3.20.). Therefore, 10D7 fragments in C3 fraction, presumably containing Fabs, detect Irga6 around PV vacuoles as efficiently as the whole 10D7 antibody, indicating that 10D7 is a high affinity antibody. Thus, 10D7 antibody preferentially recognises a specific conformation of Irga6 molecules in cells, associated with aggregation or oligomerisation.

4.5. 10D7 epitope is located in the first N-terminal α helix of Irga6 but excludes its myristoyl group and the GTP-binding domain

To be able to interpret the 10D7-Irga6 interactions properly, the 10D7 epitope was analysed in detail. Deletion constructs and single amino acid mutants of Irga6 located the 10D7 epitope between amino acid 20-25 in the Irga6 molecule, where the mutation of the threonine residue in position 21 shows the strongest effect on 10D7 binding (figures 3.21. and 3.22.). In addition, the myristoyl group and first 12 N-terminal amino acids of Irga6 protein are not part of the 10D7 epitope (figure 3.23.). The fact that the epitope is a part of the first α helix in the Irga6 molecule suggests that the GTP-binding domain itself is excluded from 10D7 recognition sequence.

4.6. Active form of Irga6 is recognised by 10D7 antibody

The possibility that 10D7 recognises Irga6 in its active, GTP-bound state was tested by immunoprecipitation experiments using the non-hydrolysable GTP analog, GTPγS. Recombinant, IFNγ-induced and transfected Irga6wt molecules were analysed. All these Irga6 proteins could form homooligomers in the presence of GTPγS ((Uthaiah et al., 2003) and figure 3.11.). However, in contrast to purified, recombinant Irga6wt, IFNγ-induced and transfected Irga6wt were expressed in fibroblasts where the other cellular components mignt affect the 10D7 binding. In the presence of the nonionic detergent Thesit, 10D7 bound more efficiently to the GTPγS-bound IFNγ-induced and transfected Irga6wt. However, 10D7 did not recognise recombinant Irga6wt, even in the presence of GTPγS (figure 3.27.). Apart from being expressed in different cells (murine fibroblasts and *E. coli*), IFNγ-induced and transfected Irga6wt differ from recombinant Irga6wt, expressed and purified from *E. coli* (Bact Irga6wt), by the N-terminal lipid modification.

IFNγ-induced Irga6 and transfected Irga6wt proteins are believed to be myristoylated at the N-terminal glycine residue *in vivo*. In the Triton X-114 partitioning assay, used to separate proteins with hydrophobic domains from hydrophilic molecules at RT (Bordier, 1981; Bhairi, 2001), IFNγ-induced Irga6 and the lower band of transfected Irga6wt partition, roughly 70:30, into the detergent phase,

indicating the partial lipophilic character of these molecules. Mutation of the N-terminal glycine residue to alanine (G2A) in Irga6 molecule results in Irga6-G2A protein partitioning exclusively into the aqueous phase, suggesting that this glycine is indeed lipid modified *in vivo* ((Martens et al., 2004) and figure 3.33.(a)). Absolute requirement of N-terminal glycine residue for myristoylation, after the initiating methionine is removed by methionine aminopeptidase, and the presence of an appropriate myristoylation sequence (M**G**QLS**T**) indicate that Irga6wt is myristoylated *in vivo*.

In contrast, recombinant Bact Irga6wt, expressed and purified from *E. coli*, cannot be myristoylated for two reasons. First, Irga6wt is expressed as GST-fusion protein in the pGEX-4T2 vector and subsequently cleaved by Thrombin in the linker region between GST and Irga6 sequence (Uthaiah et al., 2003). Thrombin cleavage results in 10 amino acids long N-terminal extension, which itself would prevent covalent binding of the myristoyl group to the recombinant Irga6wt. In addition, prokaryotes do not express enzymes necessary for protein myristoylation (Heuckeroth et al., 1988). As a consequence, Bact Irga6wt purified from *E. coli* is not myristoylated.

10D7 recognises IFNγ-induced and transfected Irga6wt preferentially in the GTP-bound form but not recombinant Bact Irga6, suggesting that not only nucleotide state of Irga6 but, in addition, the presence of the myristoyl group may be required for the exposure of the 10D7 epitope. As mentioned earlier, the GTP-binding domain and myristoyl group are not part of the 10D7 epitope. It is therefore more likely that the GTPγS binding to the Irga6wt protein results in a conformational change, involving the nucleotide binding domain and myristoyl group, which exposes or creates the 10D7 epitope in the first α helix.

To analyse further this possibility, Irga6 mutants were tested for their ability to bind to the 10D7 antibody (figure 3.29.). Two mutations in the G1 binding motif were introduced. Irga6-K82A has wild type nucleotide binding affinity but no GTPase activity, whereas Irga6-S83N essentially binds no nucleotide (Hunn, 2007). In addition, the Irga6-E106A mutant was tested, that caries a mutation in the primary interaction interface (Pawlowski, unpublished data). This mutant binds nucleotides with the wild type affinities but cannot hydrolyse GTP and is, thus, considered to be constitutively in the GTP-bound state, similarly to the K82A mutant.

Irga6wt is precipitated by 10D7 in the presence of GTPγS with up to 10 fold higher efficiency than in the absence of exogenous nucleotide. On the other hand, K82A and E106A Irga6 mutants, which are not able to hydrolyse bound GTP and are considered to be constitutively in the GTP-bound state, displayed strong binding to 10D7 independently of nucleotide added. In contrast, the S83N mutant, that exhibits essentially no GDP or GTP binding, was precipitated by 10D7 very inefficiently, even when GTPγS was added to the lysates.

Additionally, Irga6-G2A mutant, that cannot be myristoylated, was precipitated very weakly and only in the presence of GTPγS, indicating that myristoyl group has an important role in GTP-dependent conformational change of Irga6. Finally, Irga6-Δ7-12, lacking six amino acids at the N-terminus, bound strongly to 10D7, in the nucleotide-independent manner, suggesting that this region might be responsible for blocking of 10D7 epitope when Irga6 is in the GDP-bound state.

Thus, 10D7 indeed recognises GTP-bound Irga6. GTP binding to Irga6 results in a conformation change of GTP-binding domain, myristoyl group and N-terminal region between amino acids 7-12.

This leads to the conclusion that IFNγ-induced Irga6wt in the resting state is in an inactive, GDP-bound form, and therefore unable to interact with 10D7 antibody. Upon infection with *Toxoplasma gondii*, Irga6wt is found accumulating around parasitophorous vacuoles in the active, GTP-bound conformational state, with the 10D7 epitope exposed.

4.7. Model of conformational change of Irga6 induced by GTP binding

In the crystal structure of recombinant nonmyristoylated Irga6, the first N-terminal 13 amino acids were not resolved (Ghosh et al., 2004). Thus, the position of the amino acids 7 to 12 in the protein structure is not known. However, based on the 10D7 immunoprecipitation data, the following model can be proposed.

As illustrated in figure 4.1.(a), in the GDP-bound state, Irga6wt is in a hypothesized "closed" conformation, where the myristoyl group (red) together with the N-terminal 12 amino acids is folded in such way that the 10D7 epitope (aa 20-25) is covered and inaccessible to the antibody (open green circle). Upon GTP binding,

conformational change in the GTP-binding domain induces the structural change of the N-terminus, with the myristoyl group being in the exposed position, facilitating insertion of activated Irga6wt into the membrane and stabilising the molecule. In this model, amino acids 7 to 12 might act as a hinge (yellow). Reorientation of the N-terminus would then expose amino acids 20-25 and allow binding of the 10D7 antibody (closed green circle). The absence of a myristoyl group in Irga6-G2A mutant prevents the stable reorientation of the N-terminus even in the GTP-bound state, thus, keeping the 10D7 epitope hardly accessible. If the "hinge" region is missing, 10D7 epitope may be constitutively exposed. The Irga6-S83N mutant, unable to bind nucleotides, would be in the constitutive "closed" conformation and, therefore, inaccessible for 10D7 antibody binding (figure 4.1.(b)). In contrary, Irga6-K82A and Irga6-E106A mutants, which bind GTP but cannot hydrolyse it, would be locked in the "open" conformation and accessible to the 10D7 antibody (figure 4.1.(c)).

In this model, 10D7 exposure was used as an indicator of the "open" or "closed" Irga6 conformation in respect of the bound nucleotide, in the presence of nonionic detergent Thesit. The same is true for another nonionic detergent Digitonin and zwitterionic detergent CHAPS (figure 3.28.). In contrast, other nonionic detergents, n-octyl-β-D-glucopyranoside (OGP), Triton X-100 and Triton X-114 induced 10D7 epitope exposure independently of the nucleotide present (figure 3.28.). Nonionic detergents are generally considered to be mild and relatively non-denaturing, and as such, not affecting the proteins' structural features. However, it has been reported that short chain nonionic detergents, such as OGP, can often lead to deactivation of the protein (Seddon et al., 2004). In the case of Irga6wt, nonionic detergents affect the structure of the N-terminal region in a different manner. This might indicate flexibility of the myristoylated N-terminus and/or the hinge region (aa 7-12).
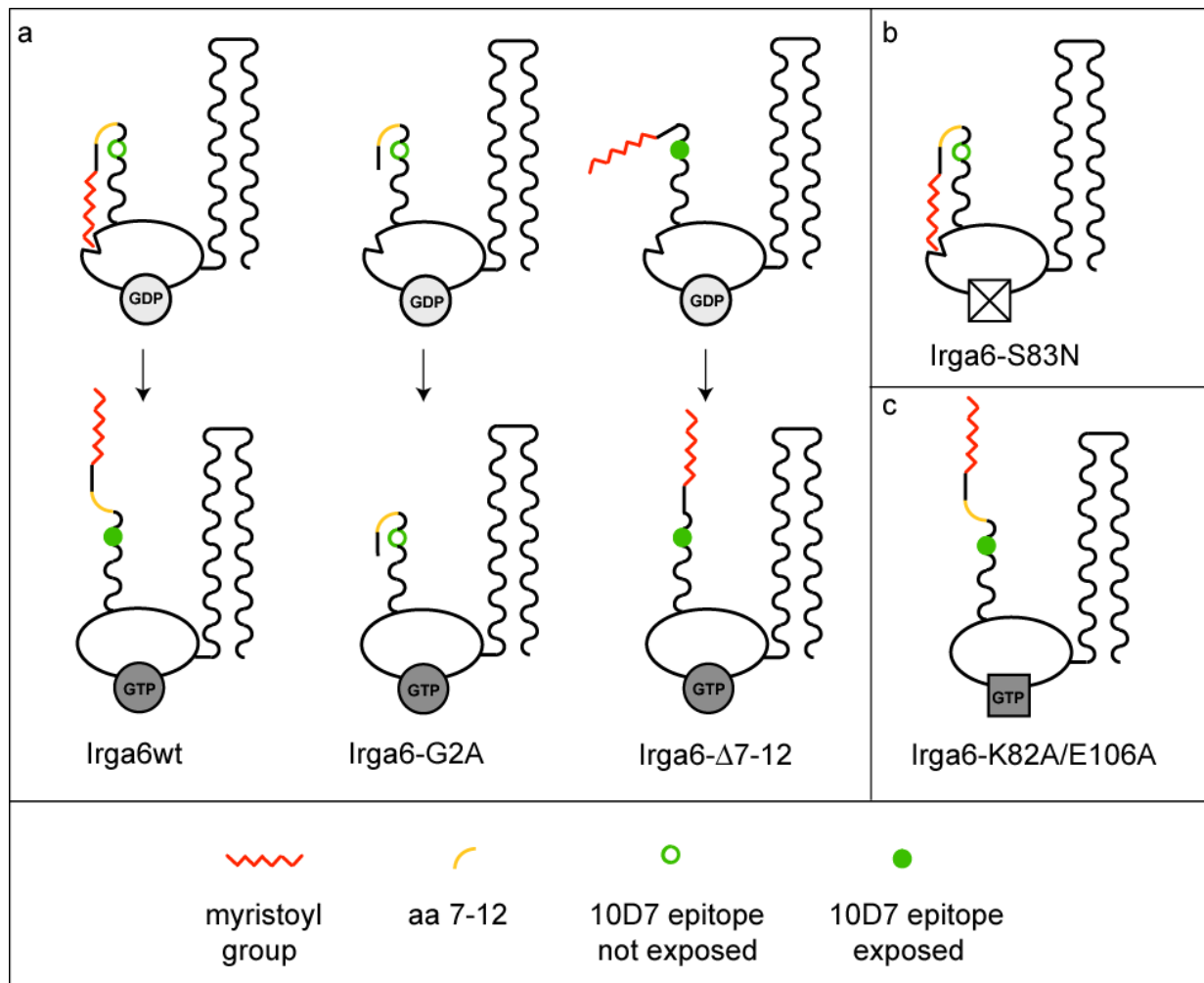
Figure 4.1. Model of Irga6 nucleotide-dependent conformational change

(a) GTP binding induces conformational change of the GTP-binding motif, myristoyl group (red) and the N-terminus, where aa 7-12 could serve as a hinge (yellow); (b) Irga6-S83N mutant is constitutively in the "closed" conformation; (c) Irga6-K82A and Irga6-E106A mutants are kept in the "open" conformation. Exposure (filled green circle) and nonexposure (open green circle) of the 10D7 epitope are used as determinants of "open" and "closed" conformation

4.8. Effects of the nucleotide state and the myristoyl group on Irga6 relocalisation to the parasitophorous vacuole membrane

Activation of Irga6wt proteins leads to the formation of Irga6 homooligomers, both *in vitro* (Uthaiah et al., 2003) and *in* and *ex vivo* (figure 3.11.). Homooligomerisation of Irga6 proteins in the presence of GTPγS, thus *ex vivo*, could be used to test the self-association properties of various Irga6 mutants. According to

the 10D7 immunoprecipitation results, it would be expected that K82A and E106A Irga6 mutants, deficient in the GTP hydrolysis, could form homooligomers even in the absence of exogenously added GTPγS. In contrast, nucleotide-binding deficient Irga6-S83N mutant would be unable to homooligomerise, regardless of nucleotide present.

Indeed, co-immunoprecipitation experiments confirmed that GTP-hydrolysis deficient mutants, K82A and E106A, do homooligomerise even in the absence of GTPγS (figure 3.12.). Conversely, the S83N mutant did not show formation of oligomers at all. Absence of myristoyl group severely impaired the ability of Irga6 to form homooligomers, indicating that this lipid modification plays a significant role in activation and, thus, in function of Irga6 *in vivo*.

The Irga6 mutant, lacking the six amino acids at the N-terminus (Irga6-Δ7-12), homooligomerised in the same manner as the wild type protein, only in the presence of GTPγS. The 10D7 epitope in this mutant, on the other hand, was constitutively exposed, regardless of the nucleotide present. These results confirmed that the 10D7 epitope exposure is not the result of GTP-dependent Irga6 homooligomerisation but rather the consequence of the conformational change of Irga6 caused by GTP binding and can be exposed in other ways too.

IFNγ-induced Irga6 binds to the membrane of the parasitophorous vacuole containing Me49 *Toxoplasma gondii* strain, and is shown to be involved in vacuolar vesiculation and disruption (Martens et al., 2005). Thus, relocalisation of Irga6 proteins to the PVM can be used as an assay to study the function of Irga6 in infected cells, in regard to its activation and membrane binding.

Irga6cTag1 in IFNγ-induced cells accumulated around *T. gondii* PV upon infection. However, the Irga6cTag1-K82A mutant, deficient in GTP-hydrolysis, not only failed to target the PVM but, additionally, acted as a dominant negative mutant, preventing IFNγ-induced Irga6wt from relocalising to the *T. gondii*-containing vacuole (Martens et al., 2005). As expected, the Irga6cTag1-E106A mutant displayed the same dominant negative effect on endogenous Irga6wt (figure 3.30. and table 3.2.). Not surprisingly, the nucleotide-binding deficient Irga6cTag1-S83N mutant did not accumulate at the PVM and also did not prevent endogenous Irga6wt from PV targeting. Nonmyristoylated Irga6cTag1-G2A bound to the PVM but inefficiently; only 19% of vacuoles were coated with G2A mutant in comparison to cells transfected with Irga6cTag1 where 70% of the vacuoles were positive for Irga6cTag1.

Interestingly, accumulation of the endogenous, IFNγ-induced Irga6wt at the PV was slightly decreased in the presence of nonmyristoylated Irga6-G2A. In contrast, transfected Irga6cTag1-Δ7-12 mutant was practically indistinguishable from the wild type protein.

Irga6 at the PVM is in the active, GTP-bound form. As GTP-bound Irga6 can self-associate *in vivo*, it can be assumed that Irga6 forms homooligomers at the vacuolar membrane. Deletion of six amino acids at the N-terminus (Δ7-12) does not affect this process. Interestingly, mutants that are unable to hydrolyse bound GTP (K82A and E106A) do not target PVM and, in addition, almost completely inhibit endogenous protein from going to the PV.

As will be discussed later, it is believed that IFNγ-induced Irga6 exist in an equilibrium between membrane bound and cytosolic pools (Martens et al., 2004). It is probably the cytosolic pool of Irga6 that is initially relocalised to the PVM. The dominant-negative effect of Irga6-K82A and -E106A mutants could be explained by a tendency of the cytosolic Irga6wt to oligomerise with constitutively active mutant proteins in cells before reaching the PVM. As the Irga6-S83N mutant practically does not bind nucleotides, it cannot target PVM nor it can interact with the endogenous Irga6 protein. Nonmyristoylated Irga6-G2A inefficiently binds to the PVM through probably two effects. As this mutant, in cell lysate, builds homooligomers very inefficiently, it might act as a chain terminator, preventing the endogenous protein from further association. Alternatively, or in addition, absence of the myristoyl group in the homooligomer may destabilise its membrane attachment and result in oligomer disassembly from the PVM.

4.9. Effect of the myristoyl group on biochemical properties of Irga6 protein

The myristoyl group is involved in Irga6 conformational change induced by GTP binding (chapter 4.6.). Lack of the myristoyl group results in an inefficient targeting of Irga6 protein to the PV (table 3.2.), indicating that the myristoyl group might be necessary for proper binding of Irga6 to the parasitophorous vacuole membrane.

Structure and biochemical properties of Irga6 protein, expressed and purified from *E. coli*, have been intensively studied *in vitro* (Uthaiah et al., 2003; Ghosh et al., 2004). However, this recombinant protein could not be myristoylated due to the N-terminal extension of the purified protein (Uthaiah et al., 2003) and also because prokaryotes do not express enzymes necessary for protein myristoylation (Heuckeroth et al., 1988). Thus, in order to study the effect of the myristoyl group on oligomerisation, GTPase activity and membrane binding *in vitro*, Irga6wt, -G2A or -S83N proteins without N-terminal fusion (Ins Irga6wt, -G2A, -S83N) were expressed and purified from insect *Sf9* cells.

Ins Irga6wt was mostly membrane bound, indicating that its membrane-binding signal is functional in insect cells (data not shown). Triton X-114 partitioning assay and mass spectrometric analysis of Ins Irga6 proteins revealed the presence of a myristoyl group at the N-termini of Ins Irga6wt and Ins Irga6-S83N. In contrast, the Ins Irga6-G2A protein was not myristoylated but N-terminally acetylated.

N-terminal acetylation is one of the most common protein modifications in eukaryotes, occurring on approximately 80–90% of the cytosolic mammalian proteins (Polevoda and Sherman, 2003). There is no simple consensus motif or dependence on a single type of residue that is identified as necessary for protein acetylation. So far, two ARF-like GTPases Arl3p and Arl8a/b are found acetylated and this modification was required for Golgi and lysosomal localisation of these proteins, respectively (Setty et al., 2004; Hofmann and Munro, 2006). However, the function of the Irga6-G2A N-terminal acetylation is not known.

In the absence of detergent, myristoylated Ins Irga6 protein was excluded from the HiLoad 26/60 Superdex 200 prep grade column, suggesting that under these conditions purified myristoylated protein forms large aggregates of over 600 kDa in molecular weight. Other large GTPases, dynamin (Hinshaw and Schmid, 1995), farnesylated hGBP1 (Fres, 2007) as well as Mx1 (Melen et al., 1992), also eluted as large oligomers in the process of purification. Even in the presence of 50% ethylene glycol, which efficiently prevents protein-protein interactions without denaturing them, Mx1 was eluting from a gel filtration column in the molecular mass range of 120-240 kDa (Melen et al., 1992). It was argued that these oligomers *in vitro* might correspond to the observed Mx1 granular structures *in vivo*.

To avoid aggregation of Ins Irga6wt, 0.05% Thesit was used during purification and final elution from the size exclusion column. However, even in the presence of

0.05% Thesit, recombinant myristoylated proteins behaved markedly different from nonmyristoylated proteins. Myristoylated Ins Irga6wt and Ins Irga6-S83N ran at 200-250 kDa in size exclusion chromatography, in contrast to nonmyristoylated Ins Irga6-G2A or Bact Irga6wt, which eluted from the column at the size of a monomer (figure 3.34.). Myristoylated Irga6 proteins, IFNγ-induced and transfected, expressed in L929 fibroblast also eluted from the Superose 6 column bigger than a monomer (approx. 150 kDa), in contrast to nonmyristoylated Irga6-G2A (figure 3.4.). It is, therefore, possible that myristoyl group itself affects the running behavior of Irga6 proteins, independently of any other protein.

Analysis of the change in hydrodynamic radius of Ins Irga6 proteins in dynamic light scattering experiments at 37°C revealed again large differences between recombinant myristoylated and nonmyristoylated Irga6 proteins. Even in the presence of detergent, nonmyristoylated Bact Irga6wt formed high molecular weight complexes only in the presence of GTP, indicating the formation of GTP-dependent Irga6 homooligomers *in vitro* (figure 3.35.). Unfortunately, due to the limited amounts of purified Ins Irga6 proteins only few measurements with these proteins could be made. In contrast to Bact Irga6wt, nonmyristoylated Ins Irga6-G2A formed higher molecular weight complexes in the presence of GTP after long incubation time (over 500 sec). As no measurement with GDP or in the absence of nucleotide was made, it is not clear whether this increase in size is GTP dependent or not.

Myristoylated Ins Irga6wt and Ins Irga6-S83N formed high molecular weight complexes much earlier, already after 180 sec. Ins Irga6wt forms complexes in the presence of both GDP and GTP. Similarly, Ins Irga6-S83N protein in the presence of GTP formed high molecular weight complexes as well, even though the same mutation in the Bact Irga6-S83N protein resulted in negligible nucleotide binding affinity (Hunn, 2007). Assuming that the S83N mutant in the Ins Irga6 protein would have the same property, high molecular weight structure formation would not be a result of nucleotide-dependent oligomerisation of myristoylated Ins Irga6 proteins. It seems more likely that the presence of myristoyl group induces formation of the Ins Irga6 complexes, probably via binding of myristoyl groups to the detergent micelle. As myristoylated Ins Irga6 aggregated in the absence of detergent, detergent micelle could be used to sequester the hydrophobic myristoyl group from the environment. In such way, more than one molecule of myristoylated Ins Irga6 proteins could associate with a micelle, resulting in a high local concentration of the protein.

10D7 antibody recognises the GTP-bound conformation of Irga6wt. It is earlier discussed that GTP binding to Irga6 molecule induces conformational change, which affects the GTP-binding domain, the N-terminal region and the myristoyl group. It is proposed that the myristoyl group in the GTP-bound cellular Irga6wt is exposed, allowing the binding of 10D7 antibody to its epitope in the presence of GTPγS, but not in Irga6-G2A nor in nucleotide binding deficient Irga6-S83N. However, incubation of 10D7 with Ins-Irga6 proteins revealed that myristoylated Ins Irga6wt and Irga6-S83N proteins were strongly immunoprecipitated, independently of the nucleotide present. In contrast, nonmyristoylated Ins Irga6-G2A was not precipitated, even in the presence of GTPγS (figure 3.36.). This indicates that purified recombinant myristoylated Irga6 proteins adopt different conformation compared to cellular Irga6 proteins. As it was discussed earlier in this chapter, recombinant myristoylated proteins might be stabilised in solution by insertion of myristoyl group into the detergent micelle, and as such are recognised by 10D7 antibody. This exposed myristoyl group might mimic the conformation of activated, membrane-bound Irga6wt protein *in vivo*. In the cells, the myristoyl group on Irga6 might be sequestered from the aqueous environment by protein-protein interaction or by insertion into the membrane.

4.10. Myristoylated Ins Irgs6wt hydrolyses GTP to GDP and GMP *in vitro*

Although nucleotide-binding affinities of Ins Irga6 were not measured, analysis of GTPase activity of Ins Irga6 proteins revealed dramatic differences between myristoylated Ins Irga6wt and nonmyristoylated Ins Irga6-G2A. While nonmyristoylated Irga6 proteins, Ins Irga6-G2A as well as Bact Irga6wt, hydrolysed GTP to GDP only, myristoylated Ins Irga6wt hydrolysed GTP to GDP and GMP (figure 3.37.).

hGBP1 is another GTPase that can hydrolyse GTP to GMP (Schwemmle et al., 1995; Praefcke et al., 1999) leaving predominantly GMP as a product of hydrolysis (85-95% at 37°C; (Kunzelmann et al., 2006)). Hydrolysis of GTP to GMP occurs by the two consecutive cleavages of γ- and β-phosphates, in a process involving a shift of the nucleotide toward the catalytic center after GTP hydrolysis by

positioning the β-phosphate of GDP at the same place as the γ-phosphate of GTP was located before (Prakash et al., 2000b). This explains the inability of hGBP1 to take GDP as a substrate from the solution (Praefcke et al., 1999).

However, it seems that Ins Irga6wt uses a different mechanism for GTP hydrolysis. First of all, the final amount of hydrolysed GMP depends on the starting concentration of GTP. Hydrolysis of 1 mM GTP by Ins Irga6wt resulted in three times more GMP as a final product, compared to the hydrolysis of 10 mM GTP (figure 3.38.), which would not be expected if the GTP hydrolysis to GMP would occur in two successive steps while the nucleotide remains bound, as in hGBP1 (Prakash et al., 2000b). A second argument against the hGBP1 model of hydrolysis for Ins Irga6wt is that the GDP concentration raised in the first hour of Ins Irga6wt hydrolysis and decreased in the next three hours (figure 3.38.(b)). Therefore, it is more likely that GTP is hydrolysed to GDP only but, as GDP concentration rises, GDP itself becomes a substrate for Ins Irga6wt and is further hydrolysed to GMP. This model would predict that GDP itself could serve as a substrate for Ins Irga6wt hydrolysis, which remains to be tested.

4.11. Model of Irga6 regulation *in vivo*

Immunity-Related GTPases (IRG) are represented by 25 coding units in the mouse genome. At least six of them are implicated in resistance against bacterial and protozoan pathogens (table 1.1.). Effects of IRG proteins in challenging pathogen infections are not redundant (Collazo et al., 2001; Butcher et al., 2005; Bernstein-Hanley et al., 2006; Miyairi et al., 2007), indicating that they may regulate each other's functions.

The function of the Irga6 protein is regulated by three GMS proteins, Irgm1, Irgm2 and Irgm3, as well as by Irgb6. These three GMSs are necessary and sufficient for proper localisation of Irga6 to the ER membrane (Schroeder, 2005). Irgm3 was shown to interact with Irga6 in immunoprecipitation and pull-down experiments most probably in the presence of GDP. In addition, ER-localised Irga6 is not visualised by the 10D7 antibody, which seems to recognise specifically the active, GTP-bound form of Irga6. It can be, therefore, postulated that GMS proteins in IFNγ-

induced cells keep Irga6 in an inactive, GDP-bound form. In this model, GMS proteins would act like Irga6 guanine-nucleotide dissociation inhibitors (figure 4.2.).

In the absence of IFNγ induction, in transfected cells, Irga6 is found in dotty structures throughout the cell. Misfolded, functionally inactive proteins, which are not degraded by the proteasome, can aggregate in the cell, forming structures called aggresomes (Kopito, 2000). However, transfected Irga6 was not found in such structures, analysed by immunofluorescence analysis and low-speed centrifugation (Kaiser, 2005). It is proposed that Irga6-containing aggregates represent the active form of this protein (figure 4.2.). Transfected Irga6 is recognised by 10D7 antibody, which binds specifically to the active form of Irga6. In addition, transfected Irga6, in the absence of INFγ-induced factors, forms GTP-dependent homooligomers *in vivo*. Interestingly, it has been reported that rough ER in cells transfected with Irga6 is distended, building abnormal voluminous structures (Kaiser, 2005). Irga6-containing structures were identified in close proximity to these deformed ER regions, indicating the necessity of tight Irga6 regulation in cells.

IFNγ-induced Irga6, which is kept inactive by GMS proteins in the resting cells, is relocalised to the parasitophorous vacuole membrane (PVM) upon infection with nonvirulent, Me 49 strain of *T. gondii* (Martens et al., 2005). Irga6 on the PVM is 10D7-positive, thus, in the active form, probably building GTP-dependent homooligomers (figure 4.2.). However, in the absence of Irgb6 on the vacuoles, Irga6 binds very inefficiently to the PVM (Hunn, 2007), indicating the possibility of Irga6-Irgb6 heterooligomers formation in infected cells. Irga6 and Irgb6 also interacted strongly in the yeast-two hybrid assay (Hunn, 2007).

The mechanism of relocalisation of Irga6, and in general all IRG proteins, from the resting localisation to the *T. gondii* vacuole is unclear. Recruitment of Irga6 to the PVM by the simple proximity of the ER to the vacuole was excluded since other typical ER markers were not found associated with the PVM (Martens et al., 2005). Even though Irga6 was reported to interact with microtubule-associated protein, Hook3 (Kaiser et al., 2004), microtubules themselves are not used to transport Irga6 to the PVM (Khaminetz, unpublished data).
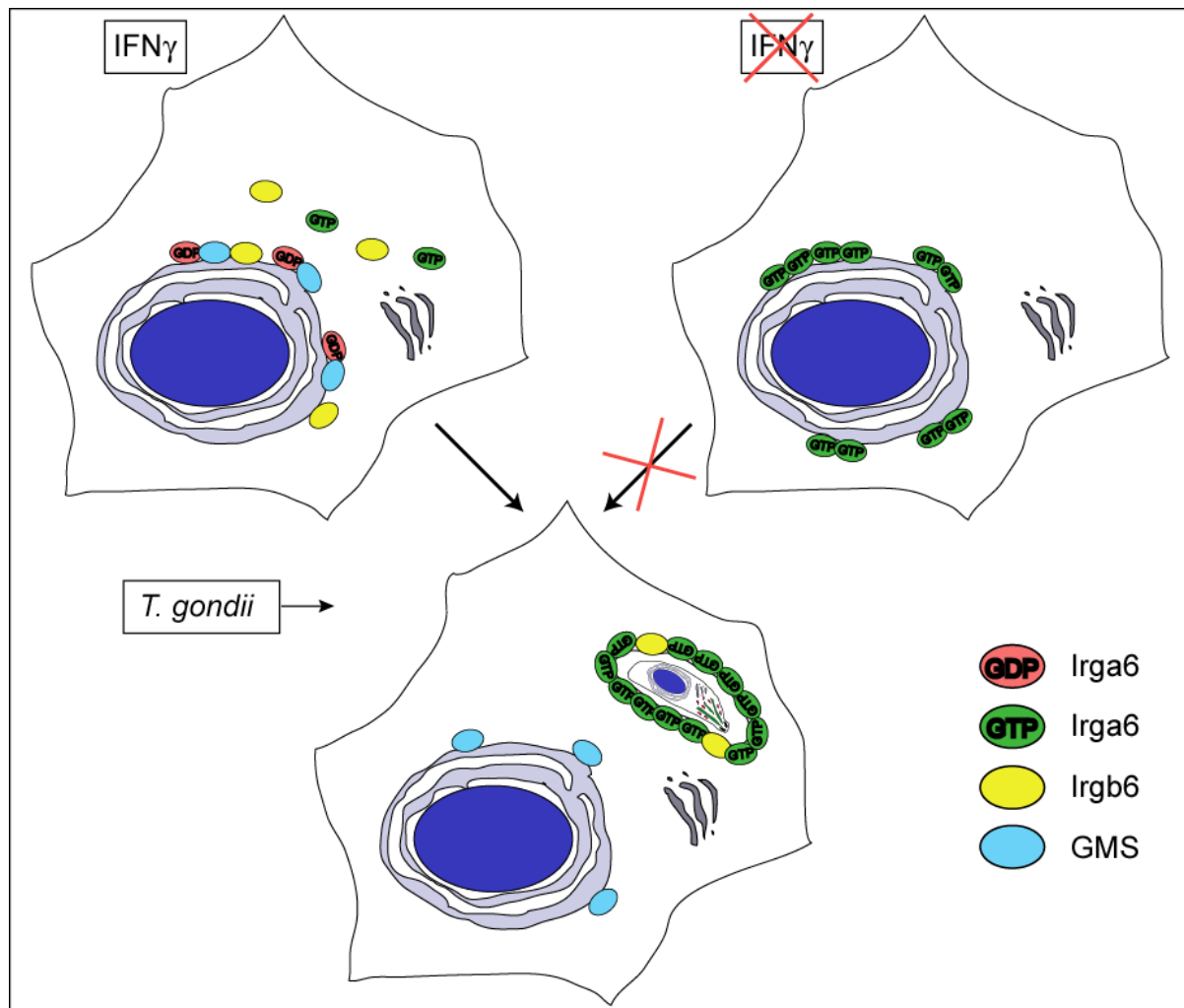
Figure 4.2. Model of relocalisation of Irga6 to the PVM

In IFNγ-induced cells, Irga6 is kept in an inactive, GDP-bound form (red oval) by GMs proteins (turquoise oval). Upon infection with nonvirulent *T. gondii*, Irga6 is relocalised to the PVM, together with Irgab6 (yellow oval) or when Irgb6 is already at the vacuole. On the PVM, Irga6 is in the active, GTP-bound form (green oval), able to form GTP-dependent homo-, and possibly, heterooligomers. In contrast, transfected Irga6wt, in cells not induced with IFNγ, cannot target the PVM, confirming the necessity of GMS and Irgb6 proteins for proper function of Irga6.

Irga6 in the IFNγ-induced cell is in a equilibrium between a membrane-bound (70%) and a soluble pool (Martens et al., 2004). However, it is believed that the soluble, cytosolic pool of Irga6 targets the PVM. As discussed earlier, membrane bound Irga6 is kept inactive by GMS proteins. Soluble Irga6 is released from the inhibitory effect of GMSs and can therefore be activated. The possibility that soluble Irga6wt can get activated is confirmed by the effect of hydrolysis-deficient mutants Irga6-K82A and Irga6-E106A on the wild type protein. These mutants, which are

unable to hydrolyse bound GTP, act as dominant-negative mutants, preventing relocalisation of endogenous Irga6 to the vacuole. They do so presumably by trapping wild type Irga6 in the GTP-dependent homoologomers, before it reaches the PVM. Since hydrolysis-deficient Irga6-K82A and -E106A mutants build homooligomers in cells but cannot target PVM, it can be postulated that GTP-bound Irga6wt binds to the PVM in its monomeric form. Inability of transfected, presumably oligomerised Irga6wt to target the PVM in the absence of IFNγ (Hunn, 2007), also argues that Irga6, which oligomerised prior to infection, cannot bind to the T. gondii-containing vacuoles.
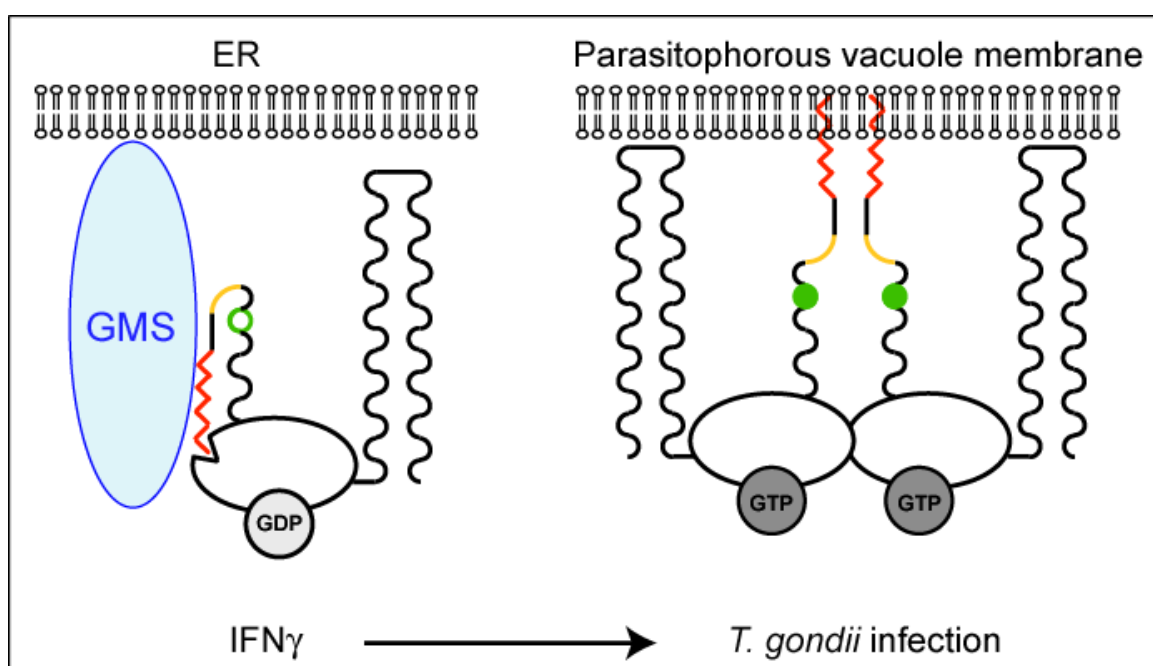
Figure 4.3. Model of Irga6 membrane interaction
In the IFNγ-induced cells, GMS mediate binding of inactive Irga6 to the ER. Upon infection, Irga6 interacts with the PVM in its GTP-bound form, probably by insertion of myristoyl group. Homooligomerisation of Irga6 could increase the avidity of this interaction, stabilising Irga6 on the vacuole.

Irga6 could interact with *T. gondii* PVM either by recognising a specific receptor on the membrane, by inserting into a lipid microdomain, or both. Since Irga6 binds efficiently to the PVM only in the presence of Irgb6, Irgb6 could act as a specific receptor for Irga6 on the parasitophorous vacuole membrane. Irga6 and Irgb6 proteins have been shown to interact in yeast-two hybrid assays (Hunn, 2007).

On the other hand, it has been reported that phosphatidylinositol 4,5-bisphosphate, $PI(4,5)P_2$, promotes the exposure of the myristoyl group (Saad et al., 2006). $PI(4,5)P_2$ is normally associated with the inner leaflet of the plasma membrane (Behnia and Munro, 2005). As parasitophorous vacuole membrane (PVM) is formed during *T. gondii* invasion by invagination of the plasma membrane (Suss-Toby et al., 1996), it is possible that the active Irga6wt, with the exposed myristoyl group, binds preferentially to the $Pi(4,5)P_2$-rich microdomains on the PVM.

However, Irga6 is absent from the cellular plasma membrane, thus simple association of Irga6 with the $Pi(4,5)P_2$-rich microdomains would not be enough for the stable interaction with PVM. It is more plausible that both Irgb6 and lipid composition of PVM are involved in targeting Irga6 to the *T. gondii* vacuole. In this model, active Irga6wt, via its exposed myristoyl group, could bind to the $Pi(4,5)P_2$ microdomains on the vacuole. This interaction could be further stabilised in the presence of Irgb6, by formation of Irga6-Irgb6 complex on the PVM. This complex would then act as a platform for building Irga6 homo- or heterooligomers.

Alternatively, Irga6 could bind to the PVM as a dimer. Biochemical analysis of recombinant, nonmyristoylated Bact Irga6wt propose that GTP-binding itself induce only minor conformational changes of Irga6 molecule. Rather dimerisation results in the major conformational change of Bact Irga6 (Pawlowski, unpublished data). If that would be the case, homodimerisation of the cytosolic Irga6 could result in exposure of myristoyl groups allowing the attachment of the Irga6 dimer to the $Pi(4,5)P_2$-containing membranes. This model would allow not only Irga6 homodimerisation in the cytosol but also formation of Irga6-Irgb6 heterodimers, which could then have higher affinity for the PVM in comparison to the Irga6 homodimer.

The myristoyl group itself is not sufficient for stable insertion of myristoylated proteins into the liposomes and membranes (Shahinian and Silvius, 1995). Homooligomerisation of Irga6 on the PVM could increase the avidity of the Irga6-membrane interaction, by providing additional hydrophobic groups and stabilising the complex (figure 4.3.). The behaviour of nonmyristoylated Irga6-G2A supports the necessity of myristoyl groups for stable integration of Irga6 into the PVM. As seen in chapter 3.9.5., Irga6-G2A has a certain inhibitory effect on targeting of the endogenous Irga6wt to the PVM. Since this mutant homooligomerises very inefficiently, measured by co-immunoprecipitation from transfected cells, Irga6-G2A might act as a chain terminator, preventing the endogenous protein from further

association to the PVM. Alternatively, or in addition, absence of the myristoyl group in the homooligomer by binding of Irga6-G2A can destabilise its membrane attachment and result in oligomer disassembly from the PVM.

If and how the insertion into the parasitophorous vacuole membrane affects the biochemical properties of Irga6 is not known. Association of dynamin with lipid vesicles results in a 1000-fold increase of its GTPase activity (Stowell et al., 1999). Similarly, addition of membranes increased GTP hydrolysis of only prenylated Rac GTPase and had hardly any effect on the nonprenylated protein (Molnar et al., 2001), emphasizing the importance of the lipid modification in the GTPase function. Significance of myristoylation on nucleotide binding affinities of the small GTPase Arf1 was also reported. In the absence of lipids, Arf1 has a higher affinity for GDP than for GTP. In contrast, in the presence of phospholipids, Arf1 affinity for GTPγS was much higher than for the GDP (Randazzo et al., 1995).

The analysis of GTPase activity of recombinant myristoylated Irga6wt revealed significant difference between the myristoylated and the nonmyristoylated protein. Nonmyristoylated Irga6 hydrolyses GTP to GDP only, in contrast to myristoylated Irga6, which hydrolyses GTP to GDP and GMP. Relation of myristoylated Irga6 hydrolysis property to its anti-pathogenic function is unknown.

Other biochemical properties of recombinant myristoylated Irga6wt remain to be studied. Binding affinity of myristoylated Irga6wt to lipid vesicles, in comparison to the nonmyristoylated protein, should be analysed. Identification of vesicle lipid compositions preferred by the myristoylated Irga6 could be used to confirm the subcellular compartmentation of the endogenous Irga6 in resting and infected cells. Finally, defining the nucleotide affinity of myristoylated Irga6wt in the presence and absence of lipid vesicles might contribute to a better understanding of the function of Irga6 in *T. gondii* infected cells, its role in the vesiculation and disruption of the parasitophorous vacuole membrane and degradation of the parasite.

5. References

Accola, M. A., Huang, B., Al Masri, A. and McNiven, M. A. (2002). The antiviral dynamin family member, MxA, tubulates lipids and localizes to the smooth endoplasmic reticulum. J Biol Chem *277*, 21829-21835.

Ames, J. B., Porumb, T., Tanaka, T., Ikura, M. and Stryer, L. (1995). Amino-terminal myristoylation induces cooperative calcium binding to recoverin. J Biol Chem *270*, 4526-4533.

Anderson, S. L., Carton, J. M., Lou, J., Xing, L. and Rubin, B. Y. (1999). Interferon-induced guanylate binding protein-1 (GBP-1) mediates an antiviral effect against vesicular stomatitis virus and encephalomyocarditis virus. Virology *256*, 8-14.

Antonny, B., Beraud-Dufour, S., Chardin, P. and Chabre, M. (1997). N-terminal hydrophobic residues of the G-protein ADP-ribosylation factor-1 insert into membrane phospholipids upon GDP to GTP exchange. Biochemistry *36*, 4675-4684.

Arnheiter, H., Skuntz, S., Noteborn, M., Chang, S. and Meier, E. (1990). Transgenic mice with intracellular immunity to influenza virus. Cell *62*, 51-61.

Baker, T. L., Zheng, H., Walker, J., Coloff, J. L. and Buss, J. E. (2003). Distinct rates of palmitate turnover on membrane-bound cellular and oncogenic H-ras. J Biol Chem *278*, 19292-19300.

Behnia, R. and Munro, S. (2005). Organelle identity and the signposts for membrane traffic. Nature *438*, 597-604.

Bekpen, C., Hunn, J. P., Rohde, C., Parvanova, I., Guethlein, L., Dunn, D. M., Glowalla, E., Leptin, M. and Howard, J. C. (2005). The interferon-inducible p47 (IRG) GTPases in vertebrates: loss of the cell autonomous resistance mechanism in the human lineage. Genome Biol *6*, R92.

Bernstein-Hanley, I., Coers, J., Balsara, Z. R., Taylor, G. A., Starnbach, M. N. and Dietrich, W. F. (2006). The p47 GTPases Igtp and Irgb10 map to the Chlamydia trachomatis susceptibility locus Ctrq-3 and mediate cellular resistance in mice. Proc Natl Acad Sci U S A *103*, 14092-14097.

Bhairi, S. M. (2001). Detergents: A guide to the properties and uses of detergents in biological systems (CALBIOCHEM).

Bhakdi, S., Bayley, H., Valeva, A., Walev, I., Walker, B., Kehoe, M. and Palmer, M. (1996). Staphylococcal alpha-toxin, streptolysin-O, and Escherichia coli hemolysin: prototypes of pore-forming bacterial cytolysins. Arch Microbiol *165*, 73-79.

Bhatnagar, R. S. and Gordon, J. I. (1997). Understanding covalent modifications of proteins by lipids: where cell biology and biophysics mingle. Trends Cell Biol *7*, 14-20.

Binns, D. D., Helms, M. K., Barylko, B., Davis, C. T., Jameson, D. M., Albanesi, J. P. and Eccleston, J. F. (2000). The mechanism of GTP hydrolysis by dynamin II: a transient kinetic study. Biochemistry *39*, 7188-7196.

Black, S. D. (2002). Properties of Detergents (Amphiphiles).

Boehm, U., Guethlein, L., Klamp, T., Ozbek, K., Schaub, A., Futterer, A., Pfeffer, K. and Howard, J. C. (1998). Two families of GTPases dominate the complex cellular response to IFN-gamma. J Immunol *161*, 6715-6723.

Bordier, C. (1981). Phase separation of integral membrane proteins in Triton X-114 solution. J Biol Chem *256*, 1604-1607.

Bourne, H. R., Sanders, D. A. and McCormick, F. (1990). The GTPase superfamily: a conserved switch for diverse cell functions. Nature *348*, 125-132.

Boyartchuk, V. L., Ashby, M. N. and Rine, J. (1997). Modulation of Ras and a-factor function by carboxyl-terminal proteolysis. Science *275*, 1796-1800.

Burger, K. N., Demel, R. A., Schmid, S. L. and de Kruijff, B. (2000). Dynamin is membrane-active: lipid insertion is induced by phosphoinositides and phosphatidic acid. Biochemistry *39*, 12485-12493.

Butcher, B. A., Greene, R. I., Henry, S. C., Annecharico, K. L., Weinberg, J. B., Denkers, E. Y., Sher, A. and Taylor, G. A. (2005). p47 GTPases regulate Toxoplasma gondii survival in activated macrophages. Infect Immun *73*, 3278-3286.

Calero, M., Chen, C. Z., Zhu, W., Winand, N., Havas, K. A., Gilbert, P. M., Burd, C. G. and Collins, R. N. (2003). Dual prenylation is required for Rab protein localization and function. Mol Biol Cell *14*, 1852-1867.

Carlow, D. A., Teh, S. J. and Teh, H. S. (1998). Specific antiviral activity demonstrated by TGTP, a member of a new family of interferon-induced GTPases. J Immunol *161*, 2348-2355.

Cerione, R. A. and Zheng, Y. (1996). The Dbl family of oncogenes. Curr Opin Cell Biol *8*, 216-222.

Charron, A. J. and Sibley, L. D. (2004). Molecular partitioning during host cell penetration by Toxoplasma gondii. Traffic *5*, 855-867.

Cheng, Y. S., Patterson, C. E. and Staeheli, P. (1991). Interferon-induced guanylate-binding proteins lack an N(T)KXD consensus motif and bind GMP in addition to GDP and GTP. Mol Cell Biol *11*, 4717-4725.

Chu, F., Shan, S. O., Moustakas, D. T., Alber, F., Egea, P. F., Stroud, R. M., Walter, P. and Burlingame, A. L. (2004). Unraveling the interface of signal recognition particle and its receptor by using chemical cross-linking and tandem mass spectrometry. Proc Natl Acad Sci U S A *101*, 16454-16459.

Collazo, C. M., Yap, G. S., Sempowski, G. D., Lusby, K. C., Tessarollo, L., Woude, G. F., Sher, A. and Taylor, G. A. (2001). Inactivation of LRG-47 and IRG-47 reveals a family of interferon gamma-inducible genes with essential, pathogen-specific roles in resistance to infection. J Exp Med *194*, 181-188.

Danino, D. and Hinshaw, J. E. (2001). Dynamin family of mechanoenzymes. Curr Opin Cell Biol *13*, 454-460.

Daumke, O., Weyand, M., Chakrabarti, P. P., Vetter, I. R. and Wittinghofer, A. (2004). The GTPase-activating protein Rap1GAP uses a catalytic asparagine. Nature *429*, 197-201.

Deretic, V. (2005). Autophagy in innate and adaptive immunity. Trends Immunol *26*, 523-528.

Di Paolo, C., Hefti, H. P., Meli, M., Landis, H. and Pavlovic, J. (1999). Intramolecular backfolding of the carboxyl-terminal end of MxA protein is a prerequisite for its oligomerization. J Biol Chem *274*, 32071-32078.

Dobrowolski, J. M. and Sibley, L. D. (1996). Toxoplasma invasion of mammalian cells is powered by the actin cytoskeleton of the parasite. Cell *84*, 933-939.

Dransart, E., Olofsson, B. and Cherfils, J. (2005). RhoGDIs revisited: novel roles in Rho regulation. Traffic *6*, 957-966.

Dufner, A. and Mak, T. W. (2006). CARD tricks: controlling the interactions of CARD6 with RICK and microtubules. Cell Cycle *5*, 797-800.

Dufner, A., Pownall, S. and Mak, T. W. (2006). Caspase recruitment domain protein 6 is a microtubule-interacting protein that positively modulates NF-kappaB activation. Proc Natl Acad Sci U S A *103*, 988-993.

Eccleston, J. F., Binns, D. D., Davis, C. T., Albanesi, J. P. and Jameson, D. M. (2002). Oligomerization and kinetic mechanism of the dynamin GTPase. Eur Biophys J *31*, 275-282.

Ehrt, S., Schnappinger, D., Bekiranov, S., Drenkow, J., Shi, S., Gingeras, T. R., Gaasterland, T., Schoolnik, G. and Nathan, C. (2001). Reprogramming of the macrophage transcriptome in response to interferon-gamma and Mycobacterium tuberculosis: signaling roles of nitric oxide synthase-2 and phagocyte oxidase. J Exp Med *194*, 1123-1140.

Farazi, T. A., Waksman, G. and Gordon, J. I. (2001). The biology and enzymology of protein N-myristoylation. J Biol Chem *276*, 39501-39504.

Feng, C. G., Collazo-Custodio, C. M., Eckhaus, M., Hieny, S., Belkaid, Y., Elkins, K., Jankovic, D., Taylor, G. A. and Sher, A. (2004). Mice deficient in LRG-47 display increased susceptibility to mycobacterial infection associated with the induction of lymphopenia. J Immunol *172*, 1163-1168.

Franco, M., Chardin, P., Chabre, M. and Paris, S. (1995). Myristoylation of ADP-ribosylation factor 1 facilitates nucleotide exchange at physiological Mg2+ levels. J Biol Chem *270*, 1337-1341.

Fres, J. (2007) Lipidmodifikation von humanem Guanylat-bindenden Protein 1. Diploma thesis.

Gelb, M. H. (1997). Protein prenylation, et cetera: signal transduction in two dimensions. Science *275*, 1750-1751.

Ghosh, A., Praefcke, G. J., Renault, L., Wittinghofer, A. and Herrmann, C. (2006). How guanylate-binding proteins achieve assembly-stimulated processive cleavage of GTP to GMP. Nature *440*, 101-104.

Ghosh, A., Uthaiah, R., Howard, J., Herrmann, C. and Wolf, E. (2004). Crystal structure of IIGP1: a paradigm for interferon-inducible p47 resistance GTPases. Mol Cell *15*, 727-739.

Goetschy, J. F., Zeller, H., Content, J. and Horisberger, M. A. (1989). Regulation of the interferon-inducible IFI-78K gene, the human equivalent of the murine Mx gene, by interferons, double-stranded RNA, certain cytokines, and viruses. J Virol *63*, 2616-2622.

Gomes, A. Q., Ali, B. R., Ramalho, J. S., Godfrey, R. F., Barral, D. C., Hume, A. N. and Seabra, M. C. (2003). Membrane targeting of Rab GTPases is influenced by the prenylation motif. Mol Biol Cell *14*, 1882-1899.

Goody, R. S., Rak, A. and Alexandrov, K. (2005). The structural and mechanistic basis for recycling of Rab proteins between membrane compartments. Cell Mol Life Sci *62*, 1657-1670.

Gorbacheva, V. Y., Lindner, D., Sen, G. C. and Vestal, D. J. (2002). The interferon (IFN)-induced GTPase, mGBP-2. Role in IFN-gamma-induced murine fibroblast proliferation. J Biol Chem *277*, 6080-6087.

Gorini, G., Medgyesi, G. A. and Doria, G. (1969). Heterogeneity of mouse myeloma gamma G globulins as revealed by enzymatic proteolysis. J Immunol *103*, 1132-1142.

Guenzi, E., Topolt, K., Cornali, E., Lubeseder-Martellato, C., Jorg, A., Matzen, K., Zietz, C., Kremmer, E., Nappi, F., Schwemmle, M.*, et al.* (2001). The helical domain of GBP-1 mediates the inhibition of endothelial cell proliferation by inflammatory cytokines. Embo J *20*, 5568-5577.

Guenzi, E., Topolt, K., Lubeseder-Martellato, C., Jorg, A., Naschberger, E., Benelli, R., Albini, A. and Sturzl, M. (2003). The guanylate binding protein-1 GTPase controls the invasive and angiogenic capability of endothelial cells through inhibition of MMP-1 expression. Embo J *22*, 3772-3782.

Gutierrez, M. G., Master, S. S., Singh, S. B., Taylor, G. A., Colombo, M. I. and Deretic, V. (2004). Autophagy is a defense mechanism inhibiting BCG and Mycobacterium tuberculosis survival in infected macrophages. Cell *119*, 753-766.

Haller, O. and Kochs, G. (2002). Interferon-induced mx proteins: dynamin-like GTPases with antiviral activity. Traffic *3*, 710-717.

Haller, O., Staeheli, P. and Kochs, G. (2007). Interferon-induced Mx proteins in antiviral host defense. Biochimie *89*, 812-818.

Halonen, S. K., Taylor, G. A. and Weiss, L. M. (2001). Gamma interferon-induced inhibition of Toxoplasma gondii in astrocytes is mediated by IGTP. Infect Immun *69*, 5573-5576.

Harlow, E., Lane, D. (1988). Antibodies; A Laboratory Manual).

Hart, M. J., Jiang, X., Kozasa, T., Roscoe, W., Singer, W. D., Gilman, A. G., Sternweis, P. C. and Bollag, G. (1998). Direct stimulation of the guanine nucleotide exchange activity of p115 RhoGEF by Galpha13. Science *280*, 2112-2114.

Hetzer, M., Gruss, O. J. and Mattaj, I. W. (2002). The Ran GTPase as a marker of chromosome position in spindle formation and nuclear envelope assembly. Nat Cell Biol *4*, E177-184.

Heuckeroth, R. O., Glaser, L. and Gordon, J. I. (1988). Heteroatom-substituted fatty acid analogs as substrates for N-myristoyltransferase: an approach for studying both the enzymology and function of protein acylation. Proc Natl Acad Sci U S A *85*, 8795-8799.

Hinshaw, J. E. (2000). Dynamin and its role in membrane fission. Annu Rev Cell Dev Biol *16*, 483-519.

Hinshaw, J. E. and Schmid, S. L. (1995). Dynamin self-assembles into rings suggesting a mechanism for coated vesicle budding. Nature *374*, 190-192.

Hoffman, G. R. and Cerione, R. A. (2002). Signaling to the Rho GTPases: networking with the DH domain. FEBS Lett *513*, 85-91.

Hofmann, I. and Munro, S. (2006). An N-terminally acetylated Arf-like GTPase is localised to lysosomes and affects their motility. J Cell Sci *119*, 1494-1503.

Hunn, J. (2007). Studies on the Evolution and Cellular Resistance Mechanisms of Immunity-Related GTPases. PhD thesis.

Hutchinson, J. P. and Eccleston, J. F. (2000). Mechanism of nucleotide release from Rho by the GDP dissociation stimulator protein. Biochemistry *39*, 11348-11359.

Janzen, C., Kochs, G. and Haller, O. (2000). A monomeric GTPase-negative MxA mutant with antiviral activity. J Virol *74*, 8202-8206.

Joiner, K. A., Fuhrman, S. A., Miettinen, H. M., Kasper, L. H. and Mellman, I. (1990). Toxoplasma gondii: fusion competence of parasitophorous vacuoles in Fc receptor-transfected fibroblasts. Science *249*, 641-646.

Kaiser, F. (2005) Molekulare Charakterisierung und funktionelle Analyse der Interferon-induzierten 47 kDa GTPase IIGP.PhD thesis.

Kaiser, F., Kaufmann, S. H. and Zerrahn, J. (2004). IIGP, a member of the IFN inducible and microbial defense mediating 47 kDa GTPase family, interacts with the microtubule binding protein hook3. J Cell Sci *117*, 1747-1756.

Kamps, M. P., Buss, J. E. and Sefton, B. M. (1985). Mutation of NH2-terminal glycine of p60src prevents both myristoylation and morphological transformation. Proc Natl Acad Sci U S A *82*, 4625-4628.

Kato, J., Kaziro, Y. and Satoh, T. (2000). Activation of the guanine nucleotide exchange factor Dbl following ACK1-dependent tyrosine phosphorylation. Biochem Biophys Res Commun *268*, 141-147.

Kjeldgaard, M., Nyborg, J. and Clark, B. F. (1996). The GTP binding motif: variations on a theme. Faseb J *10*, 1347-1368.

Klamp, T., Boehm, U., Schenk, D., Pfeffer, K. and Howard, J. C. (2003). A giant GTPase, very large inducible GTPase-1, is inducible by IFNs. J Immunol *171*, 1255-1265.

Kleinecke, J. and Soeling, H. (1979). Subcellular compartmentation of guanine nucleotides and functional relationships between the adenine and guanine nucleotide systems in isolated hepatocytes. FEBS Lett *107*, 1255-1265.

Kochs, G., Haener, M., Aebi, U. and Haller, O. (2002). Self-assembly of human MxA GTPase into highly ordered dynamin-like oligomers. J Biol Chem *277*, 14172-14176.

Kochs, G. and Haller, O. (1999a). GTP-bound human MxA protein interacts with the nucleocapsids of Thogoto virus (Orthomyxoviridae). J Biol Chem *274*, 4370-4376.

Kochs, G. and Haller, O. (1999b). Interferon-induced human MxA GTPase blocks nuclear import of Thogoto virus nucleocapsids. Proc Natl Acad Sci U S A *96*, 2082-2086.

Konstantinopoulos, P. A., Karamouzis, M. V. and Papavassiliou, A. G. (2007). Post-translational modifications and regulation of the RAS superfamily of GTPases as anticancer targets. Nat Rev Drug Discov *6*, 541-555.

Kopito, R. R. (2000). Aggresomes, inclusion bodies and protein aggregation. Trends Cell Biol *10*, 524-530.

Krug, R. M., Shaw, M., Broni, B., Shapiro, G. and Haller, O. (1985). Inhibition of influenza viral mRNA synthesis in cells expressing the interferon-induced Mx gene product. J Virol *56*, 201-206.

Kunzelmann, S., Praefcke, G. J. and Herrmann, C. (2006). Transient kinetic investigation of GTP hydrolysis catalyzed by interferon-gamma-induced hGBP1 (human guanylate binding protein 1). J Biol Chem *281*, 28627-28635.

Leipe, D. D., Wolf, Y. I., Koonin, E. V. and Aravind, L. (2002). Classification and evolution of P-loop GTPases and related ATPases. J Mol Biol *317*, 41-72.

Lindenmann, J. (1964). Inheritance Of Resistance To Influenza Virus In Mice. Proc Soc Exp Biol Med *116*, 506-509.

Lindenmann, J., Deuel, E., Fanconi, S. and Haller, O. (1978). Inborn resistance of mice to myxoviruses: macrophages express phenotype in vitro. J Exp Med *147*, 531-540.

Lindenmann, J., Lane, C. A. and Hobson, D. (1963). The Resistance Of A2g Mice To Myxoviruses. J Immunol *90*, 942-951.

Ling, Y. M., Shaw, M. H., Ayala, C., Coppens, I., Taylor, G. A., Ferguson, D. J. and Yap, G. S. (2006). Vacuolar and plasma membrane stripping and autophagic elimination of Toxoplasma gondii in primed effector macrophages. J Exp Med *203*, 2063-2071.

Mackay, D. J. and Hall, A. (1998). Rho GTPases. J Biol Chem *273*, 20685-20688.
MacMicking, J. D. (2004). IFN-inducible GTPases and immunity to intracellular pathogens. Trends Immunol *25*, 601-609.

MacMicking, J. D., Taylor, G. A. and McKinney, J. D. (2003). Immune control of tuberculosis by IFN-gamma-inducible LRG-47. Science *302*, 654-659.

Magee, T. and Seabra, M. C. (2005). Fatty acylation and prenylation of proteins: what's hot in fat. Curr Opin Cell Biol *17*, 190-196.

Marks, B., Stowell, M. H., Vallis, Y., Mills, I. G., Gibson, A., Hopkins, C. R. and McMahon, H. T. (2001). GTPase activity of dynamin and resulting conformation change are essential for endocytosis. Nature *410*, 231-235.

Martens, S. (2004) Cell-Biology of Interferon Inducible GTPases. PhD thesis.

Martens, S. and Howard, J. (2006). The interferon-inducible GTPases. Annu Rev Cell Dev Biol *22*, 559-589.

Martens, S., Parvanova, I., Zerrahn, J., Griffiths, G., Schell, G., Reichmann, G. and Howard, J. C. (2005). Disruption of Toxoplasma gondii parasitophorous vacuoles by the mouse p47-resistance GTPases. PLoS Pathog *1*, e24.

Martens, S., Sabel, K., Lange, R., Uthaiah, R., Wolf, E. and Howard, J. C. (2004). Mechanisms regulating the positioning of mouse p47 resistance GTPases LRG-47 and IIGP1 on cellular membranes: retargeting to plasma membrane induced by phagocytosis. J Immunol *173*, 2594-2606.

Maurer-Stroh, S., Eisenhaber, B. and Eisenhaber, F. (2002). N-terminal N-myristoylation of proteins: refinement of the sequence motif and its taxon-specific differences. J Mol Biol *317*, 523-540.

McCabe, J. B. and Berthiaume, L. G. (1999). Functional roles for fatty acylated amino-terminal domains in subcellular localization. Mol Biol Cell *10*, 3771-3786.

McLaughlin, S. and Aderem, A. (1995). The myristoyl-electrostatic switch: a modulator of reversible protein-membrane interactions. Trends Biochem Sci *20*, 272-276.

Melen, K., Ronni, T., Broni, B., Krug, R. M., von Bonsdorff, C. H. and Julkunen, I. (1992). Interferon-induced Mx proteins form oligomers and contain a putative leucine zipper. J Biol Chem *267*, 25898-25907.

Milligan, G., Parenti, M. and Magee, A. I. (1995). The dynamic role of palmitoylation in signal transduction. Trends Biochem Sci *20*, 181-187.

Mishra, R., Gara, S. K., Mishra, S. and Prakash, B. (2005). Analysis of GTPases carrying hydrophobic amino acid substitutions in lieu of the catalytic glutamine: implications for GTP hydrolysis. Proteins *59*, 332-338.

Mittal, R., Ahmadian, M. R., Goody, R. S. and Wittinghofer, A. (1996). Formation of a transition-state analog of the Ras GTPase reaction by Ras-GDP, tetrafluoroaluminate, and GTPase-activating proteins. Science *273*, 115-117.

Miyairi, I., Tatireddigari, V. R., Mahdi, O. S., Rose, L. A., Belland, R. J., Lu, L., Williams, R. W. and Byrne, G. I. (2007). The p47 GTPases ligp2 and Irgb10 regulate innate immunity and inflammation to murine Chlamydia psittaci infection. J Immunol *179*, 1814-1824.

Modiano, N., Lu, Y. E. and Cresswell, P. (2005). Golgi targeting of human guanylate-binding protein-1 requires nucleotide binding, isoprenylation, and an IFN-gamma-inducible cofactor. Proc Natl Acad Sci U S A *102*, 8680-8685.

Molnar, G., Dagher, M. C., Geiszt, M., Settleman, J. and Ligeti, E. (2001). Role of prenylation in the interaction of Rho-family small GTPases with GTPase activating proteins. Biochemistry *40*, 10542-10549.

Mordue, D. G., Desai, N., Dustin, M. and Sibley, L. D. (1999a). Invasion by Toxoplasma gondii establishes a moving junction that selectively excludes host cell plasma membrane proteins on the basis of their membrane anchoring. J Exp Med *190*, 1783-1792.

Mordue, D. G., Hakansson, S., Niesman, I. and Sibley, L. D. (1999b). Toxoplasma gondii resides in a vacuole that avoids fusion with host cell endocytic and exocytic vesicular trafficking pathways. Exp Parasitol *92*, 87-99.

Morisaki, J. H., Heuser, J. E. and Sibley, L. D. (1995). Invasion of Toxoplasma gondii occurs by active penetration of the host cell. J Cell Sci *108 (Pt 6),* 2457-2464.

Moss, J. and Vaughan, M. (1998). Molecules in the ARF orbit. J Biol Chem *273,* 21431-21434.

Murray, D., Ben-Tal, N., Honig, B. and McLaughlin, S. (1997). Electrostatic interaction of myristoylated proteins with membranes: simple physics, complicated biology. Structure *5,* 985-989.

Murray, D., Hermida-Matsumoto, L., Buser, C. A., Tsang, J., Sigal, C. T., Ben-Tal, N., Honig, B., Resh, M. D. and McLaughlin, S. (1998). Electrostatics and the membrane association of Src: theory and experiment. Biochemistry *37,* 2145-2159.

Nakayama, M., Yazaki, K., Kusano, A., Nagata, K., Hanai, N. and Ishihama, A. (1993). Structure of mouse Mx1 protein. Molecular assembly and GTP-dependent conformational change. J Biol Chem *268,* 15033-15038.

Nantais, D. E., Schwemmle, M., Stickney, J. T., Vestal, D. J. and Buss, J. E. (1996). Prenylation of an interferon-gamma-induced GTP-binding protein: the human guanylate binding protein, huGBP1. J Leukoc Biol *60,* 423-431.

Nelson, D. E., Virok, D. P., Wood, H., Roshick, C., Johnson, R. M., Whitmire, W. M., Crane, D. D., Steele-Mortimer, O., Kari, L., McClarty, G. and Caldwell, H. D. (2005). Chlamydial IFN-gamma immune evasion is linked to host infection tropism. Proc Natl Acad Sci U S A *102,* 10658-10663.

Olson, E. N. and Spizz, G. (1986). Fatty acylation of cellular proteins. Temporal and subcellular differences between palmitate and myristate acylation. J Biol Chem *261,* 2458-2466.

Olszewski, M. A., Gray, J. and Vestal, D. J. (2006). In silico genomic analysis of the human and murine guanylate-binding protein (GBP) gene clusters. J Interferon Cytokine Res *26,* 328-352.

Pavlovic, J., Haller, O. and Staeheli, P. (1992). Human and mouse Mx proteins inhibit different steps of the influenza virus multiplication cycle. J Virol *66*, 2564-2569.

Pechlivanis, M. and Kuhlmann, J. (2006). Hydrophobic modifications of Ras proteins by isoprenoid groups and fatty acids--More than just membrane anchoring. Biochim Biophys Acta *1764*, 1914-1931.

Peitzsch, R. M. and McLaughlin, S. (1993). Binding of acylated peptides and fatty acids to phospholipid vesicles: pertinence to myristoylated proteins. Biochemistry *32*, 10436-10443.

Perez de Castro, I., Bivona, T. G., Philips, M. R. and Pellicer, A. (2004). Ras activation in Jurkat T cells following low-grade stimulation of the T-cell receptor is specific to N-Ras and occurs only on the Golgi apparatus. Mol Cell Biol *24*, 3485-3496.

Pfeffer, S. and Aivazian, D. (2004). Targeting Rab GTPases to distinct membrane compartments. Nat Rev Mol Cell Biol *5*, 886-896.

Polevoda, B. and Sherman, F. (2003). N-terminal acetyltransferases and sequence requirements for N-terminal acetylation of eukaryotic proteins. J Mol Biol *325*, 595-622.

Ponten, A., Sick, C., Weeber, M., Haller, O. and Kochs, G. (1997). Dominant-negative mutants of human MxA protein: domains in the carboxy-terminal moiety are important for oligomerization and antiviral activity. J Virol *71*, 2591-2599.

Praefcke, G. J., Geyer, M., Schwemmle, M., Robert Kalbitzer, H. and Herrmann, C. (1999). Nucleotide-binding characteristics of human guanylate-binding protein 1 (hGBP1) and identification of the third GTP-binding motif. J Mol Biol *292*, 321-332.

Praefcke, G. J., Kloep, S., Benscheid, U., Lilie, H., Prakash, B. and Herrmann, C. (2004). Identification of residues in the human guanylate-binding protein 1 critical for nucleotide binding and cooperative GTP hydrolysis. J Mol Biol *344*, 257-269.

Praefcke, G. J. and McMahon, H. T. (2004). The dynamin superfamily: universal membrane tubulation and fission molecules? Nat Rev Mol Cell Biol *5*, 133-147.

Prakash, B., Praefcke, G. J., Renault, L., Wittinghofer, A. and Herrmann, C. (2000a). Structure of human guanylate-binding protein 1 representing a unique class of GTP-binding proteins. Nature *403*, 567-571.

Prakash, B., Renault, L., Praefcke, G. J., Herrmann, C. and Wittinghofer, A. (2000b). Triphosphate structure of guanylate-binding protein 1 and implications for nucleotide binding and GTPase mechanism. Embo J *19*, 4555-4564.

Randazzo, P. A., Terui, T., Sturch, S., Fales, H. M., Ferrige, A. G. and Kahn, R. A. (1995). The myristoylated amino terminus of ADP-ribosylation factor 1 is a phospholipid- and GTP-sensitive switch. J Biol Chem *270*, 14809-14815.

Resh, M. D. (2006). Trafficking and signaling by fatty-acylated and prenylated proteins. Nat Chem Biol *2*, 584-590.

Rich, K. A., Burkett, C. and Webster, P. (2003). Cytoplasmic bacteria can be targets for autophagy. Cell Microbiol *5*, 455-468.

Richter, M. F., Schwemmle, M., Herrmann, C., Wittinghofer, A. and Staeheli, P. (1995). Interferon-induced MxA protein. GTP binding and GTP hydrolysis properties. J Biol Chem *270*, 13512-13517.

Robertsen, B., Zou, J., Secombes, C. and Leong, J. A. (2006). Molecular and expression analysis of an interferon-gamma-inducible guanylate-binding protein from rainbow trout (Oncorhynchus mykiss). Dev Comp Immunol *30*, 1023-1033.

Rohde, C. (2007) Genetic and Functional Studies on the Conserved IRG (Immunity-related GTPase) Protein IRGC (CINEMA). PhD thesis.

Saad, J. S., Miller, J., Tai, J., Kim, A., Ghanam, R. H. and Summers, M. F. (2006). Structural basis for targeting HIV-1 Gag proteins to the plasma membrane for virus assembly. Proc Natl Acad Sci U S A *103*, 11364-11369.

Santiago, H. C., Feng, C. G., Bafica, A., Roffe, E., Arantes, R. M., Cheever, A., Taylor, G., Vieira, L. Q., Aliberti, J., Gazzinelli, R. T. and Sher, A. (2005). Mice deficient in LRG-47 display enhanced susceptibility to Trypanosoma cruzi infection associated with defective hemopoiesis and intracellular control of parasite growth. J Immunol *175*, 8165-8172.

Sasaki, T., Kaibuchi, K., Kabcenell, A. K., Novick, P. J. and Takai, Y. (1991). A mammalian inhibitory GDP/GTP exchange protein (GDP dissociation inhibitor) for smg p25A is active on the yeast SEC4 protein. Mol Cell Biol *11*, 2909-2912.

Sasaki, T., Kikuchi, A., Araki, S., Hata, Y., Isomura, M., Kuroda, S. and Takai, Y. (1990). Purification and characterization from bovine brain cytosol of a protein that inhibits the dissociation of GDP from and the subsequent binding of GTP to smg p25A, a ras p21-like GTP-binding protein. J Biol Chem *265*, 2333-2337.

Scheffzek, K. and Ahmadian, M. R. (2005). GTPase activating proteins: structural and functional insights 18 years after discovery. Cell Mol Life Sci *62*, 3014-3038.

Scheffzek, K., Ahmadian, M. R., Kabsch, W., Wiesmuller, L., Lautwein, A., Schmitz, F. and Wittinghofer, A. (1997). The Ras-RasGAP complex: structural basis for GTPase activation and its loss in oncogenic Ras mutants. Science *277*, 333-338.

Scheffzek, K., Ahmadian, M. R. and Wittinghofer, A. (1998). GTPase-activating proteins: helping hands to complement an active site. Trends Biochem Sci *23*, 257-262.

Schimmoller, F., Simon, I. and Pfeffer, S. R. (1998). Rab GTPases, directors of vesicle docking. J Biol Chem *273*, 22161-22164.

Schroeder, H., Leventis, R., Shahinian, S., Walton, P. A. and Silvius, J. R. (1996). Lipid-modified, cysteinyl-containing peptides of diverse structures are efficiently S-acylated at the plasma membrane of mammalian cells. J Cell Biol *134*, 647-660.

Schroeder, N. (2005) Dynamic Behaviour of p47 GTPases in Cells. Diploma thesis.

Schumacher, B. and Staeheli, P. (1998). Domains mediating intramolecular folding and oligomerization of MxA GTPase. J Biol Chem *273*, 28365-28370.

Schwemmle, M., Richter, M. F., Herrmann, C., Nassar, N. and Staeheli, P. (1995). Unexpected structural requirements for GTPase activity of the interferon-induced MxA protein. J Biol Chem *270*, 13518-13523.

Schwemmle, M. and Staeheli, P. (1994). The interferon-induced 67-kDa guanylate-binding protein (hGBP1) is a GTPase that converts GTP to GMP. J Biol Chem *269*, 11299-11305.

Seddon, A. M., Curnow, P. and Booth, P. J. (2004). Membrane proteins, lipids and detergents: not just a soap opera. Biochim Biophys Acta *1666*, 105-117.

Setty, S. R., Strochlic, T. I., Tong, A. H., Boone, C. and Burd, C. G. (2004). Golgi targeting of ARF-like GTPase Arl3p requires its Nalpha-acetylation and the integral membrane protein Sys1p. Nat Cell Biol *6*, 414-419.

Sever, S., Muhlberg, A. B. and Schmid, S. L. (1999). Impairment of dynamin's GAP domain stimulates receptor-mediated endocytosis. Nature *398*, 481-486.

Shahinian, S. and Silvius, J. R. (1995). Doubly-lipid-modified protein sequence motifs exhibit long-lived anchorage to lipid bilayer membranes. Biochemistry *34*, 3813-3822.

Sibley, L. D. (2004). Intracellular parasite invasion strategies. Science *304*, 248-253.

Silvius, J. R. and l'Heureux, F. (1994). Fluorimetric evaluation of the affinities of isoprenylated peptides for lipid bilayers. Biochemistry *33*, 3014-3022.

Simon, A., Fah, J., Haller, O. and Staeheli, P. (1991). Interferon-regulated Mx genes are not responsive to interleukin-1, tumor necrosis factor, and other cytokines. J Virol *65*, 968-971.

Soldati, T., Shapiro, A. D., Svejstrup, A. B. and Pfeffer, S. R. (1994). Membrane targeting of the small GTPase Rab9 is accompanied by nucleotide exchange. Nature *369*, 76-78.

Song, B. D. and Schmid, S. L. (2003). A molecular motor or a regulator? Dynamin's in a class of its own. Biochemistry *42*, 1369-1376.

Sprang, S. (2001). GEFs: master regulators of G-protein activation. Trends Biochem Sci *26*, 266-267.

Sprang, S. R. (1997). G protein mechanisms: insights from structural analysis. Annu Rev Biochem *66*, 639-678.

Staeheli, P. and Haller, O. (1985). Interferon-induced human protein with homology to protein Mx of influenza virus-resistant mice. Mol Cell Biol *5*, 2150-2153.

Staeheli, P., Haller, O., Boll, W., Lindenmann, J. and Weissmann, C. (1986). Mx protein: constitutive expression in 3T3 cells transformed with cloned Mx cDNA confers selective resistance to influenza virus. Cell *44*, 147-158.

Stickney, J. T. and Buss, J. E. (2000). Murine guanylate-binding protein: incomplete geranylgeranyl isoprenoid modification of an interferon-gamma-inducible guanosine triphosphate-binding protein. Mol Biol Cell *11*, 2191-2200.

Stowell, M. H., Marks, B., Wigge, P. and McMahon, H. T. (1999). Nucleotide-dependent conformational changes in dynamin: evidence for a mechanochemical molecular spring. Nat Cell Biol *1*, 27-32.

Strunecka, A., Strunecky, O. and Patocka, J. (2002). Fluoride plus aluminum: useful tools in laboratory investigations, but messengers of false information. Physiol Res *51*, 557-564.

Suss-Toby, E., Zimmerberg, J. and Ward, G. E. (1996). Toxoplasma invasion: the parasitophorous vacuole is formed from host cell plasma membrane and pinches off via a fission pore. Proc Natl Acad Sci U S A *93*, 8413-8418.

Sweitzer, S. M. and Hinshaw, J. E. (1998). Dynamin undergoes a GTP-dependent conformational change causing vesiculation. Cell *93*, 1021-1029.

Taylor, G. A., Collazo, C. M., Yap, G. S., Nguyen, K., Gregorio, T. A., Taylor, L. S., Eagleson, B., Secrest, L., Southon, E. A., Reid, S. W.*, et al.* (2000). Pathogen-specific loss of host resistance in mice lacking the IFN-gamma-inducible gene IGTP. Proc Natl Acad Sci U S A *97*, 751-755.

Taylor, G. A., Feng, C. G. and Sher, A. (2004). p47 GTPases: regulators of immunity to intracellular pathogens. Nat Rev Immunol *4*, 100-109.

Taylor, G. A., Jeffers, M., Largaespada, D. A., Jenkins, N. A., Copeland, N. G. and Woude, G. F. (1996). Identification of a novel GTPase, the inducibly expressed GTPase, that accumulates in response to interferon gamma. J Biol Chem *271*, 20399-20405.

Taylor, G. A., Stauber, R., Rulong, S., Hudson, E., Pei, V., Pavlakis, G. N., Resau, J. H. and Vande Woude, G. F. (1997). The inducibly expressed GTPase localizes to the endoplasmic reticulum, independently of GTP binding. J Biol Chem *272*, 10639-10645.

Tuma, P. L. and Collins, C. A. (1994). Activation of dynamin GTPase is a result of positive cooperativity. J Biol Chem *269*, 30842-30847.

Tuma, P. L. and Collins, C. A. (1995). Dynamin forms polymeric complexes in the presence of lipid vesicles. Characterization of chemically cross-linked dynamin molecules. J Biol Chem *270*, 26707-26714.

Uthaiah, R. C., Praefcke, G. J., Howard, J. C. and Herrmann, C. (2003). IIGP1, an interferon-gamma-inducible 47-kDa GTPase of the mouse, showing cooperative enzymatic activity and GTP-dependent multimerization. J Biol Chem *278*, 29336-29343.

Vestal, D. J. (2005). The guanylate-binding proteins (GBPs): proinflammatory cytokine-induced members of the dynamin superfamily with unique GTPase activity. J Interferon Cytokine Res *25*, 435-443.

Vestal, D. J., Gorbacheva, V. Y. and Sen, G. C. (2000). Different subcellular localizations for the related interferon-induced GTPases, MuGBP-1 and MuGBP-2: implications for different functions? J Interferon Cytokine Res *20*, 991-1000.

Vetter, I. R. and Wittinghofer, A. (2001). The guanine nucleotide-binding switch in three dimensions. Science *294*, 1299-1304.

Vojtek, A. B. and Der, C. J. (1998). Increasing complexity of the Ras signaling pathway. J Biol Chem *273*, 19925-19928.

Wilcox, C., Hu, J. S. and Olson, E. N. (1987). Acylation of proteins with myristic acid occurs cotranslationally. Science *238*, 1275-1278.

Worthylake, D. K., Rossman, K. L. and Sondek, J. (2000). Crystal structure of Rac1 in complex with the guanine nucleotide exchange region of Tiam1. Nature *408*, 682-688.

Zerial, M. and McBride, H. (2001). Rab proteins as membrane organizers. Nat Rev Mol Cell Biol *2*, 107-117.

Zerrahn, J., Schaible, U. E., Brinkmann, V., Guhlich, U. and Kaufmann, S. H. (2002). The IFN-inducible Golgi- and endoplasmic reticulum- associated 47-kDa GTPase IIGP is transiently expressed during listeriosis. J Immunol *168*, 3428-3436.

Zhang, H. M., Yuan, J., Cheung, P., Luo, H., Yanagawa, B., Chau, D., Stephan-Tozy, N., Wong, B. W., Zhang, J., Wilson, J. E.*, et al.* (2003). Overexpression of interferon-gamma-inducible GTPase inhibits coxsackievirus B3-induced apoptosis through the activation of the phosphatidylinositol 3-kinase/Akt pathway and inhibition of viral replication. J Biol Chem *278*, 33011-33019.

Zozulya, S. and Stryer, L. (1992). Calcium-myristoyl protein switch. Proc Natl Acad Sci U S A *89*, 11569-11573.

Zurcher, T., Pavlovic, J. and Staeheli, P. (1992a). Mechanism of human MxA protein action: variants with changed antiviral properties. Embo J *11*, 1657-1661.

Zurcher, T., Pavlovic, J. and Staeheli, P. (1992b). Nuclear localization of mouse Mx1 protein is necessary for inhibition of influenza virus. J Virol *66*, 5059-5066.

6. Summary

Immunity-Related GTPases (IRGs) are implicated in cell-autonomous resistance against intracellular bacterial and protozoan pathogens in the mouse. Members of the IRG family are involved in *Toxoplasma gondii*-vacuole vesiculation and disruption, in acidification of phagosomes containing *Mycobacterium tuberculosis*, as well as in induction of autophagy. However, how they work is unclear.

Irga6, a member of the IRG family that is myristoylated *in vivo*, accumulates at vacuoles containing *T. gondii*, in a process that requires an intact GTP-binding domain. *In vitro*, recombinant nonmyristoylated Irga6wt forms GTP-dependent, catalytically active homooligomers, characterized by increased GTPase activity. However, there is no information about Irga6 self-association in cells. Although Irga6 is lipid modified *in vivo*, the role of the myristoyl group in function and in the enzymatic properties of Irga6 has not been characterized.

This study was set to analyze the mechanism of activation of myristoylated Irga6 in cells. Furthermore, the effect of myristoyl group on enzymatic activity and function of Irga6 was studied, *in vivo* and *in vitro*.

Irga6 forms GTP-dependent homooligomers *in vivo*, in the absence of other IFNγ-induced factors. In IFNγ-induced cells, however, Irga6 is kept at the ER in an inactive, GDP-bound form through interactions with members of the GMS family. Infection with *T. gondii* results in the relocalisation of activated, GTP-bound Irga6 to the parasitophorous vacuole membrane. GTP binding promotes a conformational change of Irga6, which involves GTP-binding domain, N-terminal 12 amino acids and the myristoyl group. Myristoylation of the Irga6 protein is required for efficient binding of the enzyme to vacuoles containing *T. gondii*.

Recombinant myristoylated Irga6wt and nonmyristoylated mutant Irga6-G2A proteins show striking differences in their biochemical properties *in vitro*. In contrast to Irga6-G2A, which hydrolyses GTP to GDP only, myristoylated Irga6wt hydrolyses GTP to GDP and GMP.

Results in this study highlight the importance of lipid modification for Irga6 function *in vivo* and *in vitro*. The presented data build a platform for further analysis of myristoylated Irga6 in order to understand better the role of this enzyme in cell-autonomous resistance against pathogens.

7. Zusammenfassung

'Immunity-Related GTPases' (IRGs) spielen in Mäusen eine Rolle in der zellautonomen Resistenz gegen intrazelluläre Bakterien und Protozen. Diese GTPasen sind an der Vesikulation und Zerstörung von Toxoplasma gondii, an der Azidifizierung von Mycobacterium tuberculosis enthaltenden Phagosomen sowie der Induktion der Autophagie beteiligt. Ihre genaue Funktion bei diesen Prozessen ist jedoch noch unklar.

Eines der IRG Proteine, Irga6, das in vivo myristoyliert wird, akkumuliert an Vakuolen, die T. gondii enthalten. Dafür ist das Vorhandensein einer intakten GTP-Bindungsdomäne in Irga6 essentiell. In vitro kann nicht-myristoyliertes Irga6wt GTP-abhängige, katalytisch aktive Homooligomere ausbilden, die eine gesteigerte GTPase Aktivität aufweisen. Ob Irga6 auch in lebenden Zellen homooligomerisieren kann, war nicht bekannt. Der Einfluß der Myristoylierung von Irga6 auf die Funktion und die enzymatischen Eigenschaften des Proteins konnte noch nicht geklärt werden.

Das Ziel dieser Arbeit war, den Aktivierungsmechanismus von myristoyliertem Irga6 in vivo zu analysieren. Des weiteren sollte der Einfluß der Myristoylgruppe auf die enzymatische Aktivität und die Funktion von Irga6 sowohl in vivo als auch in vitro untersucht werden.

Es konnte gezeigt werden, daß Irg6 in Abwesenheit anderer IFNγ-induzierter Faktoren in vivo GTP-abhängige Homooligomere ausbildet. Andererseits interagiert Irga6 in IFNγ-induzierten Zellen in einer inaktiven, GDP-gebunden Form mit Mitgliedern der GMS Famile und wird dadurch am ER gehalten. Infektionen mit T. gondii führen zur Ansammlung von aktiviertem, GTP-gebundenem Irga6 an der Membran der parasitophoren Vakuole. GTP Bindung löst eine Konformationsänderung von Irga6 aus, die die GTP bindende Domäne, die 12 Aminosäuren am N-Terminus und die Myristoyl-Gruppe betrifft. Letztere ist für eine effiziente Bindung des Enzyms an die T. gondii enthaltenden Vakuolen notwendig.

Rekombinantes myristoyliertes Irga6wt und Irga6-G2A, das aufgrund eines Aminosäureaustauschs nicht myristoyliert werden kann, unterscheiden sich grundlegend in ihren biochemischen Eigenschaften in vitro: im Gegensatz zu Irga6-G2A, das GTP nur zu GDP hydrolysiert, kann Irga6wt GTP zu GDP und GMP hydrolysieren.

Die Ergebnisse dieser Arbeit unterstreichen die Bedeutung der Lipidmodifikation für die Funktion von Irga6 *in vivo* und *in vitro*. Sie bilden die Grundlage weiterer Untersuchungen an myristoylisiertem Irga6, mit dem Ziel die Funktion dieses Enzyms in der zellautonomen Resistenz gegen Krankheitserreger besser zu verstehen.

8. Acknowledgement

I'd like to thank Prof. Dr. Jonathan Howard, for giving me the opportunity to work in his lab, for all his support, advices and for making me think twice before just saying "just".

Prof. Dr. Thomas Langer for reviewing my work and being in my examination committee.

Dr. Matthias Cramer and his almighty signature, for the assistance in bureaucratic matters and his kindness.

Steffi, for being such a great roommate and for all the colours she's carrying around.

Rita, the "Cloning Queen", for all her help, experience and honesty.

Gaby, for sharing all the good and the bad times with our favourite *Sf9*s.

Christoph, for his infinite good moods and for his patience with "noch eine Frage".

Niko and Gerrit, for guiding me through the world of P-loops, interfaces and catalytic fingers.

Tobi, for his irreplaceable mega-gels.

Claudia and Bettina, for their help and kindness.

Julia, for her friendship, support, understanding, discussions and many, many more.

And all other members of the lab, present and past, for helpful discussions and the friendly atmosphere.

9. Erklärung

Ich versichere, dass ich die von mir vorgelegte Dissertation selbständig angefertigt, mit Ausnahme der Daten in Kapitel 3.3.1. und 3.3.2., die in Zusammenarbeit mit Julia Hunn erstellt wurden, die benutzten Quellen und Hilfsmittel vollständig angegeben und die Stellen der Arbeit – einschließlich Tabellen, Karten und Abbildungen-, die anderen Werken im Wortlaut oder dem Sinn nach entnommen sind, in jedem Einzelfall als Entlehnung kenntlich gemacht habe; dass diese Dissertation noch keiner anderen Fakultät oder Universität zur Prüfung vorgelegen hat; dass sie abgesehen von den unten angegebenen Teilpublikationen noch nicht veröffentlicht worden ist, sowie, dass ich eine solche Veröffentlichung vor Abschluss des Promotionsverfahrens nicht vornehmen werde.

Die von mir vorgelegte Dissertation ist von Prof. Dr. Jonathan C. Howard betreut worden.

Köln, im November 2007

10. Lebenslauf

Name: Nataša Papić

Geburtsdatum: 06.05.1975.

Geburtsort: Belgrad, Serbien

Staatsangehörigkeit: serbisch

Familienstand: ledig

Ausbildung

1982-1990   Besuch der Grundschule „Lazar Savatić" in Belgrad

1990-1994   Besuch des „Prva beogradska gimnazija" Gymnasiums in Belgrad

1994   Immatrikulation an der Biologischen Fakultät der Universität Belgrad, Serbien
                               Diplomstudiengang: Molekularbiologie und Physiologie

1994-1999   Studium der Biologie an der Universität Belgrad, Serbien

1999-2000   Diplomarbeit an dem „Institute of Molecular Genetics and Genetic Engineering", Belgrad

ab WS 2002   Promotionsstudiengang Biologie (Fachrichtung Genetik) am Institut für Genetik, Universität zu Köln, Abteilung von Prof. Dr. Jonathan C.Howard